

UC Santa Barbara

UC Santa Barbara Electronic Theses and Dissertations

Title

Soft Wearable Robotics and Haptics: Design, Engineering, and Human Factors

Permalink

<https://escholarship.org/uc/item/88c0f8wj>

Author

Zhu, Mengjia

Publication Date

2022

Peer reviewed|Thesis/dissertation

University of California
Santa Barbara

**Soft Wearable Robotics and Haptics: Design, Engineering,
and Human Factors**

A dissertation submitted in partial satisfaction
of the requirements for the degree

Doctor of Philosophy
in
Media Arts and Technology

by

Mengjia Zhu

Committee in charge:

Professor Yon Visell, Co-chair
Professor Elliot Hawkes, Co-chair
Professor Jennifer Jacobs
Professor Misha Sra

September 2022

The Dissertation of Mengjia Zhu is approved.

Professor Jennifer Jacobs

Professor Misha Sra

Professor Elliot Hawkes, Committee Co-chair

Professor Yon Visell, Committee Co-chair

July 2022

Soft Wearable Robotics and Haptics: Design, Engineering, and Human Factors

Copyright © 2022

by

Mengjia Zhu

Dedication here

Acknowledgements

This thesis would not have been completed without support from my mentors, colleagues, family, and friends. First I would like to express my deepest appreciation to my advisor, Prof. Yon Visell for your supervision and support throughout the course of my study. I greatly appreciate the opportunity to work with you and I have been learning how to be a better researcher to conduct impactful, practical, and effective research from you. Thank you for always being available to discuss research, career, and life. I would also like to thank my co-advisor, Prof. Elliot Hawkes for sharing his intelligence and providing valuable input on my research.

I would like to express my sincere gratitude to Prof. Jennifer Jacobs and Prof. Misha Sra for serving on my doctoral committee. I always found our discussions encouraging and inspiring.

Many thanks to my collaborators for their contributions to various research projects presented in this thesis: Dr. Thanh Nho Do, Dr. Shantonu Biswas, Dr. Niko Kastor, Dr. Yufei Hao, Stejara Dinulescu, Adrian Ferstera, Max Linnander, Anzu Kawazoe, Gregory Reardon, and Xinghao Huang. I am deeply grateful to Dr. Nicholas Colonnese, Dr. Amirhossein H. Memar, Dr. Aakar Gupta, Dr. Majed Samad, Dr. Priyanshu Agarwal, and Dr. Sean J. Keller who provided valuable guidance and contributions to the PneuSleeve research during my internship. I feel very honored to have the opportunity to work with you and learn from you. I am also grateful to lab members and members from collaborating labs: Yitian Shao, Bharat Dandu, Dustin Goetz, Neeli Tummula, Vedad Bassari, Mare Hirsch, Taku Hachisu, Robert Bloom III, Mark Beliaev, Simone Fani, Kelly Zhaoan Lu, Jian Jiao, Huanhuan Qin, Souradeep Chakraborty, Zhiwei Zhang, Erin Woo, Steven Delello, Dr. Hung Phan, Dr. Dang Tùng Nguyen, Jianfei Huang, Zhifang Du, Nicholas Naclerio, Matt Devlin, Charles Xiao, Luke Gockowski, David Haggerty, Anna Alvarez, and Veronica Reynolds, for making it such a fun and supportive place to work. I would like to extend my sincere thanks to all the faculty and teachers who have

taught me throughout my education.

Special thanks to my husband Wenpo Huang for his tremendous love and support during the course of my entire oversea studies. Your optimistic attitudes always light me up. Thank you for always being here and especially, for undertaking so much work and responsibilities during the most challenging but happy time when our first baby Ethan came into the world.

I would like to thank my friends, including Xindi, Weidi, Lu, Kendrick, Yuwei, Ziyue, Bao, Mert, You-Jin, Mengyu and the entire MAT community, for making my time after work so enjoyable and relaxed. I would also like to thank moms in the Santa Barbara area: Cloe, Lynx, Susan, Yan, Wenbo, Evelyn, and many others, for sharing parenting tricks, tips, anxiety, and happiness.

Finally, I would like to thank my family, without whom I would not be where I am today. Mom and Dad, thanks for always supporting my decisions and encouraging me to pursue what I believe in. Grandma, thanks for raising me up when my parents could not be with me. Thanks to my big family, my aunts, uncles, and cousins, for your care and love throughout my life.

Curriculum Vitæ

Mengjia Zhu

Education

- 2022 **Ph.D.** in Media Arts and Technology (Expected), University of California, Santa Barbara.
Research topics: soft wearable robotics and haptics.
- 2017 **M.S.** in Materials Science and Engineering, Arizona State University.
Research topics: soft assistive and rehabilitative wearable robotics.
- 2015 **B.E.** in Apparel Design and Engineering (with Distinction), Apparel Design and Engineering, Soochow University (China).
Research topics: intelligent collaborative design platform for children's garments.
- 2014 Summer School in Media, Culture and Art, King's College London, London, UK

Publications

Journal articles:

1. **M. Zhu**, S. Dinulescu, G. Reardon, A. Kawazoe, Y. Visell, Soft Robotic Garments that Share Emotion and Information, in preparation.
2. **M. Zhu**, A. Ferstera, S. Dinulescu, N. Kastor, M. Linnander, E. Hawkes, and Y. Visell, A peristaltic soft, wearable robot for compression and massage therapy (submitted to IEEE/ASME Transactions on Mechatronics), 2022.
3. **M. Zhu**, S. Biswas, S. Dinulescu, N. Kastor, E. Hawkes, and Y. Visell, Soft, Wearable Robotics and Haptics: Technologies, Trends, and Emerging Applications. Proceedings of the IEEE, vol. 110, no. 2, pp. 246-272, Feb. 2022.
4. **M. Zhu**, T. N. Do, E. Hawkes, and Y. Visell, Fluidic Fabric Muscle Sheets for Wearable and Soft Robotics. Soft Robotics, 7(2), 179-197, Apr. 2020. **Cover Article. High-Impact Article.**
5. Y. Hao, S. Biswas, E. Hawkes, T. Wang, **M. Zhu**, L. Wen, and Y. Visell, A Multimodal, Enveloping Soft Gripper: Shape Conformation, Bioinspired Adhesion, and Expansion-Driven Suction. IEEE Transactions on Robotics, vol. 37, no. 2, pp. 350-362, April 2021.

Peer-reviewed conference papers:

1. **M. Zhu**, A. H. Memar, A. Gupta, M. Samad, P. Agarwal, Y. Visell, S.J. Keller, and N. Colonnese, PneuSleeve: In-fabric Multimodal Actuation and Sensing in a Soft, Compact, and Expressive Haptic Sleeve. Proceedings of the 2020 ACM CHI Conference on Human Factors in Computing Systems, pp. 1-12, 2022. **Best Paper Honorable Mention Award.**

2. **M. Zhu**, W. Adams, and P. Polygerinos, Carpal Tunnel Syndrome Soft Relief Device for Typing Applications. 2017 Design of Medical Devices Conference (DMD), Frontiers in Biomedical Devices (Vol. 40672, p. V001T03A003), Apr. 2017. **Top 10 paper**.
3. S. Sridar, P. H. Nguyen, **M. Zhu**, Q. P. Lam, and P. Polygerinos, Development of a Soft-inflatable Exosuit for Knee Rehabilitation. 2017 IEEE/RSJ International Conference on Intelligent Robots and Systems (IROS), pp. 3722-3727, Sept. 2017.

Patents

1. Y. Visell, E. W. Hawkes, T. N. Do, **M. Zhu**, Soft Actuator and Method of Making the Same, U.S. Patent Application 17/275,731, filed February 3, 2022.
2. **M. Zhu**, W. Adams, P. Polygerinos, Devices for Treatment of Carpal Tunnel Syndrome, U.S. Patent 11,185,432, issued November 30, 2021.

Awards and Press

1. **Best Paper Honorable Mention Award**: 2020 ACM CHI Conference on Human Factors in Computing Systems.
2. **Cover Article**: Soft Robotics (April, 2020).
3. **Top 10 Paper** participated in Three-in-Five Competition (Invitation Only), 2017 Design of Medical Devices Conference (DMD).
4. **News Report**: Alliance of Advanced BioMedical Engineering: Hand-in-Glove Relief for Carpal Tunnel Syndrome, Jun. 2017.
5. **News Report**: Montecito Journal: Shape changing garment for expressive fashion, pp 43, Jun. 2022.

Research Intern, Facebook (now Meta) Reality Labs, Jun. 2019 - Sept. 2019.

Abstract

Soft Wearable Robotics and Haptics: Design, Engineering, and Human Factors

by

Mengjia Zhu

Soft robotics technologies hold substantial promise for use in wearable haptic systems, due to their ability to supply forces to the human body in a compliant, conformal, and safe manner. While existing research at the intersection of soft robotics and wearable haptics focuses on "attaching" soft actuators onto the body, it remains a challenge to seamlessly integrate soft actuators into garments in a compact, safe, and effective way. The overarching goal of my PhD research is to transform textiles into soft robotic haptic garments that are comfortable, ergonomic, and can provide multimodal, affective, and expressive haptic feedback tailored to the human sense of touch. This PhD research integrates research on the design, fabrication, and control methods for soft robotic textiles. This dissertation contributes new methods for expressive haptic feedback for large areas of the body, and guidelines for the design of haptic feedback delivered via garments, accounting for immersion, emotion, affect, and health-related benefits. At a broader level, this dissertation contributes to the fidelity, ubiquity, and social relevance of wearable haptic systems, by allowing haptics to be seamlessly integrated within garments that are widely used.

The first chapter of this dissertation gives an introduction of my PhD research and outlines the main contributions. After the introduction, the second chapter reviews emerging advances in soft wearable robotic and haptic technologies, and several promising application areas, including wearable haptic interfaces, assistive robotics, and biomedical devices [1]. It summarizes essential design considerations for such systems based on functional concerns, wearability, and ergonomics. It provides a synthetic review of design strategies that have been adopted

in numerous examples from prior research by surveying sensing and actuation technologies, materials, and fabrication methods. The chapter concludes with a discussion of frontiers, challenges, and future prospects for soft, wearable robotics. These findings guided the development of novel wearable technologies and haptic rendering methods in the following chapters of the dissertation.

The third chapter of this dissertation presents the development of a new family of soft actuators that are suitable, versatile, and effective for wearable applications. We refer to these actuators as fluidic fabric muscle sheets (FFMS) [2]. These sheet-like actuators can strain, squeeze, bend, and conform to the human body. I designed and fabricated FFMS using fabrics and elastic tubes through facile apparel engineering methods. Though the fabrication process is low-cost and straightforward, FFMS can operate at frequencies of 5 Hz or more, achieve engineering strains exceeding 100%, and exert forces exceeding their weight by more than 10,000%. I further demonstrated several potential use cases of FFMS actuators, including a miniature steerable robot, a glove for grasp assistance, garments for applying compression to the extremities, and devices for actuating small body regions or tissues via localized skin stretch.

The fourth chapter of this dissertation demonstrates how FFMS actuators can be used to realize a wearable haptic interface with integrated sensing and multimodal actuation. Using six FFMS actuators, I constructed a forearm sleeve called the PneuSleeve [3]. It is able to render a broad range of haptic feedback types including compression, skin stretch, and vibration, and is able to supply consistent feedback to users with different arm sizes and anatomies by virtue of integrated soft capacitive sensors and a closed-loop force controller. Physical characterizations showed that the actuators generated consistent and perceivable forces at frequencies of 20 Hz, as validated in engineering characterizations. Results of user studies highlight the expressiveness of the haptic effects it provides. The PneuSleeve holds the potential for enabling new interfaces, haptic notifications, navigation, gaming, AR/VR experiences, and many other

applications.

In the fifth chapter of this dissertation, informed by the preceding results, I designed and investigated a peristaltic wearable robot for supplying dynamic compression therapy via finger-sized FFMS actuators. The wearable robot can produce dynamic compression pressure exceeding 22 kPa at frequencies of 14 Hz or more, meeting the requirements for compression therapy and massage. An array of software-programmable peristaltic compression patterns can be furnished by varying frequency, amplitude, phase delay, and duration parameters. To evaluate the promise this wearable robot holds for aiding peripheral hemodynamic flow, I designed a mechanical fixture integrating artificial muscles, skin, and a vein, modeled after the human upper limb. Results showed that the wearable robot was capable of driving fluid flow at rates of up to 1 mL/min. The results matched theoretically derived predictions for peristaltic fluid transport. This dynamic compression garment holds promise for treating disorders affecting lymphatic and blood circulation.

Contents

Curriculum Vitae	vii
Abstract	ix
List of Figures	xiv
List of Tables	xxiii
1 Introduction	1
1.1 Overview	3
1.2 Contributions	5
2 Soft, Wearable Robotics and Haptics: Technologies, Trends, and Emerging Applications	8
2.1 Introduction	10
2.2 Emerging Application Domains for Soft, Wearable Robotics	12
2.3 Soft, Wearable Robotics: Design Considerations	21
2.4 Soft, Wearable Robotics: Materials and Fabrication Methods	30
2.5 Soft, Wearable Robotics: Actuation and Sensing Methods	42
2.6 Conclusion: Frontiers, Challenges, and Future Prospects	59
3 Fluidic fabric muscle sheets for wearable and soft robotics	63
3.1 Introduction	65
3.2 Design Concept and Operating Principle	71
3.3 Fabrication	74
3.4 Material Selection	76
3.5 Analytical Modeling	81
3.6 Results	85
3.7 FFMS Embodiments and Applications	93
3.8 Conclusions	98

4	PneuSleeve: In-fabric multimodal actuation and sensing in a soft, compact, and expressive haptic sleeve	103
4.1	Introduction	105
4.2	Related Work	107
4.3	Design of PneuSleeve System	111
4.4	Physical Characterization and Evaluation	117
4.5	User Study: Psychophysical Evaluation	121
4.6	User Study: Feel Effects	124
4.7	Limitations and Future Work	129
4.8	Conclusion	130
5	A peristaltic soft, wearable robot for compression and massage therapy	132
5.1	Introduction	133
5.2	Device Design and Operating Principle	137
5.3	Mechanical Characterization of the Dynamic Compression System	143
5.4	Applications for Compression Therapy and Therapeutic Massage	147
5.5	Discussion and Future Work	150
6	Conclusion	152
6.1	Future Research Directions	154
	Bibliography	159

List of Figures

2.1	Examples of soft wearable devices in diverse application areas. A. Pneumatic glove for hand rehabilitation [4]. B. Cable-driven soft prosthetic hand [5]. C. Segmented pneumatic actuation for compression therapies [6]. D. Cable-driven suit for reducing metabolic costs of walking [7]. E. Supernumerary pneumatic arm for aiding activities of daily living [8]. F. String-based wearable haptic interface for virtual reality [9]. G. Leggings knit from SMA that can contract to match the limb shape [10]. H. Expressive soft robotic garment actuated by SMAs responds to the gaze of others [11]. I. Piezoelectric garment reacts to facial expressions [12]. Images reproduced with permission. Image B is licensed under Creative Commons 4.0.	14
2.2	Examples of soft wearable robotics and haptic devices in various wearable form factors. Yellow and blue symbols represent different actuation and sensing principles respectively. A-B. Devices consist of braces and straps on the upper body [13, 14]. C. Biometric neckwear [15]. D. Responsive face prosthesis [16]. E. Haptic jackets [17]. F-G. Sleeves [18, 3]. H-I. Bracelets [19, 20]. J-K. Gloves [21, 22]. L-M. Rings on different segments of fingers [23, 24]. N-O. Thimbles [25, 26]. P-Q. Suits [27, 28]. R-S. Footwear [29, 30]. T-V. Braces and straps for lower body [31, 32, 33]. Images reproduced with permission. Images B, C, K are licensed under Creative Commons 4.0.	20
2.3	Body interfaces and mounting methods that can be used in soft, wearable robotic technologies. A. Protective pads for the elbow using stiffness-tunable hydrogels adhered to the skin [34]. B. Skin-adhered tactile stickers actuated by shape memory alloys facilitate wearability at challenging body locations, such as the ear [35]. C. Mounting configurations for a supernumerary arm [36]. D. Supernumerary finger mounted on a user’s wrist [37]. Images reproduced with permission.	22

2.4	<p>Comparison of hardness, or softness, of materials suitable for use in soft wearable robots that interface with human tissues. A class of wearable materials may include those used in the construction of textiles, such as: Silicone, polyamide (nylon), cotton, silk, wool, rayon. Some materials have known hardness values and are shown in the figure. Other materials, particularly those natural materials used in commercial textiles have hardness values that are not apparent in academic literature. Typically designers will consult a manufacturer and choose from subjective experience. Other online sources such as [38, 39] compile material data for such purposes, however, because polymer material properties vary significantly with temperature, humidity, and other testing conditions, the authors recommend performing individual testing for applications with sensitive requirements. Fiber hardness data, especially when measured via nanoindentation, is often reported in MPa, which is not directly comparable to traditional hardness scales (see text). For example, the hardness of PDMS (Dow Sylgard 184) ranges from 20 to 50 Shore A, depending on the catalyst used [40, 41]; the material hardness has been reported as 2.06 MPa [42]. The hardness of cellulose ranges from 2.7 MPa to 240 MPa depending on temperature and humidity [43, 44]. That of bone (234 to 760 MPa [45]), cartilage (2.6 MPa to 179 MPa [46, 47]), or other soft tissues [47] vary depending on test conditions and sample quality.</p>	31
2.5	<p>Few examples of functional soft and wearable robotic devices realized using various materials and relevant fabrication methods. (a) Wearable prosthetic tactile gloves with integrated resistive and capacitive sensors for monitoring finger articulation and pressure [48]. (i) Textile glove with stretchable strain and tactile sensors when grasping an object. (ii) Structure design of the resistive strain and bending sensors. (iii) Multi-layer design for the capacitive sensors. (iv) Resistive flexion sensors are placed on the back of a finger for bending motion sensing. (b) Fiber-reinforced soft robotic glove with pressurized actuator manufactured using 3D printing and soft lithography techniques for rehabilitation and training [49]. (i) Schematic of the soft robotic glove design. (ii) Pressurized soft actuator showing a combination of motions including bending, extending and twisting. (iii) Exploded view showing inextensible layers, elastomer, and fiber reinforcements. (Caption continued on the following page.)</p>	37

2.5	(Continued:) (c) Fluid-driven soft wearable actuators realized using fabrics and stitching [2]. (i) Prototype of Fluidic Fabric Muscle Sheets (FFMS). (ii) Compression garment for the lower limb made of FFMS. (iii)–(v) Stitching for the FFMS actuators may be done with (iii) hand sewing, (iv) machine sewing, or (v) machine embroidery. (d) Machine knitted wearables with tendon-based actuation [50]. (i) Sweater that has an actuatable sleeve. (ii) Knit operation that forms the main fabric. (iii) Two examples of tendon placement on the main fabric. (e) A prosthetic skin with temperature sensor array on a robot hand was made using micro-/nano-fabrication techniques including photolithography, wet etching, reactive ion etching, and deposition [51]. (i): Robotic hand with the temperature sensor array. Insert is a magnified image. (ii) and (iii) SEM image (ii) and exploded view (iii) of the temperature sensor array. (iv) and (v) Exploded view (iv) and optical microscopic image (v) of the IZO temperature sensor. Images reproduced with permission. Images E i-v licensed under Creative Commons 4.0.	38
2.6	Examples of soft and flexible actuation methods for wearable applications. A. Bidirectional cable-driven actuation for an ankle-foot-orthosis [52]. B. Fluidic actuation for bicep lifting assistance [53]. C. Twisted and super-coiled fibre actuators assist with finger bending [54]. D. Biohybrid actuation with microbial cells that adjusts the humidity of clothing microenvironment [55]. E. SMA actuator patches that create shear forces on skin for haptic feedback [56]. F. Electroactive polymer actuation that generates vibrotactile feedback [57]. G. Electrostatic actuation for joint arresting haptic feedback [58]. Images reproduced with permission. Images D (i) and (ii) are adapted with permission from [55]. Copyright 2019 American Chemical Society.	44
2.7	Examples of sensing methods for soft wearable robotic applications. A. Examples using capacitive sensors. i-ii. Sensing glove for human body articulation using a customizable, stretchable textile-silicone composite capacitive strain sensor [59]. iii-iv. Soft-matter sensor measuring elastic pressure and shear deformation [60]. B. Examples using resistive sensing. i-ii. Curvature sensor for monitoring human or robotic motion [61]. iii-iv. Array of 548 resistive sensors on a soft tactile glove for normal force readings to identify tactile information when interacting with objects [62]. C. Examples with optical sensing designs. i-ii. A soft orthotic with curvature control enabled via embedded optical fiber [63]. iii-iv. Soft prosthetic hand for shape, texture, and softness detection using stretchable optical sensing techniques [64]. D. Examples of other sensing technologies. i-ii. Stretchable and flexible piezoelectric sensor for detecting force and pressure [65]. iii. An upper limb soft wearable assistive exosuit using IMU for joint angle sensing and EMG for muscle activity sensing [66]. iv. A soft wearable pneumatic glove with commercially available flex and force sensors to capture finger movements [67]. Images reproduced with permission. Images D i, D ii licensed under Creative Commons 4.0.	54

3.1	<p>A. Examples of muscle sheets in the human body that inspired the design of FFMS [68] (reproduction rights pending). B. A functional prototype illustrating how FFMS are planar fabric structures analogous to muscle sheets. C. FFMS comprise arrays of elastic tubes that function as fluidic transmissions. In this example, corresponding to the prototype of Fig. 1B, uniaxial extension is produced when fluid pressure is increased. D-G. FFMS may be applied in a variety of ways (see Fig. 3.10): (D) deforming a soft object, (E) compressing a limb, (F) bending a flexible structure, (G) in bilayer structures that generate morphological change, among many other possibilities.</p>	72
3.2	<p>Fluidic Fabric Muscle Sheets: Concept and operating principle. A. Hollow elastic tubes are integrated in a composite fabric structure. The tubes are routed in fabric conduits that provide circumferential constraints, due to stitching. <i>Left:</i> When pressurized fluid is pumped into the elastic tubes; the tubes cannot swell radially due to the constraining stitches, and thus can produce a lengthening, similar to a relaxing sheet of muscle. <i>Right:</i> When the fluid pressure is removed, stored elastic energy in the hollow tubes and elastic fabric is released, and the entire textile shortens, like a contracting sheet of muscle. P and L represent fluid pressure and actuator length, respectively. B. <i>Left:</i> When the FFMS is operated to work against a load, as in the isometric configuration shown here, forces are produced. <i>Middle:</i> High pressures produce low forces, and vice versa. F_b and F_a correspond to states a and b in panel B. <i>Right:</i> A simple illustration of the generation of axial forces. We present a mathematical model in a subsequent section. C. <i>Left:</i> Cross section view of a single channel in the displacement operating mode. Wall thinning may result as the elastomer length increases. <i>Middle:</i> In displacement mode, higher pressures produce larger displacements, and vice versa. <i>Right:</i> In such a displacement mode, the FFMS may be used to do external work, such as lifting a mass, as shown here.</p>	73
3.3	<p>Fabricating planar fluidic fabric muscles involves several steps based, in part, on apparel engineering methods. For configurations based on non-stretchable fabrics, the fabric layers are first aligned and stacked. (A) The routing of elastic tubes is designed and layers are stitched to form conduits (B) in a pattern that determines the routing. The stitched patterns can realize single (b) or multiple (a) tube routings. The elastic tubes are then threaded (C) through the resulting fabric conduits. (D) For non-stretchable fabric layers, the fabric structure is wrinkled. (E) A port is established at one end of each channel, whose remote end is then sealed. The stitching may be done via (F) hand sewing, (G) machine sewing, or (H) computerized embroidery.</p>	75

3.4	A1-A4. Four representative FFMS prototypes illustrating different fabric and stitch combinations. A1. Two-way stretch fabric using zig-zag side stitches without wrinkling. A2. Two-way stretch fabric using zig-zag side stitches with wrinkling. A3. Two-way stretch fabric using zig-zag cross stitches without wrinkling. A4. Non-stretch fabric using straight side stitches with wrinkling. B. Cross section images of several commercially available tubes made of latex (top) and silicone (bottom, note the smaller scale). The outer diameter of the silicone tube can reach sub-millimeter scales.	79
3.5	Force testing. A. Apparatus for axial force testing. B. 3-channel FFMS. C. 10-channel FFMS with brackets for test fixture. D-F. Results for the 3-channel FFMS demonstrated consistent performance over repeated actuation, similar behavior at different actuation speeds, and surprisingly good agreement with the analytical model. G1-G4. The larger, 10-channel FFMS yielded similar results to those that we obtained with the 3-channel device. The force range was 0 to 50 N. The longer fluid circuit yielded slightly greater response latency. H. Compression force testing apparatus. I-K. The device produced compressive forces of 0 to 10 N, as 0 to 2 mL of fluid was withdrawn. The results were consistent with our analytical model, and varied little with actuation speed.	88
3.6	Displacement and compression testing. A. Apparatus for displacement testing. B-D. Results for the three-channel FFMS were consistent over repeated actuation. Similar behavior was observed for different actuation speeds. The pressure-displacement relationships were consistent with analytical predictions, despite dynamic effects, including hysteresis (see text). E1-E4. Results for the larger, 10-channel FFMS were similar to those for the smaller FFMS. F. Hydraulic operation with water was more efficient than with air. Similar efficiencies were measured for actuators with one and three channels. Error bars: 95% confidence intervals. G. Durability testing revealed consistent performance over 5000 actuation cycles. A 5% reduction in displacement was observed after this period, which we attributed to initial actuator relaxation.	90
3.7	Examples illustrating failure modes. A. Fabric tearing at stitch locations. B. Stitching failure between fabric conduits. C. Tube ballooning between stitch locations.	92
3.8	FFMS actuators are readily scaled to small and large sizes. (A,B) A large example, consisting of a 34.0 mm thickness FFMS (A: Top view, B: Side view), shown in contracted state, was sufficient to lift 15 kg (Fig. 3.10). (C-F) A small example, in contracted (C,D) and extended (E,F) states; the thickness when extended is 1.0 mm. The large and small actuators were fabricated using the same general process. A penny is used to illustrate the relative scale.	94

3.9	Composite or multi-actuated FFMS can realize dynamic, multimodal bending motion or shape change. (A) In-plane rotation realized by differential pressurization of multiple fluid channels. (B) Out-of-plane bending is realized by combining an FFMS with a second, passive layer with specified bending stiffness. (C) Biaxial bending is realized via a composite of two, orthogonally oriented FFMS sheet actuators.	96
3.10	Demonstrations. (A,D,E) Miniature soft actuators for linear motion control or compression, capable of (A) lifting a small mass, (D) compressing small tissue areas, or (E) providing tactile feedback via skin stretch. Inset: Skin stretch was easily perceived. (B) FFMS actuators can perform large mechanical work. A 10-channel device lifts a 3 kg mass. A 3-channel structure (inner tube radius 2 cm) lifts a 15 kg cinder block and chain at pressures less than 276 kPa. (F,G) FFMS can be used for compression garments for healthcare, training, and haptics. (F) A compression band yields uniform pressure on the upper limb, easily matching pressures provided by blood pressure cuffs. (G) A compression garment for the lower limb comprises three independently addressable sections (dashed boxes). Pressure variations can yield peristaltic motions suitable for undulatory massage in therapies for lymphatic and blood circulation [69], such as lymphedema [70] or venous closure [71].	99
4.1	PneuSleeve is a fabric sleeve capable of rendering complex combinations of compression, skin stretch, and vibration haptic stimuli to a user. (a) PneuSleeve prototype on forearm. Zig-zag stitches are used for integrating compression actuators with the sleeve substrate. Locking stitches are used for integrating stretch actuators with compression actuators. Lower insert illustrates the cross section of a single actuator. (b) PneuSleeve design consisting of six fluidic fabric muscle sheet actuators, two custom soft force sensors, a knit fabric sleeve base, and velcro connectors. (c) Actuation renderability of PneuSleeve. Compression actuators are used to provide compression stimuli and controlled grounding for skin stretch. All actuators can generate vibration stimuli.	106
4.2	Paired with tracking and/or communication technology, the complex multimodal haptics of PneuSleeve enable a wide range of applications.	107
4.3	Customized mutual capacitance sensor to measure force. Two silicone dielectric layers with microgrooves are oriented orthogonally between conductive fabrics to increase sensitivity. Plasma treatment is used to bond interfaces between silicone layers and conductive fabrics.	113
4.4	PneuSleeve system architecture using measured capacitance from the sensor as the feedback for the closed-loop control of the actuator compression force.	114

4.5	Block diagram of the closed-loop control regulating compression force to the user. The highlighted inner loop is embedded into the pressure regulator to reach the commanded pressure signal. The user's calibration model is used for feedforward, and an integral controller using the soft force sensor measurement is used for feedback.	115
4.6	The results of the characterization tests. Each curve corresponds to a deflation and inflation cycle at a certain displacement of the actuator endpoint. L_0 is the length of the actuator at high pressure (200 kPa) and $\Delta L = L_0 - L$ denotes the change in the actuator end-point position. The arrows on the curves indicate the deflation and inflation cycles. <i>Inserts:</i> Actuator characterization setup for quasi-static analysis.	118
4.7	Frequency response of the compression actuator for different amplitudes. Frequency axis is in log scale from 1 Hz to 50 Hz. The red dots represent the magnitude determined using the experimental data, and the lines represents a fitted spline to the experimental data. <i>Inserts:</i> Dynamic response characterization setup for the compression actuator.	119
4.8	(a) Experimental data and fitted models relating measured capacitance to compression force. (b) Experimental data for various cylinder circumferences showing consistent behavior. The unloaded capacitance, C_0 , is 6.6 pF.	120
4.9	Closed-loop control performance for a commanded sinusoidal, (a), and squared, (b), compression force. The black line indicates the desired compression force profile over time and the red line shows the tracking performance recorded from the soft force sensor on the user's arm. The root-mean-square tracking error for the sinusoidal input was 0.10 N, and the settling time for squared input was less than 0.3 s.	121
4.10	ADTs, (a), and JNDs, (b) for all six actuators embedded in PneuSleeve (Figure 4.1) in terms of $\Delta P = P_H - P$, with initial pressure $P_H = 200$ kPa. The detectability and sensitivity differences may be attributed to the type and location of the actuator.	124
4.11	Example single-cycle control signals for selected feel effects. Bold red numbers denote the index of the active actuator (Figure 4.1).	125
4.12	Box plots showing the Goodness of Fit and Goodness of Feel ratings for the 23 feel effects.	127
5.1	A. FFMS actuators are used for the peristaltic wearable robot design. These actuators are arranged in parallel to mimic peristalsis. B. The peristaltic wearable robot can be used in various locations on human limbs, including the upper arm, forearm, and lower limb. The insert demonstrates the propagation of the peristaltic wave generated. C. Peristaltic transport in biological organs such as the digestive tract involves sequential contraction and relaxation of muscles. . .	135
5.2	Schematic design of the slider-crank driving mechanism.	139

5.3	<p>Various control input designs can be used to generate spatial-temporal compression wave patterns. A. Two pistons can be used to control eight actuators for maximum efficiency, with spatial compression forces coupled at locations routed to the same motor. The sinusoidal displacements with a phase delay of $\pi/2$ on the top denote an example of the input signal for both pistons. The plot on the bottom illustrates the resulting spatial profile of the compression force at times t_0 and t_1. The two-piston driving system can also compose other spatial-temporal compression force patterns such as B and C, with the top figures showing the piston input signals, and the bottom figures showing the composed spatial waves. D. The driving system can be expanded to eight pistons to control each actuator independently. Arbitrary spatial compression force waves can be generated. E. The prototype of the two-piston driving system. F. The prototype of the eight-piston driving system.</p>	140
5.4	<p>The graphic user interface generates a user-defined waveform with input parameters such as frequency and amplitude. The interface also includes a two-step donning design of the device.</p>	141
5.5	<p>Evaluation of the force generated by a single actuator. A. Compression force testing set-up for a single actuator. B. Relationship between fluid volume and compression pressure follows a similar curve for different operation strokes ranging from 10% to 100% with the margins marked in the plot. Note that the minimum compression pressure occurs when the fluid volume is maximum. As the fluid is withdrawn from the actuator, the compression pressure increases. The inserted diagrams illustrate the extreme conditions for maximum and minimum compression pressure to occur.</p>	142
5.6	<p>Frequency response of the system. A. The hysteresis loops presented in the relationship between fluid volume and compression pressure show energy loss during the actuation. The energy loss increases with increasing frequency. Legend: commanded frequency in Hz. B. Legend: different operation stroke range in %. The experimental frequency reaches a plateau for all stroke ranges. The smaller the stroke range, the higher the experimental frequency achieved. Overall, the system is able to operate at frequencies up to about 20 Hz despite some discrepancies between commanded frequency and experimental frequency. C. As the stroke magnitude gets higher, the drop-off in stroke occurs at lower frequencies. The magnitude remains almost flat across all frequencies for 10% operation stroke range.</p>	144
5.7	<p>Motion capture results for various dynamic compression patterns including peristaltic motions (A-D, F), all-in-phase actuation (E), and sequential squeezing (G-H). The texts at the top left corner of each subfigure denote the wavelength and wave speed of each peristaltic pattern. For the sequential squeezing patterns, the texts show the squeezing time of each actuator.</p>	145

5.8	The wearable robot is configured to promote hemodynamic circulation in a limb model via peristaltic transport. A. A simplified illustration of the cross-section through the middle of upper arm [72]. B. The cross-section of the arm model used for the experiment. C. Testing apparatus for the peristaltic transport.	146
5.9	A. Experimental results of the flow rate showed a linear relationship with the wavelength, in agreement with the theoretical prediction (equation 5.7). B. Results showed that the viscosity had a weak effect on the flow rate, agreeing with the analytical predictions in [73, 74].	148
5.10	A. Our peristaltic wearable robot on user’s forearm for therapeutic massage. B. The actuator side of the wearable robot. C. The closure side of the wearable robot.	151
6.1	A. A shape changing garment for expressive fashion. Inserts show the actuated sleeve and skirt ruffles. B. A piezoelectric micro-pump I designed to generate a volumetric flow to power miniature fluidic actuators. C. An example of the future garment as a whole-body haptic suit. The colored strips denote the active components that can change length longitudinally or exert compression force radially on the body.	155

List of Tables

2.1	Elastic moduli of selected materials in wearable robotics in GPa.	29
2.2	Selected soft-robotic materials, technologies, and applications ²	48
2.3	Comparison of different actuation methods for wearable applications*	49
2.4	Selected attributes of representative sensors for wearable applications*	55
3.1	Stitch and fabric selection for FFMS actuators. Red arrows represent the stretch directions of the fabrics, and blue arrows represent the stretchability of the assembled FFMS. Longer arrows denote greater stretchability. The configuration in the red box is used for most prototypes in this work.	80
4.2	Abbreviated List of Wearable Haptic Interfaces	109
4.3	List of the 23 feel effects tested in the subjective user study. Feel effects are grouped into ‘families’ based on the similarity of their control signals. C = compression, SS = skin stretch, V = vibration, CW = clockwise, CCW = counterclockwise.	126
5.1	Theoretical viscosity and Reynolds number of glycerin-water mixtures with different glycerin concentrations in mass C_m	149

Chapter 1

Introduction

Garments are essential in our everyday life to provide aesthetics, basic protection, and social identification. Increased efforts have been put into the development of functional garments through the integration of technologies into clothing in recent years. These functional garments provide advanced functionalities such as protecting the wearer from hazards, providing a high level of breathability in sports-functional clothing, and supplying medical treatments.

Haptics is one of the prevalent application areas of functional garments. Haptics studies the science and technologies related to the sense of touch. When integrated with garments, wearable haptic systems have gained increasing popularity as a novel paradigm for human-robot interaction (HRI). With these systems grounded to the body, haptic wearables can be easily carried around to supply instantaneous haptic feedback in a more integrated manner. Among these wearable haptic systems, smartwatches earned a steady following among consumers over the past decades. Similar to phones and gaming gadgets, these devices provide notifications and alerts. However, they are limited in their capabilities to render many real-life touch interactions, such as being gripped or stroked by a hand.

A grand challenge in haptics research is to make rendered haptic feedback feel close to our real-life touch experiences [75, 76]. This challenge comes in three aspects. Firstly, many

objects we interact with in our life are soft, but many haptic actuators are rigid. Secondly, a lot of the haptic stimuli we experience are non-vibratory, but many haptic actuators are vibrotactile devices. Besides vibrations provided by these haptic devices, we also experience many other mechanical stimuli, such as pressure that is challenging to be simulated by vibrotactile methods. Thirdly, in addition to haptic communications, other applications of wearable haptic devices in the healthcare domain demands further exploration. All of the above suggests that we could contribute to the wearable haptics and robotics field by developing devices that can generate more natural, diversified, expressive, and health-beneficial haptic feedback.

By developing soft robotic wearable devices with multimodal and expressive haptic feedback, I provided four contributions motivated by this grand challenge during my PhD research. The second chapter of the dissertation presents a systematic review of the state of the art in soft wearable robotics and haptics (chapter 2), aiming to synthesize and discover the opportunities in this area. Motivated by the opportunities in the review, the third chapter of this dissertation presents a new family of soft actuators for wearable robotics and haptics applications that enable conformal interactions with the human body (chapter 3). Next, the fourth chapter presents a systematic haptic device with integrated sensing and multimodal actuation (chapter 4) using the technology developed in chapter 3. This research shows how combining different modalities of haptic stimulations can make the haptic feedback rendered more diversified and information-rich. Further informed by these findings, the fifth chapter of the dissertation presents the study of a peristaltic wearable robot for compression therapy (chapter 5). These efforts aim to enhance the fidelity, ubiquity, and social relevance of wearable haptic systems. The following sections provide a more detailed summary of the contents and contributions of the dissertation.

1.1 Overview

The goal of this dissertation is to develop soft wearables to provide multimodal and expressive haptic feedback, aiming to enhance the fidelity, ubiquity, and social relevance of wearable haptic systems. This dissertation is organized into six chapters: this introduction, three most significant published papers, one chapter (submitted for publication), and a summary.

Chapter 2 provides a survey of prior literature in the field of soft wearable robotics and haptics. It reviews emerging advances from numerous examples in promising application areas including wearable haptic interfaces, assistive robotics, and biomedical devices. It synthesizes several important design considerations related to wearability and ergonomics. It also summarizes the commonly used materials, fabrication methods, actuation, and sensing methods that facilitate the compliance engineering and functional design of soft wearable robots. It concludes with a discussion on the frontiers, challenges, and future prospects in soft wearable robotics and haptics.

One of the most important challenges identified in the review of chapter 2 is to engineer new actuation methods that meet wearability needs and functionality considerations. Motivated by this, I designed a new family of soft actuators that we refer to as Fluidic Fabric Muscle Sheets (FFMS) as presented in chapter 3 (which is based on publication [2]). These soft actuators are made of fabrics and elastomers that are readily integrated with daily garments, enabling conformal interactions through large areas of the human body. These sheet-like actuators provide forces through straining, squeezing, bending, and conforming to the human body, demonstrating potential applications in assistive exosuits, haptic wearables (chapter 4), and dynamic compression garments (chapter 5).

The findings from chapter 3 show that FFMS actuators can provide compression and skin stretch to the human body for haptic feedback. Leveraging these actuation capabilities of FFMS actuators, in chapter 4, I developed an expressive haptic sleeve (referred to as PneuSleeve,

which is based on publication [3]) with integrated sensing and multimodal actuation. In addition to supplying compression and skin stretch, PneuSleeve can deliver vibrations up to 50 Hz. These three forms of haptic feedback (compression, skin stretch, and vibration) contain distinguishable sensory information when perceived by the human. For a haptic garment, such capability of providing multiple types of stimuli is a significant design consideration to enrich the expressiveness of the device. In addition to the actuation capabilities, I further developed soft sensors integrated with closed-loop control algorithms to ensure that the compression force generated by the sleeve is consistent among different users. Results from psychophysical evaluations and user studies showed that this multimodal haptic sleeve could generate various distinguishable meaningful messages. This research contributes to methods for rendering multimodal feedback to the body and strategies for the mechanical unification of compression haptic feedback across users with different body sizes and anatomies. This research highlights the expressiveness of haptic wearables when used for various interaction applications, including navigation, social communication, and gaming.

In addition to providing expressive haptic feedback demonstrated in chapter 4, functional garments can also improve human health in medical-related fields as reviewed in chapter 2. Therefore, in chapter 5, I developed a soft wearable robot that supplies compression and massage therapies to the human extremities for blood and lymphatic circulation. This robot consists of eight FFMS actuators arranged parallelly, with each capable of providing compression pressure exceeding 22 kPa and frequencies surpassing 14 Hz, meeting the requirements for compression therapy and massage. To show how this wearable robot could potentially promote blood and lymphatic circulation, I evaluated the effect of the compression wave patterns on flow promotion in a customized mechanical model of the upper limb. Results showed that the dynamic compression patterns induced a fluid flow of up to 1 mL/min in the artificial vein. Further experiments on the fluid flow optimization revealed that the flow rate increased with the wavelength and frequency of the compression wave patterns, which agrees well with theo-

retical findings. This research provides preliminary evidence for the wearable robot to be used to improve lymphatic and blood circulation.

Chapter 6 concludes this dissertation with a summary of the main findings and a discussion on the future directions of this work.

1.2 Contributions

The key contributions of this dissertation may be summarized as follows:

1. It presents a comprehensive review at the distinctive intersection of soft robotics and wearable technologies, discussing relevant technologies, design considerations, engineering techniques, and promising application areas (chapter 2 and publication [1] in Proceedings of the IEEE). This survey synthesizes well over 200 articles with the earliest cited work from 1954, but most are recent, dating from 2015 or later. This research creates a fundamental understanding of soft wearable robotics and haptics research, aiming to synthesize and discover the opportunities in this field.
2. Motivated by the findings from the literature review in chapter 2, it presents the design of novel Fluidic Fabric Muscle Sheets (FFMS), a new family of soft actuators inspired by human thin, sheet-like muscles (chapter 3 and publication [2] in Soft Robotics). This research contributes novel design, fabrication, and modeling for soft wearable actuators based on fluidically actuated fabrics. These actuators can elongate and contract as artificial muscles, squeeze when wrapped around human extremities or soft bodies, and have various shape-changing modes such as in-plane turning, out-of-plane bending, and biaxial bending through composites made of FFMS with optional passive structures. It contributes analysis indicating that FFMS can operate at frequencies of 5 Hz or more, achieve engineering strains exceeding 100%, and exert forces >115 times their weight.

3. The intrinsic compliance and the mechanical performance empower FFMS actuators to be used for various applications in soft wearables (chapter 3 and [2]). This research provides demonstrations of FFMS actuators in several use cases including a miniature steerable robot, an assistive glove for grasp, compression garments, and devices for rendering touch feedback via localized skin stretch. This research has been featured on the cover of *Soft Robotics* (April 2020) and is one of the top-cited articles with dozens of citations from subsequent publications.
4. The capability of producing compression, vibration, and skin stretch demonstrated in chapter 3 makes FFMS actuators great candidates for multimodal haptic rendering (chapter 4 and publication [3] in *Proceedings of the 2020 CHI Conference on Human Factors in Computing Systems (ACM CHI)*). This research contributes a novel haptic sleeve, which we refer to as PneuSleeve, for rendering expressive haptic feedback for large areas of the body. It also contributes techniques for rendering consistent compression stimulations across users with different arm sizes and anatomies through the development of soft sensors and closed-loop feedback control algorithms.
5. Leveraging the capabilities of PneuSleeve, this research further contributes analysis of the expressiveness of haptic wearable interfaces using psychological characterizations and subjective assessments (chapter 4 and [3]). Results show that PneuSleeve can generate a broad range of detectable and distinctive meaningful haptic messages to a human. This paper won the Best Paper Honorable Mention award at the ACM CHI conference 2020. This research has attracted broad attention from the community, with the video presentations gaining over a thousand views on YouTube.
6. This dissertation also contributes to a peristaltic wearable robot for compression therapy (chapter 5, submitted to *IEEE/ASME Transactions on Mechatronics*). This research contributes to a novel wearable robot using FFMS actuators driven by compact customized

hydraulic systems. It contributes novel methods to improve blood and lymphatic circulations based on peristalsis. Finally, it contributes findings of the optimal driving regimes for fluid transport both theoretically and empirically.

Chapter 2

Soft, Wearable Robotics and Haptics: Technologies, Trends, and Emerging Applications

This chapter reviews the state of the art in prior literature as a general context for the research presented in this dissertation. More detailed overviews on the topics of each following chapter are presented in the introduction sections of the following chapters (chapter 3 through 5). This chapter summarizes the emerging application domains for soft wearable robotics, including health-related applications, haptic and human-computer interactions, and fashion arts. Commonly used materials, fabrication methods, sensing approaches, and actuation techniques are enumerated and discussed critically. This chapter provides research context and motivations for the design of FFMS actuators (chapter 3), the development of PneuSleeve (chapter 4), and the invention of the peristaltic wearable robot (chapter 5).

The content of chapter 2 is originally published in the following reference [1]:

M. Zhu, S. Biswas, S. I. Dinulescu, N. Kastor, E. W. Hawkes and Y. Visell, Soft, Wearable Robotics and Haptics: Technologies, Trends, and Emerging Applications. Proceedings of the IEEE, vol. 110, no. 2, pp. 246-272, Feb. 2022. ©2022 IEEE.

Adapted here with permission from the publisher, doi: 10.1109/JPROC.2021.3140049.

Abstract

Recent advances in the rapidly growing field of soft robotics highlight the potential for innovations in wearable soft robotics to meet challenges and opportunities affecting individuals, society, and the economy. Some of the most promising application areas include wearable haptic interfaces, assistive robotics, and biomedical devices. Several attributes of soft robotic systems make them well-suited for use in human-wearable applications. Such systems can be designed to accommodate the complex morphology and movements of the human body, can afford sufficient compliance to ensure safe operation in intimate proximity with humans, and can provide context-appropriate haptic feedback or assistance to their wearers. Many soft robotic systems have been designed to resemble garments or wearables that are already widely used today. Such systems could one day become seamlessly integrated into a myriad of human activities and environments. Here, we review emerging advances in wearable soft robotic technologies and systems, including numerous examples from prior research. We discuss important considerations for the design of such systems based on functional concerns, wearability, and ergonomics. We describe an array of design strategies that have been adopted in prior research. We review wearable soft robotics applications in diverse domains, survey sensing and actuation technologies, materials, and fabrication methods. We conclude by discussing frontiers, challenges, and future prospects for soft, wearable robotics.

2.1 Introduction

Recent advances in soft and functional materials, and methods of fabrication have catalyzed research in soft robotics during the past decade. Among the earliest examples of wearable soft robotics were technologies for human space exploration that were developed to support the NASA Apollo program in the 1960s [77]. Inspired by the stringent demands of human space

exploration, those explorations anticipate the utility of soft robotics for systems that assist humans in close proximity with the body. During the intervening decades, soft robotics has been used in wearable systems for first responders, rehabilitation and assistive robotics, and wearable haptic devices, among many other examples.

In this article, we review recent developments in the vibrant and diverse research area of soft wearable robotics. The many examples that we present highlight the invention and diversity of embodiments and hardware designs represented in recent work. However, their diversity also underscores the immature nature of the field. Hardware paradigms, morphologies, materials, and technologies for soft robotics remain fluid, evolving, and nonstandardized. A consequence is that the unique software and control challenges they pose are only beginning to be described, as reflected in the relatively sparse literature on software and control methods for soft robotics. As a result, the present survey is mainly focused on hardware design approaches, application-related investigations, materials, and technologies. We survey emerging application domains, including rehabilitative, therapeutic, and assistive robotics, prosthetics, haptics, and other areas. We also discuss distinguishing characteristics of soft, wearable robotic systems, including aspects of coordinated sensing, actuation, and computation. We discuss considerations arising from human wearability in soft robotic and haptic systems, and conceptual and practical implications for their design. Enabling technologies for soft robotics have advanced rapidly as a result of intense research in numerous groups and institutions. We review many of the advances and technologies in materials, fabrication, sensing, and actuation that are contributing to the development of this promising field. We conclude by discussing the potentially transformative influence that soft, wearable robotic systems could have in many human environments and activities. We discuss some of the important challenges that we argue need to be met in order to realize this potential. This survey complements recent articles that have covered developments in soft robotics or wearable technologies in particular domains – focused on biomedical or assistive devices [78, 79, 80, 81], haptic interfaces [82, 83], actuators [84, 85],

sensors [86, 87, 88], or fabrication methods [89, 90]. In contrast, we here present a holistic survey of research at the distinctive intersection of soft robotics and wearable technologies, including relevant technologies, engineering challenges, and applications. We identified hundreds of published articles or works for potential inclusion in this survey via multi-keyword search of online scholarly indices (representative keywords: soft, wearable, robotic, haptic, fluidic, garment, prosthesis, orthosis, actuators, sensors), and by cross-reference to related or citing works. We selected well over 200 articles or other sources for inclusion. The earliest cited work is from 1954, but most are recent, dating from 2015 or later.

Many developments in wearable robotics have been motivated by applications that involve complex, human-centered challenges that benefit from automation. The term *robotic* is frequently used to describe systems that integrate three key capabilities: sensing, thinking, and acting [91]. Sensors collect information from the environment or the robot itself; computation processes information, enacts decisions and control; and actuators perform mechanical work on the environment. In wearable robotics, the environment encompasses the human body and its surroundings. Designing wearable systems thus demands careful consideration of factors including safety, ergonomics, comfort, and reliability [92, 93]. It can be challenging to meet these requirements using conventional robotic design approaches that are based on rigid mechanical systems. Thus, a growing array of researchers and engineers have identified soft robotic technologies as being especially well suited for wearable application areas. We review recent work in several of these areas in Section 2.2.

2.2 Emerging Application Domains for Soft, Wearable Robotics

Many advancements in soft robotic technologies have been driven by needs in health-related areas, including rehabilitation and disability engineering [94, 78]. Wearable soft robotics may also provide therapeutic technologies offering mental and physical benefits [6, 95]. Other

researchers have investigated soft robotic technologies, including orthotic and prosthetic devices, that might augment the capabilities of the human body, by reducing the effort or energy required to perform physical activities [7, 27], or even providing additional, supernumerary limbs [8, 37]. In this section, we review an array of examples in diverse application areas.

2.2.1 Rehabilitation and Assistive Devices

Physical assistance and rehabilitation are among the most actively researched biomedical application areas for soft, wearable robotics. Assistive devices are designed to restore the body's capacities for performing physical tasks or movements that are affected by injury, disease, or congenital effects. Many activities of daily living rely on the impressive capabilities of the human hand for grasping and manipulation. Consequently, some of the most promising examples of soft robotics research include devices for assisting or restoring grasping movements of the hand [4, 96, 97, 21]. Technologies that interface with the hand are challenging to engineer because hands are kinematically complex, are used in a diverse variety of fine manipulation tasks, and have numerous moving joints. Impairments of the sensorimotor system often arise from neurological impairments, such as stroke or traumatic injury. Such impairments can often be remedied through rehabilitation exercises and resistance training. Several research groups have investigated soft, wearable robotic devices that address needs in rehabilitation. Many of these employ fluidic actuation. Polygerinos et al. developed a robotic glove for stroke patients, employing soft fiber-reinforced silicone-based actuators that can enact a variety of motions under fluid pressurization (Figure 2.1A) [4]. Zhu et al. designed a pneumatic wrist angle correction device for the rehabilitation of carpal tunnel syndrome [98]. Several tendon-driven assistive gloves have also been developed. Kang et al. created one such glove for restoring hand movements during activities of daily living [97, 21]. In it, tendons are embedded in a polymer skin, and arranged so as to assist pinch and other grasping movements



Figure 2.1: Examples of soft wearable devices in diverse application areas. A. Pneumatic glove for hand rehabilitation [4]. B. Cable-driven soft prosthetic hand [5]. C. Segmented pneumatic actuation for compression therapies [6]. D. Cable-driven suit for reducing metabolic costs of walking [7]. E. Supernumerary pneumatic arm for aiding activities of daily living [8]. F. String-based wearable haptic interface for virtual reality [9]. G. Leggings knit from SMA that can contract to match the limb shape [10]. H. Expressive soft robotic garment actuated by SMAs responds to the gaze of others [11]. I. Piezoelectric garment reacts to facial expressions [12]. Images reproduced with permission. Image B is licensed under Creative Commons 4.0.

(Figure 2.2J) [21]. While many other soft robotic gloves have also been developed, Zhang et al. investigated a different approach, based on wearable pneumatic rings that aid grasping (Figure 2.2M) [24]. Sensors in the device allow the rings to inflate in response to the grasping movements of the wearer.

The larger joints of the body are kinematically simpler than the hand but often involve larger forces or displacements, and thus produce different design requirements. Galiana et al. introduced a cable-driven rehabilitation device that corrects shoulder position based on a wearer's posture, which is sensed via an Inertial Measurement Unit (IMU) (Figure 2.2A) [13]. Among soft, wearable robotic devices for the lower limbs, Park et al. realized an ankle-foot rehabilitation system using McKibben artificial muscles (Figure 2.2R) [30]. Sridar et al. created a soft-inflatable exosuit for knee rehabilitation using structured thermoplastic polyurethane (TPU) fluidic bladders (Figure 2.2S) [31]. Further examples of soft wearable robots for movement assistance can be found in a recent review by Thalman et al. [79].

2.2.2 Prostheses and Orthotics

Prosthetics and orthotic devices augment the ability of the body to perform physical activities. Prosthetic devices provide replacements for absent limbs. Orthotic devices are used to assist with mechanical functions of the musculoskeletal system, prevent joint hypomobility and disuse atrophy, maintain fracture and joint alignment during healing, and remove damaging load to decrease pain. Several research groups have investigated soft robotic prosthetic and orthotic devices. Mohammadi et al. designed a 3D printable soft robotic prosthetic hand that has multi-articulating capabilities for daily grasping tasks (Figure 2.1B) [5]. Thalman et al. investigated a pneumatic ankle-foot orthosis to assist in inversion-eversion ankle support [99]. Further examples may be found in recent review articles that survey advances in soft robotics for prostheses [78], orthoses [100], and other needs.

2.2.3 Compression Therapies

Compression therapies are used to improve lymphatic or blood circulation [69], such as lymphedema [70] or venous closure [71]. In some cases, they are combined with cold treatment to reduce pain and swelling, as in hiloterapy. Compression devices are often designed to apply static or dynamic pressure to body surfaces, such as in the application of Intermittent Pneumatic Compression (IPC) for the treatment of lymphedema [101]. Among emerging soft robotic technologies for compression therapies, Payne et al. developed a brace-like fabric device that encloses human limbs to provide dynamic pressure stimuli that mimic manual massage (Figure 2.1C) [6], while Zhao et al. investigated a programmable robotic system for efficient, programmable intermittent pneumatic compression therapy [102].

2.2.4 Performance Augmentation

Other wearable robotic systems are designed to improve the physical performance of healthy individuals. For example, Simpson et al. showed that simply connecting the legs via an elastic element can reduce the energy required for running by $6.4 \pm 2.8\%$ [103]. Several actuated devices have also been designed to improve human movement economy by reducing the amount of energy required to complete a movement, activity, or exercise. For instance, Quinlivan et al. created a tethered, multiarticular soft exosuit that can reduce the metabolic rate of walking by nearly 23% (Figure 2.1D) [7]. Kim et al. created a portable exosuit for assisting hip extension, and showed that it can reduce the metabolic rate of treadmill walking or running by 9.3% and 4.0% respectively (Figure 2.2P) [27].

2.2.5 Extending the Human Body

Several researchers have investigated methods for augmenting the human body through soft robotic supernumerary (supplemental) limbs. Such supernumerary limbs have been designed to help their wearers compensate for injuries or impairments, to extend the working space of the healthy body, to improve task performance, or enable their wearers to perform tasks that exceed their capabilities. For example, several groups have proposed wearable, supernumerary fingers that assist stroke patients during object grasping (Figure 2.3E) [37]. Many supernumerary devices have been designed to be modular, comprising arrays of moving segments that can produce substantial motion. Some integrate multiple actuators that increase the size of the kinematic workspace of the limb. Examples include pneumatic soft poly-limbs made of silicone actuators (Figure 2.3D) [36], and supernumerary limbs based on wearable fabric actuators (Figure 2.1E) [8]. A recent review of supernumerary devices can be found in Masia et al. [104].

2.2.6 Haptic Interfaces for Human-Computer Interaction, Virtual Reality, Human-Robot Interaction, and Other Applications

Wearable robotic systems interface with the skin, which is a major component of the human haptic system, associated with the sense of touch. The haptic system integrates the skin, musculoskeletal system, and other tissues. Over the past half-century, haptic technologies, including many wearable devices, have been investigated for applications in human-computer interaction, virtual reality, neurorehabilitation, human-robot interaction, telemanipulation, sensory substitution, and many others [105, 106]. Most haptic technologies are designed to stimulate the skin, which is the largest sensory organ of the body. It is a critically important intermediary in any physical interaction with the environment and is a fundamental constituent of our ability to perceive and interact with our environment. Such interfaces provide perceptual cues in the form of forces, displacements, electrical, thermal, or other signals delivered to the skin and body [107, 108]. Two recent reviews survey additional considerations for wearable haptic devices [82, 83].

The properties of the skin, and associated ergonomic requirements (Section III, below), are motivating many researchers to investigate soft technologies for wearable haptics. Today, much of this research remains at the stage of technology development; we review several examples of such enabling technologies in later sections of this article. However, several researchers have already produced wearable, soft interfaces for haptic applications. Several soft, wearable haptic technologies have been designed to allow users to experience touching and interacting with virtual objects whose properties are simulated haptically. These include devices for providing tactile feedback to a hand or finger (Figure 2.1F [9]) in virtual reality. Others have been designed to guide navigation or actions in real or virtual environments, for example through belt-like garments [109, 110], or wrist-worn inflatable interfaces [111, 112].

2.2.7 Affective Haptic Interfaces

In addition to facilitating physical interactions with our environment, the human sense of touch also serves important functions in social communication and emotion. Emotional, or affective, states are influenced by physiological processes in the body driven by activity in the sympathetic, parasympathetic, and enteric components of the visceral motor system, and by exogenous tactile sensations felt by the skin [113]. Many forms of touch between individuals, such as handshakes or hugs, convey social and emotional information [114, 115] that depends on the social context involved and on the parameters governing the physical interaction, such as locations, forces, or sliding speeds [116]. Recent findings demonstrate that such parameters greatly influence the responses of tactile receptors, including multitudes of C-polymodal tactile afferents that innervate most skin regions, that drive emotional responses to social touch [117, 118].

These findings have influenced the development of new methods for haptic feedback related to emotion, also referred to as affective haptics. Emerging application areas for affective haptics include interfaces for mediating remote touch between individuals and wearable devices for haptic therapy [119]. The important role of mechanics in the emotional processing of touch sensations, and the soft contacts that are involved in interpersonal touch, have motivated several research groups to develop affective haptic systems using wearable, soft robotic technologies. Hiroshi et al. developed four affective haptic interfaces that provide touch, squeezing, painful and cooling sensations for therapeutic applications including anxiety disorders and Autism Spectrum Disorder [120]. Papadopoulou et al. developed a programmable shape memory alloy (SMA) actuated sleeve that provides rhythmic and thermal stimulation to promote calmness and reduce anxiety [95]. Wu et al. fabricated a segmented pneumatic sleeve that creates the illusion of a continuous lateral motion in order to mimic a stroking gesture commonly used in social touch (Figure 2.2F) [18].

2.2.8 Fashion, Art, and Design

Humans have employed soft, wearable technologies in the form of clothing since ancient times. Thus, it is unsurprising that designers in fashion, art, and other areas have explored soft, wearable robotic systems whose functionalities expand those of conventional garments, such as through adaptive garments. In some cases, the expanded functionalities of these garments allow them to adapt to the size, shape, or preferences of their wearer. A basic purpose of conventional garments is to insulate their wearer from their environment. Thus, it is unsurprising that many researchers have investigated adaptive garments that can respond dynamically to the environment of the wearer by altering their configuration, shape, or other attributes. Other functions of traditional garments include individual expression or social interaction, including privacy. Thus, many examples of adaptive garments respond to the social context in which they are worn, or to interpersonal interactions.

Originally envisioned in science fiction, one category of size-adaptive garments is that of self-lacing shoes. Companies including Puma and Nike have commercialized footwear with actuated, self-constricting laces in recent years [121, 122]. Many other self-fitting garments have been proposed, such as the sleeves developed by Granberry et al. that are actuated by nickel-titanium (NiTi)-based SMA materials (Figure 2.1G) [10].

Aesthetics, art, and personal expression have also informed many developments in soft, wearable robotics for fashion and art. Many design researchers have also investigated the opportunities that such technologies, including sensors and actuators, can provide for interaction with a wearer's environment or others within it. Drawing inspiration from human emotion and social behaviors, Albaugh created a cable-driven collar that can hide the wearer's face when desired [123]. Farahi designed expressive, gaze-actuated garments actuated via SMAs (Figure 2.1H) [11]. Gao designed animated dresses that change configuration in the presence of unfamiliar people [124]. Gao also realized interactive fashion articles integrating piezoelectric



Figure 2.2: Examples of soft wearable robotics and haptic devices in various wearable form factors. Yellow and blue symbols represent different actuation and sensing principles respectively. A-B. Devices consist of braces and straps on the upper body [13, 14]. C. Biometric neckwear [15]. D. Responsive face prosthesis [16]. E. Haptic jackets [17]. F-G. Sleeves [18, 3]. H-I. Bracelets [19, 20]. J-K. Gloves [21, 22]. L-M. Rings on different segments of fingers [23, 24]. N-O. Thimbles [25, 26]. P-Q. Suits [27, 28]. R-S. Footwear [29, 30]. T-V. Braces and straps for lower body [31, 32, 33]. Images reproduced with permission. Images B, C, K are licensed under Creative Commons 4.0.

materials, such as polyvinylidene fluoride (PVDF) sheets, that can react to the chromatic spectrum of their immediate surroundings (Figure 2.1I) [12, 125]. She also designed a pneumatic dress utilizing origami structures whose pattern changes when actuated via air pressure [126]. Extending this idea, Perovich et al. later realized a dress that unfolds when pressurized [127]. Recently, similar ideas have also manifested in prominent fashion circles. At the 2019 Paris Haute Couture fashion week, van Herpen introduced garments that, while not entirely soft, use integrated motors in order to animate a garment with rotating structures [128]. Additional examples of robotic designs in fashion from the standpoint of social robotics are described in a 2015 book chapter by Danese [129].

As the aforementioned examples demonstrate, emerging applications for wearable, soft robotics are diverse, including medical devices, haptic interfaces, performance augmentation systems, supernumerary limbs, and adaptive garments, among other categories. These new design methods, systems, and technologies evoke novel questions concerning how such systems can be designed to achieve their intended functionalities, while also meeting other requirements such as ergonomics, comfort, and safety. We review design considerations for soft, wearable robotics, with further illustrative examples, in the next section.

2.3 Soft, Wearable Robotics: Design Considerations

Soft, wearable robotic systems are being investigated for application in diverse areas. While many of these applications are relatively established, methods for the design of soft, wearable robotics are still developing. Several properties of these systems evoke important design considerations arising from their properties and context of use. Several important design considerations relate to human wearability, including safety, stability, comfort, and wearability. Others arise from the essential softness of these systems, which involve continuum mechanical media and mechanisms and soft materials that are less established in robotics. Such considera-

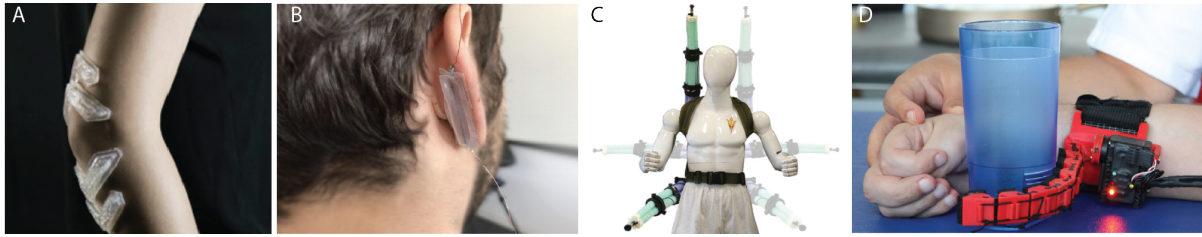


Figure 2.3: Body interfaces and mounting methods that can be used in soft, wearable robotic technologies. A. Protective pads for the elbow using stiffness-tunable hydrogels adhered to the skin [34]. B. Skin-adhered tactile stickers actuated by shape memory alloys facilitate wearability at challenging body locations, such as the ear [35]. C. Mounting configurations for a supernumerary arm [36]. D. Supernumerary finger mounted on a user's wrist [37]. Images reproduced with permission.

tions often weigh importantly in the selection of materials and technologies for soft, wearable robotics, in how these elements are integrated, in how they are designed for wearability, and in the design of methods and algorithms for control and interaction.

2.3.1 Tissue Biomechanics and Haptics

Another distinguishing aspect of soft, wearable robotic systems concerns how they interface with the skin, either by design, as in wearable haptic systems, or through the close connection of all wearable robotic devices with the body. Human skin is not only a prominent interface with the environment but is also the sensory organ of touch (the largest such organ in our body). Skin is a marvel of biological engineering, sufficiently sensitive to detect the tiny footsteps of a fly, while also strong enough that it can sustain extreme loads like those produced when lifting very heavy loads. There are two main categories of human skin. Glabrous skin covers the palmar surfaces of the hands and the soles of the feet; It is thicker and reinforced by networks of collagen fibers that endow it with shear strength and hyperelasticity, which are required to permit the manipulation of large loads. Hairy skin covers most of the body and possesses a thinner outer layer. Hairy skin is nearly two orders of magnitude more compliant than glabrous skin, readily displacing by a centimeter or more when subjected to loads of a

few Newtons. The softness of these tissues can of course make them prone to damage or discomfort when encumbered by substantial loads. Thus, an important functional and ergonomic challenge is to design methods for stably and ergonomically anchoring wearable systems on the body, especially when substantial loads are involved.

Skin also possesses sensory capabilities that arise from dense innervation by thousands of tactile receptors – sensory nerve endings that can number thousands per square centimeter of skin. Together, they capture mechanical and thermal information from the ambient environment, transmitting this sensory information in volleys of spikes that are processed in the brain. While a full account of tactile sensation would exceed the scope of this review, it is worth noting that there are several distinct sub-types of tactile sensory receptors that exist in numbers that vary with body region [108, 130]. Each type responds to distinct aspects of stimuli in the tactile range. The neural signals they produce underlie the processing of touch contact with the body, the detection of painful or noxious stimuli, and the perception of object properties such as texture, shape, or hardness [108]. They also enable the remarkable feats of dexterity of the human hand. Tactile sensitivity and spatial acuity vary with body location in a manner that depends on the manner of stimulation, such as via pressure [131], sliding contact [132], or vibration [133]. Fingertips are among the most sensitive regions of the body. Thus, it can be advantageous to integrate higher actuator densities at such locations (Figure 2.2N) [130, 25, 26]. Skin plays a further role in homeostasis, by actively regulating body heat through capillary effects and perspiration. Thus, whether through intention or accident, soft wearable technologies often greatly affect mechanical, thermal, and sensory inputs to the body in manners that should weigh into their design.

2.3.2 Design for Wearability

While biomechanical and sensorimotor considerations can inform the design of soft, wearable robotic systems, the roles they play depend upon the application involved, including the form factor of the wearable system. Two key design considerations are wearability and ergonomics.

Placement and form language can both guide the selection of form factors for wearability. Many form factors have been investigated in prior research. Among small form factors are devices worn on the upper limbs, such as thimbles (Figure 2.2N, 2.2O) [25, 26], rings (Figure 2.2L, 2.2M) [23, 24], and bracelets (Figure 2.2H, 2.2I) [19, 20]. Larger form factors for the upper body include sleeves (Figure 2.2F, 2.2G) [18, 3], gloves (Figure 2.2J, 2.2K) [21, 22], and jackets (Figure 2.2E) [17]. Those for the lower body include footwear (Figure 2.2R, 2.2S) [29, 30] and trousers [134]. Many different kinds of devices have been designed to affix to different body locations via straps (Figure 2.2A, 2.2B, 2.2T, 2.2U, 2.2V) [13, 14, 31, 32, 7]. Such approaches have commonly been used in supernumerary devices that provide supplemental artificial limbs. The locations for mounting are closely related to the functional purposes of those devices. For supernumerary arms, common mounting locations include the shoulders, waist, or back (Figure 2.3C) [36], while the wrist is a typical mounting location for supernumerary fingers (Figure 2.3D) [37]. Centuries of development in apparel engineering have informed the design of clothing that is fitted to the whole body's shape and topology; in soft robotics research, several examples of bodysuits have been proposed (Figure 2.2P, 2.2Q) [27, 28]. Other soft wearables have taken the form of accessories, including hats, scarves, and jewelry, neckwear (Figure 2.2C [15]), and face masks (Figure 2.2D [16]).

Other body interfaces involve devices that adhere to the skin. This can allow lightweight systems to be worn without any need for anchoring. Kao et al. designed texture-tunable skin overlays that stiffen when heated using hydrophilic gels (Figure 2.3A) [34]. Hamdan et al.

integrated SMAs into skin-worn actuated stickers that they refer to as “Springlets” that may be worn on challenging body locations such as the ear (Figure 2.3B) [35].

An overarching concern in the design of form factors is the size or surface area of the device. Suits cover larger body areas than sleeves, bracelets, and thimbles, while skin adhesion allows for minimal coverage. In terms of device constraints, the size of the actuators, the means of attachment or grounding to the body, and the body location are three key considerations that must be weighed during design and garment construction.

The form factor design also depends on functional and aesthetic considerations, including the required range of motion and force, biomechanical factors, weight, comfort, perception, safety, and appearance. Wearable robotic systems that exert forces on the body do so through internal forces that necessitate that the forces applied at one location be balanced by those produced elsewhere. The means of attachment and anchoring to the body must be designed to apply these forces according to application requirements. Stability is an important consideration, because if attachments shift in configuration, device functionality, comfort, or safety could be affected. Many wearable devices are designed with adjustable attachments, such as velcro or cinched straps, which allow the device to be adjusted to the user. Friction often plays an important role, since such attachments may provide normal forces that indirectly produce the shear forces needed for anchoring via friction with the skin (Figure 2.2S, 2.2T, 2.2U) [31, 32, 33]. This approach is often referred to as passive grounding. In other systems, the actuated degrees of freedom in the device may provide tunable attachment forces. For example, the PneuSleeve device uses pneumatic compression actuators and closed-loop force control to adjust and equalize grounding forces so that haptic shear forces may be applied to the skin of users, and so that different limb girths may be accommodated (Figure 2.2G) [3].

Many soft, wearable robotic systems are designed to span joints of the body. In these cases, the kinematic range of motion of the joint and limb must be accounted for in the design. For example, some wearable systems are designed to arrest or assist joint motion, as in the

haptic VR glove device of Hinchet et al. [58], which uses an electrostatic clutch to arrest finger movements. When no forces are intended to be applied at the joint in question, such as when the device is off or the joint is spanned by non-actuated regions of the device, it is often important that the normal motion and flexibility of the joint is affected as little as possible, to allow for normal activities. This can be achieved using stretchable materials or other structures that can freely accommodate joint motion at such locations. Some systems, such as tendon-driven wearables, employ curvilinear inextensible elements or channels. Such elements may be aligned with the body's lines of non-extension, such as the lines lateral to the knee joints, along which the skin undergoes little stretching during body motion [135].

In summary, a variety of human factors and application-dependent considerations must inform the design of soft, wearable robotics. Such considerations also inform the engineering of active elements of such wearable systems, as well as their control, as we review in Section 2.3.3.

2.3.3 Control Considerations for Wearability

As noted in the introduction, robotic systems are commonly considered to integrate the three key capabilities of sensing, actuation, and computation or control. Soft robotic systems typically involve continuum mechanical media, and compliant structures, in lieu of traditional mechanisms. Control methods for such continuum systems are less mature than those that have been developed for finite degree-of-freedom systems. In addition, the central role of the wearer in these systems often introduces challenges in human-in-the-loop control. Control paradigms that have been developed for continuum systems are diverse, and include classical methods for the control of low-dimensional systems, simplified techniques that leverage the intrinsic dynamics of the structures and materials involved, and emerging methods for high-dimensional control [136].

Wearable robotic systems are often designed to sense, and responsively act, in concert with their wearer, which is the setting of human-in-the-loop control. The highly adapted nature of many body movements often leads to domain-specific approaches to human-in-the-loop control, as for example in devices that assist walking mobility [137, 32], or aid individuals in grasping with a stroke-impaired hand [4]. This setting involves distinctive control demands, because the natural biomechanics of the human body must carefully factor into any design so that the movements of the wearer are assisted, rather than encumbered, and that the system operates safely. To this end, such systems are often designed to account for the biomechanics, kinematics, and sensorimotor system of their wearer in an application- and wearer-dependent fashion [80, 138]. Due to the complexity of these systems, and to differences between individuals, such factors are often integrated in a data-driven fashion, through the collection of motion or postural data from users [139, 140]. In assistive devices, a one-size-fits-all approach rarely lends itself to optimal performance due to individual differences in ability, anatomy, biomechanics, and physiology. For example, research in walking assistance reveals that when individual factors, including walking dynamics, are not accounted for, efficiency may be reduced or control may become unstable [141].

2.3.4 Mechanical Properties of Materials for Wearability

Wearing robotic devices for extended periods of time leads to unique design challenges such as user comfort, reliability, and safety [92, 93]. Indeed, soft robotic technologies are well suited for wearable applications because their softness can be matched to the properties of the materials and structures of the body [142]. The term *soft* can refer to a combination of the extensive mechanical compliance of the structure [136] and the intensive hardness, or physical softness, of the materials themselves [143, 144, 145]. In fact, these two aspects are uncorrelated, which provides designers with additional freedom to select materials that also

achieve other goals. For example, wear resistance can often be improved by selecting materials to better match the hardness of adjacent materials [146]. Attributes, such as durability, are likewise multi-faceted, depending on both material properties and design choices determining their integration and operation, and are thus difficult to analyze outside of a particular device and application. Soft, wearable devices offer advantages in comfort and safety and can accommodate variations in movement that can be challenging to integrate in rigid systems, such as robotic exoskeletons. For example, Sawiki et al. determined that a soft exosuit can be designed to provide more effective robotic walking assistance than a rigid exoskeleton [147]. This may be due to the complex, non-idealized kinematics of motion at body joints.

Soft materials may be used to provide high mechanical compliance (inverse stiffness), allowing them to conform with the body. The axial compliance C of a structure is equal to length L divided by the product of cross-section area A and the intensive elastic modulus E , i.e., $C = L/(AE)$. Similarly, the bending compliance κ of a structure is equal to the bending moment M divided by the product of the modulus of elasticity E and the second moment of area, I , i.e. $\kappa = M/(IE)$. This illustrates how, for example, in order to maximize compliance, a material of given elastic modulus E may be designed to span a large distance L on the body and to have a small cross-section area A . In particular, the elastic modulus need not necessarily be small to achieve compliance. Compliance may be achieved by high-modulus materials with small cross-sections, such as thin films, via the patterning of high-modulus materials, or via other composite material designs. For example, garments are often constructed from filaments, such as textile fibers, with a large modulus E . The compliance of the textile may be greatly altered by the manner in which the fibers are arranged – how they are piled into yarns, threads, ropes, woven, or knitted. A further factor greatly affecting the mechanics of textiles is the interaction between fibers [148]. Thus, in contrast to bulk materials, the effective elasticity of a textile or other fiber composite is often viewed as an extensive property [149]. Table 2.1 illustrates representative elastic moduli of fiber materials that are often involved in soft, wear-

Table 2.1: Elastic moduli of selected materials in wearable robotics in GPa.

Material	Reference	Max	Min	Average*
Vertebrate Cartilage	[151]	—	—	0.1
Vertebrate Ligament	[151]	—	—	0.001
Wool fibers	[152]	4.5	3.1	3.8
Cellulose (Cotton, Rayon, Viscose) fibers	[152, 153]	57	5	31
Polyester (PET, PE) fibers	[152, 153]	95	13.5	54.3
Acrylic (Polyacrylonitrile PAN) fibers	[154]	2.93	1.86	—
Environ (PVC) fibers	[155]	1.96	0.67	—
Polyamide (Nylon-6) mono-filaments	[155]	0.68	0.23	—
Polyamide (Nylon-6,6, PA66) nanofibers†	[156]	0.95	0.15	0.45
Aramid (Kevlar, Nomex) fibers	[153]	123	71	97
Bulk PDMS	[41, 157]	0.0037	0.00057	—

*Each of these materials' data was taken from many samples and not necessarily normally distributed.

†Data was obtained at room temperature.

able robotics. Bulk poly(dimethylsiloxane) (PDMS) and vertebrate tissues are also included for comparison. (It should be noted that few references report the temperature at which such data are taken. Nonetheless, in many instances experiments are likely to have been conducted at room temperature, because sample deformation becomes highly nonlinear above the glass transition temperature, if applicable. The distinction between bulk and fiber materials is particularly important because the elastic modulus of fibers is an extensive rather than an intensive property. The elastic modulus is the measure of resistance to elastic deformation, whereas hardness measures the resistance to localized plastic deformation that are more important to wearability. Indeed, hardness is often as important as elastic or other bulk moduli in the selection of materials for wearable robots. Hardness and bulk elasticity are not trivially related, and it remains theoretically challenging to correlate such properties [150].

Due to the dependence of textile mechanics on fiber arrangement, many different materials can be used to create conforming textiles, including metal fibers [149]. However, such hard materials would produce substantial abrasion of soft tissues or materials. To avoid this, materials are often selected with lower hardnesses. For example, for comfort, and to avoid abrading the skin, materials should be selected with hardness less than about 20 on the Shore A scale, or 60 on the Shore 00 scale (Figure 2.4). Where thin or fibrous materials are concerned, hardness

cannot readily be quantified using standard scales (e.g. Vickers, Rockwell, or Shore scales). For geometrically small samples, nanoindentation methods are often used for characterization, yielding hardness measures with dimensions of stress (units MPa). Examples are given in Figure 2.4. To date, few references report both conventional and nanoindentation-based hardness measures [158].

2.4 Soft, Wearable Robotics: Materials and Fabrication Methods

The use of soft materials in the design of wearable and soft robotics is motivated by human factors considerations like those described above, and by new functionalities that emerging soft materials can provide that transcend those of conventional materials. The diverse materials used in soft, wearable robotics require a variety of manufacturing methods that are often different from those employed for conventional mechanical or electronic systems. Therefore, besides device design requirements, considerations such as access to related equipment and tools are also important in the selection of materials and fabrication methods.

2.4.1 Soft material types in wearable robotics

Some advantages of many soft materials include their ease of handling, processing, and fabrication, and amenability to very large or very small scale or dimension processing [136, 159, 130, 160, 161]. In this section, we provide an overview of the categories of soft materials that are most frequently used in soft, wearable robotics. Further discussion of functional properties of these materials for sensing and actuation is provided in later sections.

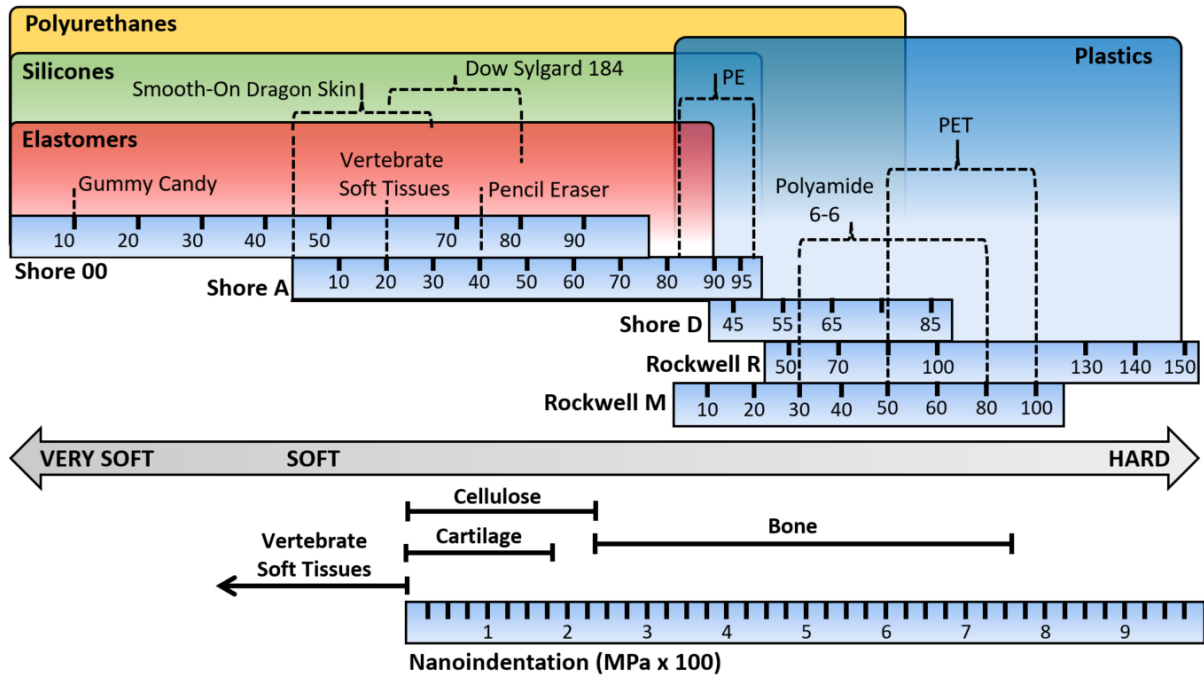


Figure 2.4: Comparison of hardness, or softness, of materials suitable for use in soft wearable robots that interface with human tissues. A class of wearable materials may include those used in the construction of textiles, such as: Silicone, polyamide (nylon), cotton, silk, wool, rayon. Some materials have known hardness values and are shown in the figure. Other materials, particularly those natural materials used in commercial textiles have hardness values that are not apparent in academic literature. Typically designers will consult a manufacturer and choose from subjective experience. Other online sources such as [38, 39] compile material data for such purposes, however, because polymer material properties vary significantly with temperature, humidity, and other testing conditions, the authors recommend performing individual testing for applications with sensitive requirements. Fiber hardness data, especially when measured via nanoindentation, is often reported in MPa, which is not directly comparable to traditional hardness scales (see text). For example, the hardness of PDMS (Dow Sylgard 184) ranges from 20 to 50 Shore A, depending on the catalyst used [40, 41]; the material hardness has been reported as 2.06 MPa [42]. The hardness of cellulose ranges from 2.7 MPa to 240 MPa depending on temperature and humidity [43, 44]. That of bone (234 to 760 MPa [45]), cartilage (2.6 MPa to 179 MPa [46, 47]), or other soft tissues [47] vary depending on test conditions and sample quality.

Polymers are organic materials that are widely used in soft and wearable robotics, for most of the reasons mentioned above. Many polymers are synthetic materials whose properties can be chemically tuned. Silicone-based polymers are often used, and they exist in great variety. They are often soft, stretchable, non-toxic, stable, and inexpensive to manufacture and purchase. This has made them a popular choice in soft robotics research. In contrast to other polymers that are based on a carbon-carbon backbone, silicone polymers are based on repeating silicon-oxygen (siloxane) groups, with two methyl groups bonded to each silicon (schematically, $-\text{R}_2\text{Si}-\text{O}-\text{SiR}_2-$, where R represents an organic group). Silicone polymers are readily available in liquid forms that can be cured or cross-linked in different ways. Curable silicones are typically polysiloxanes with additional fillers, cross-linkers, and additives that allow them to match desired characteristics. The curing or cross-linking process of these elastomers is achieved through covalent bond formation between polymer chains. This process is catalyzed through the addition of a cross-linker. Several different cross-linking methods are used, including condensation curing, platinum-catalyzed hydrosilylation, or peroxide-induced curing [162]. Thus, there are many options available for synthesizing silicone polymers with different properties.

A silicone-based elastomer that has been often used to create soft or wearable devices is PDMS. It is moderately compliant (Table 2.1) [163], inexpensive, and amenable to facile processing using established tools and methods. It can be used to create structures or substrates for functional devices that are stretchable, transparent, permeable to air, nontoxic, and biocompatible. As with other silicone polymers, the material properties of PDMS are tunable. For example, a cured pristine PDMS surface is hydrophobic, but can be modified to be hydrophilic through oxygen plasma activation or ultraviolet radiation. As with many silicone polymers, commercially available PDMS reagents, such as Sylgard 184 (Dow Corning), consist of two-part liquid compounds. The two parts are combined in ratios that may be adjusted in order to vary the elasticity that is achieved after curing. Typical values for Young's modulus of PDMS

are reported in Table 2.1.

Other commercially available silicone elastomers include platinum-catalyzed silicones, such as the commercial products Ecoflex and Dragon Skin (Smooth-On, Inc), which are low-viscosity, two-component reagents that have been widely used in soft robotics. These silicones are available with a large range of elasticity, pot life, and cure time. The tensile strain of Ecoflex ranges from 800% to above 1000%. [164] The Young's modulus varies in the range of 0.05 MPa to 1 MPa [165]. Commercial Ecoflex is a platinum-catalyzed silicone elastomer with low viscosity and is also available as a compound (with two components, which are typically mixed in a 1A:1B ratio by their volume) that can be cured either at near room temperatures, or at elevated temperatures to facilitate rapid cross-linking [164, 166]. Among other polymers polyurethane (PU), nitrile butadiene rubber, acrylic elastomer, poly(isobutylene-co-isoprene) (IIR), polyolefin (POE), poly(styrene-block-butadiene-block-styrene) (SBS) are also being used as soft materials for applications in soft and wearable robots [167].

Hydrogel materials are networks of polymer chains that have attracted great attention among researchers. They have been used to realize functional devices for soft robotics and wearable applications. Hydrogel polymers occur in natural form in the bodies of animals. As a result, many hydrogel materials are biocompatible [168]. Hydrogels typically contain between 10% and 95% water. The quantity of water can be altered through heat activation in order to tune their elasticity. This has, for example, been used to create stiffness-tunable wearable devices, such as protective pads worn on the skin (Figure 2.3A) [34]. The mechanical properties of hydrogels vary greatly. While they can be made elastic, in terms of strength, many hydrogels are brittle. Thus, while there are a number of hydrogels that can achieve a maximum strain of 200% to 2000%, their tensile fracture strength is typically in the range from 100 kPa to 10000 kPa. For example, (PBMA-b-PMAAc-b-PBMA)/PAAm (PBMA: Poly(butyl methacrylate), PMAAc: poly(methacrylic acid), PAAm: Polyacrylamide) contains 42% water and has a fracture strain of 10000 kPa, with a maximum tensile strain of 600% [169].

Many other polymer materials have been used in soft robotics. They include thermoplastic polyurethane (TPU) [31], polyurethane (PU) [64], nitrile butadiene rubber [170], and acrylic elastomers. Several recent review articles survey these materials in greater detail than can be included here [171, 172, 173, 159].

Liquid alloys are metals that are in the liquid phase at room temperatures. They have attracted great attention in recent years for applications in soft electronics and robotics. Several metal alloys remain liquid at room temperature. Mercury is the most familiar such alloy, but is toxic. Today, Gallium (Ga) alloys are more popular. Gallium has a melting temperature of 30 °C. This temperature can be decreased by addition of Indium (In) or Tin (Sn). For example, eutectic gallium-indium (EGaIn) and eutectic gallium-indium-tin (Galinstan) have melting temperatures of 15.7 °C and -19 °C, respectively. Both of these alloys possess high electrical and thermal conductivity [174]. Such liquid metals must often be encapsulated within soft substrates for applications. This is often achieved via microfluidic channels. Such liquid alloys do not store mechanical energy under tensile strain. Encapsulated liquid alloys conform to Poisson's law, which states that the total volume of incompressible liquid remains constant. Thus, the elongation of encapsulated liquid alloys yields a decrease in cross-section area [161].

Textiles, fabrics, and their products are a familiar part of many garments and products that we interact with in close proximity to our body. Wearable garments made of textiles can readily be made flexible, deformable, deployable, durable, soft, and stretchable. These attributes make them ideal for wearable devices. Most textiles are made from fibers or yarns that have woven, knit, or other composite structures. Xiong et al. have reviewed the use of functional fibers and fabrics in soft wearable robotics [175].

The stretchability of textile and fabrics typically falls in one of three categories: non-stretchable, two-way stretchable, or four-way stretchable. Non-stretchable fabrics are often

conformable but are inextensible in each planar direction. In contrast, two-way or four-way stretchable fabrics are stretchable in one or both in-plane orthogonal directions. The anisotropic arrangement and mechanical properties of many fabrics are useful in many applications. Such anisotropies arise through variations in stitching [2] or fiber reinforcement [176].

The physical properties of fabrics can be modified, often dramatically so, through post-processing, such as coating, or through their composition with similar or dissimilar materials. Such modifications often also affect other properties of the fabrics, such as breathability, that may affect their suitability for some wearable applications.

Smart materials and composites possess properties that provide additional functionality, such as electronic actuation or sensing [177, 178]. They include functional materials or composites overlapping with the categories described in the foregoing. Piezoelectric materials provide functionalities through conversion between electrical and mechanical energy [12, 179]. Many polymers or polymer structures have been designed to provide similar functionalities [25, 180]. Such materials have been used to realize sensors and actuators, as further discussed below. Another smart material category includes phase change materials. Shape memory alloys are one important category. Application or removal of heat, such as via electric current, causes such materials to transition between a martensite phase and the austenite phase, yielding bulk elongation or contraction that can perform mechanical work [181, 35].

In many cases, smart materials or composites can be chemically or structurally engineered to achieve desired performance characteristics. For example, PDMS is electrically insulating ($\rho = 4 \times 10^{13} \Omega \cdot m$) with a very low dielectric constant ($\epsilon = 2.3 - 2.8$). Both properties can be tuned by combining the PDMS bulk matrix material with suspended additives (e.g., conductive carbon powders or silver nanowires, AgNWs) [57].

This example illustrates how components of composite smart materials contribute different attributes, for example, by acting as a bulk substrate or a functional additive. The mechanical

softness of such thin films or membranes is largely dominated by their carrier substrate [182].

Many combinations are possible, and many methods have been described for tuning such materials. Thus, a large variety of smart materials have been created and used in wearable devices. To describe one integrated example, Gerratt et al. realized a wearable tactile sensing glove for prosthetics [48]. It integrated resistive and capacitive sensors for capturing finger motion and contact pressure, respectively (Figure 2.5A). The materials include elastomers, silicone foam, liquid metals, and thin-metal gold films (Figure 2.5A ii, iii). The metal films embedded in the PDMS substrate, with liquid metal wire interconnects, acted as resistive strain sensors (Figure 2.5A ii). Capacitive pressure sensors were formed from layers of silicone foam dielectric material encapsulated between conductive film layers (Figure 2.5A iii), which were then integrated in the textile glove (Figure 2.5A iv). The similar compliance of all of the materials ensured that, when combined, the wearable device retained significant compliance. We discuss the functional applications of smart materials in Section 2.5.

In summary, there are many compliant materials or composites that may be used in wearable robotics. Table-2.2 lists an array of representative examples that have been used in such applications.

2.4.2 Fabrication

A key distinction can be drawn between small-scale fabrication for research or prototyping, which may employ manual or improvised processes that do not translate to mass production, and fabrication methods that utilize, are compatible with, or may be readily translated to, large-scale manufacturing. Key features that must be considered include the materials to be used and design requirements, including dimensions and resolution. For example, if a device requires patterning with resolution on the microscale over a large area, a microprinting method might be preferred to a 3D lithography method. On the other hand, the materials involved often

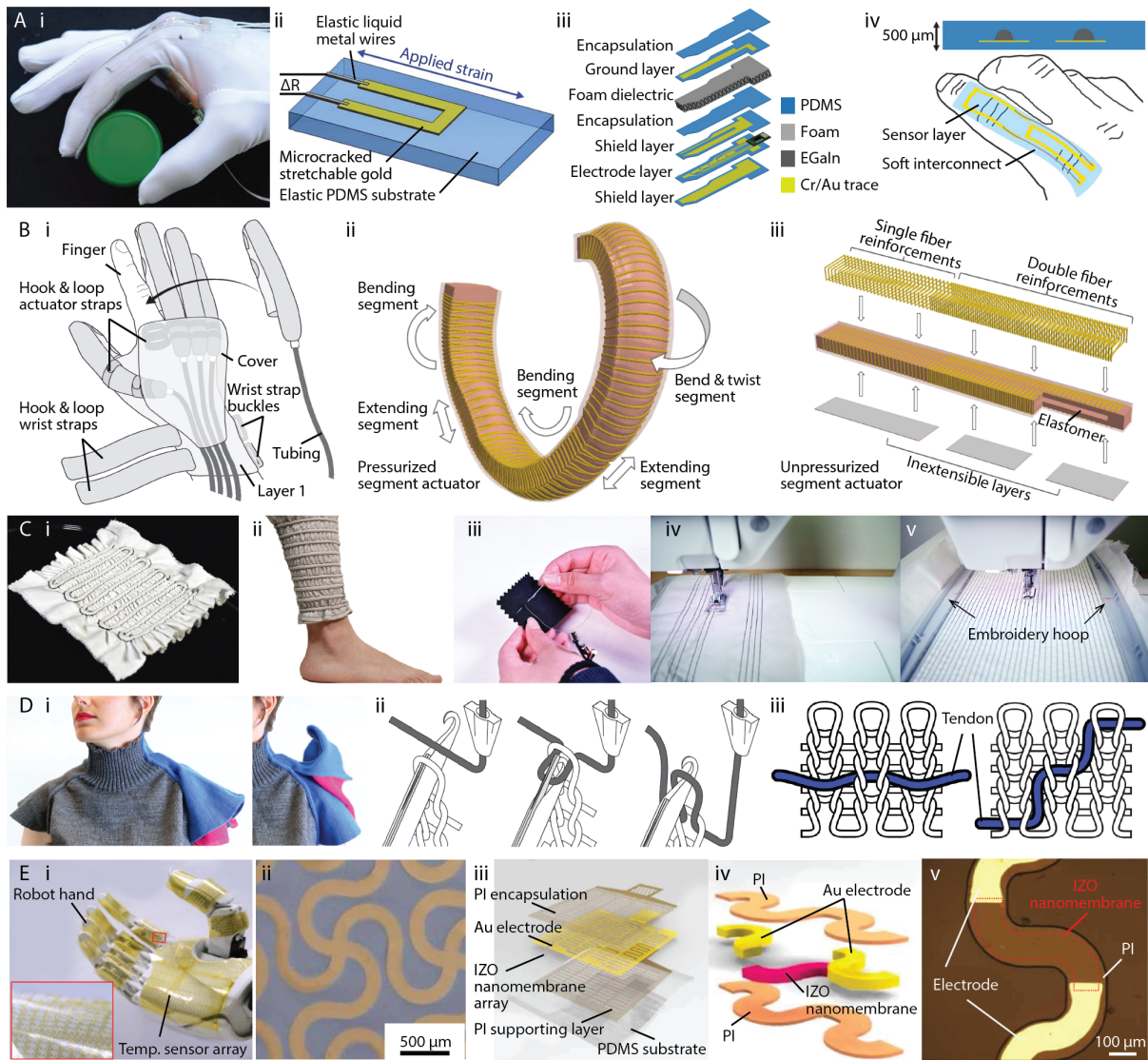


Figure 2.5: Few examples of functional soft and wearable robotic devices realized using various materials and relevant fabrication methods. (a) Wearable prosthetic tactile gloves with integrated resistive and capacitive sensors for monitoring finger articulation and pressure [48]. (i) Textile glove with stretchable strain and tactile sensors when grasping an object. (ii) Structure design of the resistive strain and bending sensors. (iii) Multi-layer design for the capacitive sensors. (iv) Resistive flexion sensors are placed on the back of a finger for bending motion sensing. (b) Fiber-reinforced soft robotic glove with pressurized actuator manufactured using 3D printing and soft lithography techniques for rehabilitation and training [49]. (i) Schematic of the soft robotic glove design. (ii) Pressurized soft actuator showing a combination of motions including bending, extending and twisting. (iii) Exploded view showing inextensible layers, elastomer, and fiber reinforcements. (Caption continued on the following page.)

Figure 2.5: (Continued:) (c) Fluid-driven soft wearable actuators realized using fabrics and stitching [2]. (i) Prototype of Fluidic Fabric Muscle Sheets (FFMS). (ii) Compression garment for the lower limb made of FFMS. (iii)–(v) Stitching for the FFMS actuators may be done with (iii) hand sewing, (iv) machine sewing, or (v) machine embroidery. (d) Machine knitted wearables with tendon-based actuation [50]. (i) Sweater that has an actuatable sleeve. (ii) Knit operation that forms the main fabric. (iii) Two examples of tendon placement on the main fabric. (e) A prosthetic skin with temperature sensor array on a robot hand was made using micro-/nano-fabrication techniques including photolithography, wet etching, reactive ion etching, and deposition [51]. (i): Robotic hand with the temperature sensor array. Insert is a magnified image. (ii) and (iii) SEM image (ii) and exploded view (iii) of the temperature sensor array. (iv) and (v) Exploded view (iv) and optical microscopic image (v) of the IZO temperature sensor. Images reproduced with permission. Images E i-v licensed under Creative Commons 4.0.

dictate the fabrication methods that can be used. For example, a microprinting method is not compatible with all materials. Here, we review some of the most used fabrication methods. A comprehensive account of the continuously growing array of fabrication methods that could be used for such devices is beyond the scope of this article.

Soft lithography and molding Soft lithography processes are extremely useful when a quasi-planar compliant substrate must be patterned over a large area with a resolution no finer than the microscale. Such processes have been widely used in manufacturing soft robotics and wearable devices [64, 179, 183]. Soft lithography processes involve creating a “master” form, on which the negative patterns are realized. An elastomer is cast and cured on this master to replicate the patterns. After curing, the elastomer replica is removed from the master, exhibiting the designed patterns. Such a master can be produced using conventional microfabrication methods, such as SU-8 photolithography, micromachining, or 3D printing.

Molding is a similar approach where liquid elastomers are patterned or shaped using a rigid frame or mold. A large variety of 3D shapes can be produced using molding techniques. Molding may or may not require thermal treatment of the liquid resins that catalyze to produce the polymer elastomer. There are different molding techniques available depending on the requirements of the device and processed materials. Examples include compression mold-

ing, replica molding, micro-transfer molding, solvent-assisted molding, and injection molding [24, 112, 21, 184, 185, 61, 186]. Numerous publications, online training videos, instructions, curricular materials, and classes provide instruction on such molding techniques, making them easy for the uninitiated to learn to use.

3D printing 3D printing technologies have greatly developed in recent years, and have been extensively used in soft and wearable devices including robotics [89, 21, 187, 188, 189, 190, 191, 37, 192]. Such technologies are often used to print rigid 3D molds for soft lithography processes. The feasible resolution is often limited by the 3D printing process. In addition to molding techniques, emerging methods of additive manufacturing allow direct printing of soft materials [90]. Currently, several commercial 3D printers can print soft materials such as hydrogels or rubbers [193]. Additionally, research has produced 3D printers that can print silicone polymers and liquid alloys in order to manufacture largely functional devices in a unitary process. Such 3D printers use computer-aided 3D design. Thus, the design of an object can comprise any shape within printing process limitations [194]. Limitations include minimum feature sizes, speed, scaling, and surface roughnesses.

A widely used method of 3D printing is based on additive deposition. It involves the expulsion of liquid or glassy-phase materials through a nozzle to construct 3D structures layer by layer. Another popular category of methods, photopolymer-based printing, cures solid structures from liquid polymer baths via optical catalysis/curing. The list of 3D printing technologies is growing, and includes: direct ink writing (DIW), stereolithography (SLA), selective laser sintering (SLS), photo-curable ink-jet printing, fused deposition modeling (FDM), and shape deposition modeling (SDM). For example, Zhao et al. realized a fiber-reinforced soft prosthetic hand, which was composed of pneumatically actuated fingers and a 3D printed rigid palm with integrated optical waveguides [64]. The waveguides were composed of elastomers and were fabricated using four-step soft lithography. A 3D-printed mold replicated the wave-

uides with high precision. In another example, Nguyen et al. developed fluid-driven soft robotic limbs that were fabricated from silicone elastomer [36]. It consists of three-chambered actuators which were made of bundles of ring-reinforced actuators (RRA). Different materials and fabrication methods were used to realize the RRA parts, primarily including a 3D printed mold and soft lithography techniques.

3D printing and molding techniques make it possible to realize complex 3D structures with a variety of soft materials and also allow the integration of different materials to generate unique functionality and material properties. For example, Polygerinos et al. realized a soft robotic glove for rehabilitation and training (Figure 2.5B i). They used fiber-reinforced rubber to create a pressurized bending actuator (Figure 2.5B ii) [49], which was composed of a molded elastomer main body, and strain limiting layers (Figure 2.5B iii).

Apparel engineering Apparel engineering methods involve the engineering of wearable structures from fabrics or other materials. Textile construction transforms fibers into textiles via knitting or weaving. Textiles are cut and recombined to form garments that are specified as patterns. Non-textile sheets, such as polymer layers, are sometimes also employed. Textiles are combined, joined, or layered via sewing, heat sealing, ultrasonic fusing, or chemical adhesives. A recent review of textile technologies provides further discussion [195]. Sewing methods include hand sewing, machine sewing, and machine embroidery; each requires different levels of machine automation or manual work. Sewing introduces holes, since fibers are threaded through the textile via a needle. In some applications, such as fluidic actuator design, even small holes present problems. In such cases, heat sealing or ultrasonic welding may be used, or holes may be sealed via post processing. Heat sealing involves the application of heat to fuse layers of materials together in order to form closed, airtight seams. This requires special materials, such as TPUs (described above). Such methods are challenging to apply in thick or multi-layered structures. Ultrasonic fusion or welding is a related method that is used to form

sealed fabric connections or closures in industry. This process is compatible with a wider range of materials that can be used with heat sealing. Examples of using apparel engineering for soft wearable robotics and haptics include the Fluidic Fabric Muscle Sheets developed by Zhu et al. (Figure 2.5C) [2], and machine-knitted tendon composite by Albaugh et al. (Figure 2.5D) [50].

Microfabrication and Nanofabrication These are the terms that refer to an array of methods that are widely used in semiconductor manufacturing, micro-electromechanical systems (MEMS), and related areas of industry and research. These methods are highly mature, and make it possible to produce devices with the fine resolution and accuracy needed in miniature devices. They can facilitate high-resolution patterning and accurate geometric registration. Microfabrication methods involve a number of variable processing steps including patterning, thin film deposition, chemical processing, plasma processing, micro-assembly, among others. The use of such methods has conventionally been limited to high modulus materials. Recent advances, including results from our lab [196], show how these methods can be used in the fabrication of soft devices. This can be achieved through careful selection of materials for compatibility with the required processing steps, including high-temperature or chemical processing, and through the use of rigid carrier substrates that constrain and control the geometry and registration of the soft materials during fabrication.

Two approaches for realizing soft electronic devices via microfabrication techniques include direct fabrication of electronic layers on soft polymers [197] or the fabrication of such layers on rigid carriers for later transfer to soft substrates [198, 51]. For example, Sim et al. fabricated electronic sensing interfaces for prosthetics using the latter approach. They produced a thin ($\sim 2\mu m$) polyimide (PI) layer on top of a rigid glass carrier substrate that was later etched away to form a freestanding structure [51]. The device was then transferred and bonded to a thin layer of PDMS to form a prosthetic skin (Figure 2.5E i, ii). Electrodes in the device were

formed from gold (Au) via electron beam evaporation, photolithography, and wet etching. Spin coating, annealing, photolithography, and wet etching were used to define the pattern geometry of the IZO nanomembrane array (Figure 2.5E iii, v) [51]. This example illustrates the many steps, selected from a standardized repertoire, that are combined to produce devices via micro-fabrication or nano-fabrication. When applied to soft materials, these methods may meet the needs of future soft, wearable robotic and haptic systems.

In addition to the techniques described above, several other methods have been used to realize soft, wearable robotics. Examples include machining [13, 199, 170, 9], laser processing [36, 58, 59, 62], and transfer printing [200, 179, 183]. Often, several fabrication methods are combined. In summary, fabrication techniques for soft wearable robotics diverge from those used in traditional manufacturing processes for rigid materials, but recent advances illustrate the advantages of adapting such traditional methods for use with soft materials. The materials involved constrain the methods that can be used to create functioning systems and devices.

2.5 Soft, Wearable Robotics: Actuation and Sensing Methods

A wide range of sensors and actuators have been used in soft wearable robotics. The selection of an appropriate actuation method depends on several factors, including functionality, ergonomics, among other considerations. Thus, it is challenging to provide general guidelines for actuation or sensing selection outside of the wearable embodiment and the application needs. For instance, to design a wearable rehabilitation device that requires high force and precise control, either cable-driven and fluidic actuation methods may be appropriate. In cable-driven applications, pressure distribution channels are often needed. The use of fluidic actuators may demand position, pressure, or additional sensors if precise control is required. Actuator prop-

erties that are undesirable in one application may prove beneficial in another. For example, in the use of shape memory alloy actuators, the delivery of ancillary heat to the skin may be avoided in some applications through insulation [35], but may be desired as a means of haptic feedback in others [95]. We discuss commonly used actuation and sensing methods further in Sections 2.5.1 and 2.5.2.

2.5.1 Actuation

Among the most intensively investigated technologies for soft robotics are actuators, which convert supplied energy into mechanical work or other responses (for example, electrical or thermal responses). In robotics and haptics, actuators are often tasked with converting orders of magnitude more energy to produce substantial displacements, forces, thermal or other changes. (Sensors, which are discussed below, are also energy transducers, but the converted energies are often very small.) Today, few soft robotic actuators can match the performance of conventional devices. This disparity has motivated ample research activity in this area. Actuators that produce forces or displacements also produce mechanical stresses and heat that must be carefully considered in relation to ergonomic requirements, safety, and operating performance. Soft materials are intrinsically insulating, which can result in more severe thermal management challenges than are encountered in many conventional mechatronic systems, further amplifying the challenge of designing actuators for many soft robotic systems.

A large variety of actuator types have been used in wearable systems. They include rigid devices such as electromagnetic motors and piezoelectric actuators. Integrating rigid actuators within soft structures involves several drawbacks that can impair system functionality, including reduced compliance and large stress gradients. Here, we focus attention on soft and flexible actuation methods, which are often well suited for use in soft, wearable robotics.

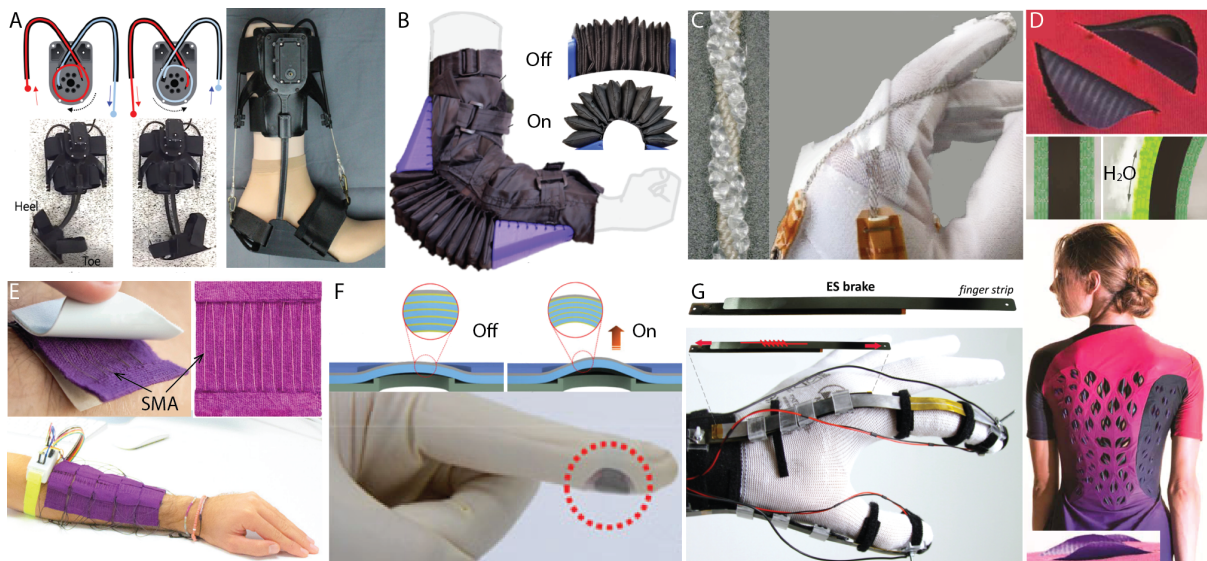


Figure 2.6: Examples of soft and flexible actuation methods for wearable applications. A. Bidirectional cable-driven actuation for an ankle-foot-orthosis [52]. B. Fluidic actuation for bicep lifting assistance [53]. C. Twisted and super-coiled fibre actuators assist with finger bending [54]. D. Biohybrid actuation with microbial cells that adjusts the humidity of clothing microenvironment [55]. E. SMA actuator patches that create shear forces on skin for haptic feedback [56]. F. Electroactive polymer actuation that generates vibrotactile feedback [57]. G. Electrostatic actuation for joint arresting haptic feedback [58]. Images reproduced with permission. Images D (i) and (ii) are adapted with permission from [55]. Copyright 2019 American Chemical Society.

Cable-driven actuation Cable-driven actuation utilizes cables – filaments, wires, or tendons – to supply forces or displacements, often via remotely positioned motors. Cables can often be selected to be thin and flexible and are thus suitable for integration in many soft, wearable devices. The forces and displacements, or mechanical work, that can be produced using such actuation schemes depend on the motor characteristics and routing details, but are often large when compared with other soft actuator technologies. Because of their capabilities, and their use of standard electromagnetic motors, such actuation methods have been used in many wearable robotic systems, including devices for rehabilitation, haptics, or other applications. In these applications, they may supply mechanical work needed for haptic force feedback, force assistance, tactile cues such as compression or skin stretch, or for driving a supernumerary limb. To list just a few of many examples: Elor et al. designed a cable-driven soft exosuit on the upper arm for upper-extremity rehabilitation in VR [192]. Kwon et al. developed an ankle-foot-orthosis with a bi-directional tendon-driven actuator for assisting both dorsiflexion and plantarflexion (Figure 2.6A) [52]. Pezent et al. designed a wrist-wearable device that supplies haptic squeezing cues via a cable-driven mechanism [201]. In addition to their capabilities, cable-driven actuation methods possess important drawbacks. When such cables are used to route large forces through conduits, control and actuation problems often arise due to friction. In wearable applications, thin cables may produce high stress concentrations on the skin, yielding discomfort or even pain. To avoid these drawbacks (while possibly amplifying frictional problems), some researchers have instead used fabric bands for the delivery of haptic cues [202], or have encapsulated cables within polymers [21].

Fluidic actuators Fluidic actuators use encapsulated gaseous or liquid fluid media to supply mechanical forces or displacements. Such actuators have been among the most widely used in soft robotics. One reason for this is that fluid volumes or channels can often be integrated within soft polymer materials that can be efficiently fabricated, yielding intrinsically compliant

actuated structures.

Fluidic actuators can produce forces, displacements, or work densities that span a large range, depending on their design and operating range of fluid volumetric displacement or fluid pressure. Indeed, conventional fluidic actuators include high-force industrial hydraulics and miniature devices for displacing biological fluids. Forces that can be produced depend on the device geometry and configuration, but typically increase monotonically with operating pressures and with the characteristic cross-section area of the fluid channel.

Soft, fluidic actuators have used fluids in liquid or gaseous phases, respectively used in hydraulic or pneumatic actuators [84]. Common fluids include air, water, oils, or other hydraulic liquids. Hydraulic actuation can be advantageous due to its incompressibility, which can provide greater efficiency, smaller fluid volumes, or simplified control, since little energy is stored in fluid compression. For similar reasons, at low to moderate pressures (for example, 0.1 to 10 MPa) – such as are typically used in soft robotics applications – hydraulic actuators can mitigate failure-related hazards, such as bursting, that are often observed in pneumatic devices, because fluid pressures drop extremely rapidly when leaks occur. Pneumatic actuation is advantageous because of the convenient availability of compressed air sources, lower mass, and the absence of liquids that could affect other device components. Fluidic actuator bandwidth depends on the operating pressure and displacement range, the actuator design, and other design details such as channel length between the power source and actuator.

Fluidic actuators can be powered (driven) via fluid flow and pressure delivered in different ways [203]. Mechanical pumps, pistons, and compressors generate fluid energy from electricity or other sources. Other sources use stored potential energy, such as compressed air reservoirs. Industrial pneumatic and hydraulic sources are often bulky, and, in the latter case, may not operate in regimes that are useful for soft robotics. Many compact pneumatic sources are readily available today [204, 205], while fewer hydraulic micropumps exist that are appropriate for most soft robotics applications. Many common fluidic power sources, such as

compressed air supplies, are not directly amenable to electric (digital or analog) control such as is normally required in integrated robotic or haptic systems. Instead, many fluidic systems use electrically controlled valves, regulators, or other devices to modulate fluid flow rates, flow directions, or pressures.

Conventional fluidic sources can increase system size or mass, or require them to be tethered to infrastructure. To avoid this, emerging research in soft robotics has been directed at identifying other methods for powering fluidic actuators. Diverse methods are described in recent literature, including the use of compressed fluid (liquid CO_2) [30], explosive combustion [206], liquid propellant [207], and low boiling point liquids [208, 209, 210], the use of inductive heating to boil liquids, generating vapor, and photothermal techniques [211]. Stretchable pumps have also been demonstrated based on charge-injection electrohydrodynamics [212].

Many fluidically-actuated soft, wearable robotic devices have been developed. Examples include an elbow flexion assistive device based on pleated fabric pneumatic actuators (Figure 2.6B) [53], a haptic glove based on pneumatic pockets [213], or devices that use fluidic actuation for particle or layer jamming to constrain or support limb movements or actions for rehabilitation, assistance, or injury prevention [214, 215].

Shape memory alloys Shape memory alloy (SMA) actuators have been used in many robotic systems, including soft, wearable devices. SMA actuators are engineered alloys, such as NiTi, that undergo thermally-controlled phase changes between two different atomic ordered (crystalline) structures. These changes produce macroscopic actuation in the form of displacement, shape, or force. Because actuation is achieved without any need for motors, mechanical actuators, or fluidic sources, SMA actuation systems can be designed to be compact, quiet, and lightweight.

The phase changes that produce SMA actuation are generated via active heating and, less often, through active cooling. Because these materials are conductors, electrical power, from

Table 2.2: Selected soft-robotic materials, technologies, and applications²

Materials	Actuation/Sensing Methods	Processing	Devices	Applications	Ref.
Silicone	Cable-driven actuation	3D printing, machining	Glove	Grasping assistance	[21]
Silicone	Pneumatic actuation, EMG sensing	Soft lithography	Rings	Grasping assistance	[24]
Silicone, foam, Au	Resistive and capacitive sensing	Soft lithography, micro-processing	E-skin	Prosthetic tactile sensation	[48]
Silicone, FEP, Au, Al	Vibrotactile actuation, piezoelectric sensing	Spin coating, deposition	Flexible patch	Vibrotactile feedback, pressure detection	[65]
Silicone, fabrics, PU rubber	Optical sensor, pneumatic actuator	Soft lithography, 3D printing	Strain sensors	prosthetic hand	[64]
Silicone, fabrics	Pneumatic actuation, EMG and IMU sensing	Soft lithography, 3D printing	Supernumerary limb	Tasks assistance	[36]
Silicone, fabrics	Capacitive sensing	Soft lithography, laser cutting	Glove	Monitoring finger motions	[59]
Silicone, fabrics, fiber	Hydraulic actuation	Soft lithography, 3D printing	Glove	Grasping rehabilitation	[4]
Silicone, fabrics, fiber	Pneumatic actuation, IMU sensing	Soft lithography	Glove	Haptic feedback on wrist	[112]
Silicone, fabrics, liquid alloy	Pneumatic actuation, IMU and resistive sensing	Soft lithography, apparel engineering	Soft orthotic footwear	Ankle-foot rehabilitation	[30]
Silicone, liquid alloy, fabrics	Resistive sensing	Soft lithography,	Sensing suit	Track joint angles and	[186],
Silicone, liquid alloy	Capacitive sensing	apparel engineering	Glove	gait phase	[185]
Silicone, liquid alloy	Capacitive sensing	Soft lithography	Glove	Joint angle measurement	[61]
Fabrics	Cable-driven actuation, IMU sensing	Soft lithography	Glove	Shear and pressure sensing	[60]
Fabrics	Cable-driven actuation, load cells and gyroscope sensing	Apparel engineering	Exosuit	Walk assistive	[27]
Fabrics	Pneumatic actuation	Apparel engineering	Exosuit	Walk assistive	[216], [7]
Fabrics, Teflon tube	Cable-driven actuation, resistive sensing	Apparel engineering	Skirt	Expressive fashion	[127]
Fabrics, tapes	SMA actuation	Apparel engineering	Glove	Grasping assistance	[199]
Fabrics, latex	Pneumatic actuation, Resistive sensing	Layer construction	Skin stickers	Tactile interfaces	[35]
Fabrics, PVDF	Piezoelectric actuation, facial expression sensing	Apparel engineering	Glove	Hand rehabilitation	[217]
Fabrics, PE-DOT/PSS	Fiber bundle actuation	Apparel engineering	Garment	Interactive garment	[12]
Fabrics, TPU	Pneumatic actuation	Wet spinning with chemical treatment	Heating glove, artificial muscle	Wearable heaters and electromechanical actuators	[218]
LDPE thermoplastic	Pneumatic actuation	Apparel engineering	Knee sleeve exosuit	Knee rehabilitation	[31]
TPU-coated fabrics	Pneumatic actuation	Heat-sealing	Wristband	Haptic guidance	[111]
ABS, thermoplastic	Cable-driven actuation	Laser cutting, CNC heat-sealing, 3D printing	Supernumerary limb	Assistive device	[8]
PU	EAP actuation	3D printing	Supernumerary finger	Grasping assistance	[37]
Silicone, AgNWs	Capacitive sensing	Soft lithography	Sleeve, glove	Tactile interfaces	[57]
Silicone, AgNWs	EAP actuation	Soft lithography	E-skin	Muscle motion sensing	[183]
Silicone, CNTs	Capacitive sensing	Soft lithography	Forearm band	Haptic communicator	[180]
Silicone, CNTs	Resistive sensing	Transfer printing	E-skin	Motion sensing	[200]
Silicone, CNTs	Resistive sensing	Dry-spinning	E-skin	Motion sensing	[219]
Silicone, graphite, CNTs	Resistive sensing	Soft lithography, bar coating	E-skin	Motion, acoustic, and biosignal sensing	[220]
Silicone, carbon powder	EAP actuation	Micro-fabrication, hot pressing	Thimbles	Vibrotactile display	[25]
Silicone, graphene, P(VDF-TrFE), Au, Ion gel	Piezoelectric sensing	Micro-/nano-fabrication	E-skin	Bending motion sensing	[179]
Silicone, rGO-on-PVDF-nanofibers	Resistive sensing	Electrospinning, spin coating	E-skin	Pressure sensing, photodetector	[221]
Silicone, rGO nanofibers, PVDF	Piezoresistive sensing	Electrospinning	E-skin	Biosignal sensing	[222]
Steel cables, Velcro	Cable-driven	Laser cutting, 3D printing	Finger caps	Haptics for VR	[9]

Materials: Au = gold, FEP = fluorinated ethylene propylene, Al = aluminum, PU = polyurethane, PVDF = polyvinylidene fluoride, PEDOT/PSS = poly(3,4-ethylenedioxythiophene)/poly(styrenesulfonate), LDPE = low-density polyethylene, TPU = thermoplastic polyurethane, ABS = acrylonitrile butadiene styrene, AgNWs = silver nanowires, CNTs = carbon nanotubes, P(VDF-TrFE) = Poly(vinylidene fluoride-co-trifluoroethylene), rGO-on-PVDF-nanofibers = reduced graphene oxide (rGO) encapsulated poly(vinylidene fluoride-trifluoroethylene) [P(VDF-TrFE)] (PVDF) nanofibers. Actuation/sensing methods: EMG = electromyography, IMU = inertial measurement unit, SMA = shape memory alloy, EAP = electroactive polymer. ¹

Table 2.3: Comparison of different actuation methods for wearable applications*

Actuation	Ref.	Compliance	Safety Hazards	Portability	Force	Stress	Displacement	Strain	Frequency
Pneumatic skin	[26]	Stretchable	Burst	Tethered	1 N	NA	NA	10%	0-100 Hz
Pneumatic sleeve	[3]	Stretchable	Burst	Tethered	4 N	200 kPa	16 mm	-33%	1-50 Hz
Hydraulic muscle	[2]	Stretchable	Burst	Tethered	13 N	500 kPa	122 mm	-50%	0.2-5 Hz
Cable-driven orthosis	[52]	Flexible	Concentrated force	Portable	70 N	NA	100 mm	NA	NA
SMA glove	[181]	Stretchable	Heat and electric current	Portable	10 N	260 kPa	50 mm	-40%	0.5 Hz
SMA stick-ers	[35]	Stretchable	Heat and electric current	Portable	3 N	600 kPa	20 mm	-44%	0.1-0.33 Hz
Coiled fibre glove	[54]	Stretchable	Heat and electric current	NA	2 N	69 MPa	2.3 mm	-23%	NA
DEA thimble	[25]	Flexible	High voltage (3.5 kV)	Tethered	14 mN	NA	450 um	NA	0-100 Hz
DEA tactile interface	[57]	Flexible	High voltage (4 kV)	Tethered	255 mN	NA	650 um	NA	0-500 Hz
Electrostatic brake	[58]	Flexible	High voltage (1 kV)	Tethered	20 N	NA	NA	NA	NA
Biohybrid suit	[55]	Flexible	Biohazards	Portable	NA	8 MPa	NA	8%	NA

*The data are collected from manuscripts, graphs, and supplementary materials of each reference with approximation. NA is used where no corresponding information is found. Positive values for strain indicate elongation, while negative values indicate contraction.

infrastructure or batteries, provides a convenient method for dynamic heat delivery, although other heat sources are also used. These advantages also imply performance drawbacks that affect SMA actuation, and that also affect other thermally-dependent actuation methods (such as nylon filament actuators, for example). While SMA actuators can be rapidly driven to their contracted phase, the speed at which these transitions can be reversed is limited by heat transport out of the SMA structure, typically via convection, radiation (when surrounded by air) or conduction (if encapsulated in another liquid or solid medium). The rate at which cooling can be achieved depends on the temperature of the ambient medium, and the size and geometry of the SMA actuators. Because SMA structures must often be massive enough to produce sufficient force, in many cases, this reversal of contraction requires more than one second. Thus, it is challenging to employ SMA actuation in applications that require high mechanical power to be produced, such as in force assistance or force feedback applications. In addition, due to the thermal mode of actuation, care must be taken in using SMA actuators close to the skin.

A variety of different behaviors can be generated through the design and arrangement of structures integrating SMA and other materials. Jeong et al. embedded helical SMA coils within stretchable polymer tubing to augment wrist motions [181]. This system produced forces of 10 N and relative displacements of 40%. SMAs have been also applied in sewed patterns on fabric patches to produce tactile feedback in social haptics (Figure 2.6E) [56]. Other researchers have coated SMA with shape memory polymer (SMP) to achieve variable stiffnesses upon direct joule heating of the embedded SMA wire [223]. Hamdan et al. designed skin-wearable tactile devices based on SMA coils for tactile feedback (Figure 2.3B) [35].

Electroactive polymers Electroactive polymers actuators (EAPs) change size or shape in response to applied electric fields. EAP actuators are most commonly used in tactile devices that apply localized mechanical stimuli to the skin. These actuators produce low forces (on the order of millinewtons, mN) and low displacements (on the order of μm), but may be actuated at high frequencies (approaching 100 Hz). The term EAP has been applied to many different actuators and materials, including dielectric elastomer EAPs, which are electrostatically actuated, and ionic actuators, which involve ion transport in conductive polymers [224]. Piezoelectric polymer EAPs, which have been used in wearable applications, produce relative displacements when an electric field is applied. This occurs due to molecular dipole alignment. Ying Gao used a piezoelectric polymer material, polyvinylidene fluoride (PVDF), to realize responsive, organically-moving garments (Figure 2.1I) [12].

Dielectric elastomer actuators (DEAs) are a class of EAPs that can be designed to be rapidly actuated through electrostatically generated Coulomb forces between electrodes separated by elastic dielectric materials. Voltage requirements are often on the order of several kilovolts (kV) or more. This can create design challenges, since electrical discharge through the air or other materials is possible at distances of a few millimeters. For the same reason, safety requirements, such as current limiting, insulator design, and suitable grounding strategies, are

often required. Risks are higher if the electrically active regions of such devices could, through failure or misuse, produce current paths that traverse the torso, since even electrical currents less than one milliamperere (mA) across the heart create risks of cardiac fibrillation. This can be avoided by confining the electrically active region of a device to a single limb, for example, and avoiding potential current paths to ground through other body regions.

DEA actuators can also be designed to be soft, thus have been used as soft replacements for vibration motors that are used in conventional devices. Koo et al. developed a soft tactile display on the fingertip using an array of EAP actuators [25] (Figure 2.2N), including 20 actuated elements 2 mm in diameter. Mun et al. integrated multilayer DEAs in a glove and sleeve for haptic feedback (Figure 2.6F) [57]. Boys et al. used hydrostatically-coupled DEA for providing haptic feedback with tunable forces and displacements [225].

Other actuation methods Many other actuation methods have been investigated for use in soft robotics. They include electrostatic brakes, electrotactile (charge- or current-based) stimulation, humidification (including moisture absorption by bacteria), and super-coiled fibre actuators, among others. Several authors have designed electrostatic brakes or clutches for arresting motion. Such clutches can produce substantial forces, as in the wearable device of Hichet et al., which generated arresting forces of 20 N for haptic feedback using voltages of 1 kV, in tandem with piezo actuators capable of providing cutaneous vibrotactile feedback (Figure 2.6G) [58]. Thus, the forces that can be produced by such devices far exceed those produced with DEA actuators operating at higher voltages. Twisted string actuators generate linear motion via the twisting of fiber strands or filaments via compact, fast rotating, low-torque motors [189]. Coiled fibre actuators are composed of polymers that produce muscle-like actuation in response to electrically-supplied Joule heating. Such actuators have been applied in wearable applications [54].

A more unusual actuation method that has been investigated for wearable technologies

consists of moisture-activated microbial cells. This actuation method was used to produce a self-ventilating garment possessing pores that opened, cooling the wearer, in response to increased moisture [55].

Table 2.3 presents several actuation methods, and reports aspects related to their wearability and functionality, including their mechanical compliance, safety considerations, portability, feasible force magnitudes, mechanical stress, absolute or relative displacement, and actuation frequency bandwidth.

2.5.2 Sensing

Sensors are critical to the functionality of robotic systems, enabling them to detect or perceive environmental stimuli, perform controlled movements, and manipulate their environments. Common sensing tasks include tracking the kinematic configuration and movements of the robot, sensing contact forces, and collecting environmental information, such as the geometry and configuration of nearby objects. Such sensing tasks mirror many of those that are performed by the sensory organs of the bodies of humans or other animals, which possess multitudes of sensors for transducing visual, auditory, and mechanical information into neural information. Such a comparison is also interesting because biology has often informed or inspired soft robotic design. However useful this analogy may be, there are gross disparities between the complexity and capabilities of biological and soft robotic systems. For example, human abilities of tactile sensing, which are important for myriad activities of touch perception, grasping, manipulation, and interaction, are enabled by numerous mechanoreceptors – end organs of the peripheral tactile sensory nervous system. A single hand possesses on the order of 10^5 such receptors, greatly exceeding the sensing density and capabilities of even the most advanced electronic skins, as further discussed in recent review articles [130, 226].

In conventional rigid robotic systems, sensing needs and solutions are heterogeneous. Kine-

matic and force sensors are among the most frequently used. A hallmark of conventional robotic systems is the integration of kinematic and force sensors within, or close to, the actuators, in configurations that form servomotors or related mechatronic drives. In contrast, in most soft robotic systems, reduced integration between sensors and actuators is common. In soft robotics, this has contributed to a large diversity of sensing methods, designs, placements, and modalities. Recent reviews include [136, 85, 227].

In the last few decades, a large number of soft, wearable, and conformable sensors to detect strain, pressure, gesture, light, temperature, motion, and many other variables have been developed for wearable robotics applications. Data collected from these sensors can be used to control the behavior of the robotic system in a physical environment, through actuation-integrated feedback control, motion or task planning, or to provide application-dependent information, including the affordance of interactivity, as in the sensing of motion or kinesthetic inputs from a user in relation to objects in a virtual environment. Sensing requirements often depend greatly on the task and application domains involved (Section 2.2), which may include healthcare, prostheses, diagnostics, movement, haptics and many others [86].

Several of the most significant sensing tasks in wearable, soft robotics concern mechanical sensing. This can include the sensing of parameters such as mechanical strain, pressure, displacement, or force. These parameters may be required for the control of a robotic system, such as a supernumerary limb, or to facilitate user-action-dependent behavior or interactivity. A great diversity of mechanical sensing methods have been used in soft robotics. An immense variety of rigid sensors have been integrated in soft and wearable devices, far more than could be profitably reviewed here. Instead, we describe prominent sensing methods based on soft or compliant materials.

One category of such sensors leverages electrical principles. These include capacitive and resistive sensors. Soft capacitive and resistive sensors have been enabled through the use of electronic or ionic (conductive or resistive) soft materials, or the integration of compliant elec-

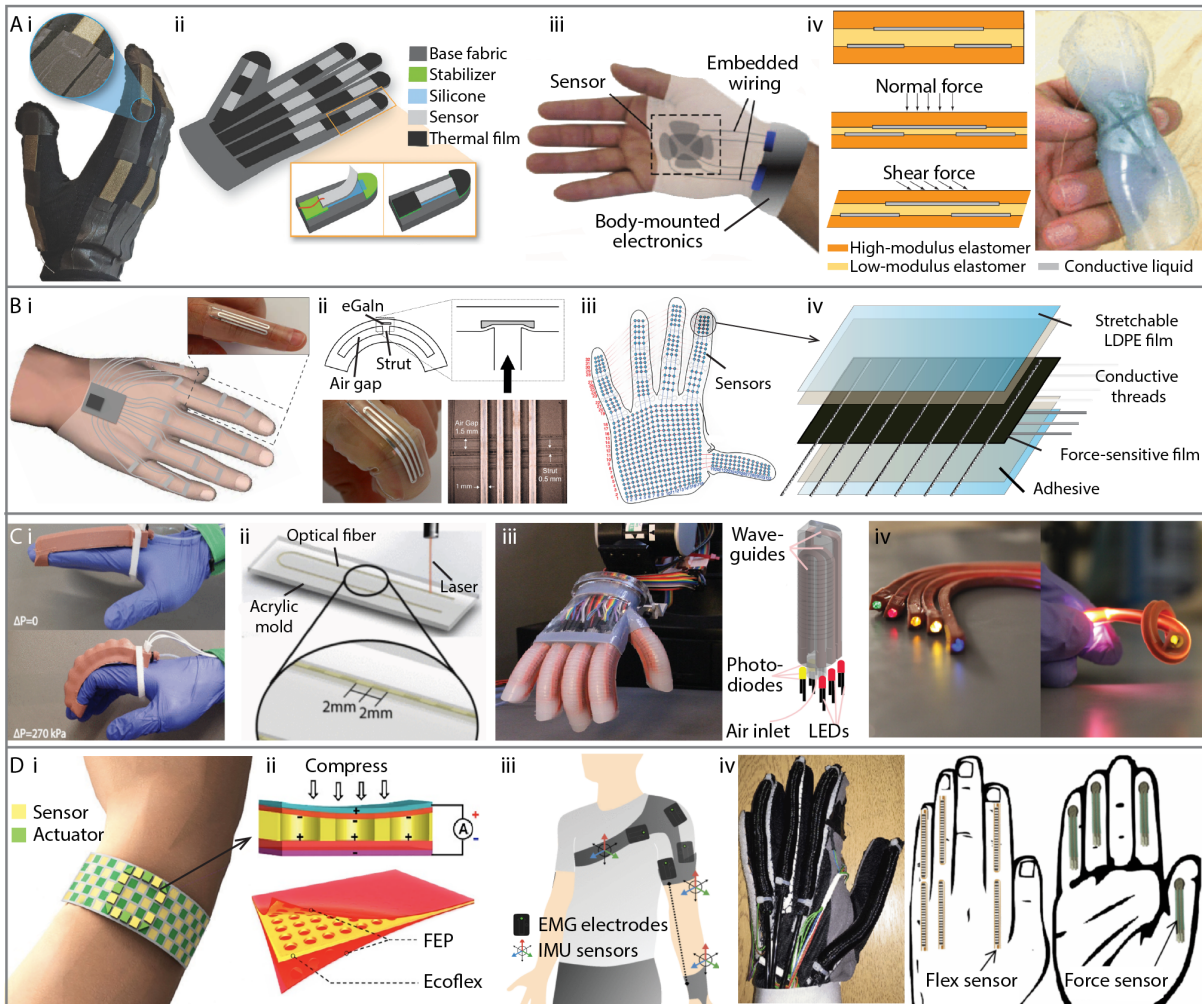


Figure 2.7: Examples of sensing methods for soft wearable robotic applications. A. Examples using capacitive sensors. i-ii. Sensing glove for human body articulation using a customizable, stretchable textile-silicone composite capacitive strain sensor [59]. iii-iv. Soft-matter sensor measuring elastic pressure and shear deformation [60]. B. Examples using resistive sensing. i-ii. Curvature sensor for monitoring human or robotic motion [61]. iii-iv. Array of 548 resistive sensors on a soft tactile glove for normal force readings to identify tactile information when interacting with objects [62]. C. Examples with optical sensing designs. i-ii. A soft orthotic with curvature control enabled via embedded optical fiber [63]. iii-iv. Soft prosthetic hand for shape, texture, and softness detection using stretchable optical sensing techniques [64]. D. Examples of other sensing technologies. i-ii. Stretchable and flexible piezoelectric sensor for detecting force and pressure [65]. iii. An upper limb soft wearable assistive exosuit using IMU for joint angle sensing and EMG for muscle activity sensing [66]. iv. A soft wearable pneumatic glove with commercially available flex and force sensors to capture finger movements [67]. Images reproduced with permission. Images D i, D ii licensed under Creative Commons 4.0.

Table 2.4: Selected attributes of representative sensors for wearable applications*

Sensing	Ref.	Compliance	Feature Size (unit: mm)	Measurement	Range	Sensitivity
Resistance liquid alloy twisted microtubules	[228]	Stretchable > 400%	Cross-section diameter: 0.5	Contact force	0-0.45 N	200%
Resistance liquid alloy sheet	[61]	Stretchable > 350%	Channel width: 1	Bending angle	0-100°	127%
Capacitive liquid alloy tactile sensing arrays	[229]	Stretchable > 500%	Cross-section diameter: 0.3	Contact pressure	0-450 kPa	140%
Capacitive silver nanowire sheet	[230]	Stretchable ≤ 50%	Pixel size: 2×2	Contact pressure Strain	0-1.2 MPa 0-35%	110% 26%
Optical waveguide	[64]	Stretchable ≈ 85%	Cross-section: 3×3	Contact force Curvature Strain	0-20 N 0-2 cm ⁻¹ 85%	9 dB 1.9 dB/cm 15 dB
RGB and IR LED photoplethysmography sensor	[231]	Stretchable	Electronics patch size: 10×10	Physiological signals	65-72 BPM	0.76%
Piezoelectric sensor patch	[65]	Flexible	Pixel diameter: 2	Contact pressure	0-1.84 Pa	0-1.5 nA
Self-powered piezoelectric sheet	[232]	Flexible	Thickness: 1	Acceleration shear force Longitudinal force	-3 to 3 g -3 to 3 g	26.7 mV/g 90.2 mV/g
Magnetic Hall effect sensing sheet	[233]	Flexible	Thickness: 7	Curvature	0-2 cm ⁻¹	85%

*The data are collected from manuscripts, graphs, and supplementary materials of each reference with approximation.

tronic or ionic materials within soft polymers or other compliant structures.

Resistance sensing Resistive sensors are based on changes in electrical resistance of a current path in response to mechanical stimuli. A simple example of such a device involves changes in the electrical resistance of a soft, conductive channel or wire in response to strain, or changes in length. In a conductive channel, the resistance R increases with length, l , and decreases with cross-section area, A , i.e. $R = \rho l/A$, where ρ is volume resistivity, a material parameter. Many soft, wearable robotic systems have employed strain sensors based on resistance. For example, Do et al. described strain-sensitive stretchable devices based on helically twisted hollow polymer fibers filled with a liquid metal, eutectic Gallium Indium [228]. Through twisting, the change in resistance in response to mechanical strain could be tuned to application requirements. Many other skin-wearable examples using resistive sensing have been used (e.g., Figure 2.7B i, ii [61]).

Capacitive sensing Capacitive sensing is based on capacitive coupling, which is the transfer of electrical energy by means of charged surfaces coupled through electric fields. A simple example of a capacitive sensor is a parallel capacitor with a soft dielectric material whose softness enables the device geometry, and thus capacitance, to change in response to applied mechanical displacements, stresses, forces, or strains. The capacitance of such a device is the ratio of change in electric charge to electric potential, depending on the device geometry and the dielectric constant of the materials. In simple devices, capacitance sensing is performed via charge or current sensing, while in more refined approaches, the capacitive device forms part of an oscillating circuit whose resonant frequency is sensed electronically in order to measure capacitance.

Atalay et al. employed capacitive sensors for strain sensing in a glove [59], while Cooper et al. produced capacitive sensors based on helically twisted fibers filled with liquid metal

[234], similar to the resistive fibers reported by Do et al. [228]. Yao and Zhu developed multimodal wearable capacitive sensors for pressure, strain, temperature, and touch contact in several application areas [230]. Figure 2.7A illustrates several more examples.

When compared with resistive sensors, capacitive sensors can be more easily integrated in two-dimensional sensing arrays, because current does not directly flow between pairs of electrodes [235, 229]. This can facilitate tactile sensing via 2D soft, skin-like devices [236, 234]. This is more challenging to achieve using arrays of resistive devices, which often involve multiple current pathways between the electrodes that are used to read out the signals. However, Sundaram et al. applied an active grounding method in order to realize a pressure sensing glove with 548 resistive sensing elements (Figure 2.7B iii, iv) [62].

Both capacitive and resistive sensors can be designed to achieve high sensitivities. Capacitive sensors involve additional design considerations because their capacitance is affected by the dielectric properties governing electric fields in their nearby environment, and not merely by their geometric and mechanical state. To reject signals produced via nearby objects that are not in contact with the sensing device, the passive design or active control of the configuration of grounded surfaces in the device can be used [237].

Optical sensors Optical sensors are widely used in wearable applications, including health monitoring [238, 231]. Such sensors have attracted interest in wearable soft robotics due to their robustness and sensitivity. Optical sensors leverage the transmission, reflection, or refraction of light to sense physical properties or changes, such as mechanical deformation. Several methods for optical sensing via soft, stretchable, compliant, or flexible materials have been investigated. Optical fibers have been used in several such investigations. Precise strain sensing can be performed via patterned optical fibers that function as Bragg gratings. Other techniques for optical sensing utilize materials that vary in refraction or luminescence, such as photonic crystals, liquid crystal materials, or mechanochromic materials [86]. Remote optical sensing

via the skin or other sensors can be used to measure light transmitted through materials or tissues. Such sensing methods have been used for curvature control of soft actuators (Figure 2.7C i, ii) [63], as well as shape, texture, and softness detection on a soft prosthetic hand (Figure 2.7C iii, iv) [64].

Piezoelectric sensors As described in Section 2.4.1, piezoelectric materials, including piezoelectric polymers, have been applied for several sensing tasks in soft robotics, including strain, force, or pressure sensing. Examples of piezoelectric sensing applications include self-powered, multifunctional pressure and shear sensors [232] as well as those developed to be used as e-skins or skin patches (Figure 2.7D i, ii) [65, 226]. Other uses of piezoelectric sensing combine them with other sensing methods to form hybrid sensing systems. One example is pyroelectric sensing, where a charge is generated in response to temperature changes and is thus primarily used for thermal detection, while another example is triboelectric sensing, where contact electrification generates a change in charge [86].

Magnetic sensors Several magnetic sensing methods have been used in soft and wearable robotic applications. In one common configuration, miniature magnets are embedded in an elastomer. Changes in the resulting magnetic field are captured via the Hall effect or other inductive sensors to measure strain, deformation, shape change, or other attributes [233, 239]. Such sensing methods are relatively noise-robust and resistant to hysteresis [240].

Multimodal sensing The sensing principles highlighted here represent a selection of those that have been used in soft and wearable robotics. Other methods include physiological sensing techniques such as electromyography and inertial sensing methods. These methods were combined in the exosuit created by Little et al. (Figure 2.7D iii) [66]. This example illustrates how sensing techniques are often combined synergistically. For example, Gerratt et al. developed a wearable tactile glove combining capacitive and resistive sensors [48], while Lacour et al.

created a skin-wearable device using piezoelectric sensors combined with thin-film transistors to detect pressure and strain [241]. Al-Fahaam et al. used commercially available flex and force sensors to capture multiple types of grasp movements in a soft wearable pneumatic glove (Figure 2.7D iii, iv) [67].

Table 2.4 presents properties of several sensing methods in relation to their wearability and functionality, including the feature sizes of the sensing components, the parameters being measured, the range of the measured parameters, and the sensitivities or signal ranges of the sensor.

2.6 Conclusion: Frontiers, Challenges, and Future Prospects

In this review, we surveyed many aspects of soft, wearable robotics in order to provide the reader with an overview of the state-of-the-art, recent trends, design considerations, and engineering knowledge and methods that are contributing to the evolution of this active, evolving domain of research.

Engineering research in soft, wearable robotics and haptics is advancing rapidly due to the promise that such technologies hold for diverse applications, in areas ranging from healthcare, to augmented and virtual technology, fashion, and industry. Advancements in soft, wearable robotics have been enabled through the development of new materials and technologies, including compliant and soft materials and systems that are able to meet the often unique design and fabrication requirements that arise in this area, and that provide sensing, actuation, and other capabilities supporting their functionality. The promising potential of soft, wearable robotics is also associated with the ability of such systems to intimately complement the capabilities of the human body, enhancing human abilities of movement, sensing, furnishing capabilities that expand performance, providing protection to the body, or supplementing human perception and cognition.

Despite the exciting nature of these developments and advancements, there are several important challenges that must be overcome in order for soft, wearable robotic and haptic systems to attain their potential.

One of the most important challenges is that of engineering new actuation methods that are compatible with the compliance of these systems, and with the softness of the materials that comprise these systems and the areas of the body with which they interface. In conventional robotic systems, established technologies including electromagnetic actuators or motors, pneumatic actuators, and hydraulic actuators, together with their accompanying mechanisms or transmissions, serve the great majority of motion control needs. While many soft analogs of each of these technologies have been developed, their capabilities often remain orders of magnitude more limited than their conventional counterparts. Advancements are needed in order for soft robotics to attain the high performance (for example, precision, speed, or operating range of forces) of conventional robotic systems. Such improvements may also require advances in methods of control engineering for soft robotic systems, which often comprise continuum systems with infinitely many degrees of freedom.

While sensing technologies are in some respects more advanced than those for actuation, here too there are opportunities for advancement. For example, as we described in the foregoing, electronic sensors cannot yet match several of the remarkable characteristics of the human skin, which is innervated with on the order of 10,000 mechanically sensitive neurons in each hand, and also provides impressive multi-modal sensing capabilities for mechanical, thermal, chemical, and noxious stimuli via a common substrate.

Control for soft, wearable robotics presents further challenges and opportunities for research. Recent research highlights the importance of human-in-the-loop considerations in control design. Further developments of these methods for soft, wearable robotics could enable such systems to perform robustly and meet the needs of myriad users.

Additional challenges arise from wearability. Many soft, wearable robotic systems are

designed to be portable. New methods for powering such systems are needed in order to facilitate this, and to avoid encumbering their wearers. Energy requirements may also be reduced through the advancement of low-power technologies for sensing, actuation, and computation.

Other challenges arise from goals of interfacing or acting upon the body. For example, emerging soft robotic systems provide assistive forces or apply forces to the environment that are reflected in their wearer, as in supernumerary limbs or prosthetics. Providing such forces via devices that are anchored to the skin and indirectly to subcutaneous tissues greatly constrains the design and performance of wearable robotics. This is a fundamental problem affecting the use of robotic wearables by endoskeletal creatures: soft tissues mediate forces between actuators and the skeleton. New ideas may be needed in order to overcome these limitations, ideally without recourse to very invasive or irreversible methods that require surgery. Examples could include minimally invasive micro-anchors that directly couple actuator forces to the skeleton. Today, implanted devices are primarily applied in medical applications. However, research in soft robotics and electronics is enabling devices that can offer greater biocompatibility than is possible with conventional technologies. In exceptional cases, body-penetrating (e.g., piercings) or implanted structures are used for body adornment. Over time, if perspectives on similarly intimate integrations of technologies with the body evolve, there could be demand for non-medical devices that are not merely wearable, but that integrate with, or within, tissues of the body itself.

Much as in any emerging area of technology, the range of potential applications of soft, wearable robotics is not yet fully understood. Past and recent history in the development of new technologies suggests that these developments will yield many applications that cannot yet be envisaged today. As we have highlighted, many emerging soft robotic technologies resemble existing wearable categories of garments, clothing, or other accessories. Such wearables are omnipresent, serving functional needs, matching cultural demands, or contributing to aesthetics or expression. Thus, it is possible that advances in soft robotics could transform the way

that many articles of apparel are viewed today. Such advances could yield robotic clothing that augments human abilities in ubiquitous arenas of human activity, such as workplaces, domestic environments, leisure environments, or the outdoors. Such developments could thus be transformative.

Efficiently combining advancements in each of these areas will require new methods for systems integration. The capabilities of conventional robotic and electronic systems, or even the highly integrated systems supporting biological organisms, provide inspiration for what future soft, wearable robotic systems could one day achieve. Such advancements may require major progress in methods of materials and manufacturing.

The computer age is less than a century old, which is remarkably short when compared with timescales involved in biological evolution. In what today seems like the distant future, it is possible that soft, wearable robotics could achieve levels of efficiency, functionality, integration, and complexity that naturally evolved systems have produced. Such a vision could point to a long-term frontier in soft wearable robotics, toward seamless and synergistic integrations of human-produced technologies with biological systems.

Chapter 3

Fluidic fabric muscle sheets for wearable and soft robotics

Advances in soft robotic technologies have enabled the development of compliant functional garments for haptics, assistive exosuits, and many other domains, as reviewed in chapter 2. Soft actuators empower garments the ability to supply forces in a compliant, conformal, and safe manner when in close contact with the human body. Despite many advances in the development of soft actuators, it remains to be a challenge to seamlessly integrate soft actuators into garments in a compact, safe, and effective way. This chapter addresses this gap through the development of a new family of fabric-based soft actuators that are readily integrated into garments already widely used. These actuators meet both the wearability needs, including compliance, versatility, safety, compactness, and the functionality needs, such as force, displacement and bandwidth, for soft wearable robotic and haptic applications. The findings from this chapter enables the development of an expressive multimodal haptic sleeve in chapter 4 and a peristaltic wearable robot in chapter 5.

The content of chapter 3 is originally published in the following reference [2]:

M. Zhu, T. N. Do, E. Hawkes, and Y. Visell, Fluidic Fabric Muscle Sheets for Wearable and Soft Robotics. *Soft Robotics*, Apr 2020.179-197, ©2020 Mary Ann Liebert, Inc..

Reproduced here with permission from the Mary Ann Liebert, doi: 10.1089/soro.2019.0033.

Abstract

Conformable robotic systems are attractive for applications in which they may actuate structures with large surface areas, provide forces through wearable garments, or enable autonomous robotic systems. We present a new family of soft actuators that we refer to as Fluidic Fabric Muscle Sheets (FFMS). They are composite fabric structures that integrate fluidic transmissions based on arrays of elastic tubes. These sheet-like actuators can strain, squeeze, bend, and conform to hard or soft objects of arbitrary shapes or sizes, including the human body. We show how to design and fabricate FFMS actuators via facile apparel engineering methods, including computerized sewing techniques, that determine the stress and strain distributions that can be generated. We present a simple mathematical model that proves effective for predicting their performance. FFMS can operate at frequencies of 5 Hertz or more, achieve engineering strains exceeding 100%, and exert forces greater than 115 times their weight. They can be safely used in intimate contact with the human body even when delivering stresses exceeding 10^6 Pascals. We demonstrate their versatility for actuating a variety of bodies or structures, and in configurations that perform multi-axis actuation, including bending and shape change. As we also show, FFMS can be used to exert forces on body tissues for wearable and biomedical applications. We demonstrate several potential use cases, including a miniature steerable robot, a glove for grasp assistance, garments for applying compression to the extremities, and devices for actuating small body regions or tissues via localized skin stretch.

3.1 Introduction

Emerging soft actuator technologies are enabling applications in robotics, healthcare, haptics, assistive technologies, and many other areas. Such soft actuators can interface with, conform to, exert forces upon, or generate shape changes in complex or compliant structures [242, 243, 244]. Wearable soft robotic devices interfaced with the human body may prove valuable for rehabilitation, movement assistance, or virtual reality [245, 30, 246, 25]. Soft actuators are also of interest for controlling motion in distributed and deformable structures. They can be used for tasks such as grasping, terrestrial locomotion, surgery, or underwater operation [4, 247, 248]. Such applications span systems of greatly varying size, ranging from millimeter-scale biomedical robots to large, deployable structures [249, 250].

Biological systems provide rich sources of information to guide the design of soft robots [251]. The motile capabilities of animals are enabled by composite systems of muscle, connective, and other tissues. The forces and motions they can produce depend on the properties of individual muscle fibers, the arrangement of fibers, and the muscle morphology and attachments. Muscle morphologies vary widely. While fusiform shapes, like the human biceps brachii, which can produce large-amplitude motion, are most common in robotics, many other morphologies exist. The present work is inspired by layered muscle sheets, like the transverse abdominis (Fig. 1A), that compress or transfer forces around the torso [252].

Here, we describe a new family of muscle-inspired actuators that we refer to as Fluidic Fabric Muscle Sheets (FFMS). They are composite fabric sheets that employ an integrated fluidic transmission comprised of arrays of hollow elastic tubes to generate in-plane stresses or strains. We show how to design and fabricate these devices using apparel engineering methods. As we demonstrate, FFMS are stretchable, conformable, safe, efficient, and scalable. In order to situate this work relative to prior research, we begin with a review of several related technologies.

3.1.1 Background

Many soft actuator technologies have been developed for applications in robotics, wearable devices, healthcare, and other areas. The FFMS sheet actuators we present here build on prior research on soft fluidic actuators, including the sheet-like actuators described below. It is useful to compare the materials, operating principles, methods of design and fabrication, and performance characteristics of such devices.

Fluidic actuators

Fluidic actuation technologies have attracted considerable attention for use in soft robotic systems because of their intrinsic compliance and the ease with which the fluids that transmit stresses may be integrated into soft media [253]. Fluidic power may be delivered in the form of fluid pressure and volume changes via a variety of pumps or charged reservoirs, enabling such systems to be designed to match a wide range of requirements. Such devices can produce larger forces, displacements, or work densities than are feasible with many emerging functional materials technologies (discussed below), facilitating practical applications.

Pneumatic Artificial Muscles, which generally shorten when filled with compressed air, come in many shapes and sizes [254]. An early, influential example is the McKibben actuator [255, 256, 257, 258]. It comprises an airtight bladder with fiber constraints that cause it to contract when the internal volume is increased through the application of pressure. The dimensions and working pressures of such actuators may be selected to match application performance requirements. However, maximum strains are typically less than 35% [259, 260], limiting applications. Many soft, fluidic actuators have been designed for pneumatic operation via compressible gases. This causes energy to be stored in gas compression during operation, which can lead to undesirable, rapid energy release on failure. Gas compression also leads to thermodynamic losses. A smaller group of soft, fluidic actuators have employed incompress-

ible fluids. The FFMS actuators can use either approach. We review some of the advantages of hydraulic operation below.

Many other variations on the idea of combining fluidic actuation with fiber constraints have been investigated [176, 261]. Recently, it has been observed that much larger strains can be realized – approaching 300% – by means of actuators that contract when the internal volume and pressure are reduced, in a manner inverse to the McKibben design. Such devices, including the Inverse Pneumatic Artificial Muscle (IPAM) [262] and Hydro-Muscle Actuators [263], integrate anisotropic components that cause them to lengthen when pressurized.

We leverage just such an “inverse” fluidic actuation strategy in the FFMS actuators described here. In contrast to the typically uniaxial and tubular forms of prior devices, which evoke fusiform muscle structures, FFMS actuators are actuated fabric-based structures, similar to muscle sheets. Anisotropic constraints in FFMS actuators are provided by the fabric structure. Different fabric patterns and assemblies can be used to realize a variety of actuation modes, including uniaxial actuation, bending, multi-axis actuation, shape-changing, and compression.

Several methods for creating mechanical anisotropies with fabrics have been previously investigated to improve the performance of fluidic actuators in devices based on individual tubes [263], air bladders [264], or other structures. In most cases, this is achieved through the intrinsic anisotropy of integral fibers. Fiber-reinforcement of the elastomer can be designed to produce desired anisotropy, and hence motion, by specifying the threading angle of the fibers [176, 261], although this complicates fabrication.

Other soft, fluidic actuator designs, including origami-inspired devices, grow longer when positive pressure is applied [163]. However, the maximum forces that can be reproduced are limited by buckling instabilities [190]. Vacuum-driven soft actuators have also been realized, attaining large peak stresses [265], but often involve large changes in cross-section area.

Other Transduction Principles for Soft Actuators

Many other methods of soft actuation have been investigated, each involving different trade-offs in performance. Shape memory alloys yield strains of up to about 5% when heated [266]. They can also yield larger strains in other configurations, such as coils [267]. Other thermally actuated transducers have been based on shape memory polymers, nylon, polyethylene, or other fibers [268, 269, 270]. Such actuators often yield low efficiencies or low-actuation speeds due to the thermal processes underlying actuation. Other devices based on shape memory polymers [271, 272] or electroactive polymer technologies, including ionic polymer-metal composites [273, 274, 275] have been designed to yield high strains, but typically only generate small forces. Soft, electrostatic actuators, including dielectric elastomer actuators, are fast and can be designed to produce large strains [276] but require high voltages and carefully controlled fabrication processes and mechanisms that preclude their use in some applications. Variations on such actuators that use fluidic electrodes overcome some of the fabrication and design challenges involved in employing such actuators, but high voltages are nonetheless required [277]. Electromagnetic soft actuators can operate at low voltages [278, 279], but often yield low work rates or require an external magnetic power source [280, 281].

Another approach to producing high forces and strains in soft, actuated structures is based on tendon- or Bowden-cable transmissions [282, 199, 283]. Achieving high performance actuation and control with such devices depends on cable routing and friction management. In addition, careful design is needed to ensure that the stresses that are produced are appropriately distributed.

Sheet-Like Soft Actuators

Various sheet-like soft actuators have been developed using actuation methods paralleling those described above. Several groups have produced such sheet-like actuators based

on shape memory alloys or thermally actuated nylons, but the tradeoffs between actuation time, forces, and strains limit the feasible mechanical power, speed, and reduce efficiencies [284, 285, 286, 287]. In addition, the temperatures or heat exchange requirements may limit wearable applications.

Multi-layered artificial muscles made of electrostatic sheet actuators have been designed to produce large forces at moderately high voltages, but require careful control over their motion during actuation, precluding out-of-plane deformation [288]. Dielectric elastomer actuation principles have also been used to realize compact sheet-like soft actuators, although large voltages (greater than 1 kV) are normally required [289, 290].

Sheet-like, fluidic soft actuators have been designed by assembling discrete pneumatic artificial muscles within a fabric, pouch, or other assembly [291]. One configuration integrated McKibben muscles within fabric layers [243]. Another consisted of thin McKibben muscles that were woven into fabric structures [292]. When driven to produce contraction along the axis of each muscle, the actuators expand, causing undesired increases in thickness, adversely affecting potential conformable or wearable applications and reducing efficiency. Other designs have resulted in low forces that preclude many applications [293]. In contrast, the FFMS actuators presented here increase in nominal length, or decrease in contraction force, when fluid pressure is applied. This is achieved with negligible tangential expansion over the normal operating range of the actuator.

Other authors have used parallel cables or strings routed within fabric structures to create sheet-like actuators [294]. Such designs can produce thin, fabric-like actuators, but require careful attention to cable actuation and friction management in order to ensure that dynamic, fast, and reversible actuation is possible. Because FFMS actuators transmit stresses via integral fluids, losses, due to viscosity and channel length (see Modeling, below) remain within ranges that permit highly dynamic operation.

3.1.2 Contributions

This paper presents FFMS, a new soft actuation technology. FFMS are planar, multimodal soft actuators that are analogous to muscle sheets. Their design also builds upon prior “inverse-type” uniaxial actuators with tubular shapes that can be compared to fusiform muscles. Here, we describe the design and fabrication of FFMS and show that this planar paradigm opens many new actuation capabilities and applications. These low-cost devices, admit multiple design options at multiple scales, facile fabrication, can conform to curved structures, produce large work densities, and achieve fast response times.

Design, Fabrication, and Modeling: We show how to design composite fabric structures to realize mechanical anisotropies that enable FFMS to generate patterns of local contractions in a conformable, planar surface as fluid is withdrawn. FFMS can be efficiently fabricated using apparel engineering methods including pattern making, computerized sewing, and wrinkling, and through the integration of a fluidic transmission based on hollow elastic tubes. We describe several alternatives for their design and assembly. We analyze the effects of fabric selection and wrinkling, tube routing, thread selection, and stitching selection, all of which can be used to tailor functionality and performance. We also present a simple mathematical model that proves effective for predicting their performance and aiding design.

Actuation Capabilities: FFMS actuators may be scaled to different sizes, depending on design requirements. We demonstrate actuators with dimensions ranging from 1 to 34 mm in thickness, and 30 to 1000 mm in length, yielding forces that can exceed 150 N, and that can produce forces more than 115 times greater than their weight. FFMS actuators can also produce uniaxial engineering strains exceeding 100%. Laboratory prototypes perform consistently in durability testing during 5000 cycles or more, with less than 5% change in displacement.

Applications: We demonstrate their use in actuating various bodies and mechanisms, and in configurations that perform multi-axis actuation, including in- or out-of-plane bending and shape change. We also demonstrate applications of FFMS methods for realizing low-profile, fabric-based actuators for new devices that exert forces on body tissues for wearable and biomedical applications. These include a glove for grasp assistance, devices for compressing small body regions or tissues, and devices for providing haptic compression or skin stretch to a finger, arm, or leg. Compression garments formed from these actuators can produce dynamic compressive pressures that scale to high, predictable values; we demonstrate prototypes that easily generate compression of 4 kPa, which is sufficient for haptic feedback, meeting requirements needed for many musculoskeletal, circulatory, wound, and lymphatic compression therapies, including peristaltic compression modes.

3.2 Design Concept and Operating Principle

FFMS actuators generate stresses or strains in a composite fabric sheet when charged with a pressurized fluid. The fluid may be compressible (pneumatic operation) or incompressible (hydraulic operation); we compare the relative merits of each later in the paper. The routing of stresses and strains is accomplished via an integral fluidic transmission composed of hollow elastic tubes. The fabric assembly directs stresses along axis of channels that are sewn into the fabrics. As fluid is pumped into the elastic tubes, their internal volume is forced to increase. Circumferential constraints imposed by the fabric cause the increased fluid volume to produce a nominal lengthening of the structure along the axis of each tube (Fig. 3.2A). This causes elastic energy to be stored in the tube-fabric structure. As the fluid pressure or volume is reduced, the stored elastic energy is released. When the FFMS is working against a load, this reduction in pressure yields a contraction force. Thus, while increased pressure produces a lengthening of the FFMS, external forces are normally produced via contraction, similar to biological muscles

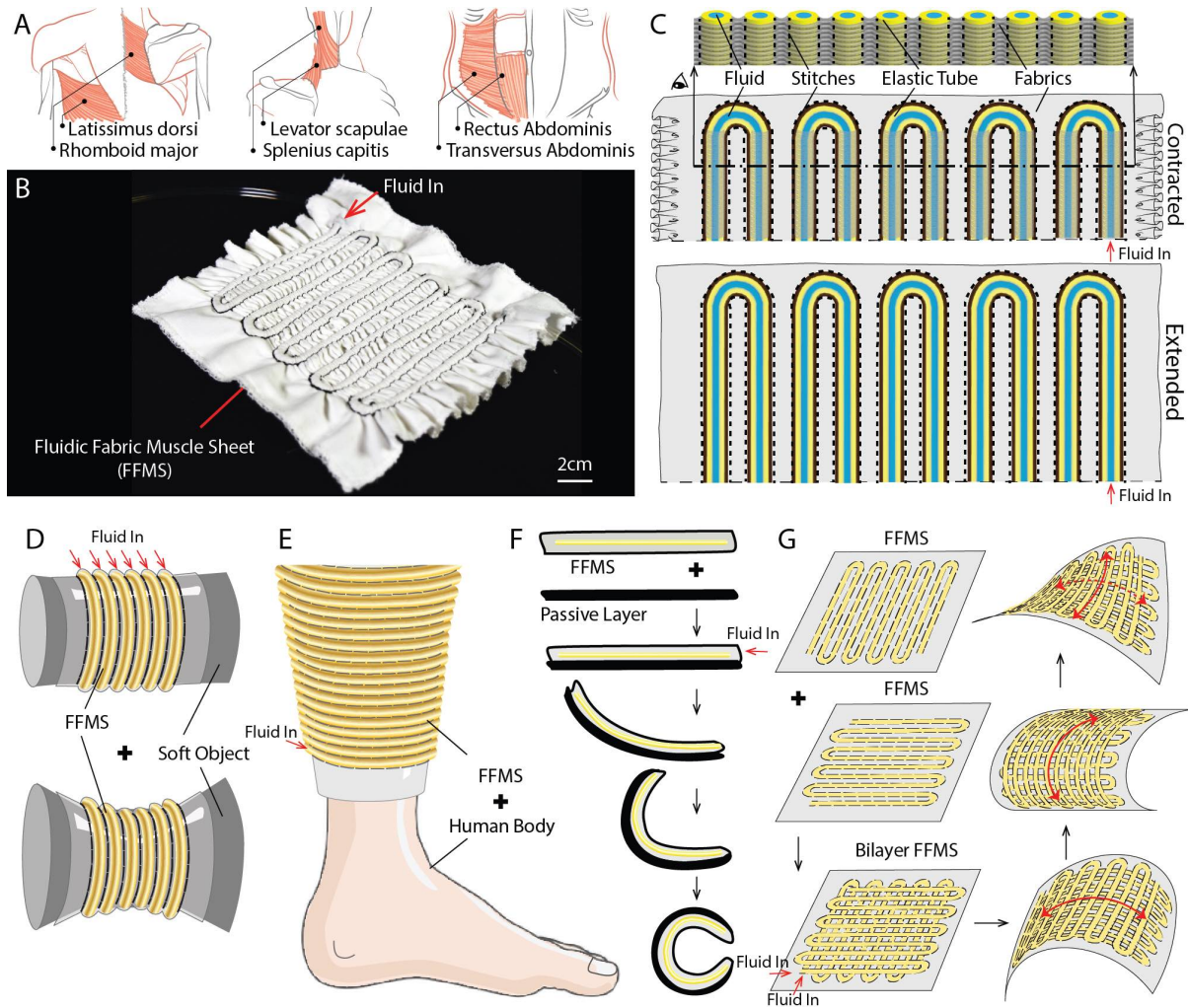


Figure 3.1: A. Examples of muscle sheets in the human body that inspired the design of FFMS [68] (reproduction rights pending). B. A functional prototype illustrating how FFMS are planar fabric structures analogous to muscle sheets. C. FFMS comprise arrays of elastic tubes that function as fluidic transmissions. In this example, corresponding to the prototype of Fig. 1B, uniaxial extension is produced when fluid pressure is increased. D-G. FFMS may be applied in a variety of ways (see Fig. 3.10): (D) deforming a soft object, (E) compressing a limb, (F) bending a flexible structure, (G) in bilayer structures that generate morphological change, among many other possibilities.

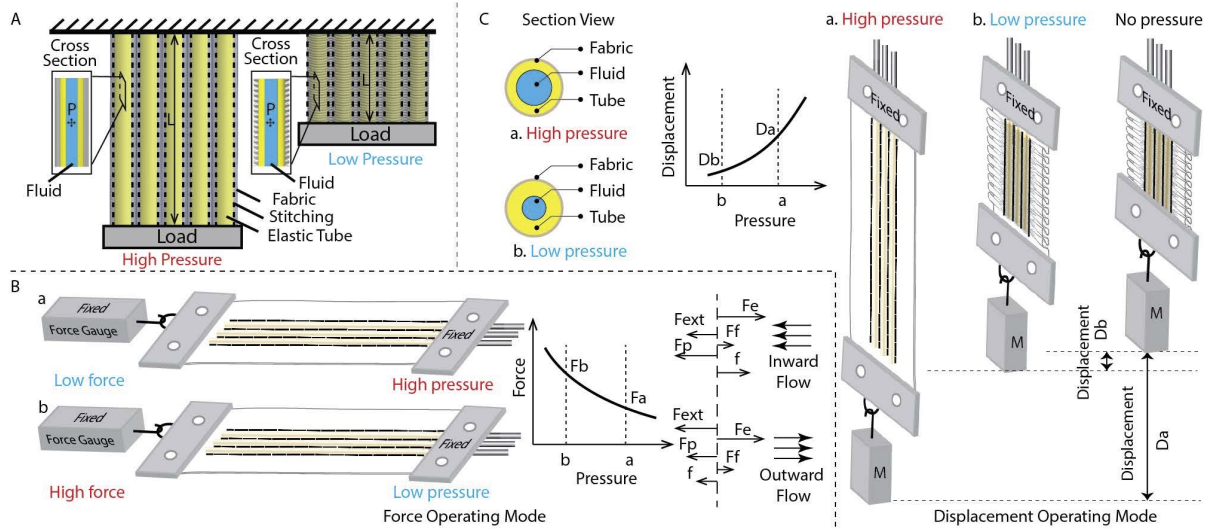


Figure 3.2: Fluidic Fabric Muscle Sheets: Concept and operating principle. A. Hollow elastic tubes are integrated in a composite fabric structure. The tubes are routed in fabric conduits that provide circumferential constraints, due to stitching. *Left:* When pressurized fluid is pumped into the elastic tubes; the tubes cannot swell radially due to the constraining stitches, and thus can produce a lengthening, similar to a relaxing sheet of muscle. *Right:* When the fluid pressure is removed, stored elastic energy in the hollow tubes and elastic fabric is released, and the entire textile shortens, like a contracting sheet of muscle. P and L represent fluid pressure and actuator length, respectively. B. *Left:* When the FFMS is operated to work against a load, as in the isometric configuration shown here, forces are produced. *Middle:* High pressures produce low forces, and vice versa. F_b and F_a correspond to states a and b in panel B. *Right:* A simple illustration of the generation of axial forces. We present a mathematical model in a subsequent section. C. *Left:* Cross section view of a single channel in the displacement operating mode. Wall thinning may result as the elastomer length increases. *Middle:* In displacement mode, higher pressures produce larger displacements, and vice versa. *Right:* In such a displacement mode, the FFMS may be used to do external work, such as lifting a mass, as shown here.

(Fig. 3.1A) [68]. As we demonstrate, the same principle can be used to realize FFMS actuators that operate in hydrostatic mode, similar to muscular hydrostats such as the tongue of many animals or trunk of the elephant. The ranges of forces and displacements that can be produced depend on the dimensions of the FFMS, operating range of applied fluids, actuation mode, and materials involved. We present a simple mathematical description of the effects of these factors below.

Depending on actuation requirements, FFMS can be operated to produce forces or displacements. In force mode (Fig. 3.2B), a muscle is pre-stretched against a load via constraints at both ends. High fluid pressures produce low forces, and vice versa. Stresses act along the longitudinal axis of the elastic tubes. This can yield axial forces, or compression forces, when the FFMS is wrapped in a nose-to-tail configuration around an object, such as a human limb (Fig. 3.10F). FFMS may also be used to generate large strains or displacements (Fig. 3.2C). Changes in displacement can be used to displace loads or to alter the shape of a structure through differential stresses or strains. Due to the radial constraint imposed by the composite fabric structure, a change in fluid volume creates a change in length. The relationship between the fluid volume in the FFMS and the channel length is approximately linear (see Section 3.6). Such a displacement can be used to perform mechanical work. As we show, in multi-layer structures, it can also be used to effect changes in the intrinsic shape of an FFMS assembly. Together, these unique capabilities make FFMS amenable to various applications.

3.3 Fabrication

The fabrication of FFMS actuators involves three main steps: Construction, patterning, and assembly of a multi-layer textile structure, routing of elastic tubes in the patterned fabric structure, and sealing and attachment of tube fittings, as illustrated in Figure 3.3A-E. The figure highlights a process based on a configuration of non-stretchable fabrics with stitching parallel

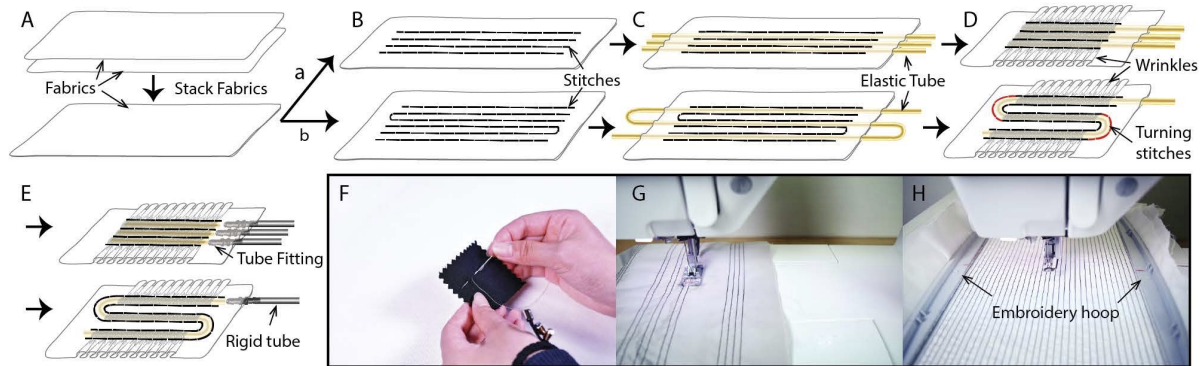


Figure 3.3: Fabricating planar fluidic fabric muscles involves several steps based, in part, on apparel engineering methods. For configurations based on non-stretchable fabrics, the fabric layers are first aligned and stacked. (A) The routing of elastic tubes is designed and layers are stitched to form conduits (B) in a pattern that determines the routing. The stitched patterns can realize single (b) or multiple (a) tube routings. The elastic tubes are then threaded (C) through the resulting fabric conduits. (D) For non-stretchable fabric layers, the fabric structure is wrinkled. (E) A port is established at one end of each channel, whose remote end is then sealed. The stitching may be done via (F) hand sewing, (G) machine sewing, or (H) computerized embroidery.

to the channels. Other stitching patterns suitable for stretchable fabrics are discussed in Section 3.4 below.

In a first step, the fabric layers are aligned and stacked. The layers are then stitched to form conduits between the fabric layers to allow tube insertion. The stitching patterns can be designed to realize configurations via a single tube and single fluid input port (Fig. 3.3a), or multiple tubes, enabling separate, independently addressable channels (Fig. 3.3b). The routing of channels in the fabric determines the distribution of strain and stress within the composite textile, which need not be uniform. To radially constrain each tube, the conduit should possess a width equal to half of the tube diameter.

Different sewing methods can be used: hand sewing (Fig. 3.3F), machine sewing (Fig. 3.3G), and computerized embroidery (Fig. 3.3H). When the pattern size fits within machine limits, computerized embroidery is preferred. It provides great accuracy, flexibility, and efficiency. When embroidery is impossible, machine sewing may be used. This involves manual movement of the fabric under the sewing foot. This is often the best option when stitching long

actuators or very large surface areas. Hand sewing is the least efficient method, but can accommodate complex paths or non-flat fabric surfaces, as are involved when stitching the turning stitches that we apply following tube insertion (Fig. 3.3D).

After sewing, the tubes are threaded through the conduits via a slender rod inserted into an end of the elastic tube. The fabric is then wrinkled along the length of the tubes in order to accommodate stretching. We have found that this wrinkling can readily be performed in a uniform, controlled fashion. Together, the proportion of wrinkling and elastic properties of the fabric and tube determine the maximum length of the muscle. This process is best suited to non-stretchable fabrics. If stretchable fabrics are used, the wrinkling step may be omitted. In a next step, one end of the elastic tube is sealed with a fixture, such as a knot, while the other is connected to a barbed tube fitting that allows the fluid to be supplied to the muscle. For large-scale FFMS (Fig. 3.8A,B), one end of the tube may be sealed with a solid barbed end plug, rather than a knot, while the other end is connected to a barbed tube fitting. To strengthen the connection between the fitting and the elastic tube, clamps may be applied. In a next step, air is purged from the channels. To stabilize the mechanical response, the muscle is fully extended and contracted several times prior to the first usage.

3.4 Material Selection

The performance of FFMS actuators depends on the selection of elastic material, fabric material, and stitching pattern. The working ranges of displacements and forces are determined by the applied fluid pressure range, the fabric and elastic tube material properties and sizes, and the manner of patterning and assembly.

3.4.1 Fabric and Stitch Selection

Forces and motions produced by the FFMS are determined by the relative magnitude of stored energy generated by the elastic tubes and the fluid pressure. To achieve the desired dynamic range of forces and motions, the axial stretchability of the fabric conduit should be maximized, while the radial expansion of the elastic tube in the operating range of fluid pressures should be minimized. A firm circumferential constraint is needed to ensure that stresses due to the fluid are directed along the axis of the tube and do not result in the tube expansion. Based on these criteria, an ideal fabric structure should possess negligible stiffness in the axial direction of the tube. This can be achieved through the use of non-stretchable fabrics, such as cotton weaves, in tandem with the wrinkling process described above. Stretchable fabrics may be used together with across-tube stitching, which can provide a radial constraint. Stretchable fabrics are uniaxially elastic (two-way stretch) or biaxially elastic (four-way stretch). These fabrics are often made of elastic fibers such as Spandex, that are spun into stretchable yarn, and integrated along weft, warp, or both directions of the weave, yielding one- or two-way stretch fabric, respectively. Alternatively, either elastic or non-elastic fibers may be used to create a knit. In a knit, stretchability depends on the design of the looping structure. This typically results in biaxial stretchability. The axial stretchability of FFMS fabric structures using stretchable fabrics can also be improved through the application of wrinkling, if required.

The routing of stresses or strains within the FFMS is achieved via fabric conduits formed from stitching applied to the fabric sheets. The stitching involves three main factors: thread material, stitch type, and stitch pattern. Near the elastic tubes, the stitching permits the fabric to impose a circumferential constraint. This ensures that fluidic stress or strain is directed along the axis of the tube (see Section 3.2). Two design criteria are involved. First, the stitching must be strong enough to constrain the fabric conduit around the elastic tubes over the entire operating regime of the FFMS. Second, it must accommodate large strains along the axial direction

of the tube. Different stitch designs and fabric choices can be used. Their selection depends on application requirements. To illustrate this, we compare three different combinations of fabric type and stitch design in Table 3.1, which shows that combinations yield distinct patterns of stretchability in the assembled FFMS (Table 3.1, blue arrows).

If a wrinkling step is omitted, a two-way or four-way stretchable fabric must be used in order to accommodate the axial strains that are required for a FFMS actuator to function. A side or cross stitch pattern may be used with either stretchable or non-stretchable fabrics, with or without wrinkling constraints (Table 3.1, red arrows). Cross stitching is preferred for use with four-way stretch fabrics, because it minimizes undesired radial expansion (i.e. ballooning) of the elastic tubes. Significant ballooning only occurs if side stitch patterns are used. Commercial two-way stretch fabrics (which are typically knits) admit fabric extension in all directions, and would yield undesirable ballooning unless a cross stitch is used. This can result in failure (see Fig. 3.7C). When non-stretchable fabric is used, wrinkling must be applied. In such cases, the range of extension is determined by the extent of wrinkling. In practice, we have designed FFMS actuators capable of greater than 300% strain using this technique. If a cross stitch is used, the amount of wrinkling is limited due to the increased fabric constraint imposed by the cross stitch, thus limiting extensibility.

Among thread types, inextensible high-strength nylon thread can provide a stiff constraint via a fine thread. There are several possible combinations of stitch designs, fabric stretchability, and wrinkling modes, which together yield distinct patterns of stretchability in the assembled FFMS (Table 3.1, blue arrows; longer arrows imply larger stretchability). When side stitches are used, zig-zag stitching is recommended for use with stretchable fabrics in order to preserve the fabric elasticity. Straight stitching is appropriate for non-stretchable fabrics, where stretching is accommodated by wrinkling. To maximize stretchability in the axial direction, and minimize radial expansion, two-way stretch fabric with side stitches and wrinkling is optimal, although non-stretch fabric with side stitches and wrinkling is also effective. Figure 3.4A

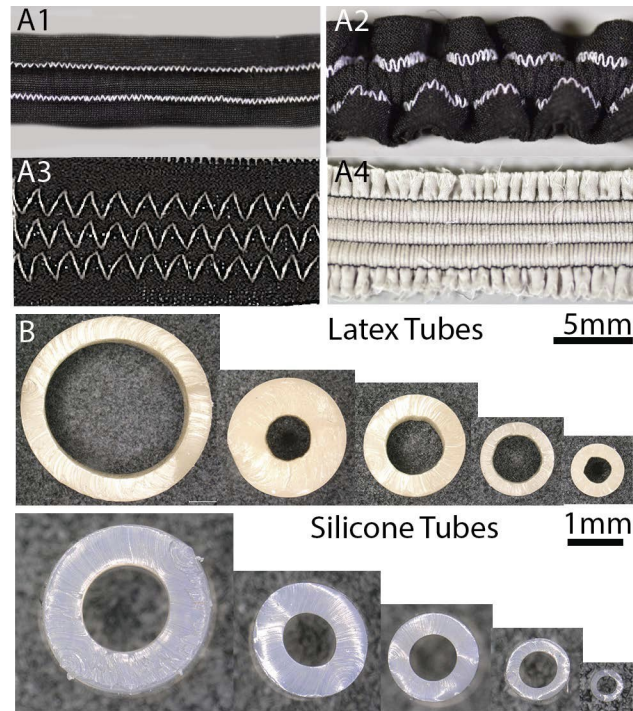


Figure 3.4: A1-A4. Four representative FFMS prototypes illustrating different fabric and stitch combinations. A1. Two-way stretch fabric using zig-zag side stitches without wrinkling. A2. Two-way stretch fabric using zig-zag side stitches with wrinkling. A3. Two-way stretch fabric using zig-zag cross stitches without wrinkling. A4. Non-stretch fabric using straight side stitches with wrinkling. B. Cross section images of several commercially available tubes made of latex (top) and silicone (bottom, note the smaller scale). The outer diameter of the silicone tube can reach sub-millimeter scales.

shows four prototypes with different combinations of fabrics and stitchings.

3.4.2 Tube and Fluid Selection

The elastic tube may be any elastomer that is compatible with the working fluid. For high force applications, tubing materials with high elastic modulus and high extensibility would be preferred. The tube can have any diameter and length compatible with the fabrication process, including very fine silicone tubing [228], or larger diameter latex rubber tubing. There are many options among commercially available tubes (Fig. 3.4B). We present a model of the actuator performance accounting for effects of tube size and material properties in Section 3.5




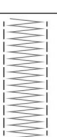
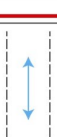
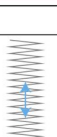
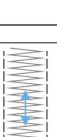
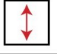
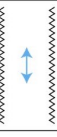
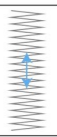
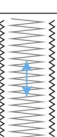
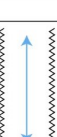
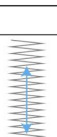
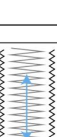


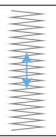
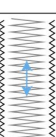
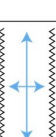
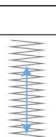
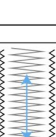
Stitches	No Fabric Wrinkling			With Fabric Wrinkling			Advantages	Disadvantages
	Side Stitch	Cross Stitch	Side + Cross	Side Stitch	Cross Stitch	Side + Cross		
Non-stretch 							No radial expansion.	Wrinkling required for stretchability.
Two-way stretch 							Wrinkling not required for stretchability.	Difficult to align layers of fabrics accurately.
Four-way stretch 							Wrinkling not required for stretchability.	Must use cross stitch to prevent radial expansion.
Advantages	Easy to insert tube.	Better constraint in radial direction.	Best constraint in radial direction and between stitches.	Easy to insert tube. Large wrinkling possible (allowing large elongation).	Better constraint in radial direction.	Best constraint in radial direction and in between stitches.		
Disadvantages	Slight radial expansion exists, especially for knit fabrics.	Difficult to insert tube. Tube may balloon between stitches.	Difficult to insert tube.	Permits radial expansion, especially for knit fabrics.	Difficult to insert tube. Limited wrinkling.	Difficult to insert tube. Limited wrinkling.		

Table 3.1: Stitch and fabric selection for FFMS actuators. Red arrows represent the stretch directions of the fabrics, and blue arrows represent the stretchability of the assembled FFMS. Longer arrows denote greater stretchability. The configuration in the red box is used for most prototypes in this work.

and experimental results for several examples in Section 3.6.

Different working fluids may be used, depending on the performance requirements, materials, and operating criteria. In hydraulic operation, FFMS can use incompressible fluids such as oils or waters, as illustrated in many of our experiments. This makes it possible to control the applied volume in the actuator and hence the actuator length, due to the circumferential constraints, and renders the quasi-static response of the actuator very simple, at the expense of increased viscosity and mass. (However, the fluid mass in many of our prototypes is on the order of a few grams). Low viscosity liquids offer improved actuation speed and efficiency. Pressures in prototypes described here are lower (less than 0.75 MPa) than those used in industrial hydraulics (e.g., 20 MPa). At such low working pressures, failures typically involve, at most, fluid leakage.

In pneumatic operation, compressible fluids such as air or other gases may be used. This can minimize mass and viscosity. Over the operating range tested in our experiments, pneumatic operation leads to increased hysteresis, lower efficiency, and increased response latency (Fig. 3.6F). Further discussion of hydraulic and pneumatic actuation methods are provided in the literature [84, 136].

3.5 Analytical Modeling

As our experiments demonstrate, FFMS actuators may be operated to yield a variety of motion or force patterns. The simplest involve the generation of axial forces through a parallel configuration of N elastic tubes. Such a structure is similar to parallel muscle sheet architectures in biology. A net external force, F_{ext} , is produced by the actuator due to the stretching of the tubes, which produce a net elastic force, F_{el} . The fabric can also contribute an elastic force, F_{fab} . The force F_{ext} exerted by the actuator decreases with increasing fluid pressure, p , due to the axial force, F_{fluid} , generated via the fluid pressure. Dissipative forces, F_d , include viscosity

and friction. Combining these factors, one can model force production as

$$F_{ext} = F_{el} + F_{fab} - F_{fluid} + F_d \quad (3.1)$$

The dissipative forces, F_d , include hydrodynamic flow resistance, $F_{d,hyd}$, and dry friction at the tube fabric interface, $F_{d,dry}$

$$F_d = F_{d,hyd} + F_{d,dry} \quad (3.2)$$

$F_{d,hyd}$ can be estimated from Newton's Law of viscosity [295],

$$F_{d,hyd} = \tau \mathcal{A} = \mu \rho \frac{\partial u}{\partial y} 2\pi r_i L \quad (3.3)$$

where τ is the shear stress of the fluid acting on the inner wall of the tube, \mathcal{A} is the contact area between the fluid and tube, μ is the kinematic viscosity, ρ is the fluid density, u is the flow velocity, $\partial u / \partial y$ is the rate of shear deformation, r_i is the tube inner radius, and L is the tube length. The dry friction $F_{d,dry}$ is given by

$$F_{d,dry} = \mathcal{F}_N \zeta = N \zeta p A_{tf}, \quad A_{tf} = 2\pi r_o L \quad (3.4)$$

where N is the number of tubes, ζ is the friction coefficient, \mathcal{F}_N is the normal force between tube and fabric, $A_{tf} = 2\pi r_o L$ is the area of the tube-fabric interface, r_o is the tube outer radius, and p is the fluid pressure. We refer to such dissipative forces when interpreting measurements of actuator efficiency and hysteresis.

In many embodiments, including the wrinkling construction described above, there is little relative motion of tube and fabric, so $F_{d,dry}$ may be neglected. In quasi-hydrostatic operation, the forces due to flow resistance $F_{d,hyd}$ may also be neglected. For fabric that is wrinkled or

stretchable, the fabric force, F_{fab} may also be neglected.¹ Assuming that these conditions hold and that the FFMS operates in a linear elastic regime with elastic modulus E and true strain $\varepsilon = \log(L - L_0)$, the net external force exerted by the actuator is:

$$F_{ext} = F_{el} - F_{fluid}, \quad (3.5)$$

where

$$F_{el} = NE\varepsilon A_{tube} = NE\varepsilon \pi(r_o^2 - r_i^2) \quad (3.6)$$

$$F_{fluid} = NpA_{fluid} = Np\pi r_i^2 \quad (3.7)$$

The result may be written

$$F_{ext} = N(E\varepsilon A_{tube} - pA_{fluid}) \quad (3.8)$$

The external force F_{ext} , reaches its maximum value if the fluid pressure $p = 0$,

$$\max_p F_{ext} = F_{ext}|_{p=0} = NE\varepsilon A_{tube}. \quad (3.9)$$

The force can be maximized by increasing the net cross section area, NA_{tube} , the elastic modulus, E , or the operating range of strains, ε . Increasing the strain may be accomplished via pretensioning, which is also aided by wrinkling. The model given by Eq. 3.8 predicts that F_{ext} decreases linearly with the increase in pressure, p . As our experiments demonstrate, despite the simplifications involved in this model, it provides a good approximation to the behavior of FFMS actuators (Sec.3.6, Fig.3.5D4 and G4).

¹Selecting a stiffer fabric, or adding non-fluidic elastic fibers to the structure, increases forces, but does not necessarily improve actuator performance, because the added elasticity does not impart any added strength to the tube that would enable it to operate at higher pressures.

The minimum external force magnitude occurs when the pressure is maximum, p_{max} . Since pressure fluctuates in dynamic operation, we take this to be the maximum quasi-hydrostatic pressure. If the operating range of forces extends down to $F_{ext} = 0$, the required maximum pressure, p_{max} is determined by the ratio of tube and fluid areas and tube elasticity,

$$p_{max} = \frac{E\varepsilon A_{tube}}{A_{fluid}}. \quad (3.10)$$

where A_{tube} is the inner cross section area of the tube. Conversely, if p_{max} is the maximum intended pressure, the tube geometry, strain, and elasticity should be selected to ensure this expression holds.

In another configuration, the actuator may be operated as a muscular hydrostat [296]. For unsupported (isochoric) operation, or for negative contraction forces, $F_{ext} < 0$, the muscle force may be produced by applying a pressures higher than the one specified in (3.10). In the absence of an external load force, $F_{ext} = 0$, a pressure p applied to hydrostatic configuration can yield a displacement, δL , with respect to the initial tube length, L_0 ,

$$\delta L = L_0 \exp\left(\frac{p}{E}\right) - L_0 \quad (3.11)$$

Such modes of operation are analogous to muscular hydrostats in biology, such as the tongues of many animals, or the elephant trunk.

FFMS actuators may also be used to compress enclosed objects. If an actuator with pressure $p > 0$ perfectly encloses a rigid cylindrical object, compressive pressures are generated as the fluid pressure p is reduced. For a cylinder of radius $r_c \gg h$, where h is the effective FFMS thickness, the thin-walled vessel equation, $\sigma_\theta = F_{ext}/A_M$ relates the compressive pressure, p_c (the force per unit area exerted on the cylinder, which may also be approximated by the internal pressure p), to the net effective cross section area, A_M , the radius, and the thickness. Solving

for p_c yields

$$p_c = \frac{hF_{ext}}{r_c A_M}. \quad (3.12)$$

3.6 Results

To evaluate the FFMS actuators, we performed mechanical testing in several experimental configurations and operating modes, using several FFMS actuators of different sizes. We also realized functional prototypes for wearable devices, haptic feedback, and soft robotics.

3.6.1 Mechanical Testing

We used three testing configurations to measure axial forces, compressive forces, and axial displacements. We complemented these evaluations with measurements of actuation efficiency and durability over thousands of cycles.

Mechanical testing was performed using two different prototypes (Fig. 3.5). The first comprised a smaller surface area FFMS with three elastic tubes (Fig. 3.5B) of dimensions 196 mm (length), 25.2 mm (width), and 4.7 mm (thickness). The fabric channel width was 5 mm. The active area spanned by the elastic tubes was measured to be 122.4 mm in length with no applied pressure. The tubes were connected via a manifold to the fluidic power source. We used latex tubes with outer diameter 3.2 mm and inner diameter 1.6 mm.

The second prototype consisted of a larger surface area FFMS with ten parallel elastic tubes (Fig. 3.5C). The tubes in this prototype were connected in series, yielding a single fluid port. The dimensions of this prototype are: 148.4 mm length, 156.6 mm width, 4.9 mm thickness, and 5 mm channel width. The active region spanned by the elastic tubes (neglecting unwrinkled end sections) was 84.1 mm.

In all experiments, distilled water was used as a working fluid. In a separate experiment, we compared the operating efficiency of water (hydraulic mode) and air (pneumatic mode).

Axial Force Testing

Axial force testing was performed using an isometric test configuration and apparatus (Fig. 3.5A). One end of the FFMS was fixed using a clamp fixture while the other end was attached to a stationary force gauge (M5-20, Mark 10). Fluid was supplied via three 10 mL syringes (inner diameter around 15 mm) driven by a displacement-controlled linear motor (A-BAR300BLC-E01, Zaber) and custom fixture. The syringe displacement was measured via an optical encoder (S6S-1000-IB, US Digital). Fluid pressure was measured using a fluid sensor (SSC Series Sensor, Honeywell) positioned near the actuator port. The actuator was pre-pressurized to approximately 650 kPa and fixed in an isometric configuration with sufficient tension to ensure that the actuator remained stationary.

The FFMS was driven via sinusoidal fluid displacement, at frequencies from 0.2 to 0.4 Hz. This yielded time-varying (measured) pressures ranging from 200 kPa to 750 kPa. The signals were recorded synchronously using a computer-in-the-loop system (QPIDE, Quanser, Inc., with Simulink, The Mathworks, Inc.). The instantaneous displacement of fluid volume was calculated from the syringe displacement and geometry.

The FFMS performance was consistent over repeated cycles. The generated axial force decreased monotonically with the increase of fluid pressure or volume (Fig. 3.5D-G). The range of forces F_{ext} (Fig. 3.5D2-D4) generated by the FFMS was 13 N (approximately 4.3 N per tube). This corresponded to a fluid volume range of 1.78 mL. The volume-force and the volume-pressure curves both exhibit hysteresis, indicating that energy was lost on each working cycle. We discuss such losses in the efficiency measurements below.

We compared the results with predictions of the analytical model (Eq. 3.8). To compute these predictions, we measured the Young's modulus of the elastic tube. Using tensile testing, we determined the Young's modulus to be 1.1 MPa for true strains, ϵ , between 0 and 1. Other parameters used for model prediction were $A_{tube} = 5.9 \times 10^{-6} \text{ m}^2$, $\epsilon = 0.8$, and $A_{fluid} = 7.7 \times$

10^{-6} m². The number of tubes was $N = 3$ for the first and $N = 10$ for the second. The experimental results and model predictions were in close agreement during slow actuation (Fig. 3.5D4). For different frequencies, ranging from 0.2 Hz to 5.0 Hz, the FFMS actuator responded in a qualitatively similar manner (Fig. 3.5E,F). The response became somewhat more complex at the highest frequencies. This can be explained by the inherent dynamics of fluid-elastomer-fabric systems.

We obtained results when testing the larger FFMS actuator with 10 parallel tubes (Fig. 3.5G1-G4). In this case, the FFMS produced forces ranging from 0 to 50 N with respect to the decrease of fluid volume (from 0 ml to 6 ml) or fluid pressure (from 620 to 180 kPa). The FFMS performance was also consistent over repeated testing cycles. Each of the ten tubes produced about 5 N. For the smaller prototype, analytical modeling yielded qualitatively good agreement with the experimental results (see Fig. 3.5G4). The results revealed a slightly nonlinear and hysteretic relationship between pressure and force, with modest discrepancies from the linear model predictions. The hysteresis can be attributed to the fact that the tubes were connected in series, requiring the fluid to traverse a much longer path. This also indicates that series connections of elastic tubes, which simplify assembly, may introduce modest response latency. From the experimental data, we estimated the latency to be approximately 100 ms at 0.2 Hz. The volume-pressure and volume-force relationships also exhibited hysteresis, indicating that energy was lost on each cycle. For small changes in fluid volume, from 0 to 2 ml, the change in force with fluid pressure was more gradual. However, the pressure-force relationship remained approximately linear.

Compression Testing

We evaluated the compression force, $F_c = p_c A$, produced using an FFMS prototype with 3 channels (Fig. 3.5H), where p_c was the compressive pressure. The actuator was wrapped around a cylinder in an isometric test fixture using a force sensor (ATI Nano17, ATI Industrial

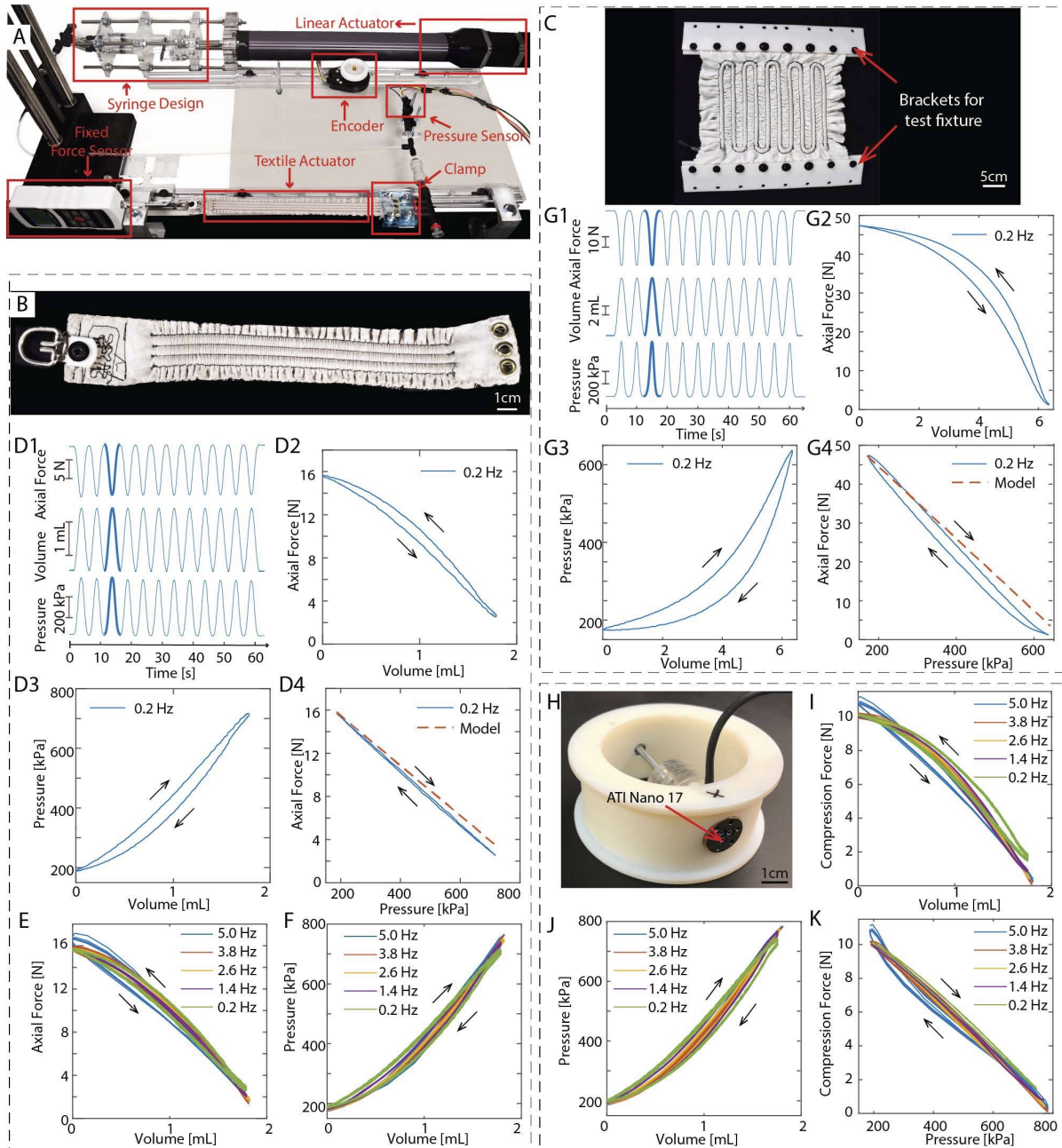


Figure 3.5: Force testing. A. Apparatus for axial force testing. B. 3-channel FFMS. C. 10-channel FFMS with brackets for test fixture. D-F. Results for the 3-channel FFMS demonstrated consistent performance over repeated actuation, similar behavior at different actuation speeds, and surprisingly good agreement with the analytical model. G1-G4. The larger, 10-channel FFMS yielded similar results to those that we obtained with the 3-channel device. The force range was 0 to 50 N. The longer fluid circuit yielded slightly greater response latency. H. Compression force testing apparatus. I-K. The device produced compressive forces of 0 to 10 N, as 0 to 2 mL of fluid was withdrawn. The results were consistent with our analytical model, and varied little with actuation speed.

Automation). The contact area, A , was 209 mm^2 . We varied the applied fluid volume from 0 to 2 mL (Fig. 3.5I). This yielded compressive forces ranging from 0 to 10 N. These values were consistent with our predictions based on the range of axial forces, F_{ext} , produced by the same device: at fluid pressure $p = 250 \text{ kPa}$, we measured the the axial force to be $F_{ext} = 13 \text{ N}$. The model predicts a compressive pressure $p_c = 44.5 \text{ kPa}$ for our text fixture configuration, which implies $F_c = p_c A = 9.3 \text{ N}$, in close agreement (error $< 5\%$) with our measurements (Fig. 3.5K). The results varied little for speeds below 5.0 Hz.

Displacement

We performed displacement testing using a configuration that was similar to the one we used in axial force testing (Fig. 3.6A). For testing, a constant force retractor (Force 4.45N, model 61115A2, McMaster-Carr) was used to replace one of the isometric constraints in the fixture described above. An optical encoder was used to record the position for the distal end of FFMS. Displacement increased with increases of fluid volume or fluid pressure. The results revealed consistent displacement across repeated actuation (Fig. 3.6B1). As predicted, the relation between volume and displacement was almost perfectly linear, reflecting the incompressibility of the medium and radial constraint provided by the textile (Fig. 3.6B2). When the fluid volume reached 4.5 mL, the FFMS attained a length increase of 70% (from 122.4 to 207.4 mm). In this case, the volume-pressure and pressure-displacement relationships exhibited greater hysteresis. We attributed this to the deformation of the nonlinear elastic materials at large displacements or high fluid volumes (Fig. 3.6B3-B4). The analytical model correctly predicted the observed ranges of displacement, but because the model was quasi-static, it did not capture hysteresis. We plan to develop a dynamic model that can capture such effects in future work. We also observed that the performance of FFMS remained consistent at higher driving frequencies. The results for the larger FFMS with 10-channels were similar to those that we observed for the smaller FFMS (see Fig. 3.6E1-E4).

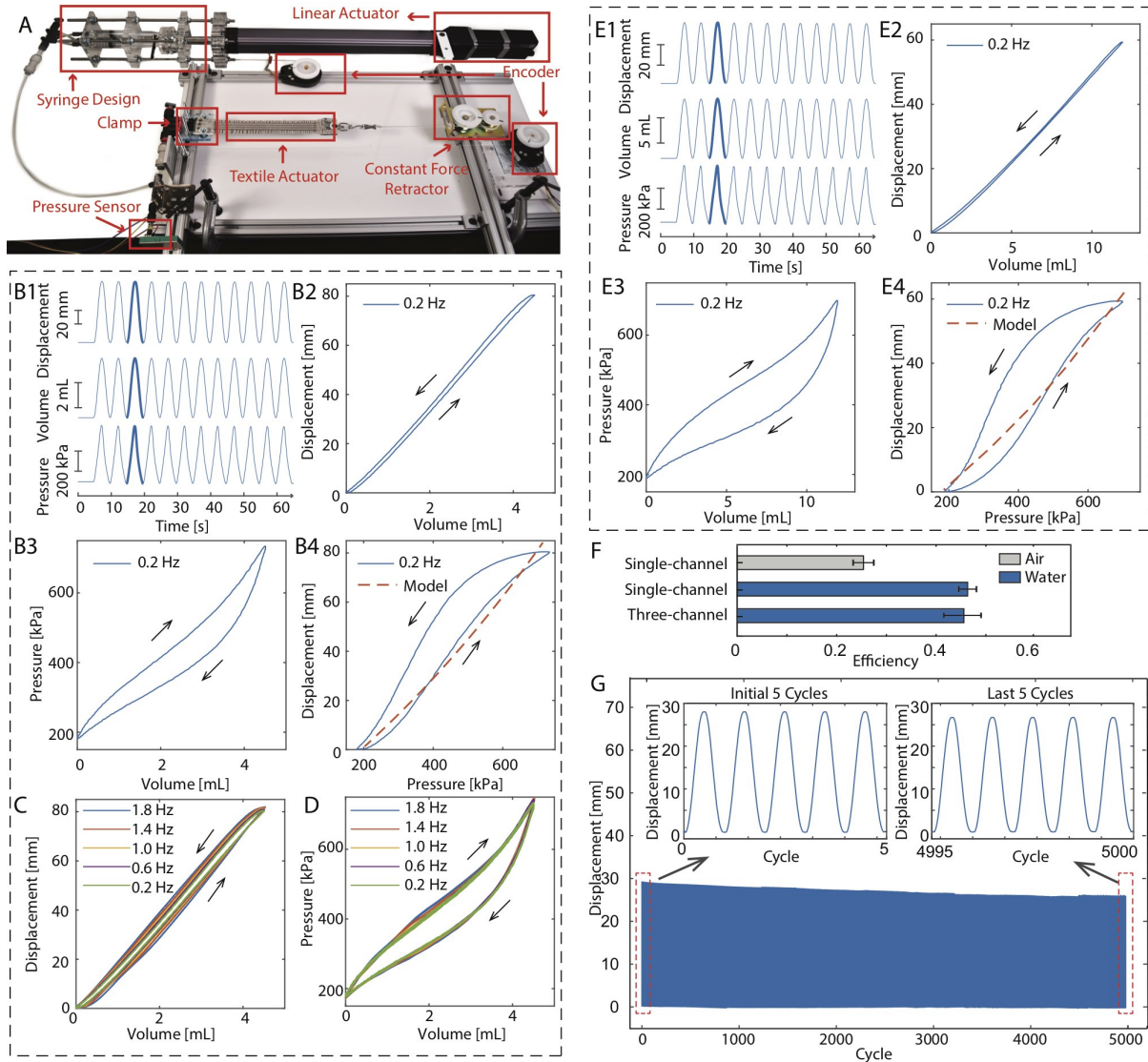


Figure 3.6: Displacement and compression testing. A. Apparatus for displacement testing. B-D. Results for the three-channel FFMS were consistent over repeated actuation. Similar behavior was observed for different actuation speeds. The pressure-displacement relationships were consistent with analytical predictions, despite dynamic effects, including hysteresis (see text). E1-E4. Results for the larger, 10-channel FFMS were similar to those for the smaller FFMS. F. Hydraulic operation with water was more efficient than with air. Similar efficiencies were measured for actuators with one and three channels. Error bars: 95% confidence intervals. G. Durability testing revealed consistent performance over 5000 actuation cycles. A 5% reduction in displacement was observed after this period, which we attributed to initial actuator relaxation.

Efficiency

We computed the energetic efficiency as the ratio of the input energy and the mechanical work over one working cycle. We measured this for a single channel FFMS with different working fluids, comprising water (hydraulic mode) and air (pneumatic mode). The FFMS (rest channel length and width 62 mm and 10 mm, tube outer and inner diameter 6.4 mm and 3.2 mm) raised a load of mass m against gravity at speed of $v = 0.1$ mm/s to height h . Input work, W_{in} , was computed as the sum of (positive) mechanical work, W_+ , performed when extending the actuator, and (negative) work, W_- , performed when withdrawing the fluid (during lifting), yielding $W_{in} = W_+ + W_-$. The energy efficiency, R , was $R = U_g/W_{in}$, where $U_g = mgh$ was the output work, or change in potential energy of the mass over one working cycle. The results were averaged over five working cycles in which the actuator returned to its initial state after displacing the mass.

The actuator efficiency was higher in hydraulic operation than in pneumatic operation (efficiency $R = 0.46$ vs. 0.25 , see Figure 3.6F). This can be explained by the additional thermodynamic losses arising from the compression of air. Other losses included those due to fluid viscosity, friction, and thermoelastic heating of the elastomer. Prior authors[263] computed the efficiency of a soft fluidic actuator by considering the work W_- performed when withdrawing the fluid as an output of the system, yielding $R = (U_g + W_-)/W_+$. However, such a calculation leads to erroneous results, since a system can be designed to make the efficiency arbitrarily close to 1 by adding and removing an increment of fluidic energy at the input without any additional production of useful work (for example, this can be achieved by adding a reservoir at the input). Applying this method to our actuator, we obtained a (erroneous) higher efficiency of $R = 0.83$ in hydraulic operation.

We also evaluated the efficiency of a hydraulically driven three-channel FFMS (rest channel length and width 44 mm and 5 mm, latex tube outer and inner diameter 3.2 mm and 1.6 mm).

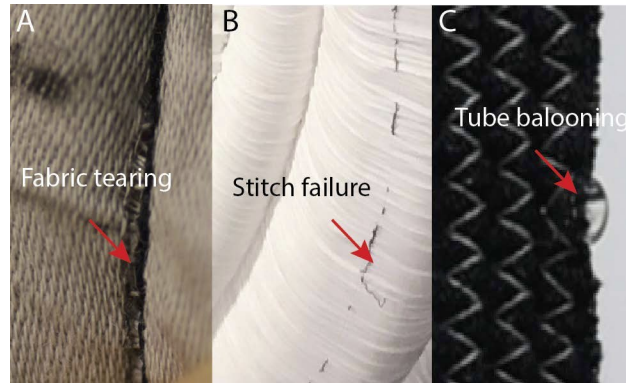


Figure 3.7: Examples illustrating failure modes. A. Fabric tearing at stitch locations. B. Stitching failure between fabric conduits. C. Tube ballooning between stitch locations.

The results were thus similar to those that we obtained with the single channel device ($R = 0.45$, based on five repeated measurements).

Durability

We evaluated the durability of FFMS (three-channel prototype (Fig. 3.6G)) by actuating it over 5000 cycles to a maximum amplitude of 28 mm. The behavior was similar throughout testing. A 5% reduction in displacement was observed after this testing cycle. We attributed this to initial relaxation of elastic tube and fabric material. The relatively consistent performance may be attributed, in part, to the operation of the tube within the elastic regime, which resulted in little plastic yielding.

Failure Modes

Actuator failure can arise due to improper selection of material, assembly, or to the operation regime. Here, we highlight three failure modes observed in our prototypes during the experiments (Fig. 3.7). As the fluid pressure increases, the elastic tubes, enclosed fabrics, and stitches are subjected to the increase of stresses. This can result in fabric tearing, stitch failure, or ballooning of the elastic tube. Fabric tearing can be minimized through the use of high-

strength or dense fabrics, ideally with thread counts exceeding 300. One failure mode was associated with large cross section elastic tube. For fixed fluid pressure, p , the force per unit length, t_s , exerted on the stitch is proportional to pr_o , where r_o is the tube outer radius. As the tube radius is increased, stitch failure will occur when t_s exceeds a critical value. Such stitch failures may be minimized through the use of high strength threads, composed of materials such as polyester or Poly-paraphenylene terephthalamide (Kevlar), through multiple (double or triple) stitching, and through the use of stronger fabrics. Another failure mode arose from insufficient radial constraints on the elastic tube, which yielded radial expansion or ballooning of the tube. We observed this to occur due to imperfections in side stitching, due to gaps between cross stitches, or due to the use of four-way stretchable fabrics. Such failures may be mitigated via uniform stitching, by avoiding four-way stretch fabric, and, where two-way stretch fabrics are used, via zig-zag stitching with fine pitch.

3.7 FFMS Embodiments and Applications

FFMS actuators are versatile, and capable of actuating a variety of bodies or structures of different scales. They can be designed to realize multiple modes of actuation that are suited to applications in robotics, healthcare, and wearable technologies, as we illustrate below.

3.7.1 Scalability

FFMS actuators can be used to realize devices of different sizes, ranging from millimeter to meter scale devices. The dimensional parameters of the FFMS include the lengths, L , of the elastic tubes, their inner and outer radii, r_i and r_o , and number, N , of elastic tubes. These parameters determine the stitched conduit width, fabric length, and fabric width. For fixed material, tube configuration, and strain, the maximum force is determined by $r_o^2 - r_i^2$. The maximum elongation, ΔL , is proportioned to L . The required maximum pressure is scale-invariant (Eq.



Figure 3.8: FFMS actuators are readily scaled to small and large sizes. (A,B) A large example, consisting of a 34.0 mm thickness FFMS (A: Top view, B: Side view), shown in contracted state, was sufficient to lift 15 kg (Fig. 3.10). (C-F) A small example, in contracted (C,D) and extended (E,F) states; the thickness when extended is 1.0 mm. The large and small actuators were fabricated using the same general process. A penny is used to illustrate the relative scale.

3.10). Commercially available elastic tubes can be used with widely varying radii, r_i, r_o , ranging from less than 1 mm to greater than 30 mm. We fabricated several prototypes to explore the scaling of FFMS actuators (Fig. 3.8) for different applications (see Fig. 3.10). Small, low-profile FFMS may be used in miniature biomedical or wearable devices, while large FFMS can be employed in higher force applications, such as orthotics or soft robotic construction machines.

3.7.2 Multimodal Actuation and Shape Change

Composite or multi-actuated FFMS can yield dynamic, multimodal motion or shape change. Here, we show how FFMS actuators can be used to realize in-plane rotation, out-of-plane bending, and biaxial bending motion (Fig. 3.9).

In-plane rotation may be realized by differentially driving multiple fluid channels to steer an actuator. Such motions may be used in soft biomedical devices [297]. In one embodiment, a 3 cm FFMS is driven via 3 elastic tubes that are independently controlled. When one of three lateral tubes is depressurized, a large-amplitude planar rotation can be achieved, yielding turning angles approaching 90 degrees (Fig. 3.9A) due to differential elongation in the three tubes.

Out-of-plane bending motion can also be achieved. We combined a passive layer of stiff fiberglass with an FFMS to produce continuous out-of-plane bending. In one embodiment, a fiberglass sheet (thickness 0.38 mm) was pre-patterned via laser engraving and stitched to the FFMS (Fig. 3.9B). Pressurizing the FFMS yielded large-amplitude bending, exceeding 180 degrees. Selecting the bending stiffness of the passive layer makes it possible to tune the actuator stiffness and generated torques. Such a configuration may be used in wearable or soft robotic applications [298].

If two FFMS layers are oriented in complementary directions, biaxial bending, or 3D shape change, may be generated. To demonstrate this capability, we stitched two 7-channel FFMS layers together in orthogonal orientations (Fig. 3.9C). The whole composite structure remained flat when the applied fluid pressure was equal in both FFMS layers. When the applied fluid pressures was unequal in each layer, bending motion was initiated about each of two orthogonal in-plane axes. Biaxial bending yielded 3D or hyperboloid shapes.

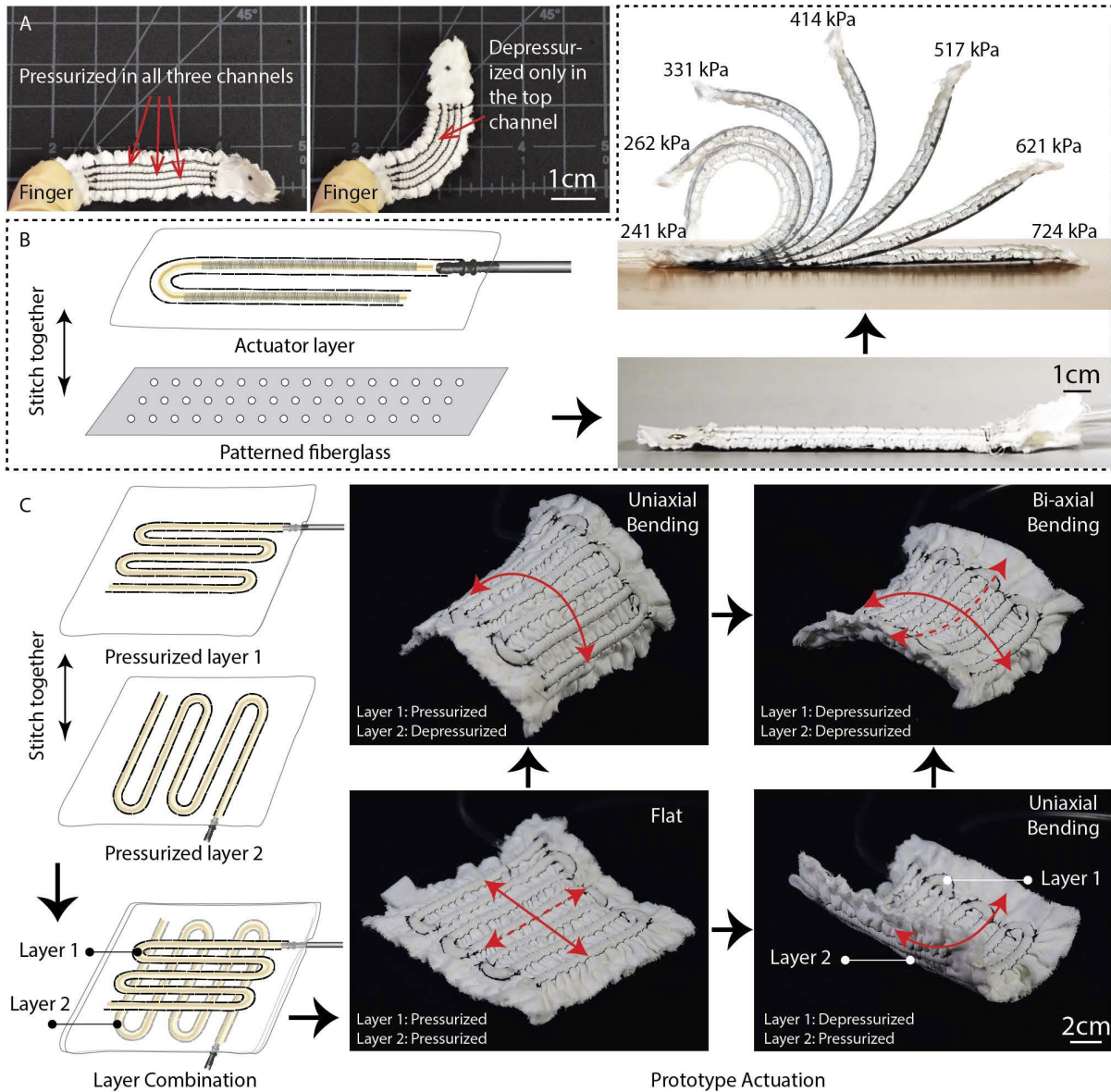


Figure 3.9: Composite or multi-actuated FFMS can realize dynamic, multimodal bending motion or shape change. (A) In-plane rotation realized by differential pressurization of multiple fluid channels. (B) Out-of-plane bending is realized by combining an FFMS with a second, passive layer with specified bending stiffness. (C) Biaxial bending is realized via a composite of two, orthogonally oriented FFMS sheet actuators.

3.7.3 Device Configurations and Applications

FFMS sheets may be used to realize motion or provide forces in applications including soft robotic motion control, wearable actuators, assistive devices, and compression garments. Some advantages of these devices include their low cost, flexible design, facile fabrication, ability to conform to curved structures, to achieve multimodal actuation at a variety of scales, to produce large work densities, and achieve fast response times, exceeding the capabilities of many other technologies. We realized several examples (Fig. 3.10 and Supplementary Video). Miniature FFMS can be used to produce linear motion, to provide skin stretch haptic feedback, or to provide compression forces to small body parts, such as a finger (Fig. 3.10D,E). We also fabricated a 3-channel FFMS that can contract from 10.5 mm in to 5 mm in length, lifting a mass of 500 g, while producing engineering strains up to 110% (Fig. 3.10A). Other compact devices can be used to apply constriction to small body parts (Fig. 3.10D, showing an FFMS of 1 mm thickness). They can also be used to realize wearable devices for providing haptic feedback via skin-stretch, yielding highly palpable tactile sensations (Fig. 3.10E).

Larger scale FFMS actuators can perform greater mechanical work. We fabricated a 10-channel device that can lift a 3 kg mass (Fig. 3.5C). This was 115 times higher than the actuator mass of 26 g (Fig. 3.10B, left). We realized a larger FFMS actuator with 3 tubes (inner latex tube of diameter 25 mm, outer diameter of 32 mm), which lifted a 15 kg mass at fluid pressures less than 276 kPa (Fig. 3.10B, right). This demonstrates how FFMS actuators can be used to perform significant mechanical work.

FFMS actuators hold promise for wearable applications such as assistive devices. We employed a configuration similar to the one we used for out-of-plane bending (Fig. 3.9C) in order to provide assistive flexion forces for two fingers during grasping (Fig. 3.10C). In this application, we pre-tensioned the fiberglass sheet layers such that the device performed flexion when pressurized and extension when depressurized (Fig. 3.10C, bottom inset). The force was suffi-

cient to open and close the hand for grasping. Such a device is useful for assisting conditions such as stroke that can often lead to chronic flexion of the fingers, preventing grasping and adversely affecting many activities of daily living [298, 4].

FFMS devices can also be used to provide compression to larger areas of the extremities. Such compressive forces are of interest for haptic feedback [17], for preventative compression therapy in deep vein thrombosis [299], for musculoskeletal recovery via blood flow restriction therapy [300, 301], for lymphatic or cardiovascular circulatory conditions [302, 303], or other biomedical devices [304, 69, 70, 71]. We created an upper limb compression device based on an FFMS arm band and measured the resulting compressive pressures using thin-film force sensors (FlexiForce A201, Tekscan Inc.). Withdrawing up to 3 mL of fluid from the band yielded uniform compression of up to 12 kPa, similar to pressures provided by blood pressure cuffs. We also demonstrate a wearable compression garment for the lower limb (Fig. 3.10G). This device is constructed from 3 elastic tubes arranged in three independently controlled sections (Fig. 3.10G, dashed boxes). Supplying different fluid pressures to different sections yields varied compressive pressures across the limb. This can be used to provide bulk compression to the limb, which is useful in recovery from some injuries or in disease treatment. It can also be used for providing dynamic peristaltic motions that can be used for undulatory massage to augment lymph and blood flow. Such devices can meet the needs for pressure garment therapy [69], lymphedema treatments [70], or venous closure treatments [71].

3.8 Conclusions

This paper presents a new family of soft actuators that we refer to as Fluidic Fabric Muscle Sheets, inspired by sheet-like biological muscles. These devices comprise fabric layers with integrated hydraulic transmissions formed from arrays of hollow elastic tubes routed in patterned fabric conduits. We demonstrate how to design and fabricate these devices using



Figure 3.10: Demonstrations. (A,D,E) Miniature soft actuators for linear motion control or compression, capable of (A) lifting a small mass, (D) compressing small tissue areas, or (E) providing tactile feedback via skin stretch. Inset: Skin stretch was easily perceived. (B) FFMS actuators can perform large mechanical work. A 10-channel device lifts a 3 kg mass. A 3-channel structure (inner tube radius 2 cm) lifts a 15 kg cinder block and chain at pressures less than 276 kPa. (F,G) FFMS can be used for compression garments for healthcare, training, and haptics. (F) A compression band yields uniform pressure on the upper limb, easily matching pressures provided by blood pressure cuffs. (G) A compression garment for the lower limb comprises three independently addressable sections (dashed boxes). Pressure variations can yield peristaltic motions suitable for undulatory massage in therapies for lymphatic and blood circulation [69], such as lymphedema [70] or venous closure [71].

facile methods that build on apparel engineering techniques including computerized sewing processes. These devices are stretchable, conformable, safe, efficient, and scalable. They are applicable to small, millimeter-scale actuators, and large meter-scale devices, and can yield forces exceeding 150 N, more than 115 times their weight, with engineering strains greater than 100%. Laboratory prototypes perform consistently in testing over thousands of cycles. Their performance can be predicted via simple mechanical modeling, aiding design. As we show, such FFMS actuators hold promise for applications in soft robotic motion control and for wearable devices for haptics, healthcare, and assistive technologies. The compressions they can produce meet requirements for several healthcare applications.

These results also point to several promising areas for future investigation. The fabrication methods we describe are simple and flexible, but further research is needed in order to align them with manufacturing techniques. FFMS actuators prove capable of performance in axial actuation, compression, and multimodal actuation, where dynamic shapes or stresses are enabled by designed routings of fluidic channels. New analytical and computational design methods would facilitate a larger variety of programmable distributions of forces and strains, and would enable greater control over such behaviors. The performance of FFMS actuators depends on the fluidic power source that is used. We highlighted advantages of hydraulic operation. Further research is needed on compact hydraulic power sources. The analytical model we present was effective for predicting actuator performance, but the model is quasi-static. In future work, we plan to extend this approach to account for dynamics, aiding precise real-time control. Our devices employ open-loop control strategies, and the performance of these devices would be further improved through the use of closed-loop controllers relying on fluidic or strain sensors. Intrinsic mechanical or physiological sensors would enable further applications. The demonstration cases we present highlight potential applications in wearable devices for human-computer interaction and virtual reality. We anticipate investigating these in future work. Our demonstrations also point to a range of potential biomedical applications for assis-

tive and therapeutic devices. These merit further research. We have highlighted applications of FFMS actuators in several forms of wearable devices. Our design and fabrication methods are amenable to realizing integrated garments that may be applied to larger body areas, including the realization of whole-body actuated suits or soft exoskeletons, which could greatly aid applications in haptic virtual reality, human space exploration, and rehabilitation. We intend to explore such garments and applications in future work.

Symbols Used

Symbol	Description
F_{fluid}	Axial force produced via fluid pressure
F_{ext}	Axial external load force
F_{el}	Axial elastic force of tubing
F_{fab}	Axial force due to fabric
F_d	Dissipative forces including viscosity and friction
$F_{d,hyd}$	Hydrodynamic flow resistance force
$F_{d,dry}$	Dry friction force at tube-fabric interface
τ	Shear stress of fluid at inner wall of tube
\mathcal{A}	Contact area between fluid and tube
μ	Kinematic viscosity of fluid
ρ	Fluid density
$\frac{\partial u}{\partial y}$	Rate of shear deformation of fluid
r_i	Tube inner radius
L	Tube length
\mathcal{F}_N	Normal force between tube and fabric
ζ	Friction coefficient
p	Fluid pressure
r_o	Tube outer radius
N	Number of elastic tubes
E	Tube elastic modulus
ε	Tube true strain
A_{tf}	Area of the tube-fabric interface
A_{tube}	Cross section area of a single tube
A_{fluid}	Cross section area of fluid inside a single tube
δL	Tube displacement
L_0	Initial tube length
h	Effective FFMS thickness
r_c	Radius of a cylindrical object
A_M	Effective axial cross section area of FFMS

Chapter 4

PneuSleeve: In-fabric multimodal actuation and sensing in a soft, compact, and expressive haptic sleeve

A key consideration in the overarching goal of this thesis is to develop expressive haptic feedback tailored to the human sense of touch. The findings from chapter 3 demonstrate the multimodal actuation capability of FFMS actuators, specifically focusing on the ability to generate compression, skin stretch, and vibration. Inspired by this work, chapter 4 presents PneuSleeve, a soft, compact, and expressive haptic sleeve that can render a broad range of haptic feedback with various distinctive meanings through multimodal actuation. Soft sensors are designed and integrated into a closed-loop controller to ensure consistent compression forces generated across users. This chapter contributes methods to enrich the expressiveness of wearable haptic garments. It also contributes techniques to supply consistent mechanotactile feedback to users with varying body sizes and anatomies.

The content of chapter 4 is reproduced from the following reference [3]:

M. Zhu, A. H. Memar, A. Gupta, M. Samad, P. Agarwal, Y. Visell, S. J. Keller, and N. Colonese, PneuSleeve: In-fabric Multimodal Actuation and Sensing in a Soft, Compact, and Expressive Haptic Sleeve. Proceedings of the 2020 CHI Conference on Human Factors in Computing Systems (ACM CHI), 2020, Association for Computing Machinery, New York, NY, USA, 1–12.

Reproduced here with permission, doi: <https://doi.org/10.1145/3313831.3376333>

Abstract

Integration of soft haptic devices into garments can improve their usability and wearability for daily computing interactions. In this paper, we introduce *PneuSleeve*, a fabric-based, compact, and highly expressive forearm sleeve which can render a broad range of haptic stimuli including compression, skin stretch, and vibration. The haptic stimuli are generated by controlling pneumatic pressure inside embroidered stretchable tubes. The actuation configuration includes two compression actuators on the proximal and distal forearm, and four uniformly distributed linear actuators around and tangent to the forearm. Further, to ensure a suitable grip force, two soft mutual capacitance sensors are fabricated and integrated into the compression actuators, and a closed-loop force controller is implemented. We physically characterize the static and dynamic behavior of the actuators, as well as the performance of closed-loop control. We quantitatively evaluate the psychophysical characteristics of the six actuators in a set of user studies. Finally, we show the expressiveness of PneuSleeve by evaluating combined haptic stimuli using subjective assessments.

4.1 Introduction

We are in the midst of a mobile interface revolution. Developments in battery technology, capacitive touch screens, symbolic input algorithms, and ever growing computation power, have made smartphones ubiquitous. Similar recent developments in optics, display, tracking, and machine perception are enabling the reinvention of mobile interfaces through augmented and virtual reality, AR/VR. Smartphone and head-mounted-display interfaces present complex and expressive visual and audio information, however, most widely-used interfaces capable of rendering haptic, or touch information today leave much to be desired in terms of wearability, and the haptic feedback they offer is often limited to simple vibrations. High-quality human computer interfaces should be capable of rendering a large set of complex and easily discernible haptic feedback, while also not encumbering the user. Ideally, these interfaces should seamlessly integrate into clothing or accessories that users already wear: jackets, shirts, bracelets, and so on.

Of all the possible wearable haptic interface locations, sleeve or armband devices offer several advantages. First, sleeves allow for a reasonable design space in terms of acceptable weight, size, power, and haptic renderable area, especially if heavier/bulkier components can be located elsewhere on the body. Secondly, sleeves leave the hands free, which is important to on-the-go AR scenarios as it allows the hands to manipulate the physical world unhindered. Finally, because shirts or jackets have sleeves, if the device can be integrated into normally-worn fabric, the device can be inconspicuous or even fashionable.

In this work, we created a lightweight fabric sleeve worn on a user's forearm *PneuSleeve*, that can render three distinct types of haptic feedback: compression around the arm, skin stretch tangent to the arm, and vibrations that result from high-frequency actuations of the compression and stretch actuators (Figure 4.1). By rendering combinations of these 'atomic' haptic stimuli in different locations and patterns in time, it is possible to communicate a large set of

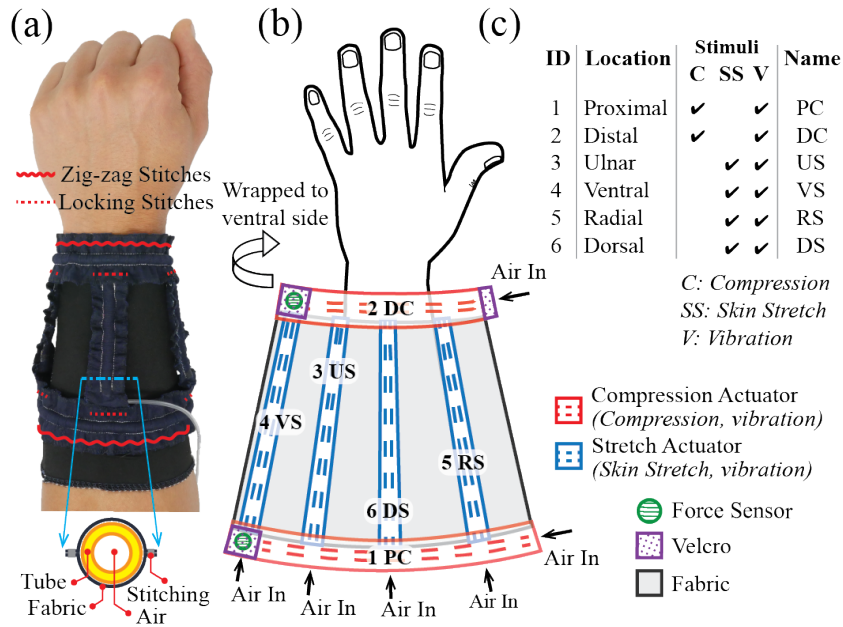


Figure 4.1: PneuSleeve is a fabric sleeve capable of rendering complex combinations of compression, skin stretch, and vibration haptic stimuli to a user. (a) PneuSleeve prototype on forearm. Zig-zag stitches are used for integrating compression actuators with the sleeve substrate. Locking stitches are used for integrating stretch actuators with compression actuators. Lower insert illustrates the cross section of a single actuator. (b) PneuSleeve design consisting of six fluidic fabric muscle sheet actuators, two custom soft force sensors, a knit fabric sleeve base, and velcro connectors. (c) Actuation renderability of PneuSleeve. Compression actuators are used to provide compression stimuli and controlled grounding for skin stretch. All actuators can generate vibration stimuli.

distinctly discernible and information rich haptic effects to the user. We hypothesize that coupling these haptic effects with audio/visual information can substantially increase the quality of a mobile human computer interface, particularly for uses in AR/VR (Figure 4.2).

In this paper, we make the following contributions:

- The design and construction of a novel fabric sleeve embedded with six soft pneumatic actuators and two customized mutual capacitance sensors. The actuators enable complex combinations of compression, skin stretch, and vibration. The two soft sensors enable closed-loop regulation of compression force.

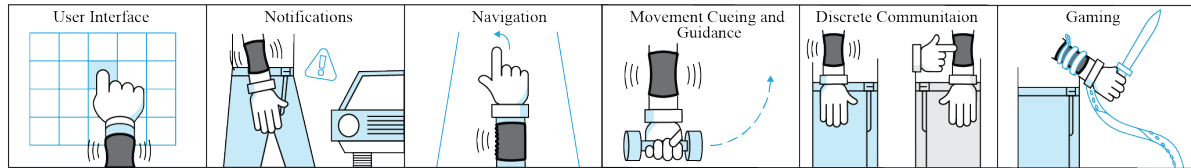


Figure 4.2: Paired with tracking and/or communication technology, the complex multimodal haptics of PneuSleeve enable a wide range of applications.

- Physical characterizations for the a) quasi-static and transient performance of the actuator, b) resolution and consistency of the sensor, and c) performance of the closed-loop compression force control system.
- Psychophysical characterization of the absolute detection thresholds (ADTs) and the just-noticeable differences (JNDs) of the six actuators in PneuSleeve.
- Subjective assessments of 23 feel effects that demonstrate PneuSleeve’s rich expression capability.

4.2 Related Work

In recent years, buoyed by developments in AR/VR, there has been a dramatic increase in interest and production of mobile, wearable, haptic interfaces. We present an abbreviated list of wearable haptic interfaces in Table 4.2. In this paper, we focus on related work for wearable haptic interfaces, and do not emphasize related work in handhelds/holdables. Wearable haptic interfaces have been implemented on many different locations on the body, where thimbles, gloves, bracelets, sleeves, and jackets, are the most popular.

Thimbles

Thimbles stimulate a user’s fingertip, which is one of the most sensitive parts of the human body, and is often involved in probing or manipulating the environment. They can provide

salient and useful haptic stimuli, however, most current thimble interfaces are bulky and do not allow interaction with physical objects. Pacchierotti et al. present a survey of over twenty thimble interfaces rendering variations of normal compression, lateral skin stretch, and vibration [82]. Most thimbles use electrically powered direct current or servo motors to position a rigid plate or tactor on the fingertip [305, 170].

Gloves

Gloves are capable of rendering haptic feedback to the entire hand, and may one day allow direct manipulation with virtual objects. However, current designs face a number of challenges regarding encumbrance, locating actuators, grounding forces, and power requirements. Pacchierotti et al. present a survey of over twenty glove interfaces rendering various haptic stimuli [82]. Similar to thimbles, most glove interfaces are powered electronically and use direct current or servo motor actuators. Notable ‘soft’ gloves using different actuation approaches are thin form factor electrostatic brakes [58] or molded elastomeric chambers with fiber reinforcements [4]. Takahashi et al. used pneumatic actuators for glove fitting and finger posture control [306], however, multi-modal actuation with user specific control methods was not implemented in their studies.

Bracelets

Bracelets are socially acceptable and leave the user’s hands free to interact with the physical world. Huang et al. used sixteen servo motors and taxels to render virtual objects with deformable rear-surfaces [312]. Pezent et al. presented a multisensory squeeze and vibrotactile bracelet using one servo motor and six linear resonant actuator vibrotactors [201]. Shim et al. developed another multimodal tactile display using wind and vibration [313]. A brushing stimulation bracelet was presented in [314], and a thermal one in [307]. Shear forces and motion rendering have also been explored in Whitmire et al.’s work [315]. The majority of pre-

Haptic Stimuli:

C = compression, SS = skin stretch, V = vibration, T = temperature, I = impedance. Actuators/Sensors: LRA = linear resonant actuator, TPU = thermoplastic polyurethane, SMA = shape memory alloy, PU = polyurethane, ERM = eccentric mass motor, cap. = mutual capacitance, FSR = force sensitive resistor.

	Form Factor	Power Source	Actuator Design	Sensor Type	Haptic Stimuli				
					C	SS	V	T	I
Zhu, 2020 (this work)	sleeve	pneumatic	tube in fabric	cap.	✓	✓	✓		
Pezent [201], 2019	bracelet	electric	motor, LRA	encoder	✓		✓		
Young [19], 2019	bracelet	pneumatic	TPU bellow		✓		✓		
Peiris [307], 2019	bracelet	electric	peltier, piezo	temp.				✓	
Hamdan [35], 2019	variable	electric	multi-layer SMA				✓		
Delazio [17], 2018	jacket	pneumatic	PU bladder	FSR	✓		✓		
Hinchet [58], 2018	glove	electric	electro-static brake	vision					✓
Raitor [308], 2017	bracelet	pneumatic	TPU bladder		✓				
Gupta [20], 2017	bracelet	electric	SMA		✓				
Pohl [309], 2017	bracelet	pneumatic	air cuff	pressure					✓
Schorr [305], 2017	thimble	electric	motor	encoder	✓		✓		
Polygerinos [4], 2015	glove	hydraulic	fiber in elastomer	pressure					✓
Tang [310], 2014	sleeve	electric	ERM, LRA	pressure			✓		
Prattichizzo [170], 2013	thimble	electric	motors	encoder	✓		✓		
Bark [311], 2009	sleeve	electric	motors	hall effect			✓		

Table 4.2: Abbreviated List of Wearable Haptic Interfaces

sented bracelets are often ‘hard’, created using rigid components, such as thermosets, motors, metals, and so on. However, there have been some ‘soft’ bracelets created using low stiffness, flexible, and stretchable components, like fabric or elastomers explored in recent years. To achieve squeeze sensation, Gupta et al, configured shape memory alloys (SMAs) around wrist [20], while Pohl et al. chose blood pressure cuffs [309]. Other multi-modal haptic stimulations combining local pressure and vibration have also been explored in Young et al.’s work [19]. These devices are soft to wear, but few combines actuation modalities include compression, vibration and skin stretch, limiting the expressiveness that one device may render.

Sleeves

Sleeves have similar advantages and disadvantages in wearable haptics to bracelets. Relative to bracelets, they present a larger renderable area, but can be more challenging to fit a diverse set of users. Tang et al. presented a sleeve composed of a grid of rigid vibrotactile actuators for treating autism [310]. Bark et al. evaluated an armband that renders skin stretch using an ultrasonic motor and cable transmission [311]. Ion et al. explored another armband that renders ‘skin drag’ using rigid components and an electric motor [316]. In Agharese et al.’s work, a soft forearm interface that grows to wraps along the users arm using pneumatic pressure was invented [317]. Hamdan et al. used multi-layer shape memory alloys (SMAs) to render various haptic stimuli based on linear extension or contraction. The connection to the user is a ‘skin sticker’ that can attach to the forearm as well as other locations. In addition, multiple pneumatic actuators have been integrated into a sleeve to create the illusion of lateral motion on the arm [18].

Jackets

Jackets present a large haptic renderable area, but face challenges in complexity, size/weight, and coupling to the human for effective transmission of haptic stimuli. Delazio et al. presented

a jacket with pneumatic airbag actuators and force sensors to increase realism [17]. Arafsha et al. presented a jacket with vibration and temperature haptic actuators to enhance emotional immersion [318]. Foo et al. used SMAs to explore user experiences of garment-based dynamic compression [319].

4.3 Design of PneuSleeve System

4.3.1 Soft Actuator Design

‘Soft’ haptic interaction devices created from composite structures of fabrics or elastomers have a key advantage over ‘hard’ devices created from rigid metals or thermosets: soft devices feature a smaller difference in mechanical impedance between the device and human, allowing for better fit, leading to more efficient sensing and transmission of haptic stimuli.

For this reason, we use Fluidic Fabric Muscle Sheets (FFMS) [2] as the actuator in PneuSleeve. FFMS actuators operate as inverse pneumatic artificial muscles (IPAMs) [262], where at high fluid pressure the actuator is in its longest state. As the pressure decreases, the actuator contracts and exerts force on the blocking element. Therefore, IPAMs can be used as either a linear, or compression actuator when wrapped around an object [2]. Contrary to McKibben muscles [255, 256] that shorten in accordance with a radial expansion, FFMS actuators change length without expanding radially. This characteristic enables them to have low profile during operation, eliminating unwanted parasitic forces generated by radial expansion of the actuator. Compared to Shape Memory Alloy (SMA) actuators [35], which contract and lengthen due to a thermally activated phase change, FFMS actuators feature faster response times without generating any unwanted thermal stimuli.

PneuSleeve consists of six single-channel pneumatic FFMS actuators: two provide radial compression on the proximal and distal forearm, and the other four generate linear stretch

at ulnar, radial, ventral, and dorsal side of the forearm. All actuators can render vibration (Figure 4.1). For linear stretch actuation, all six actuators are pressurized to their longest length. Compression actuators are first compressed to provide grounding or anchoring force for the linear stretch actuators. Then, the linear stretch actuator shortens and moves the connection points with the already compressed compression actuators, thus generating effective localized compressive shear on the skin. When the actuator is pressurized back, the skin recovers to its normal state due to its own elasticity to render extensive shear. Due to the soft nature of the actuator and fabric, occasional actuator touch with the passive sleeve is not noticeable compared to the sensation of the skin stretch. The skin stretch sensation is dominated by large deformations caused by shortening the actuators, rather than the sensation caused by bunching and releasing of the actuator.

The six FFMS actuators are fabricated using the method described in [2]. Latex tubes with outer diameter of 5.5 mm and wall thickness of 0.5 mm are used as the stretchable tubings. Non-stretch woven fabrics with straight stitching are used to construct conduits with 7.5 mm width for constraining radial expansion of the soft tubes. The lengths of the stitching for distal compression, proximal compression, and stretch actuators are 250 mm, 170 mm, and 80 mm, respectively. After inserting the tubings, the conduits are all wrinkled to 40% of their original length. Finally a barbed tube fitting is attached to the end of each latex tubing. The cross section of a single actuator is shown in Figure 4.1(a) lower insert.

4.3.2 Soft Mutual Capacitance Sensor Design

To render high-quality haptic feedback, it is important to prevent the slippage of compression actuators and maintain a suitable grounding force when skin stretch actuators are activated. Therefore, we implement a closed-loop controller to regulate grounding compression forces to users with different forearm sizes and anatomies. This control is enabled by a soft force sensor

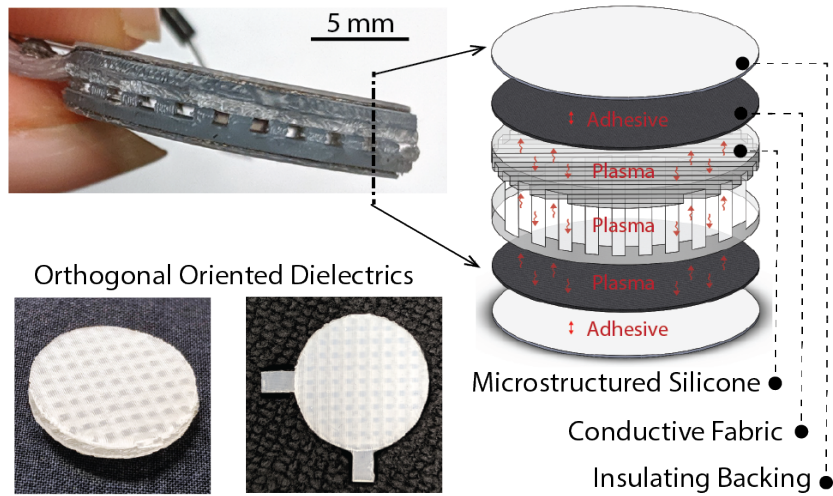


Figure 4.3: Customized mutual capacitance sensor to measure force. Two silicone dielectric layers with microgrooves are oriented orthogonally between conductive fabrics to increase sensitivity. Plasma treatment is used to bond interfaces between silicone layers and conductive fabrics.

based upon sensing mutual capacitance. We choose capacitance sensing over force sensing resistors due to its low temperature sensitivity. The capacitance C of a parallel-plate capacitor is inversely proportional to the distance d between the parallel plates when the permittivity ϵ and the electrode area A are constant ($C = \epsilon * A/d$). A change in the compression force results in a change in the gap between the electrodes and accordingly a change in the capacitance.

Based on the capacitance sensing theory, we use a layered structure of dielectrics, electrodes and insulators for the sensor (Figure 4.3). The transfer function between the capacitance and the applied force (compression force generated by the actuator in our case) is heavily dependent on the stress-strain behavior of the dielectric material. Two main performance characteristics, hysteresis and relative capacitance change ($\frac{\Delta C}{C_0}$, where C_0 is the capacitance baseline) are considered to select sensor material and geometry.

To find the most suitable dielectric materials for PneuSleeve, a variety of dielectric films including foams, 3D printed Elastomeric Polyurethane (EPU) with microgrooves and pillars, and 3D molded silicone with microgrooves [320] are fabricated and tested. Due to the small applied force (about 4 N according to Figure 4.6), microstructures are used to increase the rela-

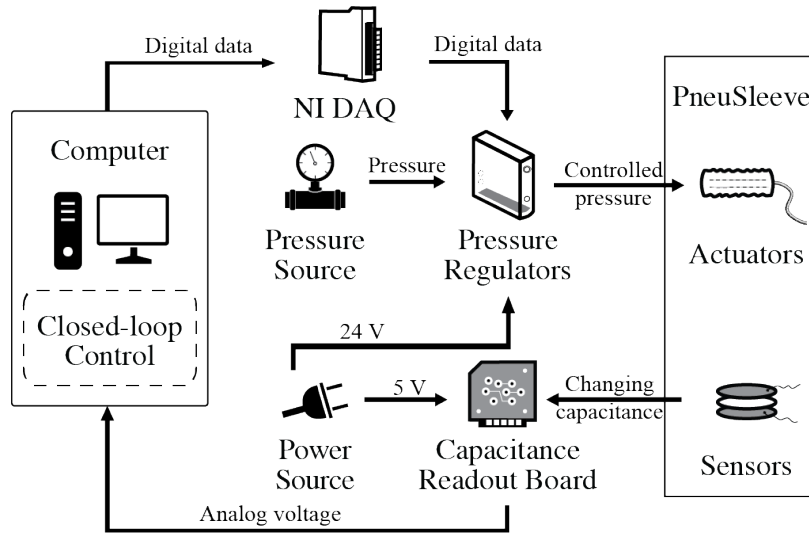


Figure 4.4: PneuSleeve system architecture using measured capacitance from the sensor as the feedback for the closed-loop control of the actuator compression force.

tive capacitance change of the sensor. Among explored dielectrics, foams show a high relative capacitance change with large hysteresis, while 3D printed EPU dielectrics reveal low hysteresis but low relative capacitance change. 3D molded silicone dielectrics with microgrooves are finally selected due to their low hysteresis and good relative change of capacitance (12% over the compression forces, Figure 4.8). Conductive fabrics are chosen as the electrodes due to their flexibility that ensures uniform layer bonding with the dielectrics. The overall shape of the sensor is designed to be circular to avoid the edge effect on the electric field caused by sharp corners.

The dielectrics are fabricated by casting Ecoflex 00-30 in a 3D printed acrylic styrene acrylonitrile (ASA) mold with microgrooves of width 1 mm, periodic width 2 mm, and height 0.75 mm. Ecoflex 00-30 is mixed and degassed before pouring into the mold, then cured at 80°C for 1 hr. Two layers of the molded dielectrics are plasma treated and bonded orthogonal to each other. Plasma treatment is also used to bond the conductive fabrics with 0.1 mm thickness to the dielectrics. Finally, acetal sheets with 0.2 mm thickness are used as the insulating layers for the electrodes with double-sided adhesives. The total thickness of the sensor is 3.9 mm.

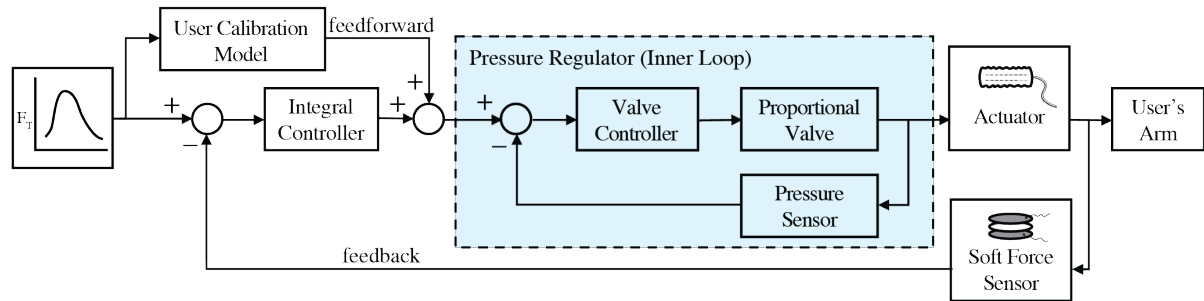


Figure 4.5: Block diagram of the closed-loop control regulating compression force to the user. The highlighted inner loop is embedded into the pressure regulator to reach the commanded pressure signal. The user’s calibration model is used for feedforward, and an integral controller using the soft force sensor measurement is used for feedback.

4.3.3 Wearable Sleeve Design

A highly elastic knit fabric base and Velcros are used to configure a sleeve form-factor combining the chosen actuator and sensor designs (Figure 4.1(b)). Velcro patches are sewn on the ends of compression actuators for radial closure and safety quick release. Sensors are placed underneath the Velcro patches on the compression actuators. All actuators are fully pressurized (200 kPa) and assembled on the fabric sleeve base using zig-zag stitches to maintain the stretchability and flexibility of the sleeve and the actuators. The connection between the ends of the stretch actuators and the the edges of the compression actuators are then reinforced with locking stitches (Figure 4.1(a)). The constructed sleeve has a total weight of 26 grams and a maximum thickness of 6 mm. With fabric as the basic construction material for the pneumatic actuators and sensors, PneuSleeve is intrinsically soft, low profile, and can be easily donned and doffed.

4.3.4 Pneumatic Control System

PneuSleeve has six pneumatic actuators and two mutual capacitance sensors. Each pneumatic actuator is controlled through an individual pressure regulator (Festo VEAB, 1-200 kPa) (Figure 4.4). The pressure regulators are proportional control three-way valves that have inlet,

outlet, and exhaust ports. The air is vented to the environment and the inlet is connected to a compressed air reservoir. Each pressure regulator is controlled using an analog output generated through a data acquisition device (NI cDAQ-9174 with NI9264 module) interfaced using a PC. The capacitance of the soft force sensor is measured through a custom-built capacitance sensing board. The measured capacitance acts as the feedback for the closed-loop control of the actuator compression force.

4.3.5 Closed-Loop Force Control

Using the real-time force feedback from the integrated soft sensor, we implement a closed-loop control strategy to apply user-specific grounding forces. Figure 4.5 shows the block diagram of the closed-loop controller. The outer feedback loop controls the compression force, which is rendered to the user by generating pressure commands to the pressure regulator. The control architecture uses a personalized calibration model to approximate the pressure-force map as a feedforward term, and employs an integral controller for its feedback loop. The calibration model improves the convergence speed of the controller and it is built once for each user after putting on the sleeve. The calibration process is conducted by deflating and inflating the compression actuators from 200 kPa to atmosphere pressure. A third degree polynomial is then fitted to the recorded data to serve as the feedforward function. The inner loop is embedded in the pressure regulator to reach the commanded pressure using its internal pressure sensor and embedded controller.

4.3.6 Noise Management

The noise in pneumatic systems mostly comes from switching action of the pressure regulators, and venting of the high pressure air to exhaust. In our system, the Festo proportional pressure regulators has a ‘silent operation’ feature based on piezo technology, which uses con-

trol frequencies above the human hearing range. To reduce the air exhaust noise, an off-the-shelf muffler is used on the regulator's exhaust port. With this arrangement, the noise for most haptic actuation in our study can be barely heard without headphones.

4.4 Physical Characterization and Evaluation

4.4.1 Quasi-Static Characterization

To characterize the relationship between pressure, force and the length of the FFMS actuator, a set of quasi-static experiments are conducted. A force sensor (ATI Nano 17) is used to measure actuator tension force as a function of input pressure controlled by a pressure regulator (Figure 4.6 inserts). A motorized linear stage is used to adjust the distance between the two ends of the actuator before the loading and unloading test of the actuator. A deflation-inflation cycle (200 kPa to atmosphere), with a duration of 40 s is performed on the actuator for discrete actuator lengths with a 4 mm step size (ΔL). Figure 4.6 shows the pressure-force curves for 5 discrete distances between the endpoints of the actuator (L). According to the functional principle of FFMS actuators, for a given pressure the actuator force decreases as L shortens [2]. The observed hysteresis effect between loading and unloading curves is mainly due to the friction between the stretchable tubing and the fabric to which it is embroidered.

4.4.2 Dynamic Frequency Response

To generate vibrations at each actuator location, the actuation needs to work at high frequencies. As the frequency of actuation becomes higher, the rendered force magnitude will be reduced due to the compressibility of air and shorter fill and drain cycles. The frequency response of an actuator provides the force magnitude that the actuator is able to render at a given frequency. A frequency response characterization is conducted for the radial compres-

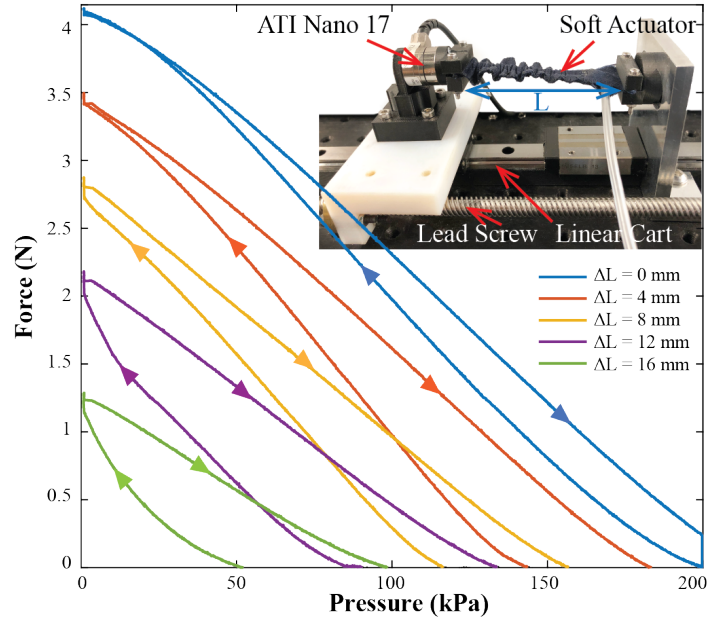


Figure 4.6: The results of the characterization tests. Each curve corresponds to a deflation and inflation cycle at a certain displacement of the actuator endpoint. L_0 is the length of the actuator at high pressure (200 kPa) and $\Delta L = L_0 - L$ denotes the change in the actuator endpoint position. The arrows on the curves indicate the deflation and inflation cycles. *Inserts:* Actuator characterization setup for quasi-static analysis.

sion actuator using a test setup with a force sensor (ATI Nano 17) (Figure 4.7 inserts). A set of sinusoidal input pressure at different frequencies (1 to 50 Hz divided into 20 equidistant steps using logarithmic spacing) is commanded to the actuator for 50 cycles each, and resulting compression force response are measured for each frequency. A fast-Fourier transform analysis is conducted on the commanded pressure data and the measured compression force data for each frequency. The force-frequency response is obtained by dividing the output amplitude corresponding to each commanded frequency with the respective input amplitude. The input signal is also normalized with the amplitude of the sinusoidal signal to obtain the frequency response in the units of force. This characterization is repeated at different amplitudes of the sinusoidal input pressure. Results indicate that the force magnitude reduces with increasing input frequency. Furthermore, with higher pressure amplitudes higher force magnitude can be achieved for a broader frequency range. This is primarily due to the way internal controller of

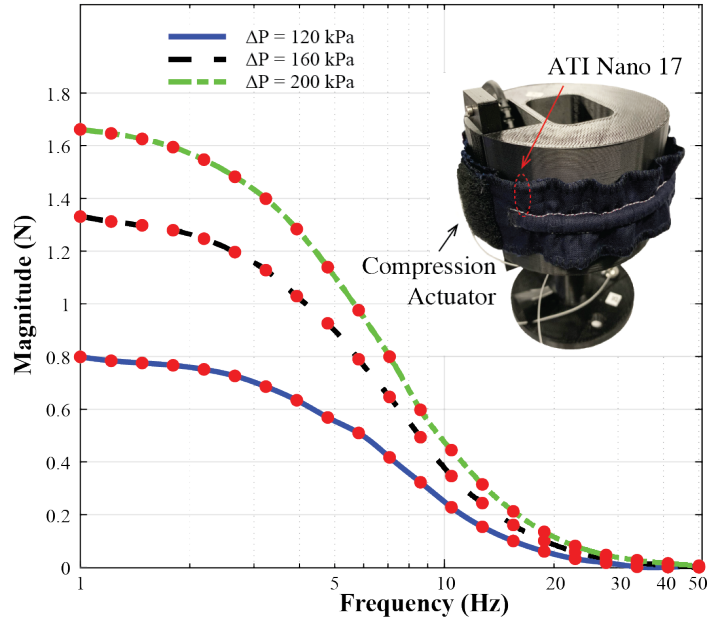


Figure 4.7: Frequency response of the compression actuator for different amplitudes. Frequency axis is in log scale from 1 Hz to 50 Hz. The red dots represent the magnitude determined using the experimental data, and the lines represent a fitted spline to the experimental data. *Inserts:* Dynamic response characterization setup for the compression actuator.

the pressure regulator functions. Although the force magnitude attenuates with the increased frequency, an easily perceptible force of 50 mN can be achieved at 20 Hz (Figure 4.7).

4.4.3 Sensor characterization

To obtain the transfer function of the capacitance sensor, the compression testing setup for dynamic characterization is adopted (Figure 4.7 inserts). The pneumatic pressure is linearly varied between 200 kPa and atmosphere pressure in a duration of 40 s for 5 cycles. Capacitance output of the sensor for all 5 cycles are highly consistent (Figure 4.8 (a)), with more than 12% relative change in capacitance under the force applied by the actuator, and a small hysteresis. A linear fit is sufficient to capture the variance of the data with R^2 of 0.9919. To further improve the accuracy, quadratic fit is used as the transfer function between compression force and capacitance.

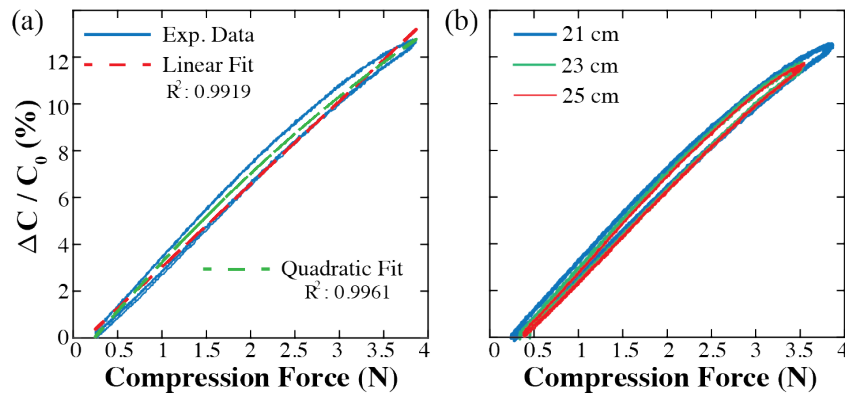


Figure 4.8: (a) Experimental data and fitted models relating measured capacitance to compression force. (b) Experimental data for various cylinder circumferences showing consistent behavior. The unloaded capacitance, C_0 , is 6.6 pF.

In addition to the hysteresis and relative capacitance change, the curvature of the forearm on different users may cause inconsistent output from the sensor. Therefore, we examined the consistency of the sensor on a set of surfaces with different curvatures. These curvatures are generated by using the cylinders in the compression setup with different circumferences (21 cm, 23 cm, and 25 cm). The results indicate that the capacitance outputs among cylinders with different circumferences are highly consistent (Figure 4.8 (b)). Although in practice user’s arms are not rigid, results demonstrate that the transfer function does not change significantly with varying arm circumferences.

4.4.4 Closed-Loop Control Response

To evaluate the performance of the proposed control method (Figure 4.5), two different types of input force profiles (F_T), including sinusoidal and squared waves, were fed to the controller while the PneuSleeve was worn by a user and tracking results were recorded. The outer control loop was set to operate at 40 Hz and the integral controller gain was set to -0.025. Considering the compressibility of the air, the tracking error and response time results indicate the suitable performance of the controller for a soft wearable actuator (Figure 4.9).

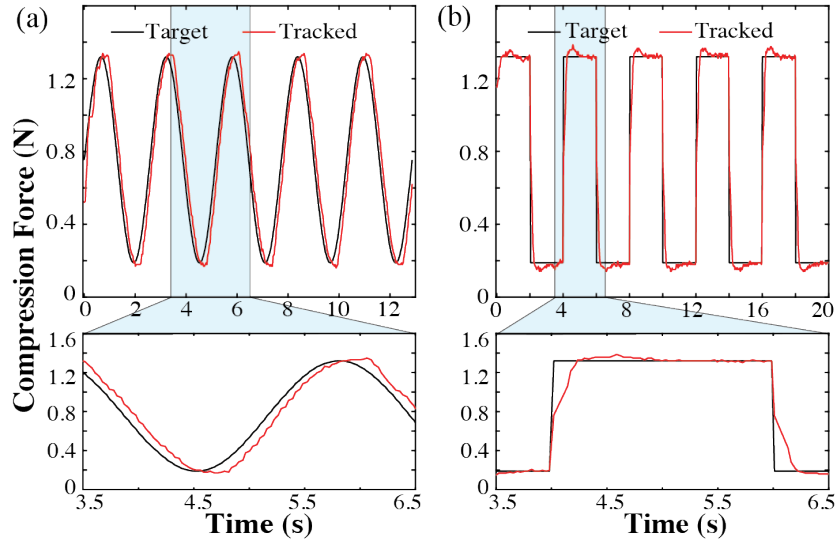


Figure 4.9: Closed-loop control performance for a commanded sinusoidal, (a), and squared, (b), compression force. The black line indicates the desired compression force profile over time and the red line shows the tracking performance recorded from the soft force sensor on the user’s arm. The root-mean-square tracking error for the sinusoidal input was 0.10 N, and the settling time for squared input was less than 0.3 s.

4.5 User Study: Psychophysical Evaluation

The aim of the user study is to evaluate the perceptual characteristics of the ‘atomic’ haptic cues provided by the PneuSleeve. Primarily, we seek to evaluate the absolute detection threshold (ADT) for compression and skin stretch actuators, as well as the just-noticeable difference (JND) for those same cues. In the following sections, we will refer to these haptic cues generically as ‘the stimulus,’ which will be either compression or skin stretch depending on the corresponding actuator. Since the actuators are their longest at high pressure, and contact and exert forces as the pressure decreases, for simplicity, the stimulus levels are reported in terms of $\Delta P = P_H - P$, where P_H is maximum pressure (200 kPa) and P is the variable controlled pressure.

4.5.1 Absolute Detection Threshold (ADT) Evaluations

We conducted ADT evaluations for the two compression actuators and the four skin stretch actuators to understand the minimum pressure required for the user to feel those sensations. We conducted a standard two-down, one-up adaptive staircase procedure in order to estimate the 71% threshold. Every stimulus was applied for a duration of 1 s. The experiment started with a stimulus of 0 kPa. For every stimulus that was not felt, the stimulus was increased by a step size of 20 kPa, and increased by the same if the stimulus was felt twice consecutively. After three reversals, the step size was changed to 2 kPa. The experiment ended after nine total reversals and the average from the last five was taken as the threshold estimate. The high initial step size of 20 kPa ensured quick jumps to the ADT vicinity thus minimizing total number of trials, after which the smaller 2 kPa step size ensured convergence to a fine-grained value.

Twelve participants (six female, six male, ages 24–34, mean = 28.5, all right-handed) took part. We recorded the arm circumferences near the distal compression actuator (range: 13.7–18 cm, mean = 15.5 cm) and the proximal compression actuator (range: 19.9–25.7 cm, mean = 22.2 cm). Participants wore the sleeve on their left forearm with the arm resting on a table and hidden from their view during the study using a box. Participants wore active noise canceling headphones playing Pink noise for complete sound insulation. The ordering of the six ADT estimation staircases (1 for each actuator) was randomized. Participants responded ‘Felt’ or ‘Not Felt’ by pressing the corresponding keyboard key after every stimulus. A random interval of 2–6 seconds between the participant’s response and the next stimulus was introduced to minimize anticipation of the stimulus at a particular instant.

4.5.2 Just-Noticeable Difference (JND) Evaluations

We conducted JND evaluations for the two compression actuators and the four skin stretch actuators. Prior work has shown that haptic sensations including pressure [309, 20] generally

follow Weber’s law. We therefore conducted the JND using a single reference value, which demonstrates that users are able to discriminate certain intensities in PneuSleeve actuators. The same participants from the ADT study did the JND study in the same session with the complete study taking about an hour. The reference stimulus was chosen to be 1.3 times the participant’s ADT. This normalizes the reference across all participants with regards to its perceived intensity. This is also preferable with respect to using a constant pressure value since depending on the arm size and stiffness, the same pressure may result in different forces on different users and the reference stimulus may be perceived differently.

We used a three-down, one-up adaptive staircase procedure to estimate the JND with participants performing a two-interval forced choice, thus targeting the 79% threshold. For every trial, participants were presented with a pair of stimuli appearing one after the other, and they judged which one felt stronger. Each pair consisted of the reference stimulus (R) and offset stimulus ($R + \Delta$). Every stimulus was applied for 1 s, and the ordering of reference and offset stimuli within a trial was randomized. The experiment started with a large offset value (Δ) of 100 kPa. For every sequence of three correct responses, the offset was decreased by a step size of 48 kPa, and increased by the same upon a single incorrect response. After two reversals, the step size was changed to 4 kPa. The experiment ended after eight total reversals and the average from the last four was taken as the JND estimate. The experiment design was finalized after initial pilots to optimize the accurate estimation of JND and the duration of the experiment.

4.5.3 ADT and JND Results Discussion

The box plots of Figure 4.10 show the distribution of the estimated ADT and JNDs with the whiskers representing first and third quartiles. The results show that thresholds are lower for the compression actuators than for the skin stretch actuators, indicating that users are more sensitive to the sensations produced by the compression actuators. We also observe a higher

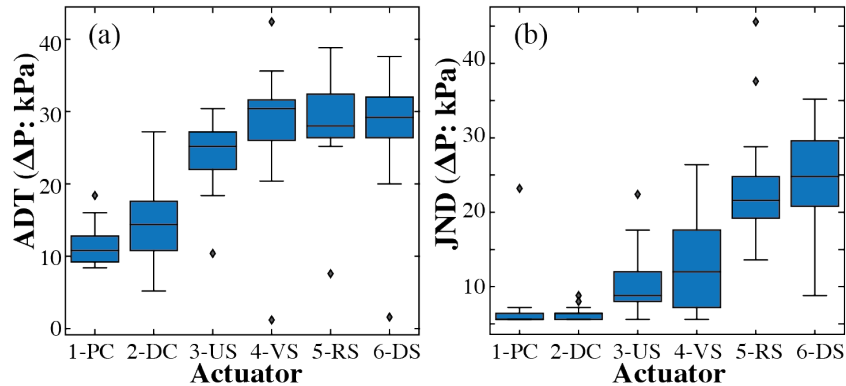


Figure 4.10: ADTs, (a), and JNDs, (b) for all six actuators embedded in PneuSleeve (Figure 4.1) in terms of $\Delta P = P_H - P$, with initial pressure $P_H = 200$ kPa. The detectability and sensitivity differences may be attributed to the type and location of the actuator.

variability in the JND estimates for the stretch actuators which is consistent with the reduced sensitivity to those actuators. However, interestingly, the estimated values of the JND for all actuators is well smaller than maximum possible ΔP that it is possible to actuate (~ 20 kPa as compared to 200 kPa). This is about one order of magnitude below the full range, plausibly providing for between 5 and 10 distinctly perceivable levels, depending on the exact Weber fraction for these sensations.

4.6 User Study: Feel Effects

Our psychophysics studies establish that PneuSleeve can stimulate varying magnitudes of compression and stretch pertaining to the six actuators. As mentioned earlier, PneuSleeve can also stimulate vibrations by actuating at higher frequencies. Here we demonstrate the expressivity of PneuSleeve using a vocabulary of 23 feel effects designed by a haptics researcher that are based on various spatio-temporal combinations of compression, stretch, and vibrations. Prior work has conducted similar feel effects studies [17, 321]. We follow a design similar to Delazio et al. [17] to see if users perceive the sensations to be good fits for their descriptions and whether they like the feeling or not. The feel effects correspond to different real-world

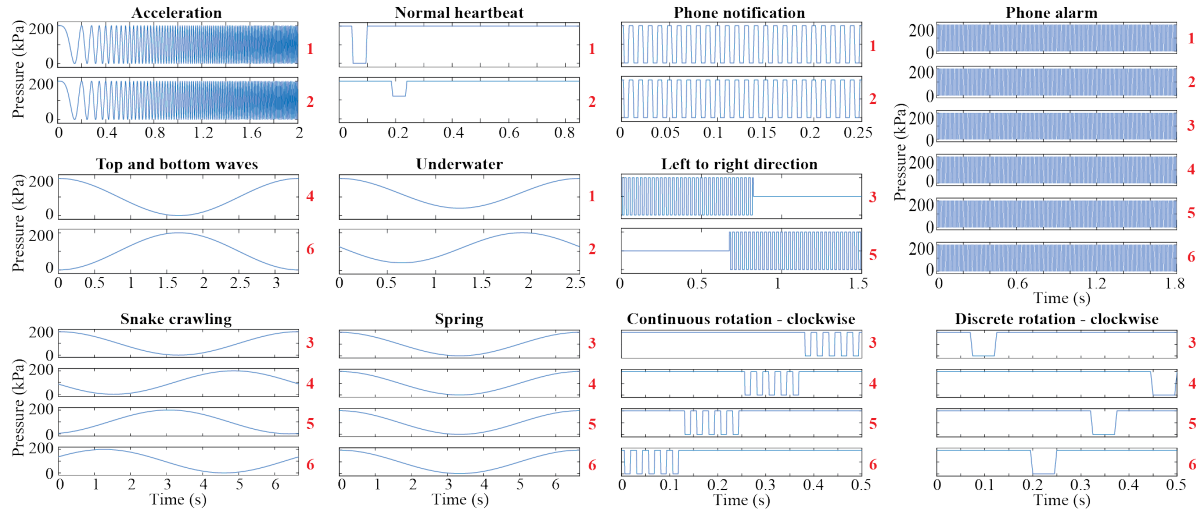


Figure 4.11: Example single-cycle control signals for selected feel effects. Bold red numbers denote the index of the active actuator (Figure 4.1).

use-cases classified into seven families as shown in Table 4.3.

4.6.1 Design of Control Signals

In practice, any signals in time series can be used as control signals for the air pressure. To form a design method for PneuSleeve, single actuator response design and combined actuation design are chosen as the two main design considerations. Single actuator response design includes the design of the waveform for a single actuation cycle, duration of the waveform, number of repeated cycles, and the time gap in between repeated cycles. The main attribution to different haptic sensations is the characteristics of the single-cycle waveform. Sinusoidal and square waves were used as the basic units to construct the waveform. Frequency, amplitude, and duty cycle can be controlled for fine tuning the effects. Combined actuation considerations include the selection of the actuators, the sequence of actuation, the phase shift, time lagging, and overlapping of signals in between selected actuators.

With these design factors, we composed 23 feel effects and grouped them into seven families based on the similarity of their control signals (Table 4.3 and Figure 4.11). Acceleration

Family	Feel Effect	Haptic Stimuli			Force Control	Active Actuators
		C	SS	V		
Accel-eration	Acceleration	✓		✓	N	1, 2
	Deacceleration	✓		✓	N	1, 2
Rotation	Continuous rotation - CW	✓	✓	✓	Y	All
	Continuous rotation - CCW	✓	✓	✓	Y	All
	Discrete rotation - CW	✓	✓		Y	All
	Discrete rotation - CCW	✓	✓		Y	All
Heart-beat	Normal heartbeat	✓		✓	N	1, 2
	Racing heartbeat	✓		✓	N	1, 2
Navi-gation	Back to front direction	✓		✓	N	1, 2
	Front to back direction	✓		✓	N	1, 2
	Bottom to top direction	✓	✓	✓	Y	1, 2, 4, 6
	Top to bottom direction	✓	✓	✓	Y	1, 2, 4, 6
	Left to right direction	✓	✓	✓	Y	1, 2, 3, 5
	Right to left direction	✓	✓	✓	Y	1, 2, 3, 5
Phone	Phone alarm	✓	✓	✓	N	All
	Phone notification	✓		✓	N	1, 2
Waves	Forward and backward waves	✓			N	1, 2
	Left and right waves	✓	✓		Y	1, 2, 3, 5
	Top and bottom waves	✓	✓		Y	1, 2, 4, 6
Special Effects	Spring	✓	✓		Y	All
	Snake crawling	✓	✓		Y	All
	Underwater	✓			N	1, 2
	Breathing	✓			N	1, 2

Table 4.3: List of the 23 feel effects tested in the subjective user study. Feel effects are grouped into ‘families’ based on the similarity of their control signals. C = compression, SS = skin stretch, V = vibration, CW = clockwise, CCW = counterclockwise.

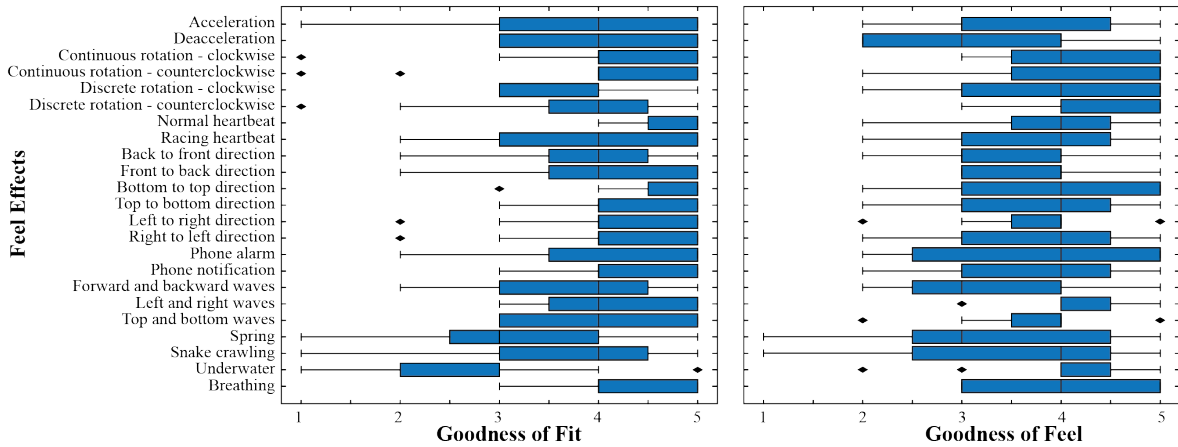


Figure 4.12: Box plots showing the Goodness of Fit and Goodness of Feel ratings for the 23 feel effects.

family features a linear change in sinusoidal frequency of the compression actuators. Rotation signals feature the sequenced actuation of the stretch actuators. The difference between continuous and discrete rotation is that continuous rotations are vibration-based. The latency of switching from one stretch actuator to the next are the same for both. Heartbeat signals have fine-tuned magnitude and delay time on two compression actuators. Navigation cues feature an overlap on the signals between actuators to make the transition smoother. Phone alarm uses long duration vibration on all six actuators at the same time intended to grab more attention from user, while phone notification has two short vibrations on two compression actuators. Waves and special effects family signals are constructed on sinusoidal waveforms with frequency less than 0.5 Hz. Opposite phase between active actuators is used in waves, while shifted phase and same phase are used in special effects, with shifted phase implemented in underwater, and snake crawling, and same phase implemented in spring and breathing. In addition to the phase difference, the active actuators are also selected differently for different effects. A grounding force of 0.5 N is used on compression rings for corresponding effects requiring controlled grounding as listed in Table 4.3.

4.6.2 Evaluation Methods

We validate these feel effects in a user study along two axes: ‘Goodness of Fit’ and ‘Goodness of Feel’. Goodness of Fit indicates how well the haptic sensations fit the name of the feel effect. Goodness of Feel indicates how well the sensation feels regardless of whether it is a good fit for the feel effect.

Eleven participants (five female, ages 26–46, mean = 31.6, 10 right-handed) participated. We recorded the arm circumferences near the distal compression actuator (range: 13.7–18 cm, mean = 15.9 cm) and the proximal compression actuator (range: 19.9–25.7 cm, mean = 22.8 cm). The feel effects were grouped into families and the ordering of the families and feel effects within the families were both randomized. The goodness metrics were explained to the participants. For each effect, participants were asked to rate the goodness of fit and feel on Likert scales of 1-5. Participants were allowed to play an effect as many number of times before their response. Participants were asked for feedback on their perceptions after each family of effects was completed.

4.6.3 Feel Effects Study Results and Discussion

Figure 4.12 shows that participants rated most feel effects high for both goodness of fit and feel. Participants found the sleeve to be comfortable overall. Multiple participants commented on liking the soft sleeve form factor. According to P3: *‘No hard material, others feel like watch, this is like a sleeve, so light weight, very nice feeling.’* Participants also compared the vibration sensations to regular vibrotactile feedback. P1: *‘With the watch vibrations there is a slight shock. The vibrations here are like light touch, they feel good.’* Participants also found the vibration based rotations to be a better fit than discrete stretch based rotations. Given that prior works have shown that sequenced vibration on the skin can lead to a feeling of apparent motion [322], the preference for vibration based rotation is reasonable.

Participants were divided on the feel of sensations which relied on strong squeeze effects, especially the deceleration, forward-backward waves, and spring. P7: *'The deceleration feels too strong initially. It reminds me of when I'm getting my blood pressure done.'* Participants had similar comments about the phone alarm, where they felt it was too strong, especially since it was actuating all the actuators simultaneously. P5: *'I like the pattern: very similar to an alarm but it's too strong. I guess an alarm is supposed to grab attention, so I think it's perfect in that sense.'*

Participants also came up with alternate interpretations of the sensations, likening the racing heartbeat to a galloping horse, the spring loading and unloading to rolling and unrolling of an arm sleeve, and the discrete rotations to an old train. One participant who was a gamer indicated the importance of context in the interpretation of these sensations. P10: *'I can imagine these sensations being useful in racing games, shooting games, also in virtual reality.'* Multiple participants alluded to applications for remote touch or emotion communication. P6: *'You can almost imagine the alarm as an angry squeeze from someone.'* P10: *'Instead of underwater, it feels more like somebody is massaging or kneading your arm.'* P8: *'It (breathing sensation) feels like a baby breathing in your arm. It's relaxing.'*

4.7 Limitations and Future Work

Our results indicate that PneuSleeve is a promising initial step toward soft multimodal haptic interfaces. However, there are several limitations and opportunities for further development. PneuSleeve is controlled using pneumatic pressure and features a compressed air reservoir for a power source and pressure regulators for individual activation. Although flexibility and mobility can be achieved by using long air tubes, the current apparatus has limited portability. This could be achieved with the advances in microelectromechanical systems and chemical engineering [203].

Our psychophysical and feel effects studies indicate that PneuSleeve is capable of rendering a rich vocabulary of different haptic effects. This opens the door for explorations on sensory substitution or augmentation studies using PneuSleeve. For the compression actuators, sensory masking may occur after some duration of stimulus and is an avenue worth investigating. Our work focuses on the haptic rendering part of the device in this work. Even though simple haptic effects already demonstrated the expressiveness of PneuSleeve, future works could study multi-sensory integration and explore how the haptic cues in different variants can be combined with visual and audio cues to further enhance user experience. User attention and perception to haptic feedback varies in mobile and on-the-go settings which may affect the detection thresholds as well as the recognition of feel effects. An analysis of PneuSleeve style haptic feedback for mobile augmented reality use cases will be useful.

Although the noise for most haptics effects in our study can be barely heard without headphones, some high frequency operations certainly produce some noise. In our user studies, we asked participants to notify the experimenter if noise were noticeable when they wore noise-canceling headphones playing pink noise at a pleasant volume. None of the participants mentioned about the noise during any of the experiments. This shows that the use of this type of regulator and muffler arrangement was sufficient for the purpose of the studies performed in this paper. For applications without headphones, high frequency noise can be further reduced by using a more advanced and customized muffler design. Other sound engineering methods, such as soundproofing foams, can be added around the regulators to further reduce the noise level.

4.8 Conclusion

We have introduced PneuSleeve, a soft, compact, and expressive haptic forearm sleeve. We used pneumatic pressure inside embroidered stretchable tubes to generate compression,

skin stretch, and vibration, haptic stimuli. We have presented the design, construction, actuation and sensing mechanisms, and the implementation of the closed-loop compression force controller. Physical experimental results validated the performance of the actuators, sensors, and performance of the controller. Psychophysical experimental results validated the quantitative perceptibility and sensitivity of the haptic stimuli. Subjective experimental results showed that the renderable haptic stimuli can present a wide range of interesting effects to the user. PneuSleeve is a new approach for soft wearable haptic interfaces.

Chapter 5

A peristaltic soft, wearable robot for compression and massage therapy

Chapter 4 demonstrates the utility of wearable haptic devices to convey expressive messages. In addition, such devices also hold promise for enhancing human lives through the delivery of massage therapies. Chapter 3 shows that FFMS actuators can supply localized compression pressure to the body. Inspired by these findings, chapter 5 presents a peristaltic wearable robot for compression and massage therapy emulating manual massage using FFMS actuators. This research provides new methods to render a variety of dynamic compression patterns on the body. Results show that the wearable robot can introduce a fluid flow in the artificial vein of a upper-limb model, holding promise to enhance blood and lymphatic circulation for many diseases, including venous ulcers, lymphedema, and blood clots.

At the time of writing, this chapter was submitted to the journal IEEE/ASME Transactions on Mechatronics under the title:

M. Zhu, A. Ferstera, S. Dinulescu, N. Kastor, M. Linnander, E. W. Hawkes, and Y. Visell, A peristaltic soft, wearable robot for compression and massage therapy.

Abstract

Soft robotics is attractive for wearable applications that require conformal interactions with the human body. Soft wearable robotic garments hold promise for supplying dynamic compression or massage therapies, such as are applied for disorders affecting lymphatic and blood circulation. In this paper, we present a wearable robot capable of supplying dynamic compression and massage therapy via peristaltic motion of finger-sized soft, fluidic actuators. We show that this peristaltic wearable robot can supply dynamic compression pressures exceeding 22 kPa at frequencies of 14 Hz or more, meeting requirements for compression and massage therapy. A large variety of software-programmable compression wave patterns can be generated by varying frequency, amplitude, phase delay, and duration parameters. We first demonstrate the utility of this peristaltic wearable robot for compression therapy, showing fluid transport in a laboratory model of the upper limb. We theoretically and empirically identify driving regimes that optimize fluid transport. We second demonstrate the utility of this garment for dynamic massage therapy. These findings show the potential of such a wearable robot for the treatment of several health disorders associated with lymphatic and blood circulation, such as lymphedema and blood clots.

5.1 Introduction

Emerging soft robotic technologies are becoming widely investigated for applications in health and medicine. Soft, wearable robotic systems are well-suited for delivering dynamic compression or massage therapy. Such therapies, when administered by a health professional, are effective in treating blood and lymphatic circulatory disorders, including chronic venous insufficiency (CVI), venous ulcers, lymphedema, and blood clots [69, 323], as well as for treating musculoskeletal injuries [324].

Compression therapy devices are expected to meet functional requirements arising from therapeutic standards that help ensure efficacy and safety or otherwise conform to norms of massage practice. Such guidelines are necessarily application-specific. Compression therapies requiring gross occlusion of venous blood flow in the lower limbs demand substantial compression pressures, amounting to 3.3 kPa, 8.0 kPa, or 9.3 kPa in the supine, sitting, or standing positions respectively [71]. Intermittent compression therapies, such as are used for lymphedema, require pressure variations to be supplied at frequencies of at least 1 Hz [304, 325]. In other applications, massage therapies are supplied for mild pain relief, easing of musculoskeletal tension, or touch elicited (i.e., haptic) emotional comfort. Examples include sports, Swedish, kinesiologic, or deep tissue massage. Such practices can involve the application of light to firm pressures, ranging from less than 12 kPa to 30 kPa or more [326].

Wearability introduces further requirements that arise from ergonomics and safety. To ensure comfort, compression garments should be soft, low-profile, and compliant. To avoid pain and avoid injury or lesions damaging soft tissues, static and dynamic forces should be distributed to avoid stress concentrations. For devices that emulate manual massage, it may be appropriate that compression is supplied via individually actuatable modules the size of a finger or hand.

Based on these requirements for compression therapies, the two existing predominant tools are graduated compression stockings (GCS) and intermittent pneumatic pressure (IPC) devices. GCS promote venous flow by applying a constant compression pressure to the limb to reduce venous caliber, preventing the static accumulation of blood [323]. GCS are convenient and low-cost while lacking the capability of dynamic pressure adjustment. IPC devices consist of single or multiple pneumatic chambers that are inflated to exert compression pressure on the limb [327]. Compared with GCS, IPC treatment features dynamic pressure modes with a wide range of pressure delivery (1-20 kPa) [328]. Studies have shown that the use of IPC instead of GCS is associated with lower incidents of venous thromboembolism (VTE) [329]. Researchers

have also shown that sequential actuation modes and high pressure in a multi-chamber device generate a higher lymphatic flow than other modes of treatment [330].

IPC devices rely on the inflation of the bladders to exert compression pressure on the skin, making it difficult to control the contact area for efficient mechanical coupling with blood vessels. It is also challenging for a user to move around when wearing them because the bladders used in IPC devices are usually bulky. The use of smaller bladders may reduce the clinical efficacy of the device due to the smaller volume of blood being expelled [331].

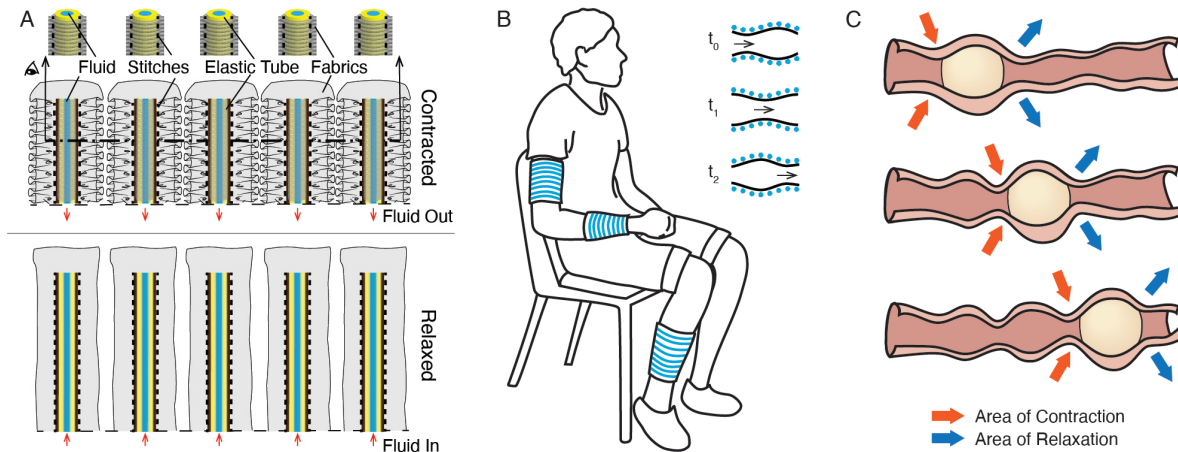


Figure 5.1: A. FFMS actuators are used for the peristaltic wearable robot design. These actuators are arranged in parallel to mimic peristalsis. B. The peristaltic wearable robot can be used in various locations on human limbs, including the upper arm, forearm, and lower limb. The insert demonstrates the propagation of the peristaltic wave generated. C. Peristaltic transport in biological organs such as the digestive tract involves sequential contraction and relaxation of muscles.

Prior researchers have investigated the modeling, control, and device designs for therapeutic massaging to overcome these limitations in IPC devices. Guan et al. proposed an evidence-based fluid-structure coupling model for the interaction between IPC soft actuator and lower limb, providing guidelines for improving the efficacy of compression therapy for venous flow promotion [332]. To address control challenges for pneumatic operations, Payne et al. incorporated closed-loop force control in pneumatic actuators with similar sizes to IPC modules [304]. Zhao et al. proposed a programmable and self-adaptive dynamic pressure delivery system with

a matrix of soft sensors for IPC therapies [102].

In addition to IPC devices, several soft, wearable robotic systems have been investigated for supplying forces to the body [1, 79] via pneumatic muscles [18], shape memory alloys [95, 266], or motor-driven tendons [21, 282]. For example, Suarez et al. created a system for robotic lymphatic drainage using three pneumatic bending fabric actuators to compress and laterally push fluid in a flexible tube [333]. Yoo et al. developed Z-folded pneumatic actuator modules to generate normal and shear forces for lymphedema massaging [334].

Pneumatic actuation has been widely used in such applications, but is often energetically inefficient, due to thermodynamic losses arising from gas compression cycles [2]. Pneumatic actuators also store substantial energy in gas compression, which can pose hazards upon soft material failure, due to rapid energy release. Shape memory alloy actuators perform mechanical work via a thermally actuated phase change; consequently, such actuators are energetically inefficient and operate at low speeds constrained by heat transport [266]. Other designs utilize tendon- or Bowden-cable transmissions. Such wearable devices require careful design to avoid painful or hazardous stress concentration [21].

To overcome some of these limitations, we present a wearable system based on fluidic fabric muscle sheets (FFMS), described in recent publications by the authors [2, 3, 1]. FFMS supply forces via soft, hydraulic transmissions integrated into finger-sized compact textile matrices (Fig. 5.1 A). They achieve greater energy efficiency and safety than many pneumatic designs, avoid stress concentration through the use of soft materials, and are capable of supplying large forces (scalable based on application requirements) and of rapid actuation at speeds exceeding 10 Hz, meeting requirements for dynamic compression and massage therapies in many application areas.

Leveraging the merits of FFMS actuators, we demonstrate a soft wearable robot that generates massage-like motions on the human limb through dynamic compression waves based on peristalsis (Fig. 5.1 B). Peristalsis is a transport mechanism produced via sequential squeezing

of muscles, as in the esophagus [335], uterus [336], ureter [337], or blood vessels [338]. Media within a peristaltic channel is transported via wave motion of the channel walls (Fig. 5.1 C). Peristaltic transport has been previously applied in robotic systems for liquid pumping [339] or swallowing robots [340]. When applied to the exterior of the body, peristalsis can supply forces similar to those used in compression and massage therapies [326].

We present the design, fabrication, and modeling of the peristaltic wearable robot and the associated control system. We characterize the compression pressure, dynamic frequency responses, and motion patterns generated by the peristaltic wearable robot. Results show that the system we designed can supply compression pressure as large as 22 kPa with frequencies up to 14 Hz, meeting the requirements for compression and massage therapy [71, 304, 325]. Our proof-of-concept demonstration for compression therapy shows that this peristaltic wearable robot is capable of driving venous flow in an artificial limb with a flow rate up to 1 mL/min. The flow rate increases linearly with peristaltic wavelength and frequency, in agreement with theoretical models we derive based on prior literature. Finally, we demonstrate that our wearable robot can deliver a wide range of massage-like motions on the forearm. This work provides a controllable and efficient method for supplying compression massage that could treat venous and lymphatic inefficiencies, as well as a means for therapeutic massage that could provide comfort or reduce anxiety.

5.2 Device Design and Operating Principle

5.2.1 Wearable Design and Fabrication

The peristaltic compression wearable aims to create dynamic compression force patterns on the wearer's limbs (Fig. 5.1 B). It consists of eight fluidic fabric muscle sheets (FFMS) actuators and leverages several benefits of this soft robotic technology [2]. FFMS actuators are

intrinsically compliant and can be scaled to sizes as small as human fingers. The modular arrangement of these actuators offers extra flexibility for personalized configurations. In addition, these actuators can be controlled efficiently with hydraulics [2] and are capable of generating a large variety of compression patterns that are easy to be detected and distinguished by humans [3]. These characteristics make FFMS an ideal candidate that meets the design requirements for compression therapy.

The operating principle of FFMS resembles Inverse Pneumatic Artificial Muscles (IPAM) [262]. When fluid pressure is high, the actuator extends to its longest state. When the fluid pressure decreases, the actuator contracts and exerts forces on the payload (Fig. 5.1 A). When wrapped around a human limb circumferentially, each actuator is capable of supplying localized compressive pressure to the limb. This working principle is intrinsically different from the IPC devices, such that a compact-sized FFMS actuator may still supply large compression pressures. The parallel arrangement of multiple actuators makes it possible to provide spatial-temporal compression patterns, including wave-like patterns that produce peristalsis.

We fabricated the actuators using the methods described in Zhu et al. [2]. The geometry of the soft latex tubing used inside the fabric conduits affects the fluid pressure required to fully operate the actuator, as well as the maximum compression force generated [2]. The actuator length should be designed such that the actuator can wrap around the human limb and produce compression pressure of at least 9.3 kPa for compression therapy. Based on these requirements and the analytical modeling in Zhu et al. [2], we specified the tubing to have an outer diameter of 4.8 mm, and an inner diameter of 3.2 mm. We selected the stitching length as 177 mm and the wrinkling ratio was 2.5. The fabricated actuators were then pre-pressurized and hand-sewn onto a stretchable sleeve for comfort using a zig-zag pattern that preserves stretchability.

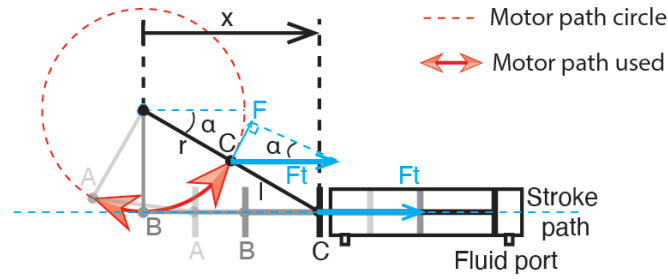


Figure 5.2: Schematic design of the slider-crank driving mechanism.

5.2.2 Design and Modeling of the Fluid Driving System

The system uses compact, servo-driven hydraulic cylinders to drive the fluid (water). The power requirements for the motors are determined by the hydraulic pressure and the speed of the actuation. A slider-crank linkage converts the rotary motion to linear motion (Fig. 5.2). The minimum stroke position occurs when the crank r is co-linear with the connecting rod l (position C). It is the initial position of the motor when fluid pressure is maximum. This design uses $l = r$ such that the minimum operation angle α between the crank and the horizontal line is 30° . The range of α is adjustable to accommodate a different fluid volume. For our actuator, the maximum α needed is 120° (position A). When the crank is vertical, the connecting rod is co-linear with the stroke path (position B). With this design, the torque τ of the motor can be related to the force acting on the piston rod of the hydraulic cylinder F_t by:

$$\tau = rF_t \sin \alpha, \quad 30^\circ \leq \alpha \leq 120^\circ \quad (5.1)$$

In a quasi-static condition, $F_t = PA$, where P is the quasi-static fluid pressure and A is the inner cross-sectional area of the hydraulic cylinder. The relationship between the crank angle α and the piston location x is obtained from the kinematics of a fourbar offset slider-crank [341]:

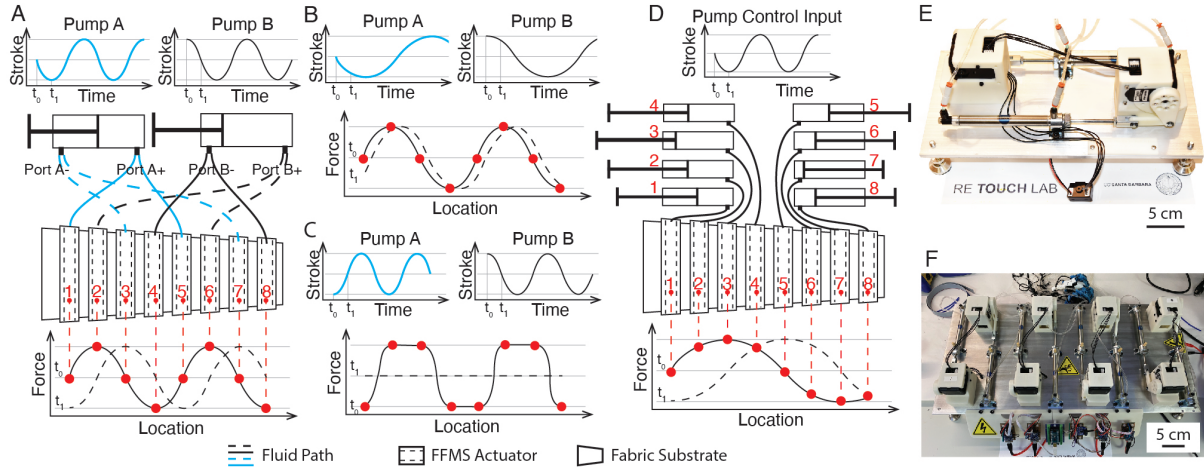


Figure 5.3: Various control input designs can be used to generate spatial-temporal compression wave patterns. A. Two pistons can be used to control eight actuators for maximum efficiency, with spatial compression forces coupled at locations routed to the same motor. The sinusoidal displacements with a phase delay of $\pi/2$ on the top denote an example of the input signal for both pistons. The plot on the bottom illustrates the resulting spatial profile of the compression force at times t_0 and t_1 . The two-piston driving system can also compose other spatial-temporal compression force patterns such as B and C, with the top figures showing the piston input signals, and the bottom figures showing the composed spatial waves. D. The driving system can be expanded to eight pistons to control each actuator independently. Arbitrary spatial compression force waves can be generated. E. The prototype of the two-piston driving system. F. The prototype of the eight-piston driving system.

$$x = r \cos \alpha + l \sqrt{1 - \left(\frac{r \cdot \sin \alpha - r}{l} \right)^2}, \quad 30^\circ \leq \alpha \leq 120^\circ \quad (5.2)$$

Our two-motor design is sufficient to produce peristaltic motions via coupled hydraulic channels (Fig. 5.3 A, E). As the piston of the hydraulic cylinder moves back and forth, the hydraulic pressure increases in one port but decreases in the other port. With two motors, the eight actuators can be connected to the four ports, with two channels sharing one port. When two sinusoidal signals with a phase delay of $\pi/2$ are fed into the two motors, a compression force pattern similar to a sinusoidal wave can be generated spatially along the wearable robot (Fig. 5.3 A). Different input signals result in distinct spatial-temporal compression force patterns (Fig. 5.3 B, C).

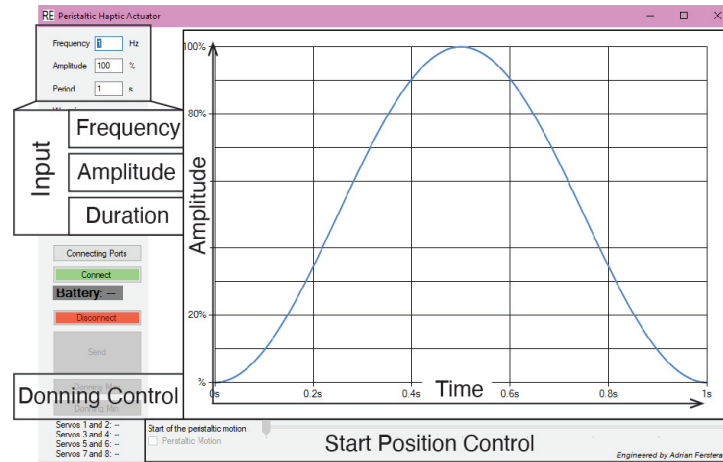


Figure 5.4: The graphic user interface generates a user-defined waveform with input parameters such as frequency and amplitude. The interface also includes a two-step donning design of the device.

The two-motor compact design uses a minimal number of motors at the cost of coupled compression forces. In many other situations, each hydraulic channel needs to be controlled independently. We designed a second driving system using eight pistons to allow independent control over individual channels to generate arbitrary compression force patterns (Fig. 5.3 D, F).

5.2.3 Software Development

Each piston is driven by a programmable high torque servo (HerklueX DRS 0602, DST Robot) that is controlled by computer via a synchronous serial communication. A software graphical user interface (GUI) enables the design of compression patterns via frequency, amplitude, duration, and phase parameters (Fig. 5.4). The motors can be powered using a rechargeable Lipo battery (14.8 V, 9 A). The software also implements a two-step donning process. First, pistons are positioned to fully pressurize one chamber in the hydraulic cylinder, allowing actuators connected to that chamber to be fastened to the arm of the user. Then, pistons are positioned to fully pressurize the other chamber, allowing the rest of the actuators to be fastened.

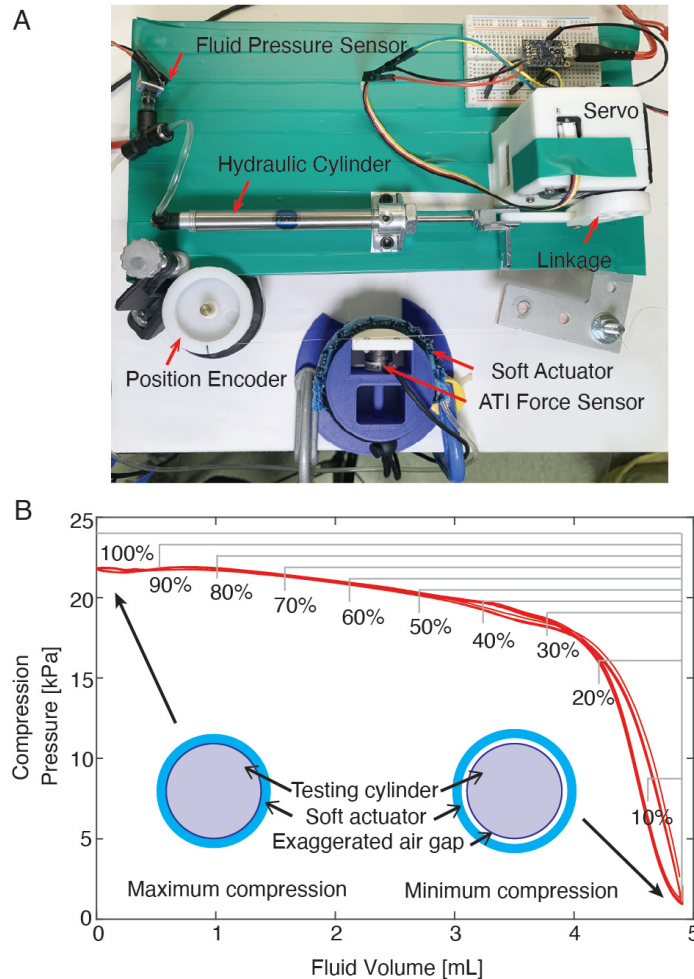


Figure 5.5: Evaluation of the force generated by a single actuator. A. Compression force testing set-up for a single actuator. B. Relationship between fluid volume and compression pressure follows a similar curve for different operation strokes ranging from 10% to 100% with the margins marked in the plot. Note that the minimum compression pressure occurs when the fluid volume is maximum. As the fluid is withdrawn from the actuator, the compression pressure increases. The inserted diagrams illustrate the extreme conditions for maximum and minimum compression pressure to occur.

5.3 Mechanical Characterization of the Dynamic Compression System

Various peristaltic, all-in-phase, and sequential squeezing spatial-temporal compression patterns can be delivered through time-varying signals for a single actuator, as well as multiple actuators at different locations. In this section, we evaluate the compression force generated by a single actuator, the dynamic frequency response of the system, and the large range of dynamic compression motion patterns that the peristaltic wearable robot is capable of generating.

5.3.1 Single Actuator Compression Force Testing

We characterized the compression force of a single actuator by wrapping it around a cylindrical testing fixture with a force sensor (ATI Nano17; ATI Industrial Automation) (Fig. 5.5 A). The force sensor measures part of the compression force exerted on the arc segment with a central angle of 68.9 degrees. The diameter of the cylinder in the testing setup is 63.7 mm to mimic the size of a human limb. Different design parameters of the testing fixture, such as the cylinder radius, can affect the compression pressure measurement. Applying the hoop stress equation yields the following expression for the compression pressure:

$$P_c = \frac{t_{act}\sigma_{act}}{R} = \frac{F}{A_c}, \quad (5.3)$$

where P_c represents the compression pressure, t_{act} and σ_{act} are the thickness and the axial stress of the actuator, R is the radius of the cylinder wrapped by the actuator, F is the force measured from the ATI nano 17, A_c is the contact area between the actuator and the testing cylinder. A position encoder measured the instantaneous stroke of the hydraulic cylinder and a pressure sensor was used to monitor hydraulic pressure. All sensing signals were recorded synchronously using a real-time computer-in-the-loop system with a sampling rate of 100 Hz

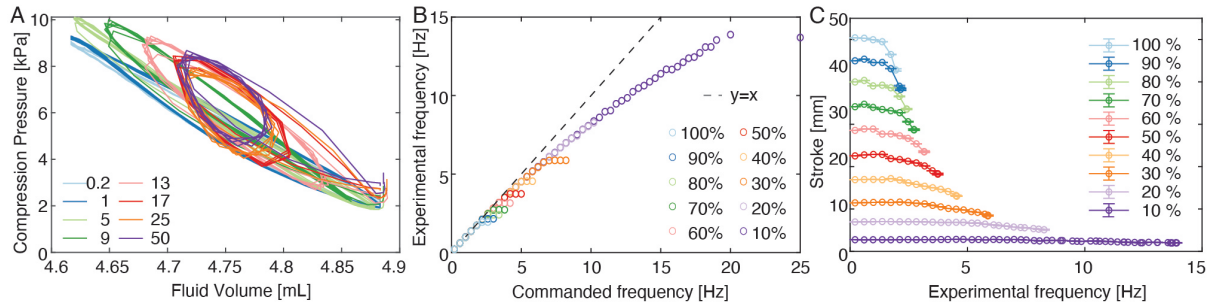


Figure 5.6: Frequency response of the system. A. The hysteresis loops presented in the relationship between fluid volume and compression pressure show energy loss during the actuation. The energy loss increases with increasing frequency. Legend: commanded frequency in Hz. B. Legend: different operation stroke range in %. The experimental frequency reaches a plateau for all stroke ranges. The smaller the stroke range, the higher the experimental frequency achieved. Overall, the system is able to operate at frequencies up to about 20 Hz despite some discrepancies between commanded frequency and experimental frequency. C. As the stroke magnitude gets higher, the drop-off in stroke occurs at lower frequencies. The magnitude remains almost flat across all frequencies for 10% operation stroke range.

(QPIDE; Quanser, Inc., with Simulink, The MathWorks, Inc.).

Results showed that compression pressure decreased with increasing fluid volume in the actuator, which is consistent with the model presented in Zhu et al. [2] (Fig. 5.5 B). The resting state of the actuator is when the fluid volume is maximum, leading to minimum compression pressure. When fluid volume is withdrawn from the actuator, the compression pressure increases. This relationship was approximately linear both before and after fluid volume of 4 mL, with a larger slope for fluid volume between 4 mL and 5 mL. The maximum compression pressure decreased with operation stroke range, as the margins illustrated in Fig. 5.5 B.

5.3.2 Dynamic Frequency Response of the System

We evaluated the system's dynamic frequency response at frequencies ranging from 0.2 Hz to 50 Hz with stroke amplitudes from 10% to 100%. The stroke of the piston was measured, and the actual frequency (experimental frequency) was obtained using spectrum analysis of the data. Fig. 5.6 A shows the results for the stroke amplitude of 10%. Compression pressure decreased as frequency increased up to 17 Hz, above which the compression pressure and the

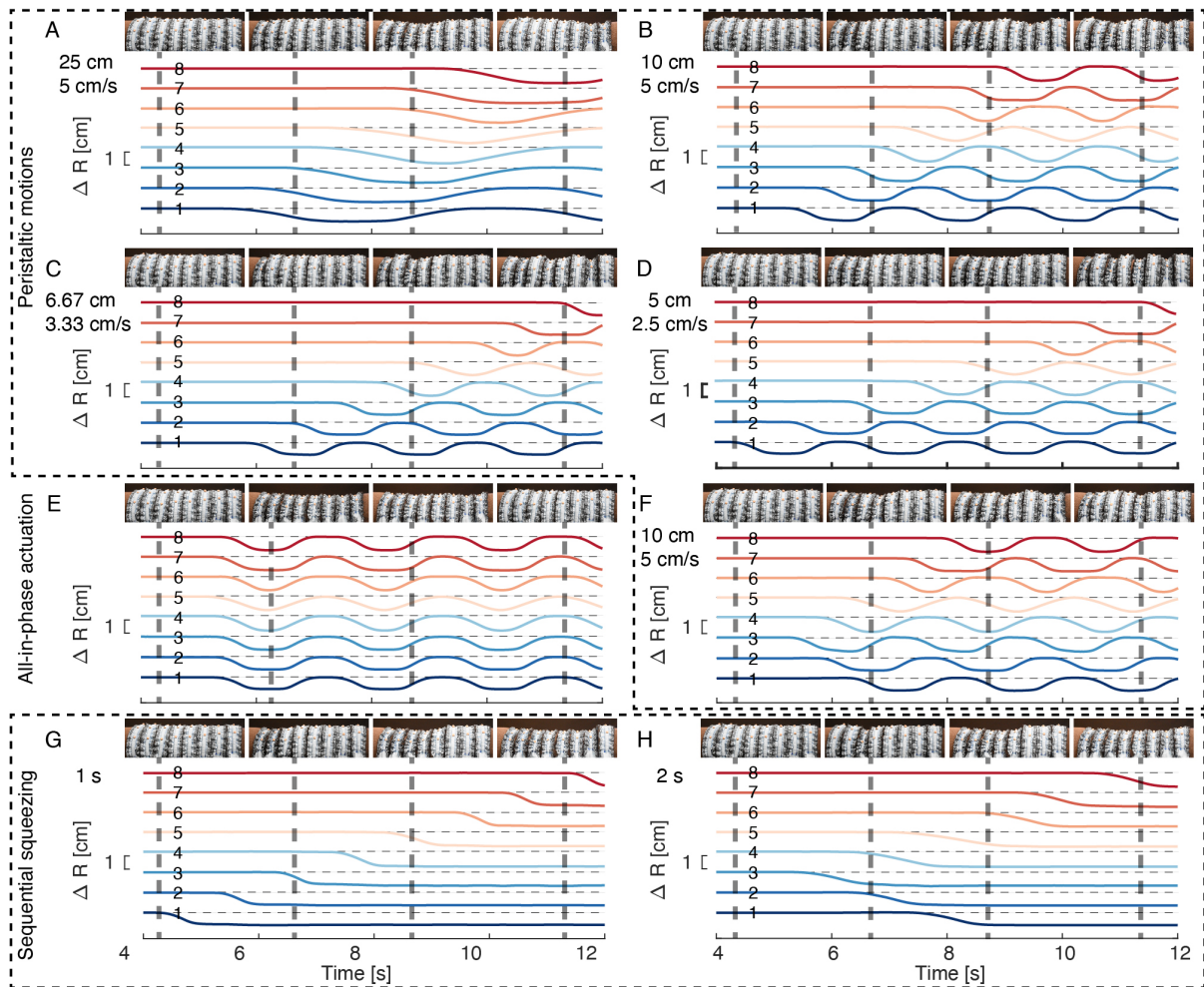


Figure 5.7: Motion capture results for various dynamic compression patterns including peristaltic motions (A-D, F), all-in-phase actuation (E), and sequential squeezing (G-H). The texts at the top left corner of each subfigure denote the wavelength and wave speed of each peristaltic pattern. For the sequential squeezing patterns, the texts show the squeezing time of each actuator.

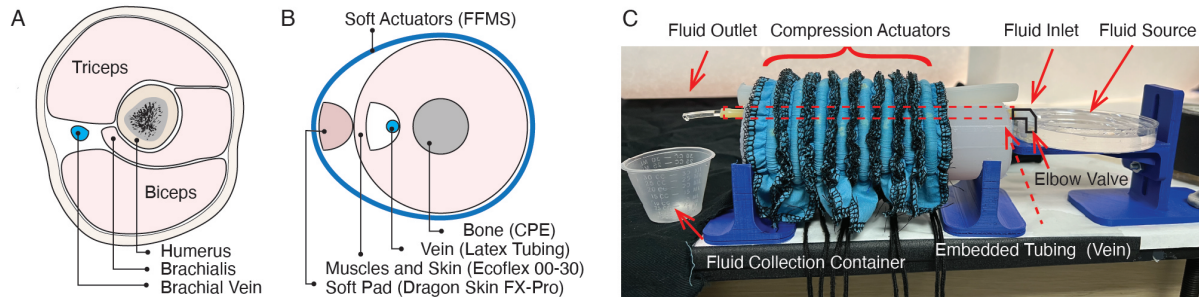


Figure 5.8: The wearable robot is configured to promote hemodynamic circulation in a limb model via peristaltic transport. A. A simplified illustration of the cross-section through the middle of upper arm [72]. B. The cross-section of the arm model used for the experiment. C. Testing apparatus for the peristaltic transport.

fluid volume had similar ranges. Results also revealed that the system was capable of operating at frequencies up to 20 Hz (Fig. 5.6 B). Motor power constrained the stroke amplitude in that the lower the maximum stroke used, the higher frequency achieved. The magnitude decrement was more prominent for larger maximum stroke (Fig. 5.6 C), while little magnitude decrement was observed when operating with 10% stroke.

5.3.3 Dynamic Compression Motion Patterns

We characterized the dynamic spatial compression motion patterns by measuring shape deformation with an optical motion capture system (Flex 13; OptiTrack). Twenty-four reflective markers (5 mm diameter) were distributed on the surface of the wearable robot, with three on each actuator. Compression patterns were generated and the dynamic positions of each marker are measured. Fig. 5.7 shows the average radius changes of the three markers on each actuator over time. Five peristaltic motions were composed by varying wavelength, wave speed, and the starting actuator (Fig. 5.7 A-D, F), along with an all-in-phase synchronized compression pattern (Fig. 5.7 E). Two sequential squeezing patterns were also evaluated with squeezing times of 1 s and 2 s respectively (Fig. 5.7 G-H). These results mechanically validated that the wearable robot was capable of generating different compression patterns on a soft body.

5.4 Applications for Compression Therapy and Therapeutic Massage

We demonstrated applications of the peristaltic wearable robot for compression therapy to promote blood circulation and for therapeutic massage therapy.

5.4.1 Compression Therapy for Blood Flow Promotion

Peristaltic action on a flexible tube can introduce fluid flow, thus, can be used to promote blood flow in the veins, to treat various medical conditions [69, 323, 324]. To demonstrate the ability of the peristaltic compression robot to promote blood circulation, we designed and fabricated an upper arm model (Fig. 5.8 B) that mimics the anatomy of the human upper arm (Fig. 5.8 A) [72]. The muscles (triceps, biceps, and brachialis muscles) and skin were realized using a soft silicone material (Ecoflex 00-30, shore hardness 00-30, Smooth-On, Inc., Macungie, PA). A rigid 3D printed bone structure was fabricated in CPE (Ultimaker filament). A latex tube was placed adjacent to the bone, representing the brachial vein. A soft strip made of stiffer silicone with a shore hardness of 2A (Dragon Skin FX-Pro, Smooth-On, Inc., Macungie, PA) was used to direct compression pressure to the vein.

The limb apparatus is shown in Fig. 5.8 C. Vegetable glycerin served as the fluid for transport in the artificial vein, as it can be mixed with water for different viscosity values [342]. Peristaltic compression patterns were generated when each motor rotated sinusoidally with an onset delay time of Δt between adjacent actuators:

$$\alpha = A \sin(2\pi f(t + (n - 1)\Delta t)), \quad (5.4)$$

where α is the rotation degree for the motor, n indexes the actuator channel, t is the time variable, A and f are the amplitude and frequency of the sinusoidal wave respectively. The

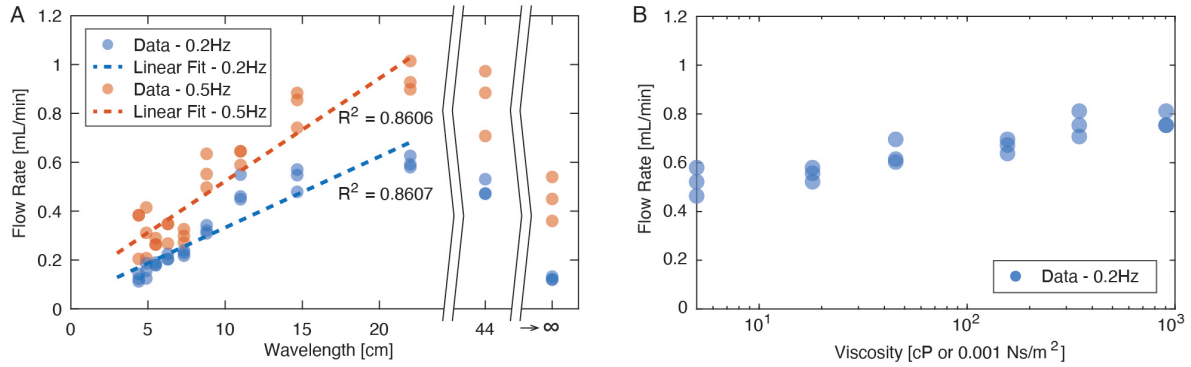


Figure 5.9: A. Experimental results of the flow rate showed a linear relationship with the wavelength, in agreement with the theoretical prediction (equation 5.7). B. Results showed that the viscosity had a weak effect on the flow rate, agreeing with the analytical predictions in [73, 74].

spatial wave generated by all the actuators is described as:

$$y(x, t) = A' \cos\left(\frac{2\pi}{\lambda}x - 2\pi f(t - \Delta t)\right), \quad (5.5)$$

where y and x are the vertical and horizontal position variables, A' and λ are the amplitude and wavelength of the spatial wave respectively.

The peristaltic compression robot was wrapped around the limb model, with a spacing of about 1.1 cm between adjacent actuators. During peristaltic actuation, a flow was induced, transporting fluid from the source through an elbow connector to the collection container (Fig. 5.8 C). From the theory of peristaltic flow in flexible tubes [73], when the pressure change over one wavelength $\Delta P_\lambda = 0$, the time average peristaltic flow \bar{Q} in a tube depends on the average radius of the tube a , wave amplitude b , and wavespeed c as follows:

$$\bar{Q} = \frac{\pi c b^2}{2} \frac{16a^2 - b^2}{2a^2 + 3b^2} \quad (5.6)$$

When the frequency f of the peristaltic wave is constant, the time average flow increases with

Table 5.1: Theoretical viscosity and Reynolds number of glycerin-water mixtures with different glycerin concentrations in mass C_m .

C_m	Density	Dynamic viscosity [cP]	Reynolds number
0.5	1.12	5.57	0.6427
0.7	1.17	20.88	0.1799
0.8	1.20	53.96	0.0714
0.9	1.23	193.24	0.0204
0.95	1.24	438.10	0.0091
1	1.26	1,178.64	0.0034

wavelength λ due to the increase in unoccluded volume:

$$\bar{Q} = \frac{\pi \lambda f b^2}{2} \frac{16a^2 - b^2}{2a^2 + 3b^2} \quad (5.7)$$

Frequencies of 0.2 Hz and 0.5 Hz were tested. Different peristaltic compression patterns were generated with onset delay time stepping between 0 ms (all-in-phase actuation) and 1125 ms (90phase shift) by 125 ms (9phase shift). Each wave pattern was repeated three times, and the fluid volume collected in the container was measured.

We found that the flow rate was higher for peristaltic motions than all-in-phase actuation when the wavelength was larger than about 5 cm. The time-average flow rate increased with the wavelength following a linear relationship (Fig. 5.9 A), in agreement with theoretical predictions (equation 5.7). The maximum flow rate was achieved when the wavelength was about 22 cm. When the wavelength further increased to 44 cm, the flow rate decreased. This may be due to the boundary conditions in the testing configuration, as the total length of actuation (about 9.2 cm) was much smaller than the wavelength of 44 cm. When the wavelength was very large, the wave pattern resembled all-in-phase actuation and the fluid reflux counteracting with the peristaltic flow was large. This decrement for wavelengths above 22 cm was also presented when frequency increased to 0.5 Hz. The overall flow rate for 0.5 Hz was slightly larger than 0.2 Hz, in agreement with theoretical predictions (equation 5.7).

The dynamic viscosity of glycerin at temperature 22 is about 1179 cP, which is much larger

than the normal blood viscosity values (between 3.3 cP and 5.5 cP) [343]. Blood is also a non-Newtonian fluid whose viscosity changes depending on the hemodynamic conditions. Here, we evaluated the effect of fluid viscosity on induced flow rate. The viscosity of the transported fluid was varied by mixing glycerin with water at different weight percentages. The theoretical viscosity of the glycerin-water mixture was obtained using published results [342] (Table 5.1).

Experimental results showed that viscosity had a weak effect on the flow rate (Fig. 5.9 B). The flow rate decreased as the viscosity decreased. This finding is consistent with predictions in the literature that show that viscosity have little effect on the flow rate when viscous forces are dominant (small Reynolds numbers) [73, 74].

5.4.2 Therapeutic Massage with a Haptic Sleeve

Wave-like peristaltic compression can also be used to emulate manual massage therapy for stress reduction and muscle relaxation. Papadopoulou et al. developed an affective sleeve that produces sequential compression and warmth on the forearm using shape memory alloys (SMAs) [95].

We adapted our peristaltic wearable robot to supply massaging patterns (Fig. 5.10). Different massage patterns may be generated by varying actuation frequency, amplitude (operation stroke range), the phase time delay between adjacent actuators, and the initialization location for the wave. A supplementary video shows several examples illustrating patterns of haptic massage feedback generated by the device.

5.5 Discussion and Future Work

This article presents a peristaltic soft, wearable robot for robotic compression therapy. Although IPC has remained the main tool for automated compression therapy for decades, little device renovation has been done to improve the spatial arrangement due to the limitations of

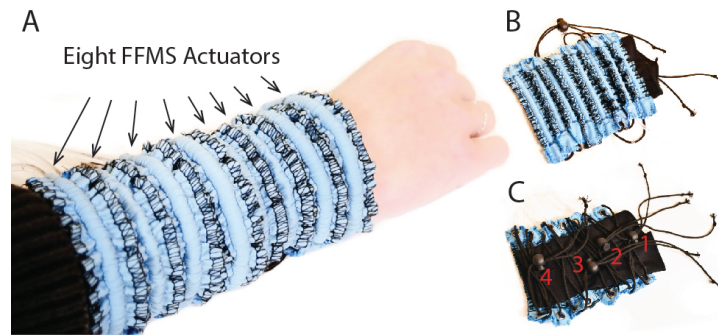


Figure 5.10: A. Our peristaltic wearable robot on user's forearm for therapeutic massage. B. The actuator side of the wearable robot. C. The closure side of the wearable robot.

pneumatic operation. We present a novel peristaltic wearable robot that has finely distributed modules with a width comparable to the size of a finger for localized compression. We also implement a modular hydraulic actuation system for efficient control compared to commonly used pneumatic wearables. Each module is able to generate compression pressure up to 22 kPa and frequency up to 14 Hz, meeting the requirements for compression therapy and therapeutic haptic massage [71, 304, 325]. With programmable frequency, amplitude, phase delay, and duration, it is capable of rendering a large range of spatial-temporal wave patterns. We further demonstrate the application of the peristaltic wearable robot for blood flow promotion and therapeutic haptic massage.

The theoretical and experimental results demonstrate the device's ability to drive fluid flow in a model limb via peristaltic transport, and provide a quantitative model that parameters governing the peristaltic pattern to the flow rate and fluid properties. These findings indicate that such systems may hold substantial promise for the treatment of lymphatic and blood circulation inefficiencies, which are associated with several health disorders. The model arm used in our experiments is in reality quite different than a real arm. Future translational research aimed at designing and evaluating the clinical efficacy of such a peristaltic robotic sleeve is warranted.

Chapter 6

Conclusion

This dissertation is motivated by the longstanding goal of designing and engineering soft, expressive, and ergonomic haptic garments at the intersection of different domains relating to soft robotics, functional wearables, and haptics, as reviewed in chapter 2. Despite numerous advances in haptic displays, this goal is far from being achieved due to the complexity of human touch and perception, the engineering challenges for soft wearable devices, and the diversity in human physical anatomies and psychological behaviors. This thesis addresses these challenges by designing soft actuators that are conformal to the human body (chapter 3); integrating multimodal actuation for expressive haptic rendering (chapter 4); and composing dynamic compression patterns for massage therapies via a peristaltic wearable robot (chapter 5).

In contrast to many innovations in haptic devices, this thesis proposes a new category of haptic wearables that could be readily integrated into daily garments. Chapter 3 presents a novel fabric-based actuator (FFMS) design accounting for wearability, safety, and functionality. The fabrication methods I developed utilize low-cost materials and easily-accessible apparel engineering methods. These actuators can strain, squeeze, bend, and conform to the human body, providing forces or deformations on the skin. They can achieve strains exceeding 100%, exert forces greater than 115 times their weight, and operate at frequencies of 5 Hz or

more. I further demonstrated several applications for these actuators, including several artificial muscles in different scales, assistive glove for grasping, compression garments for the extremities, and devices for actuating small skin tissues via localized skin stretch. Not only does this work contribute to the design, fabrication, and modeling of FFMS actuators, but it also lays the technical foundation for chapter 4 and chapter 5.

One of the most notable challenges in haptic engineering concerns the expressiveness of the device. While researchers have combined different types of haptic stimulations in their devices to enrich the information conveyed, none of them can render compression, skin stretch, and vibration all together in a soft and compact wearable device. To address this gap, chapter 4 focuses on building a multimodal expressive haptic sleeve that renders compression, skin stretch, and vibration, leveraging the capabilities of FFMS actuators developed in chapter 3. This research shows that this multimodal actuation can convey a broad range of distinct meaningful haptic messages to the user. This research also addresses the challenge of inconsistency in biomechanics among users by developing soft capacitive sensors integrated with a closed-loop control strategy to control the compression force. Results from psychophysical evaluations and subjective assessments show that a large range of different haptic messages can be generated and these haptic messages are easily detectable, distinguishable, and recognizable by the user.

Finally, taking inspiration from the literature review, the development of FFMS actuators, as well as the expressiveness of PneuSleeve through chapters 2 to 4, chapter 5 presents work addressing challenges from another perspective by developing haptic wearables that could potentially improve human health. This work expands existing compression therapy devices with a more compact wearable robot using finger-scale FFMS actuators. The customized driving systems made from low-cost and off-the-shelf components offer a large amount of flexibility for personalized demands. In addition, I demonstrated the efficacy of this wearable robot for fluid transport in a mechanical model of the upper limb, emulating blood transport in the human body. Finally, I identified the optimal driving regimes for fluid transport both theoretically

and empirically.

6.1 Future Research Directions

This dissertation contributes to haptic garments at the intersection of soft robotics, wearable technologies, and haptic rendering on large areas of the skin. The promising findings from this research suggest several future research directions, some of which I am currently pursuing with my colleagues.

- The comprehensive literature review from chapter 2 highlights the potential of soft robotic and haptic garments to complement the capabilities of the human body by providing protection and recovery strategies, augmenting the physical performance of healthy individuals, facilitating physical interactions with our environment, supplementing human abilities of perception and cognition, and evolving the aesthetic approaches addressing expanded functionalities, human emotions, and social behaviors. While this thesis mainly addresses wearable garments, more research is needed for tabletop devices such as encounter-type haptic devices.
- Chapter 3 presents the design, fabrication, and modeling of FFMS actuators, a new family of soft actuators that have potential to be easily integrated into daily garments. Although this research demonstrates the FFMS actuators meet both the wearability requirements and the functionality needs for soft wearable robotics and haptics, it focuses on the actuation aspects. Chapter 4 complements chapter 3 with the development of soft sensors for compression force sensing, enabling closed-loop control to ensure that the compression forces rendered are consistent across different users. More research is needed on strain sensing for FFMS actuators for their displacement operating mode. Although the fabrication techniques described in this research are low-cost and easily ac-

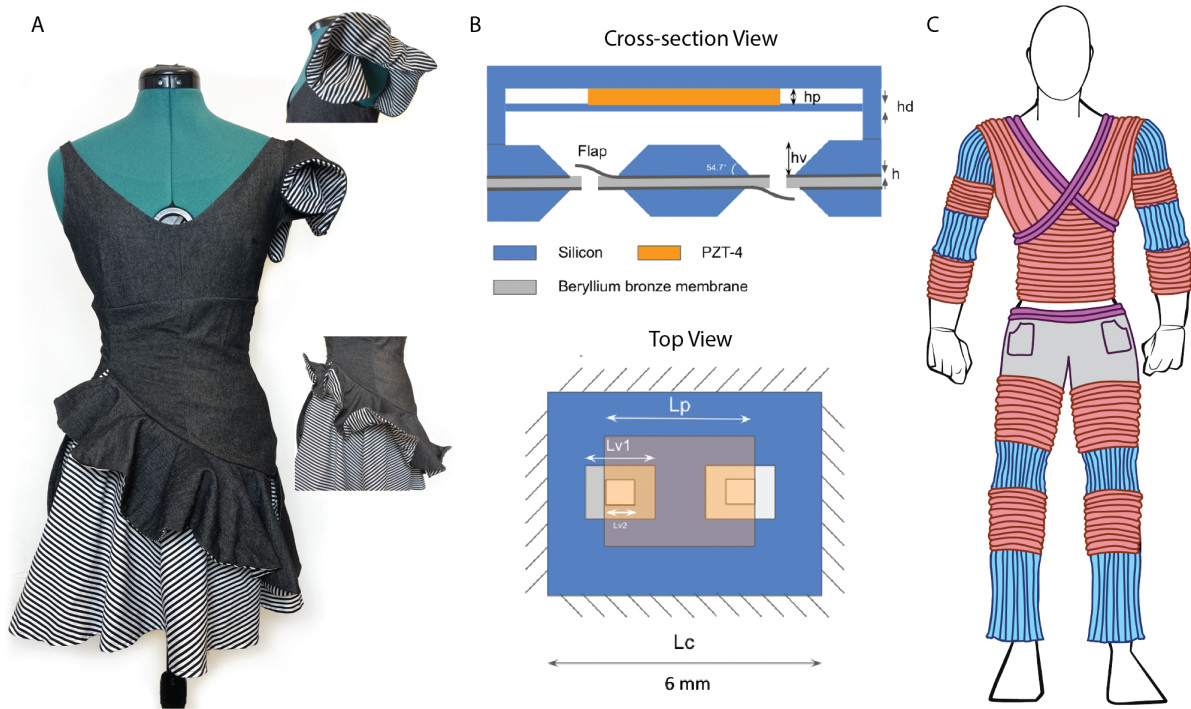


Figure 6.1: A. A shape changing garment for expressive fashion. Inserts show the actuated sleeve and skirt ruffles. B. A piezoelectric micro-pump I designed to generate a volumetric flow to power miniature fluidic actuators. C. An example of the future garment as a whole-body haptic suit. The colored strips denote the active components that can change length longitudinally or exert compression force radially on the body.

cessible, further research is needed to align them with manufacturing techniques. While chapter 3 demonstrates the scalability of FFMS actuators ranging from millimeter scales to centimeter scales, many other applications require further scaling up or down of the sizes. These applications would require more research on the materials synthesis and fabrication techniques.

- The expressiveness achieved through multimodal actuation in chapter 4 raises interesting questions of whether we can leverage other sensory channels such as vision for the design of expressive garments. The emergence of shape-changing garments opens the opportunity in this field. I am currently working on an expressive garment that changes shape to reflect the wearer's internal states. By engineering the stretchability anisotropy

across the FFMS actuator, bending and twisting motions could be generated. When integrated with components of a garment, these motions empower the garment to change shape as expressive representations. For example, in the shape changing garment I designed in Figure 6.1 A, the sleeve and the skirt ruffle flip and reveal the inner pattern in various dynamic patterns. These motion patterns can be used to express the user's internal states, such as the heart rates or the brain activities of the wearer, when integrated with sensors.

- Chapter 5 demonstrates a proof-of-concept method to enhance blood circulation using a model upper arm through robotic haptic therapies. However, the effects of this wearable robot on other locations of the body remain under-explored. Chapter 5 also evaluates the effect of wavelength, wave speed, and viscosity on the introduced flow rate in the artificial vein. Another important factor that may change the flow rate is the spacing between the actuators, which needs more investigation. Furthermore, future research is needed to validate the clinical efficacy of such a wearable robot for the treatment of lymphatic disorders.
- Chapter 5 focuses on improving human physical health through massage therapies. In addition, massage can also affect our emotions by reducing stress and increasing relaxation. Therefore, I and my colleagues are designing haptic apparels that convey various emotions and information. Such capabilities are evaluated via behavioral experiments using semantic differential scaling, factor analysis, and emotion self-appraisal. This research paves the way for turning everyday garments into intimate companions to provide social and emotional support to the wearer.
- While this thesis focuses on the development and applications of FFMS, other device innovations could open up many opportunities for wearable robotic and haptic devices. For example, variable stiffness could be achieved using magnetorheological fluid with

varying magnetic field. The development of MEMS pumps could untether fluidic actuators from compressed fluid sources [344]. For example, I have designed a piezoelectric MEMS pump for one of my courses during my PhD (Figure 6.1 B). This pump is in sub-centimeter scale and uses piezoelectric actuation together with two flaps to generate a unidirectional flow in the fluid channel. Analytical modeling shows that a driving voltage of 200 V and frequency of 30 kHz can produce a pressure of 6 MPa in the fluid and a volumetric flow rate of 0.033 mL/s. When integrated with miniature actuators that do not require high power and large fluid volume, these pumps and their powering systems can be easily integrated with garments. These device innovations build up the affordance of the device, broadening the sphere of possible use cases.

- Recent development of intelligent systems sheds lights on smart wearable systems where individual components could be working more effectively and coherently together in a collaborative manner. For example, biological sensing methods (e.g. skin conductance) could be integrated with future wearables to track the mental states of the wearer, and machine learning methods could be used to learn from user's status to guide the actuation of the garment for personalized support.

The various findings presented in this thesis open up many opportunities for future wearable interfaces to both provide assistance with physical tasks (e.g. rehabilitation devices, HCI devices) and aid in social interactions (e.g. via haptic messages), enabling users to feel and understand haptic interactions rendered using soft devices that are compact, safe, and versatile. These findings also raised possibilities of whole-body garment scenarios to enable superhero capabilities such as the Iron Man suit in the movie *Avengers: Infinity War*, or render realistic touch feedback like the suit in the movie *Ready Player One*. Figure 6.1 C illustrates one example of such garment using FFMS actuators. These FFMS actuators are arranged on the body to provide compression and skin stretch, enabling full-body haptic rendering and motion assis-

tance. The results of this dissertation could inform many developments of such next-generation wearable interfaces that are fidelitous, ubiquitous, and socially relevant.

Bibliography

- [1] M. Zhu, S. Biswas, S. I. Dinulescu, N. Kastor, E. W. Hawkes, and Y. Visell, *Soft, wearable robotics and haptics: Technologies, trends, and emerging applications*, *Proceedings of the IEEE* **110** (2022), no. 2 246–272.
- [2] M. Zhu, T. N. Do, E. Hawkes, and Y. Visell, *Fluidic fabric muscle sheets for wearable and soft robotics*, *Soft Robotics* **7** (2020), no. 2 179–197.
- [3] M. Zhu, A. H. Memar, A. Gupta, M. Samad, P. Agarwal, Y. Visell, S. J. Keller, and N. Colonnese, *Pneusleeve: In-fabric multimodal actuation and sensing in a soft, compact, and expressive haptic sleeve*, in *Proceedings of the 2020 CHI Conference on Human Factors in Computing Systems*, pp. 1–12, 2020.
- [4] P. Polygerinos, Z. Wang, K. C. Galloway, R. J. Wood, and C. J. Walsh, *Soft robotic glove for combined assistance and at-home rehabilitation*, *Robotics and Autonomous Systems* **73** (2015) 135–143.
- [5] A. Mohammadi, J. Lavranos, H. Zhou, R. Mutlu, G. Alici, Y. Tan, P. Choong, and D. Oetomo, *A practical 3d-printed soft robotic prosthetic hand with multi-articulating capabilities*, *Plos one* **15** (2020), no. 5 e0232766.
- [6] C. J. Payne, E. G. Hevia, N. Phipps, A. Atalay, O. Atalay, B. R. Seo, D. J. Mooney, and C. J. Walsh, *Force control of textile-based soft wearable robots for mechanotherapy*, in *Proceedings - IEEE International Conference on Robotics and Automation*, pp. 5459–5465, Institute of Electrical and Electronics Engineers Inc., sep, 2018.
- [7] B. Quinlivan, S. Lee, P. Malcolm, D. Rossi, M. Grimmer, C. Siviyy, N. Karavas, D. Wagner, A. Asbeck, I. Galiana, *et. al.*, *Assistance magnitude versus metabolic cost reductions for a tethered multiarticular soft exosuit*, *Sci. Robot* **2** (2017), no. 2 1–10.
- [8] P. H. Nguyen, I. B. Imran Mohd, C. Sparks, F. L. Arellano, W. Zhang, and P. Polygerinos, *Fabric soft poly-limbs for physical assistance of daily living tasks*, in *Proceedings - IEEE International Conference on Robotics and Automation*, vol. 2019-May, pp. 8429–8435, Institute of Electrical and Electronics Engineers Inc., may, 2019.

- [9] C. Fang, Y. Zhang, M. Dworman, and C. Harrison, *Wireality: Enabling complex tangible geometries in virtual reality with worn multi-string haptics*, in *Proceedings of the 2020 CHI Conference on Human Factors in Computing Systems*, pp. 1–10, 2020.
- [10] R. Granberry, K. Eschen, B. Holschuh, and J. Abel, *Functionally graded knitted actuators with niti-based shape memory alloys for topographically self-fitting wearables*, *Advanced Materials Technologies* (2019).
- [11] “Caress of the Gaze.” Behnaz Farahi, 2015, behnazfarahi.com/caress-of-the-gaze/.
- [12] Gao, Ying. Ying Gao - Designer, 2016, yinggao.ca/interactifs/neutralite-cant-and-wont/.
- [13] I. Galiana, F. L. Hammond, R. D. Howe, and M. B. Popovic, *Wearable soft robotic device for post-stroke shoulder rehabilitation: Identifying misalignments*, in *2012 IEEE/RSJ International Conference on Intelligent Robots and Systems*, pp. 317–322, IEEE, 2012.
- [14] M. Xiloyannis, D. Chiaradia, A. Frisoli, and L. Masia, *Physiological and kinematic effects of a soft exosuit on arm movements*, *Journal of neuroengineering and rehabilitation* **16** (2019), no. 1 1–15.
- [15] M. Chen, J. Yan, and Y. Yu, *Biometric Perception Interface*, in *International Workshop on Haptic and Audio Interaction Design - HAID2019*, (Lille, France), Mar., 2019.
- [16] Adi Meyer, Silvia Rueda and Sirou Peng, “Aposema: Soft Robotic Mask.” Interactive Architecture Lab, 19 Sept. 2017, www.interactivearchitecture.org/lab-projects/aposema-soft-robotic-mask.
- [17] A. Delazio, K. Nakagaki, R. L. Klatzky, S. E. Hudson, J. F. Lehman, and A. P. Sample, *Force jacket: Pneumatically-actuated jacket for embodied haptic experiences*, in *Proceedings of the 2018 CHI Conference on Human Factors in Computing Systems*, p. 320, ACM, 2018.
- [18] W. Wu and H. Culbertson, *Wearable haptic pneumatic device for creating the illusion of lateral motion on the arm*, in *2019 IEEE World Haptics Conference (WHC)*, pp. 193–198, IEEE, 2019.
- [19] E. M. Young, A. H. Memar, P. Agarwal, and N. Colonnese, *Bellowband: A pneumatic wristband for delivering local pressure and vibration*, in *2019 IEEE World Haptics Conference (WHC)*, pp. 55–60, IEEE, 2019.
- [20] A. Gupta, A. A. R. Irudayaraj, and R. Balakrishnan, *Hapticclench: Investigating squeeze sensations using memory alloys*, in *Proceedings of the 30th Annual ACM Symposium on User Interface Software and Technology*, pp. 109–117, ACM, 2017.

- [21] B. B. Kang, H. Choi, H. Lee, and K.-J. Cho, *Exo-glove poly ii: A polymer-based soft wearable robot for the hand with a tendon-driven actuation system*, *Soft robotics* **6** (2019), no. 2 214–227.
- [22] H. K. Yap, J. H. Lim, F. Nasrallah, and C.-H. Yeow, *Design and preliminary feasibility study of a soft robotic glove for hand function assistance in stroke survivors*, *Frontiers in neuroscience* **11** (2017) 547.
- [23] T. Han, F. Anderson, P. Irani, and T. Grossman, *Hydroring: Supporting mixed reality haptics using liquid flow*, in *Proceedings of the 31st Annual ACM Symposium on User Interface Software and Technology*, pp. 913–925, 2018.
- [24] X. Zhang, A. Shtarbanov, J. Zeng, V. K. Chen, V. M. Bove, P. Maes, and J. Rekimoto, *Bubble: Wearable assistive grasping augmentation based on soft inflatables*, in *Extended Abstracts of the 2019 CHI Conference on Human Factors in Computing Systems*, p. LBW2313, ACM, 2019.
- [25] I. M. Koo, K. Jung, J. C. Koo, J.-D. Nam, Y. K. Lee, and H. R. Choi, *Development of soft-actuator-based wearable tactile display*, *IEEE Transactions on Robotics* **24** (2008), no. 3 549–558.
- [26] H. A. Sonar, A. P. Gerratt, S. P. Lacour, and J. Paik, *Closed-loop haptic feedback control using a self-sensing soft pneumatic actuator skin*, *Soft robotics* **7** (2020), no. 1 22–29.
- [27] J. Kim, G. Lee, R. Heimgartner, D. A. Revi, N. Karavas, D. Nathanson, I. Galiana, A. Eckert-Erdheim, P. Murphy, D. Perry, *et. al.*, *Reducing the metabolic rate of walking and running with a versatile, portable exosuit*, *Science* **365** (2019), no. 6454 668–672.
- [28] “Full Body Haptic Feedback & Motion Capture Tracking VR Suit.” TESLASUIT, teslasuit.io/.
- [29] J. Chung, R. Heimgartner, C. T. O’Neill, N. S. Phipps, and C. J. Walsh, *Exoboot, a soft inflatable robotic boot to assist ankle during walking: Design, characterization and preliminary tests*, in *2018 7th IEEE International Conference on Biomedical Robotics and Biomechatronics (Biorob)*, pp. 509–516, IEEE, 2018.
- [30] Y.-L. Park, B.-r. Chen, N. O. Pérez-Arancibia, D. Young, L. Stirling, R. J. Wood, E. C. Goldfield, and R. Nagpal, *Design and control of a bio-inspired soft wearable robotic device for ankle–foot rehabilitation*, *Bioinspiration & biomimetics* **9** (2014), no. 1 016007.
- [31] S. Sridar, P. H. Nguyen, M. Zhu, Q. P. Lam, and P. Polygerinos, *Development of a soft-inflatable exosuit for knee rehabilitation*, in *2017 IEEE/RSJ International Conference on Intelligent Robots and Systems (IROS)*, pp. 3722–3727, IEEE, 2017.

- [32] Y. Ding, M. Kim, S. Kuindersma, and C. J. Walsh, *Human-in-the-loop optimization of hip assistance with a soft exosuit during walking*, *Science Robotics* **3** (2018), no. 15 eaar5438.
- [33] Y. Ding, I. Galiana, A. T. Asbeck, S. M. M. De Rossi, J. Bae, T. R. T. Santos, V. L. De Araujo, S. Lee, K. G. Holt, and C. Walsh, *Biomechanical and physiological evaluation of multi-joint assistance with soft exosuits*, *IEEE Transactions on Neural Systems and Rehabilitation Engineering* **25** (2016), no. 2 119–130.
- [34] H.-L. Kao, M. Bamforth, D. Kim, and C. Schmandt, *Skinmorph: texture-tunable on-skin interface through thin, programmable gel*, in *Proceedings of the 2018 ACM International Symposium on Wearable Computers*, pp. 196–203, 2018.
- [35] N. A.-h. Hamdan, A. Wagner, S. Voelker, J. Steimle, and J. Borchers, *Springlets: Expressive, flexible and silent on-skin tactile interfaces*, in *Proceedings of the 2019 CHI Conference on Human Factors in Computing Systems*, p. 488, ACM, 2019.
- [36] P. H. Nguyen, C. Sparks, S. G. Nuthi, N. M. Vale, and P. Polygerinos, *Soft Poly-Limbs: Toward a New Paradigm of Mobile Manipulation for Daily Living Tasks*, *Soft Robotics* **6** (feb, 2019) 38–53.
- [37] I. Hussain, G. Salvietti, G. Spagnoletti, M. Malvezzi, D. Cioncoloni, S. Rossi, and D. Prattichizzo, *A soft supernumerary robotic finger and mobile arm support for grasping compensation and hemiparetic upper limb rehabilitation*, *Robotics and Autonomous Systems* **93** (2017) 1–12.
- [38] “Hardness Rockwell M.” Rockwell Hardness Testing and Measure of Plastics, omnexus.specialchem.com/polymer-properties/properties/hardness-rockwell-m.
- [39] “Hardness Shore D.” Shore D Hardness Test (Durometer Scale) - Hardness of Plastic Materials, omnexus.specialchem.com/polymer-properties/properties/hardness-shore-d.
- [40] F. Schneider, T. Fellner, J. Wilde, and U. Wallrabe, *Mechanical properties of silicones for mems*, *Journal of Micromechanics and Microengineering* **18** (2008), no. 6 065008.
- [41] I. Johnston, D. McCluskey, C. Tan, and M. Tracey, *Mechanical characterization of bulk sylgard 184 for microfluidics and microengineering*, *Journal of Micromechanics and Microengineering* **24** (2014), no. 3 035017.
- [42] W.-Y. Zhang, J. P. Labukas, S. Tatic-Lucic, L. Larson, T. Bannuru, R. P. Vinci, and G. S. Ferguson, *Novel room-temperature first-level packaging process for microscale devices*, *Sensors and Actuators A: Physical* **123** (2005) 646–654.
- [43] C. Ganser, F. Weber, C. Czibula, I. Bernt, R. Schennach, and C. Teichert, *Tuning hardness of swollen viscose fibers*, *Bioinspired, Biomimetic and Nanobiomaterials* **3** (2014), no. 3 131–138.

- [44] C. Ganser, U. Hirn, S. Rohm, R. Schennach, and C. Teichert, *Afm nanoindentation of pulp fibers and thin cellulose films at varying relative humidity*, *Holzforschung* **68** (2014), no. 1 53–60.
- [45] P. K. Zysset, X. E. Guo, C. E. Hoffler, K. E. Moore, and S. A. Goldstein, *Elastic modulus and hardness of cortical and trabecular bone lamellae measured by nanoindentation in the human femur*, *Journal of biomechanics* **32** (1999), no. 10 1005–1012.
- [46] A. A. Mieloch, M. Richter, T. Trzeciak, M. Giersig, and J. D. Rybka, *Osteoarthritis severely decreases the elasticity and hardness of knee joint cartilage: A nanoindentation study*, *Journal of clinical medicine* **8** (2019), no. 11 1865.
- [47] D. M. Ebenstein and L. A. Pruitt, *Nanoindentation of biological materials*, *Nano Today* **1** (2006), no. 3 26–33.
- [48] A. P. Gerratt, H. O. Michaud, and S. P. Lacour, *Elastomeric electronic skin for prosthetic tactile sensation*, *Advanced Functional Materials* **25** (2015), no. 15 2287–2295, [<https://onlinelibrary.wiley.com/doi/pdf/10.1002/adfm.201404365>].
- [49] P. Polygerinos, K. C. Galloway, E. Savage, M. Herman, K. O’Donnell, and C. J. Walsh, *Soft robotic glove for hand rehabilitation and task specific training*, in *2015 IEEE international conference on robotics and automation (ICRA)*, pp. 2913–2919, IEEE, 2015.
- [50] L. Albaugh, S. Hudson, and L. Yao, *Digital fabrication of soft actuated objects by machine knitting*, in *Proceedings of the 2019 CHI Conference on Human Factors in Computing Systems*, p. 184, ACM, 2019.
- [51] K. Sim, Z. Rao, Z. Zou, F. Ershad, J. Lei, A. Thukral, J. Chen, Q.-A. Huang, J. Xiao, and C. Yu, *Metal oxide semiconductor nanomembrane-based soft unnoticeable multifunctional electronics for wearable human-machine interfaces*, *Science advances* **5** (2019), no. 8 eaav9653.
- [52] J. Kwon, J.-H. Park, S. Ku, Y. Jeong, N.-J. Paik, and Y.-L. Park, *A soft wearable robotic ankle-foot-orthosis for post-stroke patients*, *IEEE Robotics and Automation Letters* **4** (2019), no. 3 2547–2552.
- [53] C. M. Thalman, Q. P. Lam, P. H. Nguyen, S. Sridar, and P. Polygerinos, *A novel soft elbow exosuit to supplement bicep lifting capacity*, in *2018 IEEE/RSJ International Conference on Intelligent Robots and Systems (IROS)*, pp. 6965–6971, IEEE, 2018.
- [54] M. Hiraoka, K. Nakamura, H. Arase, K. Asai, Y. Kaneko, S. W. John, K. Tagashira, and A. Omote, *Power-efficient low-temperature woven coiled fibre actuator for wearable applications*, *Scientific reports* **6** (2016) 36358.

- [55] W. Wang, L. Yao, C.-Y. Cheng, T. Zhang, H. Atsumi, L. Wang, G. Wang, O. Anilonyte, H. Steiner, J. Ou, *et. al.*, *Harnessing the hygroscopic and biofluorescent behaviors of genetically tractable microbial cells to design biohybrid wearables*, *Science advances* **3** (2017), no. 5 e1601984.
- [56] S. Muthukumarana, D. S. Elvitigala, J. P. Forero Cortes, D. J. Matthies, and S. Nanayakkara, *Touch me gently: Recreating the perception of touch using a shape-memory alloy matrix*, in *Proceedings of the 2020 CHI Conference on Human Factors in Computing Systems*, pp. 1–12, 2020.
- [57] S. Mun, S. Yun, S. Nam, S. K. Park, S. Park, B. J. Park, J. M. Lim, and K.-U. Kyung, *Electro-active polymer based soft tactile interface for wearable devices*, *IEEE Transactions on Haptics* **11** (2018), no. 1 15–21.
- [58] R. Hinchet, V. Vechev, H. Shea, and O. Hilliges, *Dextres: Wearable haptic feedback for grasping in vr via a thin form-factor electrostatic brake*, in *The 31st Annual ACM Symposium on User Interface Software and Technology*, pp. 901–912, ACM, 2018.
- [59] A. Atalay, V. Sanchez, O. Atalay, D. M. Vogt, F. Haufe, R. J. Wood, and C. J. Walsh, *Batch fabrication of customizable silicone-textile composite capacitive strain sensors for human motion tracking*, *Advanced Materials Technologies* **2** (2017), no. 9 1700136, [<https://onlinelibrary.wiley.com/doi/pdf/10.1002/admt.201700136>].
- [60] P. Roberts, D. D. Damian, W. Shan, T. Lu, and C. Majidi, *Soft-matter capacitive sensor for measuring shear and pressure deformation*, in *2013 IEEE International Conference on Robotics and Automation*, pp. 3529–3534, 2013.
- [61] R. K. Kramer, C. Majidi, R. Sahai, and R. J. Wood, *Soft curvature sensors for joint angle proprioception*, in *2011 IEEE/RSJ International Conference on Intelligent Robots and Systems*, pp. 1919–1926, IEEE, 2011.
- [62] S. Sundaram, P. Kellnhofer, Y. Li, J.-Y. Zhu, A. Torralba, and W. Matusik, *Learning the signatures of the human grasp using a scalable tactile glove*, *Nature* **569** (2019), no. 7758 698–702.
- [63] Huichan Zhao, Rukang Huang, and R. F. Shepherd, *Curvature control of soft orthotics via low cost solid-state optics*, in *2016 IEEE International Conference on Robotics and Automation (ICRA)*, pp. 4008–4013, 2016.
- [64] H. Zhao, K. O’Brien, S. Li, and R. F. Shepherd, *Optoelectronically innervated soft prosthetic hand via stretchable optical waveguides*, *Science Robotics* **1** (dec, 2016).
- [65] J. Zhong, Y. Ma, Y. Song, Q. Zhong, Y. Chu, I. Karakurt, D. B. Bogy, and L. Lin, *A flexible piezoelectret actuator/sensor patch for mechanical human–machine interfaces*, *ACS nano* **13** (2019), no. 6 7107–7116.

- [66] K. Little, C. W. Antuvan, M. Xiloyannis, B. A. P. S. de Noronha, Y. G. Kim, L. Masia, and D. Accoto, *Imu-based assistance modulation in upper limb soft wearable exosuits*, in *2019 IEEE 16th International Conference on Rehabilitation Robotics (ICORR)*, pp. 1197–1202, 2019.
- [67] H. Al-Fahaam, S. Davis, and S. Nefti-Meziani, *Power assistive and rehabilitation wearable robot based on pneumatic soft actuators*, in *2016 21st international conference on methods and models in automation and robotics (MMAR)*, pp. 472–477, IEEE, 2016.
- [68] R. Drake, A. W. Vogl, and A. W. Mitchell, *Gray's Anatomy for Students E-Book*. Elsevier Health Sciences, 2014.
- [69] R. Duffield and J. Kalkhoven, *Effects of compression garments in strength, power and speed based exercise*, in *Compression Garments in Sports: Athletic Performance and Recovery*, pp. 63–78. Springer, 2016.
- [70] M. J. Brennan and L. T. Miller, *Overview of treatment options and review of the current role and use of compression garments, intermittent pumps, and exercise in the management of lymphedema*, *Cancer: Interdisciplinary International Journal of the American Cancer Society* **83** (1998), no. S12B 2821–2827.
- [71] B. Partsch and H. Partsch, *Calf compression pressure required to achieve venous closure from supine to standing positions*, *Journal of vascular surgery* **42** (2005), no. 4 734–738.
- [72] A. C. Eycleshymer and D. M. Schoemaker, *A cross-section anatomy*. D. Appleton, 1911.
- [73] C. Barton and S. Raynor, *Peristaltic flow in tubes*, *The Bulletin of mathematical biophysics* **30** (1968), no. 4 663–680.
- [74] M. Y. Jaffrin, *Inertia and streamline curvature effects on peristaltic pumping*, *International Journal of Engineering Science* **11** (1973), no. 6 681–699.
- [75] H. Culbertson and K. J. Kuchenbecker, *Importance of matching physical friction, hardness, and texture in creating realistic haptic virtual surfaces*, *IEEE transactions on haptics* **10** (2016), no. 1 63–74.
- [76] K. J. Kuchenbecker, J. Fiene, and G. Niemeyer, *Improving contact realism through event-based haptic feedback*, *IEEE transactions on visualization and computer graphics* **12** (2006), no. 2 219–230.
- [77] Smith, P., *Body Covering*. Museum of Contemporary Crafts, the American Craft Council, New York, NY, 1968.

- [78] M. Cianchetti, C. Laschi, A. Menciassi, and P. Dario, *Biomedical applications of soft robotics*, *Nature Reviews Materials* **3** (2018), no. 6 143–153.
- [79] C. Thalman and P. Artemiadis, *A review of soft wearable robots that provide active assistance: trends, common actuation methods, fabrication, and applications*, *Wearable Technologies* **1** (2020).
- [80] C. Walsh, *Human-in-the-loop development of soft wearable robots*, *Nature Reviews Materials* **3** (2018), no. 6 78–80.
- [81] Q. Wang, P. Markopoulos, B. Yu, W. Chen, and A. Timmermans, *Interactive wearable systems for upper body rehabilitation: a systematic review*, *Journal of neuroengineering and rehabilitation* **14** (2017), no. 1 1–21.
- [82] C. Pachierotti, S. Sinclair, M. Solazzi, A. Frisoli, V. Hayward, and D. Prattichizzo, *Wearable haptic systems for the fingertip and the hand: taxonomy, review, and perspectives*, *IEEE Transactions on Haptics* **10** (2017), no. 4 580–600.
- [83] P. B. Shull and D. D. Damian, *Haptic wearables as sensory replacement, sensory augmentation and trainer—a review*, *Journal of neuroengineering and rehabilitation* **12** (2015), no. 1 1–13.
- [84] M. De Volder and D. Reynaerts, *Pneumatic and hydraulic microactuators: a review*, *Journal of Micromechanics and microengineering* **20** (2010), no. 4 043001.
- [85] Y. Bahramzadeh and M. Shahinpoor, *A review of ionic polymeric soft actuators and sensors*, *Soft Robotics* **1** (2014), no. 1 38–52.
- [86] M. Xie, K. Hisano, M. Zhu, T. Toyoshi, M. Pan, S. Okada, O. Tsutsumi, S. Kawamura, and C. Bowen, *Flexible multifunctional sensors for wearable and robotic applications*, *Advanced Materials Technologies* **4** (2019), no. 3 1800626, [<https://onlinelibrary.wiley.com/doi/pdf/10.1002/admt.201800626>].
- [87] A. Hatamie, S. Angizi, S. Kumar, C. M. Pandey, A. Simchi, M. Willander, and B. D. Malhotra, *Review—textile based chemical and physical sensors for healthcare monitoring*, *Journal of The Electrochemical Society* **167** (jan, 2020) 037546.
- [88] A. Nag, S. C. Mukhopadhyay, and J. Kosel, *Wearable flexible sensors: A review*, *IEEE Sensors Journal* **17** (2017), no. 13 3949–3960.
- [89] J. Z. Gul, M. Sajid, M. M. Rehman, G. U. Siddiqui, I. Shah, K.-H. Kim, J.-W. Lee, and K. H. Choi, *3d printing for soft robotics—a review*, *Science and technology of advanced materials* **19** (2018), no. 1 243–262.
- [90] Z. X. Khoo, J. E. M. Teoh, Y. Liu, C. K. Chua, S. Yang, J. An, K. F. Leong, and W. Y. Yeong, *3d printing of smart materials: A review on recent progresses in 4d printing*, *Virtual and Physical Prototyping* **10** (2015), no. 3 103–122.

- [91] M. Siegel, *The sense-think-act paradigm revisited*, in *1st International Workshop on Robotic Sensing, 2003. ROSE'03.*, pp. 5–pp, IEEE, 2003.
- [92] H. Abidi and M. Cianchetti, *On intrinsic safety of soft robots*, *Frontiers in Robotics and AI* **4** (2017) 5.
- [93] R. A. Bilodeau and R. K. Kramer, *Self-healing and damage resilience for soft robotics: a review*, *Frontiers in Robotics and AI* **4** (2017) 48.
- [94] C.-Y. Chu and R. M. Patterson, *Soft robotic devices for hand rehabilitation and assistance: a narrative review*, *Journal of neuroengineering and rehabilitation* **15** (2018), no. 1 9.
- [95] A. Papadopoulou, J. Berry, T. Knight, and R. Picard, *Affective sleeve: Wearable materials with haptic action for promoting calmness*, in *International Conference on Human-Computer Interaction*, pp. 304–319, Springer, 2019.
- [96] F. Connolly, D. A. Wagner, C. J. Walsh, and K. Bertoldi, *Sew-free anisotropic textile composites for rapid design and manufacturing of soft wearable robots*, *Extreme Mechanics Letters* **27** (2019) 52–58.
- [97] B. B. Kang, H. Lee, H. In, U. Jeong, J. Chung, and K.-J. Cho, *Development of a polymer-based tendon-driven wearable robotic hand*, in *2016 IEEE International Conference on Robotics and Automation (ICRA)*, pp. 3750–3755, IEEE, 2016.
- [98] M. Zhu, W. Adams, and P. Polygerinos, *Carpal tunnel syndrome soft relief device for typing applications*, in *2017 Design of Medical Devices Conference*, American Society of Mechanical Engineers Digital Collection, 2017.
- [99] C. M. Thalman and H. Lee, *Design and validation of a soft robotic ankle-foot orthosis (sr-af) exosuit for inversion and eversion ankle support*, in *2020 IEEE International Conference on Robotics and Automation (ICRA)*, pp. 1735–1741, IEEE, 2020.
- [100] A. J. Veale and S. Q. Xie, *Towards compliant and wearable robotic orthoses: A review of current and emerging actuator technologies*, *Medical engineering & physics* **38** (2016), no. 4 317–325.
- [101] J. Feldman, N. Stout, A. Wanchai, B. Stewart, J. Cormier, and J. Armer, *Intermittent pneumatic compression therapy: a systematic review*, *Lymphology* **45** (2012), no. 1 13–25.
- [102] S. Zhao, R. Liu, X. Wu, C. Ye, and A. W. Zia, *A programmable and self-adaptive dynamic pressure delivery and feedback system for efficient intermittent pneumatic compression therapy*, *Sensors and Actuators A: Physical* **315** (2020) 112285.

- [103] C. S. Simpson, C. G. Welker, S. D. Uhlrich, S. M. Sketch, R. W. Jackson, S. L. Delp, S. H. Collins, J. C. Selinger, and E. W. Hawkes, *Connecting the legs with a spring improves human running economy*, *Journal of Experimental Biology* **222** (2019), no. 17 jeb202895.
- [104] L. Masia, I. Hussain, M. Xiloyannis, C. Pacchierotti, L. Cappello, M. Malvezzi, G. Spagnoletti, C. Antuvan, D. Khanh, M. Pozzi, and D. Prattichizzo, *Soft wearable assistive robotics: exosuits and supernumerary limbs*, in *Wearable Exoskeleton Systems: Design, control and applications*, pp. 219–254. Institution of Engineering and Technology, mar, 2018.
- [105] B. Hannaford and A. M. Okamura, *Haptics*, in *Springer Handbook of Robotics*, pp. 1063–1084. Springer, 2016.
- [106] Y. Visell, *Tactile sensory substitution: Models for enaction in hci*, *Interacting with Computers* **21** (2009), no. 1-2 38–53.
- [107] L. Jones, *Haptics*. The MIT Press, 09, 2018.
- [108] L. A. Jones, *Human hand function*. Oxford University Press, Oxford ; New York, 2006.
- [109] R. W. Lindeman, Y. Yanagida, H. Noma, and K. Hosaka, *Wearable vibrotactile systems for virtual contact and information display*, *Virtual Reality* **9** (2006), no. 2-3 203–213.
- [110] J. B. V. Erp, H. A. V. Veen, C. Jansen, and T. Dobbins, *Waypoint navigation with a vibrotactile waist belt*, *ACM Transactions on Applied Perception (TAP)* **2** (2005), no. 2 106–117.
- [111] M. Raitor, J. M. Walker, A. M. Okamura, and H. Culbertson, *WRAP: Wearable, restricted-aperture pneumatics for haptic guidance*, in *Proceedings - IEEE International Conference on Robotics and Automation*, pp. 427–432, Institute of Electrical and Electronics Engineers Inc., jul, 2017.
- [112] E. H. Skorina, M. Luo, and C. D. Onal, *A soft robotic wearable wrist device for kinesthetic haptic feedback*, *Frontiers in Robotics and AI* **5** (2018) 83.
- [113] D. Purves and S. M. Williams, *Neuroscience. 2nd edition*. Sinauer Associates, 2001.
- [114] G. Huisman, *A touch of affect: mediated social touch and affect*, in *Proceedings of the 14th ACM International Conference on Multimodal Interaction, ICMI 2012*, (United States), pp. 317–320, Association for Computing Machinery (ACM), 10, 2012. 10.1145/2388676.2388746.
- [115] J. T. Suvilehto, E. Glerean, R. I. M. Dunbar, R. Hari, and L. Nummenmaa, *Topography of social touching depends on emotional bonds between humans*, *Proceedings of the National Academy of Sciences* (2015) [<https://www.pnas.org/content/early/2015/10/21/1519231112.full.pdf>].

- [116] G. K. Essick, F. McGlone, C. Dancer, D. Fabricant, Y. Ragin, N. Phillips, T. Jones, and S. Guest, *Quantitative assessment of pleasant touch*, *Neuroscience & Biobehavioral Reviews* **34** (2010), no. 2 192–203.
- [117] C. J. Cascio, D. Moore, and F. McGlone, *Social touch and human development*, *Developmental Cognitive Neuroscience* **35** (2019) 5–11.
- [118] R. Ackerley, K. Saar, F. McGlone, and H. Backlund Wasling, *Quantifying the sensory and emotional perception of touch: differences between glabrous and hairy skin*, *Frontiers in Behavioral Neuroscience* **8** (2014) 34.
- [119] M. A. Eid and H. Al Osman, *Affective haptics: Current research and future directions*, *IEEE Access* **4** (2015) 26–40.
- [120] C. Vaucelle, L. Bonanni, and H. Ishii, *Design of haptic interfaces for therapy*, in *Proceedings of the SIGCHI Conference on Human Factors in Computing Systems*, CHI '09, (New York, NY, USA), p. 467–470, Association for Computing Machinery, 2009.
- [121] “PUMA® INTRODUCES SELF-LACING TRAINING SHOE FIT INTELLIGENCE.” PUMA SE, 2019, about.puma.com/en/newsroom/corporate-news/2019/2019-01-31-puma-introduces-self-lacing-training-shoe.
- [122] “Nike HyperAdapt 1.0.” Nike HyperAdapt 1.0. Nike SNKRS, 2017, www.nike.com/launch/t/hyperadapt-1-0/.
- [123] “Lea Albaugh.” Clothing for Moderns, 2014, lea.zone/clothing-for-moderns.html.
- [124] Levy, Natasha. “Ying Gao’s Dresses Become Animated ‘in the Presence of Strangers.’” Dezeen, Dezeen, 23 Oct. 2017, www.dezeen.com/2017/10/22/ying-gaos-dresses-become-animated-in-the-presence-of-strangers/.
- [125] Gao, Ying. Ying Gao - Designer, 2019, yinggao.ca/interactifs/flowing-water-standing-time/.
- [126] Gao, Ying. Ying Gao - Designer, 2006, yinggao.ca/interactifs/walking-city/.
- [127] L. Perovich, P. Mothersill, and J. B. Farah, *Awakened apparel: embedded soft actuators for expressive fashion and functional garments*, in *Proceedings of the 8th International Conference on Tangible, Embedded and Embodied Interaction*, pp. 77–80, ACM, 2014.
- [128] Iris Van Herpen, 2019, www.irisvanherpen.com/home.
- [129] E. Danese, *Fashion tech and robotics*, in *Social robots from a human perspective*, pp. 129–138. Springer, 2015.
- [130] S. Biswas and Y. Visell, *Emerging material technologies for haptics*, *Advanced Materials Technologies* **4** (2019), no. 4 1900042.

- [131] S. Weinstein, *Intensive and extensive aspects of tactile sensitivity as a function of body part, sex and laterality*, *The skin senses* (1968).
- [132] R. Ackerley, I. Carlsson, H. Wester, H. Olausson, and H. Backlund Wasling, *Touch perceptions across skin sites: differences between sensitivity, direction discrimination and pleasantness*, *Frontiers in Behavioral Neuroscience* **8** (2014) 54.
- [133] A. Wilska, *On the vibrational sensitivity in different regions of the body surface*, *Acta Physiologica Scandinavica* **31** (1954), no. 2-3 285–289.
- [134] The Right Trousers, therighttrousers.com/.
- [135] A. S. Iberall, *The use of lines of nonextension to improve mobility in full-pressure suits*, tech. rep., RAND DEVELOPMENT CORP CLEVELAND OH, 1964.
- [136] P. Polygerinos, N. Correll, S. A. Morin, B. Mosadegh, C. D. Onal, K. Petersen, M. Cianchetti, M. T. Tolley, and R. F. Shepherd, *Soft robotics: Review of fluid-driven intrinsically soft devices; manufacturing, sensing, control, and applications in human-robot interaction*, *Advanced Engineering Materials* **19** (2017), no. 12 1700016.
- [137] J. Zhang, P. Fiers, K. A. Witte, R. W. Jackson, K. L. Poggensee, C. G. Atkeson, and S. H. Collins, *Human-in-the-loop optimization of exoskeleton assistance during walking*, *Science* **356** (2017), no. 6344 1280–1284.
- [138] P. Beckerle, G. Salvietti, R. Unal, D. Prattichizzo, S. Rossi, C. Castellini, S. Hirche, S. Endo, H. B. Amor, M. Ciocarlie, *et. al.*, *A human–robot interaction perspective on assistive and rehabilitation robotics*, *Frontiers in neurorobotics* **11** (2017) 24.
- [139] S. H. Collins, M. B. Wiggin, and G. S. Sawicki, *Reducing the energy cost of human walking using an unpowered exoskeleton*, *Nature* **522** (2015), no. 7555 212–215.
- [140] F. A. Panizzolo, I. Galiana, A. T. Asbeck, C. Siviyy, K. Schmidt, K. G. Holt, and C. J. Walsh, *A biologically-inspired multi-joint soft exosuit that can reduce the energy cost of loaded walking*, *Journal of neuroengineering and rehabilitation* **13** (2016), no. 1 43.
- [141] J. M. Hausdorff, *Gait dynamics, fractals and falls: finding meaning in the stride-to-stride fluctuations of human walking*, *Human movement science* **26** (2007), no. 4 555–589.
- [142] H. Banerjee, Z. T. H. Tse, and H. Ren, *Soft robotics with compliance and adaptation for biomedical applications and forthcoming challenges*, *International Journal of Robotics and Automation* **33** (2018), no. 1.
- [143] N. Kastor, V. Vikas, E. Cohen, and R. D. White, *A definition of soft materials for use in the design of robots*, *Soft robotics* **4** (2017), no. 3 181–182.

- [144] A. Chen, R. Yin, L. Cao, C. Yuan, H. Ding, and W. Zhang, *Soft robotics: Definition and research issues*, in *2017 24th international conference on mechatronics and machine vision in practice (M2VIP)*, pp. 366–370, IEEE, 2017.
- [145] K. Chubb, D. Berry, and T. Burke, *Towards an ontology for soft robots: what is soft?*, *Bioinspiration & biomimetics* **14** (2019), no. 6 063001.
- [146] N. Kastor, *Design, manufacturing, and control of soft foam robots*. PhD thesis, Tufts University, 2018.
- [147] G. S. Sawicki, O. N. Beck, I. Kang, and A. J. Young, *The exoskeleton expansion: improving walking and running economy*, *Journal of NeuroEngineering and Rehabilitation* **17** (2020), no. 1 1–9.
- [148] A. Manich, P. Marino, M. De Castellar, M. Saldivia, and R. Sauri, *Viscoelastic modeling of natural and synthetic textile yarns*, *Journal of Applied Polymer Science* **76** (2000), no. 14 2062–2067.
- [149] A. R. Bunsell, *Handbook of tensile properties of textile and technical fibres*. Elsevier, 2009.
- [150] K. Larson, *Dow white paper: Can you estimate modulus from durometer hardness for silicones? yes, but only roughly ... and you must choose your modulus carefully!*, Tech. Rep. 11-3716-01 A S2D, Dow Chemical, 2019.
- [151] S. Vogel, *Comparative biomechanics: life's physical world*. Princeton University Press, 2013.
- [152] Y. Elmogahzy and R. Farag, *Tensile properties of cotton fibers: importance, research, and limitations*, in *Handbook of Properties of Textile and Technical Fibres*, pp. 223–273. Elsevier, 2018.
- [153] J. Baltussen and M. Northolt, *The elastic extension of polymer fibers in the glassy state: Experimental results*, *Journal of Rheology* **41** (1997), no. 3 575–598.
- [154] A. Ismail, M. Rahman, A. Mustafa, and T. Matsuura, *The effect of processing conditions on a polyacrylonitrile fiber produced using a solvent-free free coagulation process*, *Materials Science and Engineering: A* **485** (2008), no. 1-2 251–257.
- [155] K. Higuchi and H. Takai, *Stress-strain diagram, young's modulus and poisson's ratio of textile fibers*, *Journal of the Textile Machinery Society of Japan* **7** (1961), no. 1 4–12.
- [156] E. Zussman, M. Burman, A. Yarin, R. Khalfin, and Y. Cohen, *Tensile deformation of electrospun nylon-6, 6 nanofibers*, *Journal of Polymer Science Part B: Polymer Physics* **44** (2006), no. 10 1482–1489.

- [157] Z. Wang, A. A. Volinsky, and N. D. Gallant, *Crosslinking effect on polydimethylsiloxane elastic modulus measured by custom-built compression instrument*, *Journal of Applied Polymer Science* **131** (2014), no. 22.
- [158] E. Broitman, *Indentation hardness measurements at macro-, micro-, and nanoscale: a critical overview*, *Tribology Letters* **65** (2017), no. 1 1–18.
- [159] H.-R. Lim, H. S. Kim, R. Qazi, Y.-T. Kwon, J.-W. Jeong, and W.-H. Yeo, *Advanced soft materials, sensor integrations, and applications of wearable flexible hybrid electronics in healthcare, energy, and environment*, *Advanced Materials* **32** (2020), no. 15 1901924.
- [160] W. A. D. M. Jayathilaka, K. Qi, Y. Qin, A. Chinnappan, W. Serrano-García, C. Baskar, H. Wang, J. He, S. Cui, S. W. Thomas, *et. al.*, *Significance of nanomaterials in wearables: A review on wearable actuators and sensors*, *Advanced Materials* **31** (2019), no. 7 1805921.
- [161] X. Wang, R. Guo, and J. Liu, *Liquid metal based soft robotics: materials, designs, and applications*, *Advanced Materials Technologies* **4** (2019), no. 2 1800549.
- [162] J. Mark, *Overview of Siloxane Polymers*, vol. 729, pp. 1–10. American Chemical Society, 05, 2000.
- [163] R. V. Martinez, C. R. Fish, X. Chen, and G. M. Whitesides, *Elastomeric origami: programmable paper-elastomer composites as pneumatic actuators*, *Advanced functional materials* **22** (2012), no. 7 1376–1384.
- [164] S. P. Lacour, *Stretchable thin-film electronics*, *Stretchable Electronics* (2012) 81–109.
- [165] B. Mosadegh, A. D. Mazzeo, R. F. Shepherd, S. A. Morin, U. Gupta, I. Z. Sani, D. Lai, S. Takayama, and G. M. Whitesides, *Control of soft machines using actuators operated by a braille display*, *Lab on a Chip* **14** (2014), no. 1 189–199.
- [166] Y. Fouillet, C. Parent, G. Gropplero, L. Davoust, J. L. Achard, F. Revol-Cavalier, and N. Verplanck, *Stretchable material for microfluidic applications*, *Proceedings* **1** (2017), no. 4.
- [167] K. Asaka and H. Okuzaki, *Soft actuators: materials, modeling, applications, and future perspectives*. Springer Nature, 2019.
- [168] J. Shintake, H. Sonar, E. Piskarev, J. Paik, and D. Floreano, *Soft pneumatic gelatin actuator for edible robotics*, in *2017 IEEE/RSJ International Conference on Intelligent Robots and Systems (IROS)*, pp. 6221–6226, IEEE, 2017.
- [169] Z. Qiao, J. Parks, P. Choi, and H.-F. Ji, *Applications of highly stretchable and tough hydrogels*, *Polymers* **11** (2019), no. 11 1773.

- [170] D. Prattichizzo, F. Chinello, C. Pacchierotti, and M. Malvezzi, *Towards wearability in fingertip haptics: a 3-dof wearable device for cutaneous force feedback*, *IEEE Transactions on Haptics* **6** (2013), no. 4 506–516.
- [171] T. Q. Trung and N.-E. Lee, *Recent progress on stretchable electronic devices with intrinsically stretchable components*, *Advanced Materials* **29** (2017), no. 3 1603167.
- [172] J. Onorato, V. Pakhnyuk, and C. K. Luscombe, *Structure and design of polymers for durable, stretchable organic electronics*, *Polymer Journal* **49** (2017), no. 1 41–60.
- [173] S. J. Benight, C. Wang, J. B. Tok, and Z. Bao, *Stretchable and self-healing polymers and devices for electronic skin*, *Progress in Polymer Science* **38** (2013), no. 12 1961–1977.
- [174] M. D. Dickey, *Stretchable and soft electronics using liquid metals*, *Advanced Materials* **29** (2017), no. 27 1606425.
- [175] J. Xiong, J. Chen, and P. S. Lee, *Functional fibers and fabrics for soft robotics, wearables, and human–robot interface*, *Advanced Materials* **33** (2021), no. 19 2002640.
- [176] J. Bishop-Moser, G. Krishnan, C. Kim, and S. Kota, *Design of soft robotic actuators using fluid-filled fiber-reinforced elastomeric enclosures in parallel combinations*, in *2012 IEEE/RSJ International Conference on Intelligent Robots and Systems*, pp. 4264–4269, IEEE, 2012.
- [177] T. Someya, *Stretchable electronics*. John Wiley & Sons, 2012.
- [178] M. V. Gandhi and B. Thompson, *Smart materials and structures*. Springer Science & Business Media, 1992.
- [179] Q. Sun, W. Seung, B. J. Kim, S. Seo, S.-W. Kim, and J. H. Cho, *Active matrix electronic skin strain sensor based on piezopotential-powered graphene transistors*, *Advanced Materials* **27** (2015), no. 22 3411–3417.
- [180] H. Zhao, A. M. Hussain, A. Israr, D. M. Vogt, M. Duduta, D. R. Clarke, and R. J. Wood, *A wearable soft haptic communicator based on dielectric elastomer actuators*, *Soft Robotics* (2020).
- [181] J. Jeong, I. B. Yasir, J. Han, C. H. Park, S.-K. Bok, and K.-U. Kyung, *Design of Shape Memory Alloy-Based Soft Wearable Robot for Assisting Wrist Motion*, *Applied Sciences* **9** (sep, 2019) 4025.
- [182] J. A. Rogers, T. Someya, and Y. Huang, *Materials and mechanics for stretchable electronics*, *science* **327** (2010), no. 5973 1603–1607.

- [183] S.-R. Kim, J.-H. Kim, and J.-W. Park, *Wearable and transparent capacitive strain sensor with high sensitivity based on patterned ag nanowire networks*, *ACS applied materials & interfaces* **9** (2017), no. 31 26407–26416.
- [184] P. Polygerinos, S. Lyne, Z. Wang, L. F. Nicolini, B. Mosadegh, G. M. Whitesides, and C. J. Walsh, *Towards a soft pneumatic glove for hand rehabilitation*, in *2013 IEEE/RSJ International Conference on Intelligent Robots and Systems*, pp. 1512–1517, IEEE, 2013.
- [185] Y. Mengüç, Y.-L. Park, E. Martinez-Villalpando, P. Aubin, M. Zisook, L. Stirling, R. J. Wood, and C. J. Walsh, *Soft wearable motion sensing suit for lower limb biomechanics measurements*, in *2013 IEEE International Conference on Robotics and Automation*, pp. 5309–5316, IEEE, 2013.
- [186] Y. Mengüç, Y.-L. Park, H. Pei, D. Vogt, P. M. Aubin, E. Winchell, L. Fluke, L. Stirling, R. J. Wood, and C. J. Walsh, *Wearable soft sensing suit for human gait measurement*, *The International Journal of Robotics Research* **33** (2014), no. 14 1748–1764.
- [187] J. M. Canino and K. B. Fite, *Haptic feedback in lower-limb prosthesis: Combined haptic feedback and emg control of a powered prosthesis*, in *2016 IEEE EMBS International Student Conference (ISC)*, pp. 1–4, IEEE, 2016.
- [188] H. K. Yap, N. Kamaldin, J. H. Lim, F. A. Nasrallah, J. C. H. Goh, and C.-H. Yeow, *A magnetic resonance compatible soft wearable robotic glove for hand rehabilitation and brain imaging*, *IEEE transactions on neural systems and rehabilitation engineering* **25** (2016), no. 6 782–793.
- [189] M. Hosseini, R. Meattini, A. San-Millan, G. Palli, C. Melchiorri, and J. Paik, *A semg-driven soft exosuit based on twisted string actuators for elbow assistive applications*, *IEEE Robotics and Automation Letters* (2020).
- [190] S. Li, D. M. Vogt, D. Rus, and R. J. Wood, *Fluid-driven origami-inspired artificial muscles*, *Proceedings of the National academy of Sciences* **114** (2017), no. 50 13132–13137.
- [191] Y. Hao, S. Biswas, E. W. Hawkes, T. Wang, M. Zhu, L. Wen, and Y. Visell, *A multimodal, enveloping soft gripper: Shape conformation, bioinspired adhesion, and expansion-driven suction*, *IEEE Transactions on Robotics* **37** (2020), no. 2 350–362.
- [192] A. Elor, S. Lessard, M. Teodorescu, and S. Kurniawan, *Project butterfly: Synergizing immersive virtual reality with actuated soft exosuit for upper-extremity rehabilitation*, in *2019 IEEE Conference on Virtual Reality and 3D User Interfaces (VR)*, pp. 1448–1456, IEEE, 2019.

- [193] S. Hong, D. Sycks, H. F. Chan, S. Lin, G. P. Lopez, F. Guilak, K. W. Leong, and X. Zhao, *3d printing of highly stretchable and tough hydrogels into complex, cellularized structures*, *Advanced materials* **27** (2015), no. 27 4035–4040.
- [194] J. Choi, O.-C. Kwon, W. Jo, H. J. Lee, and M.-W. Moon, *4d printing technology: A review*, *3D Printing and Additive Manufacturing* **2** (2015), no. 4 159–167.
- [195] V. Sanchez, C. J. Walsh, and R. J. Wood, *Textile technology for soft robotic and autonomous garments*, *Advanced Functional Materials* **31** (2021), no. 6 2008278.
- [196] S. Biswas, A. Schoeberl, Y. Hao, J. Reiprich, T. Stauden, J. Pezoldt, and H. O. Jacobs, *Integrated multilayer stretchable printed circuit boards paving the way for deformable active matrix*, *Nature communications* **10** (2019), no. 1 1–8.
- [197] J. Kim, G. A. Salvatore, H. Araki, A. M. Chiarelli, Z. Xie, A. Banks, X. Sheng, Y. Liu, J. W. Lee, K.-I. Jang, *et. al.*, *Battery-free, stretchable optoelectronic systems for wireless optical characterization of the skin*, *Science advances* **2** (2016), no. 8 e1600418.
- [198] S. Biswas, A. Schöberl, M. Mozafari, J. Pezoldt, T. Stauden, and H. O. Jacobs, *Deformable printed circuit boards that enable metamorphic electronics*, *NPG Asia Materials* **8** (2016), no. 12 e336–e336.
- [199] H. In, B. B. Kang, M. Sin, and K.-J. Cho, *Exo-glove: a wearable robot for the hand with a soft tendon routing system*, *IEEE Robotics & Automation Magazine* **22** (2015), no. 1 97–105.
- [200] L. Cai, L. Song, P. Luan, Q. Zhang, N. Zhang, Q. Gao, D. Zhao, X. Zhang, M. Tu, F. Yang, *et. al.*, *Super-stretchable, transparent carbon nanotube-based capacitive strain sensors for human motion detection*, *Scientific reports* **3** (2013), no. 1 1–9.
- [201] E. Pezent, A. Israr, M. Samad, S. Robinson, P. Agarwal, H. Benko, and N. Colonnese, *Tasbi: Multisensory squeeze and vibrotactile wrist haptics for augmented and virtual reality*, in *2019 IEEE World Haptics Conference (WHC)*, pp. 1–6, IEEE, 2019.
- [202] M. Bianchi, E. Battaglia, M. Poggiani, S. Ciotti, and A. Bicchi, *A wearable fabric-based display for haptic multi-cue delivery*, in *2016 IEEE haptics symposium (HAPTICS)*, pp. 277–283, IEEE, 2016.
- [203] M. Wehner, M. T. Tolley, Y. Mengüç, Y.-L. Park, A. Mozeika, Y. Ding, C. Onal, R. F. Shepherd, G. M. Whitesides, and R. J. Wood, *Pneumatic energy sources for autonomous and wearable soft robotics*, *Soft robotics* **1** (2014), no. 4 263–274.
- [204] V. V. Singh and J. Wang, *Nano/micromotors for security/defense applications. a review*, *Nanoscale* **7** (2015), no. 46 19377–19389.

- [205] D. J. Laser and J. G. Santiago, *A review of micropumps*, *Journal of micromechanics and microengineering* **14** (2004), no. 6 R35.
- [206] R. F. Shepherd, A. A. Stokes, J. Freake, J. Barber, P. W. Snyder, A. D. Mazzeo, L. Cademartiri, S. A. Morin, and G. M. Whitesides, *Using explosions to power a soft robot*, *Angewandte Chemie International Edition* **52** (2013), no. 10 2892–2896.
- [207] M. Goldfarb, E. J. Barth, M. A. Gogola, and J. A. Wehrmeyer, *Design and energetic characterization of a liquid-propellant-powered actuator for self-powered robots*, *IEEE/ASME transactions on mechatronics* **8** (2003), no. 2 254–262.
- [208] K. Narumi, H. Sato, K. Nakahara, Y. ah Seong, K. Morinaga, Y. Kakehi, R. Niiyama, and Y. Kawahara, *Liquid pouch motors: Printable planar actuators driven by liquid-to-gas phase change for shape-changing interfaces*, *IEEE Robotics and Automation Letters* **5** (2020), no. 3 3915–3922.
- [209] M. Boyvat, D. M. Vogt, and R. J. Wood, *Ultrastrong and high-stroke wireless soft actuators through liquid–gas phase change*, *Advanced Materials Technologies* **4** (2019), no. 2 1800381.
- [210] M. Garrad, G. Soter, A. T. Conn, H. Hauser, and J. Rossiter, *Driving soft robots with low-boiling point fluids*, in *2019 2nd IEEE International Conference on Soft Robotics (RoboSoft)*, pp. 74–79, IEEE, 2019.
- [211] L. Gockowski, S. Seshadri, J. Lee, M. Sroda, M. Helgeson, J. Read de Alaniz, E. Hawkes, and M. Valentine, *Photothermal actuation of a fluidic soft muscle*, *Bulletin of the American Physical Society* (2020).
- [212] V. Cacucciolo, J. Shintake, Y. Kuwajima, S. Maeda, D. Floreano, and H. Shea, *Stretchable pumps for soft machines*, *Nature* **572** (2019), no. 7770 516–519.
- [213] S. Cai, P. Ke, T. Narumi, and K. Zhu, *Thermairglove: A pneumatic glove for thermal perception and material identification in virtual reality*, .
- [214] S. Hauser, M. Robertson, A. Ijspeert, and J. Paik, *Jammjoint: A variable stiffness device based on granular jamming for wearable joint support*, *IEEE Robotics and Automation Letters* **2** (2017), no. 2 849–855.
- [215] W. H. Choi, S. Kim, D. Lee, and D. Shin, *Soft, multi-dof, variable stiffness mechanism using layer jamming for wearable robots*, *IEEE Robotics and Automation Letters* **4** (2019), no. 3 2539–2546.
- [216] J. Bae, S. M. M. De Rossi, K. O’Donnell, K. L. Hendron, L. N. Awad, T. R. T. Dos Santos, V. L. De Araujo, Y. Ding, K. G. Holt, T. D. Ellis, *et. al.*, *A soft exosuit for patients with stroke: Feasibility study with a mobile off-board actuation unit*, in *2015 IEEE International Conference on Rehabilitation Robotics (ICORR)*, pp. 131–138, IEEE, 2015.

- [217] H. Al-Fahaam, S. Davis, and S. Nefti-Meziani, *Power assistive and rehabilitation wearable robot based on pneumatic soft actuators*, in *2016 21st International Conference on Methods and Models in Automation and Robotics (MMAR)*, pp. 472–477, 2016.
- [218] J. Zhou, M. Mulle, Y. Zhang, X. Xu, E. Q. Li, F. Han, S. T. Thoroddsen, and G. Lubineau, *High-ampacity conductive polymer microfibers as fast response wearable heaters and electromechanical actuators*, *Journal of Materials Chemistry C* **4** (2016), no. 6 1238–1249.
- [219] S. Ryu, P. Lee, J. B. Chou, R. Xu, R. Zhao, A. J. Hart, and S.-G. Kim, *Extremely elastic wearable carbon nanotube fiber strain sensor for monitoring of human motion*, *ACS nano* **9** (2015), no. 6 5929–5936.
- [220] M. Amjadi, M. Turan, C. P. Clementson, and M. Sitti, *Parallel microcracks-based ultrasensitive and highly stretchable strain sensors*, *ACS applied materials & interfaces* **8** (2016), no. 8 5618–5626.
- [221] Y. Ai, Z. Lou, S. Chen, D. Chen, Z. M. Wang, K. Jiang, and G. Shen, *All rgo-on-pvdf-nanofibers based self-powered electronic skins*, *Nano Energy* **35** (2017) 121–127.
- [222] Z. Lou, S. Chen, L. Wang, K. Jiang, and G. Shen, *An ultra-sensitive and rapid response speed graphene pressure sensors for electronic skin and health monitoring*, *Nano Energy* **23** (2016) 7–14.
- [223] T. P. Chenal, J. C. Case, J. Paik, and R. K. Kramer, *Variable stiffness fabrics with embedded shape memory materials for wearable applications*, in *2014 IEEE/RSJ International Conference on Intelligent Robots and Systems*, pp. 2827–2831, IEEE, 2014.
- [224] Y. Bar-Cohen, *Artificial muscles using electroactive polymers (eap): Capabilities, challenges and potential*, .
- [225] H. Boys, G. Frediani, M. Ghilardi, S. Poslad, J. C. Busfield, and F. Carpi, *Soft wearable non-vibratory tactile displays*, in *2018 IEEE International Conference on Soft Robotics (RoboSoft)*, pp. 270–275, IEEE, 2018.
- [226] R. Dahiya, *E-skin: From humanoids to humans [point of view]*, *Proceedings of the IEEE* **107** (2019), no. 2 247–252.
- [227] J. Hughes, U. Culha, F. Giardina, F. Guenther, A. Rosendo, and F. Iida, *Soft manipulators and grippers: a review*, *Frontiers in Robotics and AI* **3** (2016) 69.
- [228] T. N. Do and Y. Visell, *Stretchable, twisted conductive microtubules for wearable computing, robotics, electronics, and healthcare*, *Scientific reports* **7** (2017), no. 1 1–12.

- [229] B. Li, Y. Gao, A. Fontecchio, and Y. Visell, *Soft capacitive tactile sensing arrays fabricated via direct filament casting*, *Smart Materials and Structures* **25** (2016), no. 7 075009.
- [230] S. Yao and Y. Zhu, *Wearable multifunctional sensors using printed stretchable conductors made of silver nanowires*, *Nanoscale* **6** (2014) 2345–2352.
- [231] S. Biswas, Y. Shao, T. Hachisu, T. Nguyen-Dang, and Y. Visell, *Integrated soft optoelectronics for wearable health monitoring*, *Advanced Materials Technologies* (2020) 2000347.
- [232] M. Xie, Y. Zhang, M. J. Krašny, C. Bowen, H. Khanbareh, and N. Gathercole, *Flexible and active self-powered pressure, shear sensors based on freeze casting ceramic–polymer composites*, *Energy Environ. Sci.* **11** (2018) 2919–2927.
- [233] S. Ozel, N. A. Keskin, D. Khea, and C. D. Onal, *A precise embedded curvature sensor module for soft-bodied robots*, *Sensors and Actuators A: Physical* **236** (2015) 349–356.
- [234] C. B. Cooper, K. Arutselvan, Y. Liu, D. Armstrong, Y. Lin, M. R. Khan, J. Genzer, and M. D. Dickey, *Stretchable capacitive sensors of torsion, strain, and touch using double helix liquid metal fibers*, *Advanced Functional Materials* **27** (2017), no. 20 1605630.
- [235] B. Li, A. K. Fontecchio, and Y. Visell, *Mutual capacitance of liquid conductors in deformable tactile sensing arrays*, *Applied Physics Letters* **108** (2016), no. 1 013502.
- [236] B. Li, Y. Shi, A. Fontecchio, and Y. Visell, *Mechanical imaging of soft tissues with a highly compliant tactile sensing array*, *IEEE Transactions on Biomedical Engineering* **65** (2017), no. 3 687–697.
- [237] B. Li, Y. Shi, H. Hu, A. Fontecchio, and Y. Visell, *Assemblies of microfluidic channels and micropillars facilitate sensitive and compliant tactile sensing*, *IEEE Sensors Journal* **16** (2016), no. 24 8908–8915.
- [238] Z. S. Ballard and A. Ozcan, *Wearable optical sensors*, in *Mobile Health*, pp. 313–342. Springer, 2017.
- [239] M. Luo, Y. Pan, E. H. Skorina, W. Tao, F. Chen, S. Ozel, and C. D. Onal, *Slithering towards autonomy: a self-contained soft robotic snake platform with integrated curvature sensing*, *Bioinspiration & biomimetics* **10** (2015), no. 5 055001.
- [240] S. Ozel, E. H. Skorina, M. Luo, W. Tao, F. Chen, Y. Pan, and C. D. Onal, *A composite soft bending actuation module with integrated curvature sensing*, in *2016 IEEE International Conference on Robotics and Automation (ICRA)*, pp. 4963–4968, IEEE, 2016.

- [241] S. P. Lacour, I. Graz, D. Cotton, S. Bauer, and S. Wagner, *Elastic components for prosthetic skin*, in *2011 Annual International Conference of the IEEE Engineering in Medicine and Biology Society*, pp. 8373–8376, 2011.
- [242] H. K. Yap, H. Y. Ng, and C.-H. Yeow, *High-force soft printable pneumatics for soft robotic applications*, *Soft Robotics* **3** (2016), no. 3 144–158.
- [243] J. W. Booth, D. Shah, J. C. Case, E. L. White, M. C. Yuen, O. Cyr-Choiniere, and R. Kramer-Bottiglio, *Omniskins: Robotic skins that turn inanimate objects into multifunctional robots*, *Science Robotics* **3** (2018), no. 22 eaat1853.
- [244] D. Rus and M. T. Tolley, *Design, fabrication and control of soft robots*, *Nature* **521** (2015), no. 7553 467.
- [245] Y. S. Song, Y. Sun, R. Van Den Brand, J. Von Zitzewitz, S. Micera, G. Courtine, and J. Paik, *Soft robot for gait rehabilitation of spinalized rodents*, in *2013 IEEE/RSJ International Conference on Intelligent Robots and Systems*, pp. 971–976, Ieee, 2013.
- [246] Y.-L. Park, B.-r. Chen, C. Majidi, R. J. Wood, R. Nagpal, and E. Goldfield, *Active modular elastomer sleeve for soft wearable assistance robots*, in *2012 IEEE/RSJ International Conference on Intelligent Robots and Systems*, pp. 1595–1602, IEEE, 2012.
- [247] S. Cotin, H. Delingette, and N. Ayache, *Real-time elastic deformations of soft tissues for surgery simulation*, *IEEE transactions on Visualization and Computer Graphics* **5** (1999), no. 1 62–73.
- [248] F. G. Serchi, A. Arienti, and C. Laschi, *Biomimetic vortex propulsion: toward the new paradigm of soft unmanned underwater vehicles*, *IEEE/ASME Transactions On Mechatronics* **18** (2013), no. 2 484–493.
- [249] G. H. Kwon, J. Y. Park, J. Y. Kim, M. L. Frisk, D. J. Beebe, and S.-H. Lee, *Biomimetic soft multifunctional miniature aquabots*, *Small* **4** (2008), no. 12 2148–2153.
- [250] W. Wang, H. Rodrigue, and S.-H. Ahn, *Deployable soft composite structures*, *Scientific reports* **6** (2016) 20869.
- [251] S. Kim, C. Laschi, and B. Trimmer, *Soft robotics: a bioinspired evolution in robotics*, *Trends in biotechnology* **31** (2013), no. 5 287–294.
- [252] C. Cutter, *A Treatise on anatomy, physiology, and hygiene*. JB Lippincott & Company, 1852.
- [253] A. D. Marchese, R. K. Katzschmann, and D. Rus, *A recipe for soft fluidic elastomer robots*, *Soft Robotics* **2** (2015), no. 1 7–25.

- [254] F. Daerden and D. Lefeber, *Pneumatic artificial muscles: actuators for robotics and automation*, *European journal of mechanical and environmental engineering* **47** (2002), no. 1 11–21.
- [255] H. Schulte Jr, *The characteristics of the mckibben artificial muscle (1961) the application of external power in prosthetics and orthotics*, *National Academy of Sciences-National Research Council, Washington DC, Appendix H* (1961) 94–115.
- [256] M. Gavrilović and M. Marić, *Positional servo-mechanism activated by artificial muscles*, *Medical and Biological Engineering* **7** (1969), no. 1 77–82.
- [257] C.-P. Chou and B. Hannaford, *Measurement and modeling of mckibben pneumatic artificial muscles*, *IEEE Transactions on robotics and automation* **12** (1996), no. 1 90–102.
- [258] B. Tondu and P. Lopez, *Modeling and control of mckibben artificial muscle robot actuators*, *IEEE control systems* **20** (2000), no. 2 15–38.
- [259] B. Tondu and P. Lopez, *Théorie d'un muscle artificiel pneumatique et application à la modelisation du muscle artificiel de mckibben*, *Comptes rendus de l'Académie des sciences. Série II, Mécanique, physique, chimie, astronomie* **320** (1995), no. 3 105–114.
- [260] I. W. Hunter, J. M. Hollerbach, and J. Ballantyne, *A comparative analysis of actuator technologies for robotics*, *Robotics Review* **2** (1991) 299–342.
- [261] F. Connolly, P. Polygerinos, C. J. Walsh, and K. Bertoldi, *Mechanical programming of soft actuators by varying fiber angle*, *Soft Robotics* **2** (2015), no. 1 26–32.
- [262] E. W. Hawkes, D. L. Christensen, and A. M. Okamura, *Design and implementation of a 300% strain soft artificial muscle*, in *2016 IEEE International Conference on Robotics and Automation (ICRA)*, pp. 4022–4029, IEEE, 2016.
- [263] S. Sridar, C. J. Majeika, P. Schaffer, M. Bowers, S. Ueda, A. J. Barth, J. L. Sorrells, J. T. Wu, T. R. Hunt, and M. Popovic, *Hydro muscle-a novel soft fluidic actuator*, in *Robotics and Automation (ICRA), 2016 IEEE International Conference on*, pp. 4014–4021, IEEE, 2016.
- [264] L. Cappello, K. C. Galloway, S. Sanan, D. A. Wagner, R. Granberry, S. Engelhardt, F. L. Haufe, J. D. Peisner, and C. J. Walsh, *Exploiting textile mechanical anisotropy for fabric-based pneumatic actuators*, *Soft robotics* **5** (2018), no. 5 662–674.
- [265] D. Yang, M. S. Verma, J.-H. So, B. Mosadegh, C. Keplinger, B. Lee, F. Khashai, E. Lossner, Z. Suo, and G. M. Whitesides, *Buckling pneumatic linear actuators inspired by muscle*, *Advanced Materials Technologies* **1** (2016), no. 3.
- [266] K. Otsuka and C. M. Wayman, *Shape memory materials*. Cambridge university press, 1999.

- [267] S. Kim, E. Hawkes, K. Cho, M. Jolda, J. Foley, and R. Wood, *Micro artificial muscle fiber using niti spring for soft robotics*, in *Intelligent Robots and Systems, 2009. IROS 2009. IEEE/RSJ International Conference on*, pp. 2228–2234, IEEE, 2009.
- [268] C. S. Haines, M. D. Lima, N. Li, G. M. Spinks, J. Foroughi, J. D. Madden, S. H. Kim, S. Fang, M. J. de Andrade, F. Göktepe, *et. al.*, *Artificial muscles from fishing line and sewing thread*, *science* **343** (2014), no. 6173 868–872.
- [269] F. Li, Y. Chen, W. Zhu, X. Zhang, and M. Xu, *Shape memory effect of polyethylene/nylon 6 graft copolymers*, *Polymer* **39** (1998), no. 26 6929–6934.
- [270] K. Takashima, J. Rossiter, and T. Mukai, *Mckibben artificial muscle using shape-memory polymer*, *Sensors and Actuators A: Physical* **164** (2010), no. 1-2 116–124.
- [271] C. Liu, H. Qin, and P. Mather, *Review of progress in shape-memory polymers*, *Journal of Materials Chemistry* **17** (2007), no. 16 1543–1558.
- [272] C.-S. Zhang and Q.-Q. Ni, *Bending behavior of shape memory polymer based laminates*, *Composite Structures* **78** (2007), no. 2 153–161.
- [273] K. Jung, J. Nam, and H. Choi, *Investigations on actuation characteristics of ipmc artificial muscle actuator*, *Sensors and Actuators A: Physical* **107** (2003), no. 2 183–192.
- [274] S. Guo, Y. Ge, L. Li, and S. Liu, *Underwater swimming micro robot using ipmc actuator*, in *Mechatronics and Automation, Proceedings of the 2006 IEEE International Conference on*, pp. 249–254, IEEE, 2006.
- [275] N. Bhat and W.-j. Kim, *Precision force and position control of an ionic polymer metal composite*, *Proceedings of the Institution of Mechanical Engineers, Part I: Journal of Systems and Control Engineering* **218** (2004), no. 6 421–432.
- [276] F. Carpi, D. De Rossi, R. Kornbluh, R. E. Pelrine, and P. Sommer-Larsen, *Dielectric elastomers as electromechanical transducers: Fundamentals, materials, devices, models and applications of an emerging electroactive polymer technology*. Elsevier, 2011.
- [277] N. Kellaris, V. G. Venkata, G. M. Smith, S. K. Mitchell, and C. Keplinger, *Peano-hasel actuators: Muscle-mimetic, electrohydraulic transducers that linearly contract on activation*, *Science Robotics* **3** (2018), no. 14 eaar3276.
- [278] R. Guo, L. Sheng, H. Gong, and J. Liu, *Liquid metal spiral coil enabled soft electromagnetic actuator*, *Science China Technological Sciences* **61** (2018), no. 4 516–521.

- [279] T. N. Do, H. Phan, T.-Q. Nguyen, and Y. Visell, *Miniature soft electromagnetic actuators for robotic applications*, *Advanced Functional Materials* **28** (2018), no. 18 1800244.
- [280] C. Pawashe, S. Floyd, and M. Sitti, *Modeling and experimental characterization of an untethered magnetic micro-robot*, *The International Journal of Robotics Research* **28** (2009), no. 8 1077–1094.
- [281] T. N. Do, T. E. T. Seah, H. K. Yu, and S. J. Phee, *Development and testing of a magnetically actuated capsule endoscopy for obesity treatment*, *PloS one* **11** (2016), no. 1 e0148035.
- [282] U. A. Hofmann, T. Bützer, O. Lambercy, and R. Gassert, *Design and evaluation of a bowden-cable-based remote actuation system for wearable robotics*, *IEEE Robotics and Automation Letters* **3** (2018), no. 3 2101–2108.
- [283] W. Wei, Z. Qu, W. Wang, P. Zhang, and F. Hao, *Design on the bowden cable-driven upper limb soft exoskeleton*, *Applied bionics and biomechanics* **2018** (2018).
- [284] M. C. Yuen, R. A. Bilodeau, and R. K. Kramer, *Active variable stiffness fibers for multifunctional robotic fabrics.*, *IEEE Robotics and Automation Letters* **1** (2016), no. 2 708–715.
- [285] A. Masuda, Q.-Q. Ni, A. Sone, R.-X. Zhang, and T. Yamamura, *Preliminary characterization and modeling of sma-based textile composites*, in *Smart Structures and Materials 2004: Modeling, Signal Processing, and Control*, vol. 5383, pp. 94–103, International Society for Optics and Photonics, 2004.
- [286] K. Kobayashi and S. Hayashi, *Woven fabric made of shape memory polymer*, July 7, 1992. US Patent 5,128,197.
- [287] T. L. Buckner and R. Kramer-Bottiglio, *Functional fibers for robotic fabrics*, *Multifunctional Materials* **1** (2018), no. 1 012001.
- [288] T. Niino, S. Egawa, H. Kimura, and T. Higuchi, *Electrostatic artificial muscle: compact, high-power linear actuators with multiple-layer structures*, in *Micro Electro Mechanical Systems, 1994, MEMS'94, Proceedings, IEEE Workshop on*, pp. 130–135, IEEE, 1994.
- [289] H. Zhao, A. M. Hussain, M. Duduta, D. M. Vogt, R. J. Wood, and D. R. Clarke, *Compact dielectric elastomer linear actuators*, *Advanced Functional Materials* **28** (2018), no. 42 1804328.
- [290] M. Duduta, E. Hajiesmaili, H. Zhao, R. J. Wood, and D. R. Clarke, *Realizing the potential of dielectric elastomer artificial muscles*, *Proceedings of the National Academy of Sciences* **116** (2019), no. 7 2476–2481.

- [291] R. Niiyama, X. Sun, C. Sung, B. An, D. Rus, and S. Kim, *Pouch motors: Printable soft actuators integrated with computational design*, *Soft Robotics* **2** (2015), no. 2 59–70.
- [292] Y. Funabora, *Flexible fabric actuator realizing 3d movements like human body surface for wearable devices*, in *2018 IEEE/RSJ International Conference on Intelligent Robots and Systems (IROS)*, pp. 6992–6997, IEEE, 2018.
- [293] M. Watanabe and H. Tsukagoshi, *Suitable configurations for pneumatic soft sheet actuator to generate traveling waves*, *Advanced Robotics* **32** (2018), no. 7 363–374.
- [294] D. S. Shah, M. C.-S. Yuen, L. G. Tilton, E. J. Yang, and R. Kramer-Bottiglio, *Morphing robots using robotic skins that sculpt clay*, *IEEE Robotics and Automation Letters* (2019).
- [295] C. K. Batchelor and G. Batchelor, *An introduction to fluid dynamics*. Cambridge university press, 1967.
- [296] W. M. Kier and K. K. Smith, *Tongues, tentacles and trunks: the biomechanics of movement in muscular-hydrostats*, *Zoological journal of the Linnean Society* **83** (1985), no. 4 307–324.
- [297] P. Berthet-Rayne, G. Gras, K. Leibrandt, P. Wisanuvej, A. Schmitz, C. A. Seneci, and G.-Z. Yang, *The i 2 snake robotic platform for endoscopic surgery*, *Annals of biomedical engineering* **46** (2018), no. 10 1663–1675.
- [298] T. Noritsugu, H. Yamamoto, D. Sasakil, and M. Takaiwa, *Wearable power assist device for hand grasping using pneumatic artificial rubber muscle*, in *SICE 2004 Annual Conference*, vol. 1, pp. 420–425 vol. 1, Aug, 2004.
- [299] C. Mazzone, F. C. Grandi, P. Sandercock, M. Miccio, and R. Salvi, *Physical methods for preventing deep vein thrombosis in stroke*, *Cochrane Database of Systematic Reviews* (2002), no. 1.
- [300] J. P. Loenneke, J. M. Wilson, P. J. Marín, M. C. Zourdos, and M. G. Bemben, *Low intensity blood flow restriction training: a meta-analysis*, *European journal of applied physiology* **112** (2012), no. 5 1849–1859.
- [301] R. P. Lowery, J. M. Joy, J. P. Loenneke, E. O. de Souza, M. Machado, J. E. Dudeck, and J. M. Wilson, *Practical blood flow restriction training increases muscle hypertrophy during a periodized resistance training programme*, *Clinical physiology and functional imaging* **34** (2014), no. 4 317–321.
- [302] M. King, A. Deveaux, H. White, and D. Rayson, *Compression garments versus compression bandaging in decongestive lymphatic therapy for breast cancer-related lymphedema: a randomized controlled trial*, *Supportive Care in Cancer* **20** (2012), no. 5 1031–1036.

- [303] J. Williamson, J. Mitchell, H. Olesen, P. Raven, and N. Secher, *Reflex increase in blood pressure induced by leg compression in man.*, *The Journal of physiology* **475** (1994), no. 2 351–357.
- [304] C. J. Payne, E. G. Hevia, N. Phipps, A. Atalay, O. Atalay, B. R. Seo, D. J. Mooney, and C. J. Walsh, *Force control of textile-based soft wearable robots for mechanotherapy*, in *2018 IEEE International Conference on Robotics and Automation (ICRA)*, pp. 5459–5465, IEEE, 2018.
- [305] S. B. Schorr and A. M. Okamura, *Fingertip tactile devices for virtual object manipulation and exploration*, in *Proceedings of the 2017 CHI Conference on Human Factors in Computing Systems*, pp. 3115–3119, ACM, 2017.
- [306] N. Takahashi, H. Takahashi, and H. Koike, *Soft exoskeleton glove enabling force feedback for human-like finger posture control with 20 degrees of freedom*, in *2019 IEEE World Haptics Conference (WHC)*, pp. 217–222, IEEE, 2019.
- [307] R. L. Peiris, Y.-L. Feng, L. Chan, and K. Minamizawa, *Thermalbracelet: Exploring thermal haptic feedback around the wrist*, in *Proceedings of the 2019 CHI Conference on Human Factors in Computing Systems*, p. 170, ACM, 2019.
- [308] M. Raitor, J. M. Walker, A. M. Okamura, and H. Culbertson, *Wrap: Wearable, restricted-aperture pneumatics for haptic guidance*, in *2017 IEEE International Conference on Robotics and Automation (ICRA)*, pp. 427–432, IEEE, 2017.
- [309] H. Pohl, P. Brandes, H. Ngo Quang, and M. Rohs, *Squeezeback: pneumatic compression for notifications*, in *Proceedings of the 2017 CHI Conference on Human Factors in Computing Systems*, pp. 5318–5330, ACM, 2017.
- [310] F. Tang, R. P. McMahan, and T. T. Allen, *Development of a low-cost tactile sleeve for autism intervention*, in *2014 IEEE International Symposium on Haptic, Audio and Visual Environments and Games (HAVE) Proceedings*, pp. 35–40, IEEE, 2014.
- [311] K. Bark, J. Wheeler, G. Lee, J. Savall, and M. Cutkosky, *A wearable skin stretch device for haptic feedback*, in *World Haptics 2009-Third Joint EuroHaptics conference and Symposium on Haptic Interfaces for Virtual Environment and Teleoperator Systems*, pp. 464–469, IEEE, 2009.
- [312] D.-Y. Huang, R. Guo, J. Gong, J. Wang, J. Graham, D.-N. Yang, and X.-D. Yang, *Retroshape: Leveraging rear-surface shape displays for 2.5 d interaction on smartwatches*, in *Proceedings of the 30th Annual ACM Symposium on User Interface Software and Technology*, pp. 539–551, ACM, 2017.
- [313] Y. A. Shim, J. Lee, and G. Lee, *Exploring multimodal watch-back tactile display using wind and vibration*, in *Proceedings of the 2018 CHI Conference on Human Factors in Computing Systems*, p. 132, ACM, 2018.

- [314] E. Strasnick, J. R. Cauchard, and J. A. Landay, *Brushtouch: Exploring an alternative tactile method for wearable haptics*, in *Proceedings of the 2017 CHI Conference on Human Factors in Computing Systems*, pp. 3120–3125, ACM, 2017.
- [315] E. Whitmire, H. Benko, C. Holz, E. Ofek, and M. Sinclair, *Haptic revolver: Touch, shear, texture, and shape rendering on a reconfigurable virtual reality controller*, in *Proceedings of the 2018 CHI Conference on Human Factors in Computing Systems*, p. 86, ACM, 2018.
- [316] A. Ion, E. J. Wang, and P. Baudisch, *Skin drag displays: Dragging a physical tactor across the user’s skin produces a stronger tactile stimulus than vibrotactile*, in *Proceedings of the 33rd Annual ACM Conference on Human Factors in Computing Systems*, pp. 2501–2504, ACM, 2015.
- [317] N. Agharese, T. Cloyd, L. H. Blumenschein, M. Raitor, E. W. Hawkes, H. Culbertson, and A. M. Okamura, *Hapwrap: Soft growing wearable haptic device*, in *2018 IEEE International Conference on Robotics and Automation (ICRA)*, pp. 1–5, IEEE, 2018.
- [318] F. Arafsha, K. M. Alam, and A. El Saddik, *Emojacket: Consumer centric wearable affective jacket to enhance emotional immersion*, in *2012 international conference on innovations in information technology (IIT)*, pp. 350–355, IEEE, 2012.
- [319] E. W. Foo, J. W. Lee, C. Compton, S. Ozbek, and B. Holschuh, *User experiences of garment-based dynamic compression for novel haptic applications*, in *Proceedings of the 23rd International Symposium on Wearable Computers*, pp. 54–59, ACM, 2019.
- [320] B. Zhuo, S. Chen, M. Zhao, and X. Guo, *High sensitivity flexible capacitive pressure sensor using polydimethylsiloxane elastomer dielectric layer micro-structured by 3-d printed mold*, *IEEE Journal of the Electron Devices Society* **5** (2017), no. 3 219–223.
- [321] A. Israr, S. Zhao, K. Schwalje, R. Klatzky, and J. Lehman, *Feel effects: Enriching storytelling with haptic feedback*, *ACM Trans. Appl. Percept.* **11** (Sept., 2014).
- [322] A. Israr and I. Poupyrev, *Tactile brush: drawing on skin with a tactile grid display*, in *Proceedings of the SIGCHI Conference on Human Factors in Computing Systems*, pp. 2019–2028, ACM, 2011.
- [323] H. Partsch, *Compression therapy: clinical and experimental evidence*, *Annals of vascular diseases* (2012) ra–12.
- [324] J. D. Crane, D. I. Ogborn, C. Cupido, S. Melov, A. Hubbard, J. M. Bourgeois, and M. A. Tarnopolsky, *Massage therapy attenuates inflammatory signaling after exercise-induced muscle damage*, *Science translational medicine* **4** (2012), no. 119 119ra13–119ra13.

- [325] K. Delis, Z. Azizi, R. Stevens, J. Wolfe, and A. Nicolaidis, *Optimum intermittent pneumatic compression stimulus for lower-limb venous emptying*, *European Journal of Vascular and Endovascular Surgery* **19** (2000), no. 3 261–269.
- [326] L. Roberts, *Effects of patterns of pressure application on resting electromyography during massage*, *International journal of therapeutic massage & bodywork* **4** (2011), no. 1 4.
- [327] A. Chen, S. Frangos, S. Kilaru, and B. Sumpio, *Intermittent pneumatic compression devices—physiological mechanisms of action*, *European Journal of Vascular and Endovascular Surgery* **21** (2001), no. 5 383–392.
- [328] P. S. Moran, C. Teljeur, P. Harrington, and M. Ryan, *A systematic review of intermittent pneumatic compression for critical limb ischaemia*, *Vascular Medicine* **20** (2015), no. 1 41–50.
- [329] Y. M. Arabi, M. Khedr, S. I. Dara, G. S. Dhar, S. A. Bhat, H. M. Tamim, and L. Y. Afesh, *Use of intermittent pneumatic compression and not graduated compression stockings is associated with lower incident vte in critically ill patients: a multiple propensity scores adjusted analysis*, *Chest* **144** (2013), no. 1 152–159.
- [330] S. Kitayama, J. Maegawa, S. Matsubara, S. Kobayashi, T. Mikami, K. Hirotomi, and S. Kagimoto, *Real-time direct evidence of the superficial lymphatic drainage effect of intermittent pneumatic compression treatment for lower limb lymphedema*, *Lymphatic research and biology* **15** (2017), no. 1 77–86.
- [331] A. J. COMEROTA, *Intermittent pneumatic compression for dvt prophylaxis*, *Supplement to endovascular today* (2011) 3–5.
- [332] D. Guan, R. Liu, C. Fei, S. Zhao, and L. Jing, *Fluid–structure coupling model and experimental validation of interaction between pneumatic soft actuator and lower limb*, *Soft robotics* **7** (2020), no. 5 627–638.
- [333] E. Suarez, J. J. Huaroto, A. A. Reymundo, D. Holland, C. Walsh, and E. Vela, *A soft pneumatic fabric-polymer actuator for wearable biomedical devices: Proof of concept for lymphedema treatment*, in *2018 IEEE International Conference on Robotics and Automation (ICRA)*, pp. 5452–5458, IEEE, 2018.
- [334] H. J. Yoo, W. Kim, S.-Y. Lee, J. Choi, Y. J. Kim, Y. Nam, K.-J. Cho, *et. al.*, *Wearable lymphedema massaging modules: Proof of concept using origami-inspired soft fabric pneumatic actuators*, in *2019 IEEE 16th International Conference on Rehabilitation Robotics (ICORR)*, pp. 950–956, IEEE, 2019.
- [335] W. G. Paterson, *Esophageal peristalsis*, *GI Motility online* (2006).

- [336] N. P. M. Kuijsters, W. G. Methorst, M. S. Q. Kortenhorst, C. Rabotti, M. Mischi, and B. C. Schoot, *Uterine peristalsis and fertility: current knowledge and future perspectives: a review and meta-analysis*, *Reproductive biomedicine online* **35** (2017), no. 1 50–71.
- [337] P. Edmond, J. A. Ross, and I. S. Kirkland, *Human ureteral peristalsis*, *The Journal of urology* **104** (1970), no. 5 670–674.
- [338] J. Misra and S. Pandey, *Peristaltic transport of blood in small vessels: study of a mathematical model*, *Computers & Mathematics with Applications* **43** (2002), no. 8-9 1183–1193.
- [339] M. Jaffrin and A. Shapiro, *Peristaltic pumping*, *Annual review of fluid mechanics* **3** (1971), no. 1 13–37.
- [340] F. Chen, S. Dirven, W. Xu, and X. Li, *Soft actuator mimicking human esophageal peristalsis for a swallowing robot*, *IEEE/ASME Transactions on Mechatronics* **19** (2013), no. 4 1300–1308.
- [341] R. L. Norton, *Design of Machinery: An Introduction to the Synthesis and Analysis of Mechanisms and Machines*, pp. 178–180. McGraw Hill, third ed., 2004.
- [342] N.-S. Cheng, *Formula for the viscosity of a glycerol- water mixture*, *Industrial & engineering chemistry research* **47** (2008), no. 9 3285–3288.
- [343] E. Nader, S. Skinner, M. Romana, R. Fort, N. Lemonne, N. Guillot, A. Gauthier, S. Antoine-Jonville, C. Renoux, M.-D. Hardy-Dessources, *et. al.*, *Blood rheology: key parameters, impact on blood flow, role in sickle cell disease and effects of exercise*, *Frontiers in physiology* **10** (2019) 1329.
- [344] H. Li, J. Liu, K. Li, and Y. Liu, *A review of recent studies on piezoelectric pumps and their applications*, *Mechanical Systems and Signal Processing* **151** (2021) 107393.